Advanced Numerical Techniques for Dynamic and Aerodynamic Analysis of Bridges

By

Hamidreza Naderian

A thesis submitted to the Faculty of Graduate and Postdoctoral Studies in partial fulfillment of the requirements for the degree of Doctor of Philosophy

The Doctor of Philosophy Program in Civil Engineering is a joint program with Carleton University, administered by the Ottawa-Carleton Institute of Civil Engineering

Department of Civil Engineering
University of Ottawa
Ottawa, Canada
February 2017

Abstract: To meet the economic, social and infrastructure needs of the community for safe and efficient transportation systems, long span bridges have been built throughout the world. Long span bridges are one of the most challenging kinds of structures in civil engineering. The cable-stayed bridges are of great interest mainly as an alternative and a more economic solution than the one of suspension bridges. In addition, the fiber reinforced polymer (FRP) composites are, nowadays, successfully used for constructing modern bridges, where the significant weight saving provides additional benefits. Because of the great flexibility, modern long-span cable-stayed bridges are usually very susceptible to dynamic loads especially to the earthquake and strong winds. Therefore, the earthquake-resistant and wind-resistant designs become one of key issues for successful construction of bridges.

The objective of the present research is to develop a very efficient spline finite strip technique, for modelling and analysis of both conventional and hybrid FRP cable-stayed bridges. The study falls into the categories of bending, free vibration, seismic, and aerodynamic flutter analysis. The spline finite strip method (SFSM) is one of the most efficient numerical methods for structural analysis of bridges, reducing the time required for estimating the structural response without affecting the degree of accuracy. In the finite strip method, the degrees of freedom could be significantly reduced due to the semi-analytical nature of this method. However, the previous versions of SFSM are not able to model the entire bridge system. For that reason, the structural interactions between different structural components of the bridge could not be handled. In addition, the vibrations and displacements of the towers and cables could not be investigated. In the present formulation, all these obstacles have been eliminated. Moreover, the proposed finite strip technique is very efficient and accurate due to the drastic reduction in the formulation time, simplicity of data preparation, rapid rate convergence of the results, and the semi-analytical nature.

Last but not least, and for the first time, a fully finite strip solution is extended to the area of wind engineering. Using the spline finite strip discretization, the aerodynamic stiffness and mass properties of the long-span cable-stayed bridge are derived. The aerodynamic properties along with the structural properties of long-span plates and bridges are formulated in the aerodynamic equation of motion and are used to analyze the flutter problem.

The accuracy and efficiency of the proposed advanced finite strip method is verified against the finite element and field measurement results. The results demonstrate that this methodology and the associated computer code can accurately predict the dynamic and aerodynamic responses of the conventional and FRP long-span cable-stayed bridge systems. The outcome of the present research will lead to a comprehensive structural analysis of bridges in the framework of the proposed discretization which is more efficient and straightforward than the finite element analysis.

Acknowledgments

First and foremost, I would like to express my deepest admirations to my supervisor, Prof. Moe M. S. Cheung, for his continuous support, motivation, and immense knowledge. His guidance helped me in not only my PhD research but also in all aspects of my life. I could not have imagined having a better advisor and mentor.

I would also like to express my sincere gratitude to my other supervisors, Prof. Elena Dragomirescu and Prof. Majid Mohammadian for their supports during my PhD, especially after the death of Prof. Moe Cheung. I highly appreciate their contributions of time to make my PhD experience productive and stimulating.

I would like to thank the committee of my PhD thesis, Prof. Mark F. Green from Queens University, Prof. Abhijit Sarkar from Carleton University, and Prof. Magdi Mohareb and Prof. Martin Noël from University of Ottawa for their insightful comments and encouragement, and for the challenging questions which inspired me to widen my research from various perspectives.

In particular, I am so grateful to Prof. Andrea Fitzpatrick, a great mentor from the department of Visual Arts at University of Ottawa for encouraging and endorsing me towards my PhD.

Last but not least, I would like to thank Dr. Diman Ghazi for her valuable advice during my PhD studies.

Dedicated to the memory of

Professor Moe M. S. Cheung

List of Figures

List of Tables

Nomenclature

A_i^*: Aerodynamic derivatives associated with self-excited aerodynamic drag force M_f

[A]: laminate extensional stiffness matrix

a_g: Ground acceleration of the earthquake

B: deck width

[B]: laminate-coupling stiffness matrix

[C]: Damping matrix

$[C_s]$: Structural damping matrix

$[C_{aer}]$ Global aerodynamic damping matrix

CS1: One-dimensional column strip

$C(K_w)$: Theodorsen's functions

C_b: Damping matrix associated with the restrained degrees of freedom δ_b

C_s: Damping matrix associated with the unrestrained degrees of freedom δ_s

C_{sb}: Coupling damping matrix

[D]: Laminate-bending stiffness matrix

$[D_{FRP}]$: Material property matrix of the laminated FRP

D_f: Aerodynamic drag force

e: a vector indicating the degrees of freedom influenced by the ground motion

E_1: Modulus of elasticity of the lamina in longitudinal direction

E_2 : Modulus of elasticity of the lamina in transverse direction

$\{f_{aer}\}$: Aerodynamic forces vector

$\{f_{FRP}\}$: Force vector of a laminate FRP

$\{F_{aer}\}$: Global self-excited aerodynamic force

$f_{\exp}(Hz)$: Measured frequencies

$f_{FEM}(Hz)$: FE frequencies

$f_{FSM}(Hz)$: FS frequencies

G_{12} : shear modulus of the lamina

h: the width of the transitions section

H_i^*: Aerodynamic derivatives associated with self-excited aerodynamic lift force L_f

H: the width of the normal section

$[K]$: Global stiffness matrix

$[K_{aer}]$: Global aerodynamic stiffness matrix

$[k_{FRP}]$ Stiffness matrix of a laminate FRP

$[K_s]$: Global structural stiffness matrix

K_b: Stiffness matrix associated with the restrained degrees of freedom δ_b

K_s: Stiffness matrix associated with the unrestrained degrees of freedom δ_s

K_{sb}: Coupling stiffness matrix

K_w: Non-dimensional reduced frequency

L1: First lateral bending of deck

L2: Second lateral bending of deck

L3: Third lateral bending of deck

L: Length of the plate strip

L_f: Aerodynamic Lift force

$[M]$: Global mass matrix

{M}: Moments vector

$[m_{FRP}]$: Mass matrix of a laminate FRP strip

$[M_s]$: Global structural mass matrix

M_f: Aerodynamic Pitching moments

M_x Bending moment about the x axis per unit length in the middle surface of the laminate

M_y: Bending moment about the y axis per unit length in the middle surface of the laminate

M_{xy}: Twisting moment per unit length in the middle surface of the laminate

M_b: Mass matrix associated with the restrained degrees of freedom δ_b

M_s: Mass matrix associated with the unrestrained degrees of freedom δ_s

M_{sb}: Coupling mass matrix

[N]: Shape function matrix

{N}: In-plane forces vector

$[N_t]$: Transverse shape function

N_x: Shear forces along x axis per unit length

N_y: Shear forces along y axis per unit length

N_{xy}: Membrane and shear forces per unit length

$\{P(t)\}$: External force vector

$P_b(t)$: Reaction force vector

P_i^*: Aerodynamic derivatives associated with self-excited aerodynamic drag force D_f

Q_{ij} : Components of the lamina stiffness matrix

r: the total number of longitudinal sections on a nodal line

T1: First torsional mode of deck

T2: Second torsional mode of deck

T3: Third torsional mode of deck

U: Wind velocity

u: membrane displacement function

U_f: Flutter critical speed

v: membrane displacement function

V1: First vertical bending of deck

V2: Second vertical bending of deck

V3: Third vertical bending of deck

V4: Fourth vertical bending of deck

V5: Fifth vertical bending of deck

w: Flexural displacement function

$\ddot{x}_g(t)$: Ground acceleration excitation

y_r: Dynamic displacement vector of δ_s

y_s: Pseudo-static displacement vector of δ_s

α: Rayleigh damping factor

β: Rayleigh damping factor

$\{\delta_i\}$: Displacement parameter vector of knot *i*

$\{\dot{\delta}\}$: Vector of the first derivative of displacements

$\{\ddot{\delta}\}$: Vector of the second derivative of the displacements

$\{\Delta_i\}$: Displacement vector of knot *i*

δ_b: Absolute displacement vector of restrained (support) degrees of freedom

$\dot{\delta}_b$: Absolute velocity vector of restrained (support) degrees of freedom

$\ddot{\delta}_b$: Absolute acceleration vector of restrained (support) degrees of freedom

δ_s: Absolute displacement vector of unrestrained degrees of freedom

$\dot{\delta}_s$: Absolute velocity vector of unrestrained degrees of freedom

$\ddot{\delta}_s$: Absolute acceleration vector of unrestrained degrees of freedom

$\bar{\Phi}_i$: Amended boundary local spline

$\Phi_i(y_j)$: B3-spline function of knot *i* at knot *j*

λ: Newmark's parameter

ξ: Structural damping ratios

γ: Newmark's parameter

ω : Natural frequency

ω_f : Flutter angular frequency

ρ_{air}: Air density

ρ : Mass density of the strip

ψ_x: Independent rotations about x axis

ψ_y : Independent rotations about y axis

$\{\varepsilon\}$: Mid-surface strains vector

$\{\kappa\}$: Mid-surface curvatures vectors

List of acronyms

2D: Two-dimensional

3D: Three-dimensional

BEM: Boundary Element Method

CFRP: Carbon fiber reinforced plastic

CHBDC: Canadian Highway Bridge Design Code

CS: Column Strip

FSM: Finite Strip Method

FEM: Finite Element Method

FRP: Fiber reinforced polymer

FSI: Fluid-structure interaction

GFRP: Glass fiber reinforced polymer

IFSM: Integrated Finite Strip Method

IMEX R-K: Implicit-Explicit Runge-Kutta

KSM Bridge: Kap Shui Mun Bridge

R-K: Runge-Kutta

RVM: Random vibration method

RSM: Response spectrum method

SFSM: Spline Finite Strip Method

SHM: Structural health monitoring

SMART-1: Strong Motion Array in Taiwan, phase I

ULSCSB: Ultra-Long Cable-stayed Bridge

THM: Time History Method

WVB: wind–vehicle–bridge

Chapter 1
Introduction

1.1 Introduction

Bridges play an indispensable role in the transportation systems and with the rapid developments of this infrastructure, longer span bridges are constructed. Numerous large cities around the world are located near wide lakes and rivers, where in order to facilitate the transportation, there is a high-demand of building long-span bridges. In general, there are two types of long-span bridges namely the suspension bridges and the cable-stayed bridges. The later one has attracted more attention from the bridge engineers and manufactures. However performing structural investigations for such massive structures with large number of degrees of freedom was always a challenge, thus engineers are limited by the assumptions they have to work with when designing the cable-stayed and suspension bridges.

1.2 Research Motivation

Recently, the main concern of the researchers and designers of long-span cable-stayed bridges is extending the span length of the cable-stayed bridge as much as possible. The use of advanced composite FRP materials in building different components of the bridge, such as the deck, cables, etc. is one of the practical solutions. However, these new construction materials can cause some problems like instability of the towers and the deck under seismic and wind loading. Moreover, with the increase in the span length the height of the tower should increase as well, and this may lead to buckling phenomena in towers.

The structural response of long-span bridges under dynamic and aerodynamic loads is very complicated. Therefore, powerful computational techniques are required that can accurately analyze and predict the structural behavior of these massive structures. This is a key point in successful and optimal design of long-span cable-stayed bridges. Most of the bridge analyses are performed with the well-known finite element method. In the case of long-span bridges with thousands of degrees of freedom and at the same time having high nonlinear behavior under dynamic and aerodynamic forces, the finite element analysis might be

inefficient. In fact, the nonlinearities of the flexible bridge structures lead to a considerable redistribution of internal forces and subsequently the need for performing iterative analysis is justified. This results in decreasing significantly the convergence rate of the standard FEM in dynamic analysis problems. One solution is to use very fine meshes for each structural element. However, this causes the FE method to process a massive number of degrees of freedom. In spite of the development of some relatively new techniques, like mesh-free method for accelerating the FEM analysis, the mentioned difficulties still remain for large-scale models such as dynamic and aerodynamic of long-span cable-stayed bridges.

From the construction point of view, long-span bridges have been built from the same small selection of materials for the last 100 years, generally steel and concrete, with occasional usage of aluminum or timber. However, fiber reinforced polymer (FRP) composites have been used in aerospace and marine applications for over 50 years and nowadays are increasingly used for bridge structures around the world. Fiber reinforced polymer (FRP) composite materials have shown great potential as an alternative bridge construction materials to conventional ones. Composites have also been used very successfully for opening the bridge spans, where the significant weight saving provides additional benefit, reducing the cost of mechanical part required to open the bridge and to allow the water traffic to pass. It seems that the benefits of using FRP composites will be even more significant for the construction of long-span bridges. It has been shown that the FRP composites have the potential to revolutionize the construction of long span-bridges, by producing more efficient and cost-effective structures. They will also increase drastically the durability of the structure, reducing through-life costs and disruption due to required maintenance. Bridges with FRP decks are gaining popularity, and there is a growing need to understand the behavior of the FRP constructed bridge decks. The acceptance of the FRP materials in bridge engineering is mainly due to their superior properties, such as high strength-to-weight ratio, better durability, corrosion resistance, and resistance to fatigue, over the steel and concrete materials. On the other hand, the characteristics of the FRP constructed decks such as mass, stiffness, and damping are significantly different from those of the traditional concrete and steel decks, which could result in a different performance of the FRP deck bridges from traditional bridges.

Despite the great potential for popularizing the FRP materials in ultra-long span cable-stayed bridges, conventional analysis and design methods do not have yet proper discretization procedures to account for the hybrid FRP cable-stayed bridges structural behaviour, which due to the complexity of the failure mechanisms and anisotropic nature of FRP laminated deck might become a tedious investigation. In contrast with the traditional steel and concrete materials, which are typically modelled as isotropic materials, FRP composites are highly anisotropic depending on the type of the fibers, matrix, and the orientation of each lamina. As a result, the structural performance of long-span cable-stayed FRP bridges, especially the dynamic and aerodynamic characteristics, is totally different from the conventional cable-stayed bridges, due to the longer span, lighter weight and more flexible structural system achieved by applying the FRP construction material. In addition, the highly non-linear material properties coupled with the geometrical complexity of the structure, cause the structural analysis and design of cable-stayed FRP bridges to become extremely more complex and challenging. Taking the above features into account, an optimal numerical technique for modeling the structural behavior of FRP laminated bridge structures is highly desired.

Last, but not the least, the aeroelastic flutter phenomenon is an important factor in successful analysis, design, and construction of long-span cable-stayed bridges. The potential collapse of the structure due to flutter instability response under the wind effects is vital for the bridge design. However, the mechanism of wind-induced flutter of long-span bridges is still very complicated and profound, involving many variables and patterns of vibrations. The flutter, as an aerodynamic problem is an iterative and time consuming analysis. The evaluation of bridge aerodynamic instability is traditionally based on direct wind tunnel testing and theoretical analysis methods. With the development of computer technology and computational fluid dynamics algorithms, the theoretical flutter analysis method is expected to further develop to meet the advanced computational methods employed for numerical analysis of aerodynamic flutter for long-span cable-stayed bridges.

1.3 Objectives

The finite strip method (FSM), as a very efficient semi-analytical numerical tool dating back to 1970's, has shown a great potential to be efficiently employed for analyzing the

bridge structures reducing the time required for analysis without affecting the degree of accuracy. A continuously differentiable smooth series, like B3 splines, in the longitudinal direction reduces the complex 3D problem to a 2D problem. Finite strip method is therefore an ideal platform for the traditional time-consuming dynamic analysis of long span cable-stayed bridges. However, because of some limitations, FSM is not as popular as the finite element method.

Current practice of finite strip method in bridge analysis is limited to the analysis of the super-structure subjected to static and dynamic loadings, given the simulated boundary conditions at the piers, towers, cables, etc. Consequently, the structural interactions between the bridge deck and the piers, towers, cables, etc. (sub-structures) cannot be modeled using the conventional FS methods. On the other hand, due to the nature of finite strip method, it is not possible to insert an extra component at an intermediate point within a strip. Currently, the effects of the sub-structure can be modelled by combining the finite strip bridge deck with sub-structures modeled by other types of element, such as the boundary elements. In this way, the structural interactions between the bridge deck and the sub-structure can be handled via an iterative process. Nonetheless, this could be applicable for simple types of structures under static and quasi-static loading only. In the case of complicated structures like long-span cable-stayed bridges or structures under dynamic and aerodynamic excitations, such as non-uniform seismic analysis or aeroelastic flutter analysis, such simplifications can no longer be effective. With certain improvements in the formulation of the finite strip method, it is estimated that the methodology can still be employed for the dynamic and aerodynamic analyses of long-span cable-stayed bridges, with very good accuracy, and remarkable computational efficiency. To achieve this, several objectives must be considered in the current research project. Developing an Integrated Finite Strip Method (IFSM) for long-span cable-stayed FRP bridges by modeling the FRP deck, piers and towers, cables, and the bearings together, in the environment of spline finite strip method (SFSM) is one of these objectives. Then, the methodology will be further extended to the seismic analysis of long-span cable-stayed bridges using the time domain method. By considering the anisotropic material properties, as well as the coupling effects within the FRP laminated deck in the formulation of the integrated finite strip solution, the IFSM methodology will be extended for modelling and analyzing the hybrid FRP long-span cable-

stayed bridges. Eventually, the final important objective of the current research is to extend the integrated finite strip to the area of wind engineering. In this regard, the finite strip formulation will be applied to derive the aerodynamic flutter properties of long-span cable-stayed bridges. Consequently, the flutter analysis can be performed by IFSM.

The property matrices derived from the integrated finite strip method will be used for bending analysis, and free vibration analysis of long-span cable-stayed bridges through which the natural frequencies and mode shapes of both conventional and FRP long-span cable-stayed bridges as well as continuous multi-span FRP bridges for different modes will be obtained.

In the framework of the finite strip solution, the time history method is proposed for the dynamic analysis and particularly for the seismic analysis of both conventional and FRP cable-stayed bridges. The method will be used for seismic response of long-span cable-stayed FRP bridges under uninform and nonuniform excitations. Finally, the integrated finite strip methodology will be used to formulate the aerodynamic flutter frequency analysis of longs-span cable-stayed bridges.

The proposed integrated finite strip solution will be formulated and programmed on a desktop workstation. The programs are used to study the static, free vibration, seismic, and flutter analyses of long-span bridges. The numerical results will be comparted with those obtained from finite element analysis as well as with the field tests data, to emphasize the accuracy and efficiency of the proposed method. The comparison must demonstrate that the convergence and efficiency of the method is very high as well as the simplicity of the input data and that the analysis can be performed in minimal computational time.

1.4 Outline of the thesis

In the following, a brief explanation about different types of long-span bridges and the advantages of cable-stayed bridges will be presented. An introduction about the finite strip method along with comparing it with finite element method is described.

In Chapter 2, a brief history of the modern long-span cable-stayed bridges will be explained. In addition, the development of the finite strip method and its capability to be used in different structural engineering problems will be presented. The limitations of the existing finite strip methods in modeling long-span cable-stayed bridge are discussed as well. In addition, the past research on the use of FRP laminated plates in bridge structures will be

reviewed. At the end of Chapter 2, the aerodynamic flutter studies on long-span bridges are discussed.

In Chapter 3, an integrated finite strip solution is proposed for long-span cable-stayed bridges. The presently developed method has its roots in the well-known spline finite strip method; which is itself based on the conventional finite strip method. Thereafter, the developed method is applied to the bending and free vibration analyses of Kap Shui Mun Bridge, an existent long-span cable-stayed bridge in Hong Kong.

In terms of dynamic analysis, the time history method is employed in the framework of the integrated finite strip method for seismic analysis of long-span cable-stayed bridges. This study is presented in Chapter 4. The numerical results are presented for seismic analysis of Kap Shui Mun Bridge under uniform and nonuniform excitations.

In order to model and analyze the long-span cable-stayed FRP bridge, first, the so called laminate spline strip model to be integrated in the IFSM, is developed in Chapter 5. The anisotropic nature of the FRP laminates, as well as the coupling effects between membrane and flexural displacements are modelled in the finite strip procedure, through introducing appropriate constitutive equations. The integration of the laminate spline strip with the integrated finite strip formulation will enable this method to simulate the FRP bridge structures. The method is applied to structural analysis of a variety of FRP laminated plates and plate-assemblies with different boundary conditions as well as continuous multi-span FRP bridges.

In Chapter 6, the proposed integrated finite strip method of laminated FRP decks is applied to long-span cable-stayed FRP bridges. Free vibration and time history seismic analysis of a laminated FRP deck long-span cable-stayed bridge is performed and is exemplified through a number of case studies.

Last but not least, the integrated finite strip method is extended to the area of wind engineering in Chapter 7. Using spline finite strip discretization, the aerodynamic stiffness and damping properties are derived and meshed with the integrated finite strip method in order to perform the flutter analysis of long-span cable-stayed bridges. In addition, a very simple scheme is proposed to amend the spline finite strip method for modelling different boundary conditions. Through numerical examples, the flutter behavior of flat plates and

long-span cable-stayed bridges is investigated. This process suggests a very efficient optimal scheme for dynamic and aerodynamic analysis of long-span cable-stayed bridges.

The finite strip results are validated against finite element method as well as field tests data. The results will show that the methodology can be successfully used for different analysis targets, from bending and free vibration, to seismic and flutter analyses of long-span cable-stayed FRP bridges.

Based on the concluding results, the future work of the research is proposed in Chapter 8, which involves the aerodynamic analysis of long-span cable-stayed hybrid composite FRP bridges, and developing an optimized numerical Runge-Kutta scheme for solving the flutter equation as a complex eigenvalue problem.

1.5 Long-span bridges

1.5.1 Suspension bridges

The suspension bridge as shown in Fig. 1.1, has two cables strung across the towers and the deck is hung on vertical suspenders attached to these suspension cables. The weight of the suspension cables is supported by the towers while the cables in turn support the weight of the vertical suspenders and the bridge traffic. James Finley (1756 – 1828) was the first designer and builder of the modern suspension bridges. In Fig. 1.2, the Chain Bridge invented by Finley in 1808 and located at Falls of Schuylkill, Philadelphia, Pennsylvania is illustrated.

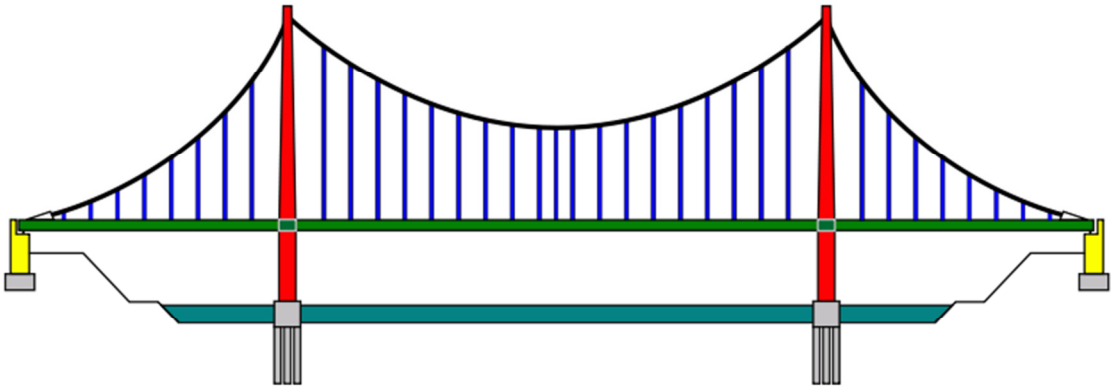

Fig. 1.1 Long-span suspension bridge [1.1]

1.5.2 Cable-stayed bridges

Cable-stayed bridges, shown in Fig. 1.3, are very similar to suspension bridges. However, their cables are connected directly to the towers. The cantilever-based construction allows them to be constructed from the inside out. In contrast with suspension bridges, multiple towers can be easily used to extend the length of the cables-stayed bridges when practical.

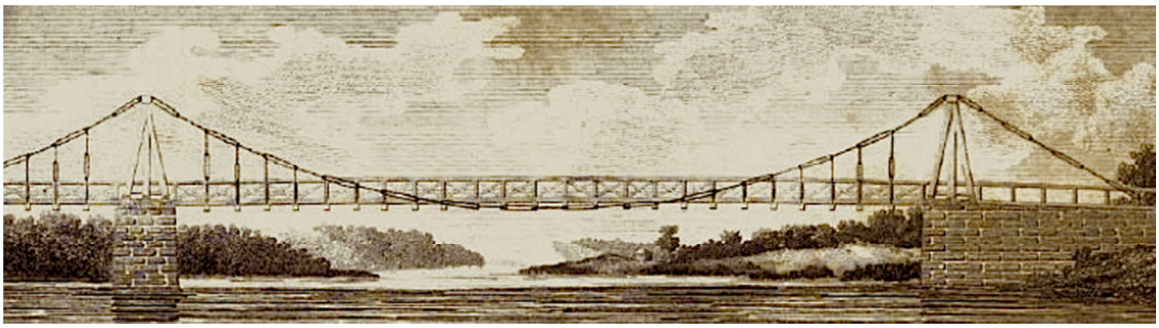

Fig. 1.2 Chain Bridge at Falls of Schuylkill, Philadelphia, Pennsylvania [1.2]

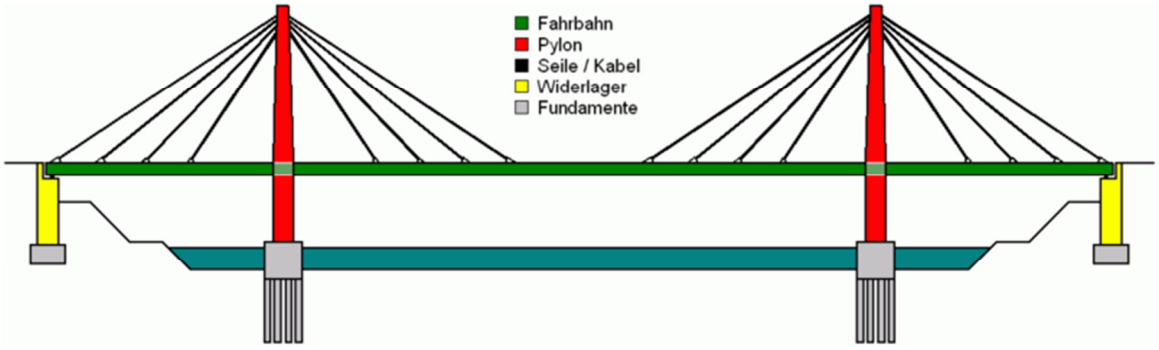

Fig. 1.3 Long-span cable-stayed bridge [1.1]

1.5.3 Comparison between suspension and cable-stayed bridges

There are differences between long-span cable-stayed and suspension bridges. Some of them are described in the following.

In cable-stayed bridges, the individual segments of the bridge can be constructed at remote locations, while the suspension bridges require the building of suspension cables across the entire span before the deck installation begins first. Moreover, the cable-stayed bridges have

the advantage of not requiring massive anchorages at the ends of the cables while for suspension bridges the anchorages are needed and they should be strong enough against the tension and angular pulling loads. In cable-stayed bridge the stiffness is much greater than the suspension bridge, which means that the deformations of the deck under live loads are reduced. On the other hand, cable-stayed bridges can be constructed by cantilevering out from the tower. In fact, the cables act both as temporary and permanent supports for the bridge deck.

In recent years, cable-stayed designs dominate most of the massive bridge projects. However, there are many other factors including engineering data and cost restrictions that affect the decision of engineers and designers to select between the suspension and cable-stayed bridges. Besides all the advantages of cable-stayed bridges, it is noticeable that suspension bridges can generally have longer spans. In Tables 1.1 and 1.2 the list of the world's longest cable-stayed and suspension bridges are given [1.3, 1.4]. Russky Bridge recently constructed in Russia has the longest span of 1104 m between cable-stayed bridges while Akashi Bridge located in Japan has the main span of 1991 m and is the longest one among the suspension bridges. It is worth noting that Akashi Bridge is the longest suspension bridge since 1998.

1.6 Bridge analysis methods

There are typically five methods for analyzing the bridges which are widely used and recognized by bridge design codes [1.5]. They are grillage energy methods, orthotropic plate theory methods, folded plate methods, finite element methods, and finite strip methods. In the present research, the focus is on finite strip method which is believed to be the most efficient method for static and dynamic analysis of long-span cable-stayed bridges. In addition, all the future research in this study will be carried out in the framework of the finite strip method. In the following sections, the reasons why finite strip solution is superior to other methods in terms of analysis of bridges will be discussed.

Table 1.1 The longest cable-stayed bridges in the world [1.3]

Rank	Name	Location	Country	Main span	Construction year
1	Russky Bridge	Vladivostok, Easten Bosphorus Strait	Russia	1,104 m	2012
2	Sutong Bridge	Suzhou, Nantong	China	1,088 m	2008
3	Stonecutters Bridge	Rambler Channel	Hong Kong	1,018 m	2009
4	E'dong Bridge	Huangshi	China	926 m	2010
5	Tatara Bridge	Seto Inland Sea	Japan	890 m	1999
6	Pont de Normandie	Le Havre	France	856 m	1995
7	Jingyue Bridge	Jingzhou	China	816 m	2010
8	Incheon Bridge	Incheon	South Korea	800 m	2009
9	Zolotoy Bridge	Vladivostok	Russia	737 m	2012
10	Shanghai Yangtze River Bridge	Shanghai	China	730 m	2009

Table 1.2 The longest suspension bridges in the world [1.4]

Rank	Name	Location	Country	Main span	Construction year
1	Akashi Kaikyō Bridge	Kobe - Awaji Island	Japan	1,991 m	1998
2	Xihoumen Bridge	Zhoushan	China	1,650 m	2009
3	Great Belt Bridge	Korsør - Sprogø (Region Zealand)	Denmark	1,624 m	1998
4	Yi Sun-sin Bridge	Gwangyang - Yeosu (South Jeolla Province)	South Korea	1,545 m	2012
5	Runyang Bridge	Yangzhou - Zhenjiang	China	1,490 m	2005
6	Nanjing Fourth Yangtze Bridge	Nanjing	China	1,418 m	2012
7	Humber Bridge	Hessle - Barton-upon-Humber	United Kingdom	1,410 m	1981
8	Jiangyin Bridge	Jiangyin -Jingjiang	China	1,385 m	1999
9	Tsing Ma Bridge	Tsing Yi - Ma Wan	Hong Kong	1,377 m	1997
10	Hardanger Bridge	Brurvik - Brimnes	Norway	1,310 m	2013

1.7 An alternative for the finite element method

There is no doubt that the finite element method had dominated the field of numerical modeling of structures. Nevertheless, various other methods like the finite strip [1.6, 1.7] and the boundary element [1.8] methods play an important role on their specialized areas. In the finite element method, one needs to discretize the problem in every dimension. It will consequently require more unknowns and degrees of freedom for solving the problem than other numerical methods. With the use of super-computers, millions of unknowns can be handled in the finite element environment. Although the cost of such kind of computations has decreased, there is still a need to use more efficient tools, in particular, for modelling massive structures. In addition, the computation costs usually multiply by the order of magnitude when a more refined or a higher dimensional analysis is needed. Moreover, for many problems involving structures of regular geometric shape and simple boundary conditions the use of finite element method is not only unnecessary but also excessive. Therefore, in order to reduce the computational costs and the CPU core requirements, alternative methods are evidently desirable.

The finite strip method which has been first developed by Y. K. Cheung [1.9] is one of the alternative methods to FEM. In the FSM, the structure is subdivided into a number of longitudinal strips for which the displacement field is defined by simple polynomials in the transverse direction and continuous harmonic functions in the longitudinal direction. The philosophy of the finite strip method is similar to Kantorovich method which is used for the purpose of reducing partial differential equations to a lower order or ordinary equations. In the finite strip method the order reduction is achieved either by using separation of variables approach or by transformation approach. A comparison between classical finite strip method and finite element method, made by Chenug and Tham [1.7], is listed in Table 1.3. The later comparison is limited to classical finite strip method. The classical finite strip method has some limitations. For instance, FSM can deal only with problems of simply supported end conditions. Moreover, it cannot handle shear forces and internal supports in the analysis. Researchers have tried to eliminate the above mentioned problems by developing new forms of finite strip method. Among the proposed finite strip methods, the spline finite strip method is the most pervasive one.

Table 1.3 Comparison between finite strip and finite element methods

Finite Element Method	Finite Strip Method
Applicable to any geometry, boundary conditions, and material properties. Extremely versatile and powerful	More often used for structures with prismatic geometric sections and with or without intermediate elastic supports. In dynamic analysis the method is used for structures with different boundary conditions and with discrete supports.
Usually a large number of equations and matrices with comparatively large bandwidth. Can be expensive and sometimes inefficient	Usually much smaller number of equations and matrices with narrow bandwidth, especially true for problems with an opposite pair of simply supported ends. Consequently, much shorter time for solution of comparable accuracy
Large quantities of input data and easier to make mistakes. Requires automatic mesh and load generation schemes.	Very small amount of input data owing to the small number of mesh lines involved due to the reduction in dimensional analysis
Many lower order elements will not yield correct stresses at the nodes and stress averaging or interpolation techniques must be used in the interpolation of results	Because of the semi analytical nature and the continuity C2, more accurate results are obtained
Requires a large amount of core and is more difficult to program.	Requires smaller amount of cores and is easier to program. Because only a few eigenvalues are needed, the first two or three terms of the series will normally yield sufficiently accurate results. Matrix can usually be solved by standard eigenvalue subroutines.

With the advent of spline finite strip method [1.10] the flexibility of the method has drastically increased. The B3-spline functions replace trigonometric and hyperbolic series in the longitudinal interpolation functions used for analyzing plates and shells. Among its characteristics, one can mention dealing with multi-span or column-supported structures. In fact, B3-spline functions are the solution of a beam under a point load deflection. Consequently, the spline finite strip method is also capable of simulating point loads with high convergence rate. In addition to being nearly as versatile as the standard finite element

method, the spline finite strip method can achieve a higher order continuity C2 with smaller number of degrees of freedom.

References

[1.1] https://www.quora.com/What-is-the-difference-between-the-cable-stayed-bridge-and-a-suspension-bridge

[1.2] https://en.wikipedia.org/wiki/Chain_Bridge_at_Falls_of_Schuylkill

[1.3] List of longest cable-stayed bridges

http://en.wikipedia.org/wiki/List_of_longest_cable-stayed_bridge_spans

[1.4] List of longest suspension bridges

http://en.wikipedia.org/wiki/List_of_longest_suspension_bridge_spans

[1.5] Cheung, M.S., Li, W., Chidiac, S. E., (1996) Finite strip analysis of bridges, 1st Edition. London: E & FN Spon,

[1.6] Cheung Y. K., (1976) Finite strip method in structural analysis. Oxford: Pergamon

[1.7] Cheung Y. K., Tham L. G. (1998) The finite strip method, USA: CRC Press; 1998

[1.8] L. C. Wrobel; M. H. Aliabadi (2002) The Boundary Element Method. New Jersey: Wiley.

[1.9] Cheung, Y. K., (1968) The finite strip method in the analysis of elastic plates with two opposite simply supported ends, Proc. Inst. Civ. Eng., 40, 1-7

[1.10] Cheung, Y.K., Fan, S.C., Wu, C.Q., (1982) Spline finite strip in structural analysis, Proc. Int. Conf. Fin. Elem. Meth., Shanghai, 704-709.

Chapter 2
Literature Review

2.1 The history of modern long-span cable-stayed bridges

The history of cable-stayed bridges dates back to sixteenth century. However, the construction of modern cable-supported bridges became popular since 1950's**.** The interesting point is that many early suspension bridges were cable-stayed construction.

The first modern cable-stayed bridges are Albert Bridge, a concrete-deck bridge constructed in 1952 (Fig. 2.1), and Strömsund Bridge (Fig. 2.2). From the Figures 2.1 and 2.2 it is obvious that early bridges from this period were constructed by few stay cables. This caused substantial erection costs. Thus, more modern bridge structures tend to use many more cables.

Fig. 2.1 Albert Bridge, London

2.2 Development of the finite strip method

The finite strip method (FSM) was first created by Y. K. Cheung [2.1] in order to perform analysis of elastic plates with simply supported end conditions. The original idea for the FSM was to reduce the dimensions of a long span structure via the implementation of an

Fig. 2.2 Strömsund Bridge

analytical solution along the longitudinal direction. Powell et al. [2.2] developed the finite strip method for modeling the rectangular slab bridges. Afterwards, researchers and engineers carried out studies to a considerable extent on expanding the theory and application of the finite strip method in the area of structural engineering. Various methodologies have been proposed for a variety of structures including plates, shells, laminated plates, bridges, tall buildings, etc. [2.3]. The nature of the finite strip method is such that it deals well with the problems in which the structure has a harmonic and deterministic response in the longitudinal direction under the applied loading. Among such kinds of problems, one can mention the buckling and vibration of plates, plate-structures, and bridge structures. This method has been further applied to the linear-elastic, nonlinear and dynamic analyses. Among the vast number of publications in the field of finite strip method, the following are worth to be highlighted.

M. S. Cheung carried out research on rectangular slabs with general end boundary conditions and box girder bridges [2.4]. Based on the finite strip analysis, Cheung et al. and Zienkiewicz et al. [2.5, 2.6] developed the finite layer and finite prism methods for analyzing thick slabs and thick bridge boxes respectively.

In the area of dynamic analysis, Cheung and Cheung [2.7] first proposed the finite strip solution for free vibration analysis of thin-walled structures with different boundary conditions.

It has been tried to combine the finite strip method with other numerical method to increase the capability of the analysis. In this regard, Cheung and his colleagues [2.8, 2.9] combined

it with finite element and boundary element methods and they used it for analysis of irregular plates and slab girder bridges.

Cheung et al. [2.10] proposed a precise finite strip solution in which the precise integration method along the space coordinate is combined with the semi-analytical analysis of prismatic domain structures.

In the field of structural stability, the first use of the finite strip method appears to be the work of Prezemieniecki [2.11], who showed how this technique can be used to predict the initial elastic local buckling of plates and sections made of plates under biaxial compression. His approach utilized the approximate finite strip formulation of Cheung and Cheung [2.12]. Plank and Wittrick [2.13] employed complex finite strip method to investigate buckling under combined loading of thin-walled structures. The advantage of their method over the formulations of the conventional finite strip method is that it can handle shear forces. Wittrick [2.14] developed an exact finite strip method for buckling analysis of stiffened panels in compression. Schafer et al [2.15-2.17] derived a constrained finite strip method based on the generalized beam theory for decomposing the buckling modes of thin-walled open cross-section members. The author used the finite strip method for a number of applications in the field of buckling of plates and plate-assemblies, the most fascinating of which is the torsional and flexural buckling of composite FRP structural plates and buckling analysis of cold-formed steel structures [2.18-2.21].

2.2.1 Spline finite strip method

In the conventional finite strip method, the structure is subdivided into a number of longitudinal strips for which the displacement field is defined by simple polynomials in the transverse direction and continuous harmonic functions in the longitudinal direction. Thus it yields much lower number of degrees of freedom than the finite element method. However, it bears the drawbacks that it usually allows only simple boundary conditions, simple structural geometries and simple loading types to be analyzed. Some efforts have been made to make the conventional finite strip method capable of modeling different boundary end conditions [2.22, 2.23].

In order to overcome the shortcomings of the semi-analytical finite strip method with boundary conditions, concentrated loads, and continuous spans, the spline finite strip

method was created by Cheung et al [2.24, 2.25]. Nowadays the spline finite strip method is universal and acceptable than the initial semi-analytical finite strip method.

The spline finite strip method can be considered as a special form of the finite element method and at the same time is an evolved version of the finite strip method. In this technique, the displacement functions in the longitudinal directions are B3 spline at the expense of more degrees of freedom in comparison with conventional finite strip method. The advantage of the latter method over the conventional one, is the ability of handling more complex types of loadings, geometries, and boundary conditions.

The spline FSM has been successfully applied to the analyses of many types of structural problems such as box girder bridges, circular plates, skew plates and the plates of arbitrary shape. Fan and Cheung [2.26] used the spline finite strip method for analysis of shallow shells. Tham [2.27] has successfully extended the application of SFSM to the analysis of space structures. Hancock et al. were the first researchers who applied SFSM for elastic and inelastic buckling of thin flat-walled structures subjected to longitudinal compression and bending, transverse compression, as well as shear [2.28, 2.29]. Some researchers tried to use other types of splines like x-spline functions in the finite strip environment that was able to solve the problems defined for some irregular shaped structures [2.30].

The isoparametric spline FSM was introduced in modeling structures of awkward geometry for the plane structures [2.31], and it was extended to the shell analysis [2.32]. Researchers at the University of Sydney extended the application of the ISFSM to inelastic materials and geometric nonlinear analysis of perforated thin-walled steel structures [2.33].

Chen et al. [2.34, 2.35] introduced the unequally spaced B3-spline functions in the analysis of stiffened plates and folded plate structures with intermediate supports. The method allows one to describe the accurate response in the region of high stress gradients, or at the locations of abrupt geometric changes by spacing knots more closely. It is worth to mention that the recently developed integrated finite strip method is based on the use of unequally spaced B3-spline functions.

Dawe [2.36] carried out an extensive research on the use of both conventional and spline finite strip methods in determining the behavior of composite laminated, prismatic plate and shell structures based on the thin plate theory. He used the method for analyzing a variety of problems like buckling stresses and natural frequencies of single span and multi-span

structures, post-buckling response of plate structures**,** thermal buckling and the transient response to dynamic loading of flat plates. Wang and Zhang [2.37] introduced a layerwise B-spline finite strip method for free vibration analysis of both thick and thin composite laminated plates. In this method, the composite laminated plates are divided into a number of numerical layers in the thickness direction.

In the area of aerodynamics, the finite strip method has been extended to flutter analysis by Cheung and his colleagues [2.38, 2.39]. However, the extension is not a pure finite strip solution but it is combined with the finite element method.

Among other successful applications of the spline finite strip method, one can mention the linear elastic analysis of arbitrarily shaped plates and shells conducted by Chen et al. [2.40] and Li et al [2.41, 2.42], free vibration of arbitrarily shaped plates and shells by Li [2.41] and Cheung et al. [2.43]. In terms of nonlinear analysis, the studies include the elastic geometric nonlinear and postbuckling analysis of arbitrarily shaped thin plates and shells by Cheung and Zhu [2.44-2.48], nonlinear analysis of thin-walled plates and plate assemblies by Hancock et al. [2.49], and nonlinear analysis of thick and laminated plates by Kong and Cheung [2.50].

2.2.2 Finite strip modeling of bridges

The field of the finite strip analysis in bridge engineering has been extended to bridges with different geometric and boundary conditions, including circularly curved slab and box girder bridges [2.51, 2.52], skew slab and box girder bridges [2.53, 2.54], continuous slab and box girder bridges [2.55, 2.56], hunched continues slab and box girder bridges [2.57, 2.58].

Static analysis of right box girder bridges with various types of end and interior supports by spline finite strip method were first carried out by Cheung et Al. [2.59]. Afterwards, they extended the spline finite strip solution to the analysis of hunched, continuous slab and box-girder bridges [2.60-2.62].

2.2.3 Limitations of existing finite strip methods

The scientific literature pertinent to the application of the finite strip method on long-span cable-stayed bridges is limited to modelling of the bridge deck. Other structural components like towers (pylons), piers, cables and bearing are modeled by applying special boundary

conditions which is a real disadvantage of the finite strip method in bridge modeling. This problem could be overcome by introducing an integrated finite strip solution, in which all structural components can be modeled by strip elements, and with transition sections between them. As a result, it makes the numerical analysis of complicated bridges like suspension and cable-stayed bridges possible.

2.2.4 Literature review on FRP plates and bridges

The FRP plates and decks are usually assumed to act as isotropic or orthotropic laminated materials [2.63, 2.64]. Different methodologies have been developed for bending and stress analyses of composite laminated structures, including laminated FRP plates, such as mesh-free methods [2.65], finite element methods [2.66-2.72], and other analytical techniques [2.73-2.75].

2.2.4.1 Finite strip method for composite laminated plates

Dawe et al, [2.76-2.80] carried out an extensive research on the use of spline finite strip methods in determining the behavior of composite laminated, prismatic plate and shell structures based on the thin plate theory. They used the method for analyzing a variety of problems including buckling stresses and natural frequencies of single span and multi-span structures, and for investigating the post-buckling response of plate structures [2.81-2.83], thermal buckling [2.84] and the transient response to dynamic loading of flat plates. Wang and Zhang [2.85] introduced a layerwise B-spline finite strip method for free vibration analysis of both thick and thin composite laminated plates. In this method, the composite laminated plates are divided into a number of numerical layers in the thickness direction. Recently, Beena et al. [2.86] used the means of spline finite strip method for modeling and conducting the linear static analysis of functionally graded plates. However, his study is limited to simply supported boundary conditions. Qiao et al. [2.87] used FSM for post-buckling analysis of composite plates under shear and compression. Although a considerable research has been carried out on the use of spline finite strip method for composite laminated plates, the elastic bending and stress analyses of laminated FRP plates have not been yet addressed in the literature to the best knowledge of the author.

2.2.4.2 Hybrid FRP deck bridges

Research shows that the stiffness of advanced composite materials including FRP is coupled to the geometry of the structure [2.88, 2.89]. To the knowledge of the author, the first all composite cable-stayed bridge is the Aberfeldy Footbridge, in the UK, where the main structure is a cable-stayed bridge made by glass fiber reinforced polymer (GFRP) deck, and suspended by Parafil-Aramid ropes and GFRP towers. Salim et al [2.90] carried out research on the analysis and design of FRP composite deck-and-stringer bridges. By the means of pultruded FRP shapes, Qiao et al [2.91] suggested a systematic approach for analysis of FRP deck bridges. Bridge engineering researchers at the University of California, San Diego in collaboration with the Federal Highway Administration, built a 4-lane traffic way composite cable-stayed bridge with the length of 137.2 m and the A-frame pylon of 57.9 m [2.92]. In spite of the state of the art research reports on the application of FRP materials used for short span bridges, there is still lack of research on the FRP based long span cable-stayed bridges. Almansour and Cheung [2.93-2.96] proposed a comprehensive multi-scale design approach of hybrid FRP bridge in the frameworks of both micro and macro levels. They performed a number of case studies which resulted in developing different types of FRP deck sections for long-span cable-stayed bridges. The studies by Virlogeux showed that a very thin deck section can support the static and traffic loads applied to a cable-stayed bridge [2.97]. Through some experimental tests, Burgueno et al. [2.98] investigated the dynamic characteristics of composite FRP bridges. Cheung and his research group at Hong Kong University of Science and Technology and Sichuan University carried out an extensive analytical and experimental research on micro-scale and macro-scale design of the FRP deck, for a number of existing bridges [2.99-2.101]. As a result, the cable-stayed bridge is redesigned by replacing the composite steel-concrete deck with the advanced composite CFRP materials based on the loading condition and the design requirements. The design process considers the multi-scale design approach introduced by Cheung and Almansour [2.95, 2.96], considering the FRP laminated material configuration and micro-material properties.

2.2.5 Review on aerodynamic flutter of bridges

The determination of the dynamic and aerodynamic characteristics of the bridge is a crucial step in solving the flutter problem for bridges. Since 1960s, a number of publications have

dealt with both analytical and experimental studies on flutter of long-span bridges. Tanaka et al. [2.102], and Ge et al. [2.103] investigated the flutter of plates and bridges by multi-mode and full-mode approaches. Huang et al. [2.104] studied the aerodynamic behavior of bridges under skew wind by performing a series of section model tests. Dowell et al. [2.105] investigated the flutter of rectangular plates under the three-dimensional axial flow through some numerical and experimental tests. Wu et al. [2.106] presented a framework for linear and nonlinear aeroelastic analysis of cable-supported bridges. The topic of the bridge flutter is still highly demanding and researchers try to develop different types of experimental and analytical techniques for better understanding of the flutter phenomenon [2.107-2.113]. Cheung and his colleagues [2.114] used a combination of spline finite strip method and finite element method for flutter analysis of long-span cable-stayed bridges. Despite the merits of their suggested method, there still seems to be considerable concerns regarding the efficiency and accuracy of the solution which will be discussed in details in Chapter 7.

References

[2.1] Cheung, Y. K., (1968) The finite strip method in the analysis of elastic plates with two opposite simply supported ends, Proc. Inst. Civ. Eng., 40, 1-7

[2.2] Powell, G. H., Ogden, D. W., (1969) Analysis of orthotropic steel plate bridge decks, Proc. ASCE, 95 (ST5), 909-922

[2.3] Cheung Y. K., Tham L. G. (1998) The finite strip method, USA: CRC Press; 1998

[2.4] M. S. Cheung, Wenchang Li, (1989) Analysis of continuous, haunched box-girder bridges by finite strips, Journal of Structural Engineering, Vol. 115, No. 5, May

[2.5] Cheung, Y. K., Chakrabarti, S., (1971), Analysis of simply supported thick layered plates, ASCE, 97(EM3), 1039-1044

[2.6] Zienkiewicz, O. C., Too, J.J.M., (1972), The finite prism in analysis of thick simply supported bridge boxes, Proc,. Inst. Civ. Eng. 53, 147-172

[2.7] Cheung, M. S., Cheung, Y. K., (1971) Natural vibrations of thin flat-walled structures with different boundary conditions, J Sound Vibr ;18:325–37

[2.8] Cheung, M.S., Li, W., Chidiac, S. E., (1996) Finite strip analysis of bridges, 1st Edition. London: E & FN Spon,

[2.9] Cheung, M. S., Akhras G., Li, W., (1994) Combined boundary element, finite strip analysis of bridges, Journal of Structural Engineering, Vol. 120, No. 3, March

[2.10] Zhong, W.X., Cheung, Y.K., Li, Y., (1998) The precise finite strip method, Comput. Struct., 69 (6), 773-783.

[2.11] Przemieniecki JS. (1973) Finite element structural analysis of local instability. AIAA J;11:33–9.

[2.12] Cheung M.S., Cheung Y.K., (1971) Natural vibration of thin flat walled structures with different boundary conditions. J Sound Vib;18(3):325–37.

[2.13] Plank RJ, Wittrick W.H., (1974) Buckling under combined loading of thin flat walled structures by a complex finite strip method. Int J Numer Methods Eng;8:323–39.

[2.14] Wittrick W.H., (1968) A unified approach to the initial buckling of stiffened panels in compression. Aeronaut Quart;19:265–83.

[2.15] Ada´ny S, Schafer B.W., (2006) Buckling mode decomposition of single-branched open cross-section members via finite strip method: derivation. Thin-Wall Struct;44:563–84.

[2.16] Adány S, Schafer B.W., (2006) Buckling mode decomposition of single-branched open cross-section members via finite strip method: application and examples. Thin-Walled Structures;44:585–600.

[2.17] Adány S, Schafer B.W., (2008) A full modal decomposition of thin-walled, single-branched open cross-section members via the constrained finite strip method. J Construct Steel Res; 64:12–29.

[2.18] Naderian, H. R., Ronagh, H. R., Azhari, M., (2012), Global Buckling Behavior of Composite FRP Cruciform Section Columns by Complex Finite Strip Method, Proceedings of the 6th International Conference on Advanced Composite Materials in Bridges and Structures, Kingston, Ontario, Canada, 22 – 25 May 2012.

[2.19] Naderian, H. R., Ronagh, H. R., Azhari, M., (2011), Torsional and Flexural Buckling of Composite FRP Columns with Cruciform Sections Considering Local Instabilities, Journal of Composite Structures, Volume 93, Issue 10, September 2011, Pages 2575-2586.

[2.20] Naderian, H. R., Azhari, M., Ronagh, H. R., (2010), Distortional Buckling of Stiffened Cold-Formed Steel Channel Sections, Proceedings of the 10th International Conference on Computational Structures Technology, Valencia, Spain

[2.21] Naderian, H. R., Azhari, M., Ronagh, H. R., (2010), Stability of Unstiffened and Stiffened Cold Formed Steel I- Sections by the Bubble Finite Strip Method, Proceedings of the 10th International Conference on Computational Structures Technology, Valencia, Spain,

[2.22] Bradford M.A, Azhari M. (1995) Buckling of plates with different end conditions using the finite strip method, J Comput Struct; 56(1):75–83

[2.23] Li, Z., Schafer, B.W., (2013) Constrained finite strip method for thin-walled members with general end boundary conditions; Journal of Engineering Mechanics

[2.24] Cheung, Y.K., Fan, S.C., Wu, C.Q., (1982) Spline finite strip in structural analysis, Proc. Int. Conf. Fin. Elem. Meth., Shanghai, 704-709.

[2.25] Fan, S. C., (1982) Spline finite strip in structural analysis, PhD thesis, Department of Civil Engineering, the University of Hong Kong

[2.26] S. C. Fan, Y. K. (1983) Cheung, Analysis of shallow shells by spline finite strip method, Eng. Struct., Vol. 5, October

[2.27] Tham LG., (1990) Application of spline finite strip method in the analysis of space structures. Thin-Walled Structures; 10:235–246

[2.28] Lau, S. C. W., and Hancock, G. J. (1986) Buckling of thin flat-walled structures by a spline finite strip method." Thin-Walled Structures, 4(4), 269-294

[2.29] Lau, S. C. W., and Hancock, G. J. (1989) Inelastic buckling analyses of beams, columns and plates using the spline finite strip method, Thin-Walled Structures, 7(3-4), 213-238

[2.30] H.Y. Yang, K.P. Chong, (1934) Finite Strip Method with X-spline Functions, Computers and Structure, Vol. 18.No. I, pp. W-132,

[2.31] Au FTK, Cheung YK., (1993) Isoparametric spline finite strip for plane structures. Computers and Structures; 48(1):23 – 32.

[2.32] Cheung YK, Au FTK., (1995) Isoparametric spline □nite strip for degenerated shells. Thin-Walled Structures; 21:65 – 92

[2.33] Yao, Z., Rasmussen K.J.R., (2010) Material and geometric non- linear isoparametric spline finite strip analysis of perforated thin-walled steel structures, Research report R910, March 2010, School of Civil Engineering, University of Sydney

[2.34] Chen CJ, Gutkowski RM, Puckett JA. (1991) B-Spline compound strip analysis of stiffened plates under transverse loading. Computers and Structures; 34(2):337–347.

[2.35] Chen CJ, Gutkowski RM, Puckett JA. (1991) Spline compound strip analysis of folded plate structures with intermediate supports. Computers and Structures; 39(3/4):369–379.

[2.36] Dawe, D.J., (2002) Use of the finite strip method in predicting the behaviour of composite laminated structures, ompositeStructures57, 11–36

[2.37] Wang, S., Zhang, Y., (2004) Vibration analysis of rectangular composite laminated plates using layerwise B-spline finite strip method, Composite structures,;(68), 349-358.

[2.38] Lau, David T., Cheung, M. S., Cheng, S. H., (2000) 3D Flutter analysis of bridges by spline finite strip method, Journal of Structural Engineering, Vol. 126, No. 10, October

[2.39] Cheng, S. H., Lau, David T., Cheung, M. S., (2003) Comparison of numerical techniques for 3D flutter analysis of cable-stayed bridges, Computers and Structures 81 2811–2822

[2.40] Chen, M. J., Tham, L. G., and Cheung, Y. K. (1984). Analysis of thin parallelogram plates' bending by spline- finite-strip method, Applied mathematics and mechanics, 5(6), 1727.

[2.41] Li, W. Y. (1988), Spline finite strip analysis of arbitrarily shaped plates and shells, PhD thesis, Univ. of Hong Kong.

[2.42] Li, W. Y., Cheung, Y. K., and Tham, L. G. (1986) Spline Finite Strip Analysis of General Plates, Journal of Engineering Mechanics, 112(1), 43-54.

[2.43] Cheung, Y. K., Tham, L. G., and Li, W. Y. (1988), Free vibration and static analysis of general plate by spline finite strip, Computational Mechanics, 3(3), 187-197.

[2.44] Cheung, Y. K., and Dashan, Z. (1987) Large deflection analysis of arbitrary shaped thin plates, Computers & Structures, 26(5), 811-814

[2.45] Zhu, D. S., (1988) Nonlinear static and dynamic analysis of plates and shells by spline finite strip method, PhD thesis, Univ. of Hong Kong

[2.46] Zhu, D. S., and Cheung, Y. K. (1989), Postbuckling analysis of shells by spline finite strip method, Computers and Structures, 31(3), 357-364

[2.47] Zhu, D. S., and Cheung, Y. K. (1996), Postbuckling analysis of circular cylindrical shell under combined loads, Computers & Structures, 58(1), 21-26

[2.48] Cheung, Y. K., and Zhu, D. S., (1989), Postbuckling analysis of circular cylindrical shells under external pressure, Thin-Walled Structures, 7(3-4), 239-25

[2.49] Kwon, Y. B., and Hancock, G. J. (1991) A nonlinear elastic spline finite strip analysis for thin-walled sections, Thin-Walled Structures, 12(4), 295-319

[2.50] Kong, J., and Cheung, Y. K., (1995) Generalized spline finite strip for the analysis of plates, Thin-Walled Structures, 22(3), 181-202

[2.51] Cheung, Y. K., (1969), The analysis of cylindrical orthotropic curved bridge decks, IABSE publications, 29-II, 41-52

[2.52] Cheung, Y. K., Cheung, M. S., (1969), Analysis of curved box girder bridges by finite strip method, IABSE publications, 31/I, 1-19

[2.53] Brown, T. G., Ghali, A., (1972) Finite strip analysis of skew slabs, Proc. McGill-EIC Conference in Finite Element Method in Civil Engineering, 1141-1151

[2.54] Brown, T. G., Ghali, A., (1975) Semi-analytic solution of skew box girder bridges, Proc. Inst. Civ. Eng., part 2, 59, 487-500

[2.55] Cheung, M. S., Cheung, Y. K., Ghali, A., (1970) Analysis of slab and girder bridges by the finite strip method, Build. Sci., 5 (2), 95-105

[2.56] Loo, Y. C., (1975), The finite strip analysis of multispan box-girder bridges with intermediate stiffening members, British Steel Corporation Fellowship Final Report, University of Dundee

[2.57] Cheung, M. S., Li, W., (1988) Analysis of haunched bridges by finite strip method, Computers and Structures, 28 (5), 621-626

[2.58] Cheung, M. S., Li, W., (1988) Analysis of continuous haunched box-girder bridges by the finite strips, Journal of Structural Engineering, 115 (5), 1076-1087

[2.59] Y. K. Cheung, *S.* C. Fan, (1983) Static analysis of right box girder bridges by spline finite strip method, *Proc. Instn Ciu. Engrs,* Part 2, 75, June, 311-323

[2.60] Cheung, M.S., Li, W., (1990) Analysis of haunched, continuous bridges by spline finite strips, Comput. Struct;36(2), 287-300.

[2.61] Cheung, M.S., Li, W., Jaeger, L.G., (1992) Spline finite strip analysis of continuous haunched box- girder bridges, Can. J. Civil Eng.;(19), 724-728.

[2.62] Cheung, M. S., Li, W., (1992) Spline finite strip analysis of continuous haunched box-girder bridges, Canadian Journal of Civil Engineering

[2.63] Naderian, H. R., Ronagh, H. R., Azhari, M., (2011) Torsional and flexural buckling of composite FRP columns with cruciform sections considering local instabilities, Composite Structures 93 (10), 2575-2586

[2.64] Naderian, H. R., Ronagh, H. R., Azhari, M., (2012), Global Buckling Behavior of Composite FRP Cruciform Section Columns by Complex Finite Strip Method, Proceedings of the 6th International Conference on Advanced Composite Materials in Bridges and Structures, Kingston, Ontario, Canada, 22 – 25 May 2012.

[2.65] Peng, L.X. , Liew K.M. , Kitipornchai S. , (2011) Bending Analysis of Folded Laminated Plates by the FSDT Meshfree Method, Procedia Engineering, Volume 14, 2011, Pages 2714-2721

[2.66] Yingqing Huang, Shenglin Di, Changchun Wu, Huiyu Sun, (2002) Bending analysis of composite laminated plates using a partially hybrid stress element with interlaminar continuity, Computers & Structures, Volume 80, Issues 5–6, March 2002, Pages 403–410

[2.67] Nguyen Duc Thai, Michele D'Ottavio, Jean-François Caron, (2013) Bending analysis of laminated and sandwich plates using a layer-wise stress model, Composite Structures, Volume 96, February 2013, Pages 135–142

[2.68] Amale Mahi, El Abbas Adda Bedia, Abdelouahed Tounsi, (2015) A new hyperbolic shear deformation theory for bending and free vibration analysis of isotropic, functionally graded, sandwich and laminated composite plates, Applied Mathematical Modelling, Volume 39, Issue 9, 1 May 2015, Pages 2489–2508

[2.69] Xiaodan Teng, Y.X. Zhang, (2014) Nonlinear finite element analyses of FRP-strengthened reinforced concrete slabs using a new layered composite plate element, Composite Structures, Volume 114, August 2014, Pages 20–29

[2.70] Aysun Baltaci, Mehmet Sarikanat, Hasan Yildiz, (2007) Static stability of laminated composite circular plates with holes using shear deformation theory, Finite Elements in Analysis and Design, Volume 43, Issues 11–12, August 2007, Pages 839–846

[2.71] B. Saboori, S.M.R. Khalili, (2011) Static analysis of tapered FRP transmission poles using finite element method, Finite Elements in Analysis and Design, Volume 47, Issue 3, March 2011, Pages 247–255

[2.72] Yin Fan, Hai Wang,(2016) Nonlinear bending and postbuckling analysis of matrix cracked hybrid laminated plates containing carbon nanotube reinforced composite layers in

thermal environments, Composites Part B: Engineering, Volume 86, 1 February 2016, Pages 1–16

[2.73] M.M. Alipour, (2016) An analytical approach for bending and stress analysis of cross/angle-ply laminated composite plates under arbitrary non-uniform loads and elastic foundations, Archives of Civil and Mechanical Engineering, Volume 16, Issue 2, February 2016, Pages 193–210

[2.74] M. Filippi, E. Carrera, (2016) Bending and vibrations analyses of laminated beams by using a zig-zag-layer-wise theory, Composites Part B: Engineering, Volume 98, 1 August 2016, Pages 269–280

[2.75] J.L. Mantari, F.G. Canales, (2016) A unified quasi-3D HSDT for the bending analysis of laminated beams, Aerospace Science and Technology, Volume 54, July 2016, Pages 267–275

[2.76] Wang, S., Dawe, D.J., (1997) Spline finite strip analysis of the buckling and vibration of composite prismatic plate, International Journal of Mechanical Sciences, Volume 39, Issue 10, October 1997, Pages 1161–1180

[2.77] Dawe, D.J., (2002) Use of the finite strip method in predicting the behaviour of composite laminated structures, Composite Structures 57, 11–36

[2.78] Wang S, Dawe DJ. (1999) Buckling of composite shell structures using the spline finite strip method. Compos Part B 1999;30B:351–64.

[2.79] Tan D, Dawe DJ. (1998) Buckling and vibration analysis of composite laminated plates and shells using general spline function. Compos Struct 1998;40:25–42.

[2.80] Dawe DJ, Tan D. (1999) Finite strip buckling and free vibration analysis of stepped rectangular composite laminated plates. Int J Numer Meth Engng 1999;46:1313–34.

[2.81] Dawe DJ, Wang S. (1998) Postbuckling analysis of thin rectangular laminated plates by spline FSM. Thin-Walled Struct 1998;30:159– 79.

[2.82] Wang S, Dawe DJ. (1999) Spline FSM postbuckling analysis of shear deformable rectangular laminates. Thin-Walled Struct 1999;34: 163–78.

[2.83] Dawe DJ, Wang S. (2000) Postbuckling analysis of composite laminated panels. AIAA J 2000;38:2160–70.

[2.84] Dawe DJ, Ge S. (2000) Thermal buckling of shear-deformable composite laminated plates by the spline finite strip method. Comput Meth Appl Mech Engng 2000;185:347–66. 312.

[2.85] Wang, S., Zhang, Y., (2004) Vibration analysis of rectangular composite laminated plates using layerwise B-spline finite strip method, Composite structures,;(68), 349-358

[2.86] Beena, K.P., Parvathy, U., (2014) Linear static analysis of Functionally Graded Plate using Spline Finite Strip Method, Composite Structures 117 (2014) 309–315

[2.87] Qingyuan Chen, Pizhong Qiao, (2014) Post-buckling analysis of composite plates under combined compression and shear loading using finite strip method, Finite Elements in Analysis and Design, Volume 83, June 2014, Pages 33–42

[2.88] R.M. Jones, (1999), Mechanics of composite materials, Second Edition, Taylor & Francis, 1999.

[2.89] J. Reddy, (2004), Mechanics of Laminated Composite Plates and Shells: Theory and Analysis, CRC Press, New York.

[2.90] H.A. Salim, J.F. Davalos, P. Qiao, S.A. Kiger, (1997), Analysis and design of fiber reinforced plastic composite deck-and-stringer bridges, Composite Structures, 38(1), (1997), 295-307.

[2.91] P. Qiao, Julio, F. Davalos, B. Brown, (2000) A systematic analysis and design approach for single-span FRP deck/stringer bridges, Composites: Part B 31, (2000), 593 - 609.

[2.92] Q.W. Zhang, T.Y.P. Chang, C.C. Chang, (2001) Finite-Element Model Updating For The Kap Shui Mun Cable-Stayed Bridge, Journal Of Bridge Engineering, 6(4), (2001), 285-293

[2.93] H. Almansour, M.S. Cheung, (2010) Structural performance of laminated FRP box girder bridge deck compared to slab on prestressed concrete girder bridge, The 8th Canada Japan Joint Workshop on Composites, Montreal, Canada, July 26-29, (2010), 1-32

[2.94] H.H. Almansour, M.S. Cheung, Ben Y.B. Chan, (2010), Analysis and design of hybrid long span cable-stayed bridges using multi-scale modeling techniques, Proceedings of the International Conference on Computing in Civil and Building Engineering, the University of Nottingham

[2.95] ALMANSOUR, H.H., CHEUNG, M.S., (2003), Finite element modeling of a CFRP composite deck for long span cable-stayed bridge. Proc. JCJC-III, Ueda, Nagano, Japan.

[2.96] H.H. Almansour, (2006), The performance of hybrid long-span cable-stayed bridges using advanced composites, department of civil and environmental engineering, the University of Ottawa

[2.97] M. Virlogeux, (1999), Recent evolution of cable-stayed bridges, Engineering Structures, 21(8) (1999), 737–755.

[2.98] R. Burgueno, V.M. Karbhari, F. Seible, R.T. Kolozes, Experimental dynamic characterization of an FRP composite bridge, superstructure assembly, Composite Structures, 54, (2001),427 - 444.

[2.99] Chao, Wang, (2015), "Damage modelling of FRP composite bridge decks", PhD thesis, department of civil and environmental engineering, Hong Kong University of Science and Technology

[2.100] Chan, Ben Y.B., Cheung, Moe M.S. Chao, Wang, (2013), Nonlinear dynamic analysis of fiber reinforced ultra-long span cable stayed bridges, Journal of Bridge Structures 9 (2013) 3–19

[2.101] Zhao Peng, Xie Ling-zhi, Moe MS Cheung (2015) Analysis and design procedure of hybrid long-span cable-stayed bridge using advanced composite material, Journal of Reinforced Plastics and Composites, 2015, 0(0) 1–24

[2.102] Ge, Y.J., Tanaka, H., (2000), Aerodynamic flutter analysis of cable-supported bridges by multi-mode and full-mode approaches, J. Wind Eng. Ind. Aerodyn: 86, 123–153.

[2.103] Ding, Q.S., Chen, A.R., Xiang, H.F., (2002), Coupled flutter analysis of long-span bridges by multimode and full order approaches, J Wind Eng Ind Aerodyn: 90, 1981–1993.

[2.104] Ming-Hui Huang, Yuh-Yi Lin and Ming-Xi Weng, (2012), Flutter and Buffeting Analysis of Bridges Subjected to Skew Wind, Journal of Applied Science and Engineering, Vol. 15, No. 4, pp. 401E413 (2012) 401

[2.105] S. Chad Gibbs, Ivan Wang, Earl Dowell, (2012), Theory and experiment for flutter of a rectangular plate with a fixed leading edge in three-dimensional axial flow, Journal of Fluids and Structures 34 (2012) 68–83

[2.106] Teng Wu, Ahsan Kareem, Yaojun Ge, (2013), Linear and nonlinear aeroelastic analysis frameworks for cable-supported bridges, Nonlinear Dynamics, November 2013, Volume 74, Issue 3, pp 487–516

[2.107] E.S. Kreis and J.C. Andr´e, (2005), A numerical inquiry into the flutter phenomenon in long-span bridges, Latin American Journal of Solids and Structures 2 (2005) 321–337

[2.108] Masaru Matsumoto, Hisato Matsumiya, Shinya Fujiwara, Yasuaki Ito, (2008) New Consideration on Flutter Properties basing on SBS -Fundamental Flutter Mode, Similar Selberg's Formula, Torsional Divergence Instability, and New Coupled Flutter Phenomena affected by Structural Coupling, BBAA VI International Colloquium on: Bluff Bodies Aerodynamics & Applications Milano, Italy, July, 20-24 2008

[2.109] Duc-Huynh Phan, Ngoc-Trung Nguyen, (2013), Flutter and Buffeting Control of Long-span Suspension Bridge by Passive Flaps: Experiment and Numerical Simulation, Int'l J. of Aeronautical & Space Sci. 14(1), 46–57 (2013) DOI:10.5139/IJASS.2013.14.1.46

[2.110] Thomas Canor, Luca Caracoglia, Vincent Denoël, (2015), Application of random eigenvalue analysis to assess bridge flutter probability, Journal of Wind Engineering and Industrial Aerodynamics, Volume 140, May 2015, Pages 79–86

[2.111] Gui-hua Xie, Jie Yin, Rong-gui Liu, Bei Chen, Dong-sheng Cai, (2017), Experimental and numerical investigation on the static and dynamic behaviors of cable-stayed bridges with CFRP cables, Composites Part B: Engineering, Volume 111, 15 February 2017, Pages 235-242

[2.112] Yongxin Yang, Rui Zhou, Yaojun Ge, Xiaojie Zou, Lihai Zhang, (2017), Flutter characteristics of twin-box girder bridges with vertical central stabilizers, Engineering Structures, Volume 133, 15 February 2017, Pages 33-48

[2.113] N Lee, H Lee, C Baek, S Lee, (2016) Aeroelastic analysis of bridge deck flutter with modified implicit coupling method, Journal of Wind Engineering and Industrial Aerodynamics, Volume 155, August 2016, Pages 11–22

[2.114] Lau, D. T., Cheung, M. S., and Cheng, S. H., (2000) "3D flutter analysis of bridges by spline finite strip method." J. Struct. Eng., 10.1061/(ASCE)0733-9445(2000)126:10(1246), 1246–1254.

Chapter 3

Integrated finite strip analysis for long-span cable-stayed bridges*

* This chapter has been published in the journal of Computers and Structures as " Naderian, Hamidreza., Cheung, Moe M. S., Shen, Zhenyuan., Dragomirescu, Elena., (2015) Integrated Finite Strip Analysis of long-span cable-stayed bridges, Computers and Structures 158 (2015) 82–97"

Abstract_ An integrated finite strip discretization scheme is proposed for modeling long-span cable-stayed bridges. So-called column strips and cable strips model the towers and cables respectively. Also, the structural interactions between different components can be considered in the analysis by defining so-called transition sections. The static and free vibration analyses are performed for Kap Shui Mun Bridge by the integrated finite strip method. The numerical results are verified against other methods. The proposed solution proves to be very efficient in yielding accurate results, in a minimum amount of time while the convergence of the method is still very high.

Keywords: Long-span bridge; cable-stayed bridge; integrated finite strip method; column strip; cable strip; Kap Shui Mun bridge

3.1 Introduction

Bridges play an indispensable role in infrastructure systems. There are many large cities around the world located near wide lakes and rivers where, in order to facilitate the transportation, there is a certain need to build long-span bridges. With the rapid development of the transportation technology, longer span bridges are constructed nowadays.

In general, there are two types of long-span bridges, namely suspension bridges and cable-stayed bridges. The later one has attracted more attention from the bridge engineers and manufactures. The cantilever-based construction allows them to be constructed from the inside out. In contrast with suspension bridges, multiple towers can be easily used to extend the length of the cable-stayed bridges when practical. In recent years, the design of cable-stayed bridges dominates most of the major bridge projects. However, there are other factors including engineering data and cost restrictions that affect the decision of engineers and designers to select between suspension and cable-stayed bridges. Besides all the advantages of cable-stayed bridges, it is noticeable that suspension bridges can generally have longer spans. Russky Bridge recently constructed in Russia has the longest span of 1104 m among cable-stayed bridges while Akashi Bridge located in Japan has the main span of 1991 m and is the longest between suspension bridges since 1998.

There are typically five methods for analyzing the bridges which are widely used and recognized by bridge design codes [3.1]. They are grillage energy methods, orthotropic plate theory methods, folded plate methods, finite element methods, and finite strip methods. Most of the bridge structural investigations are performed with the well-known finite element method [3.2-3.6]. Nevertheless, various other methods such as finite strip [3.7] and boundary element [3.8] methods play an important role on their specialized areas.

In the case of long-span bridges with thousands of degrees of freedom and in the same time with high nonlinearity behavior under dynamic and aerodynamic forces, the finite element analysis seems to become inefficient. In the finite element method, one requires to discretize the problem in every dimension. It will consequently require more unknowns and degrees of freedom for solving the problem than other numerical methods. With the use of super-computers, millions of unknowns can be handled in the finite element environment. Although the cost of such kind of computations has decreased, there is still a need to use more efficient tools, in particular, for certain structures of massive dimensions. Besides, the

computation costs usually multiply by order of magnitude when a more refined or a higher dimensional analysis is needed. Moreover, for many problems with regular geometric shape and simple boundary conditions the use of finite element method is not only unnecessary but also extravagant. In order to reduce the computational costs and core requirements, alternative methods are therefore evidently desirable.

The finite strip method (FSM) is one of the most efficient numerical methods for structural analysis of bridges, reducing the time required for performing the structural analysis, without affecting the results accuracy. In the FSM, the structure is subdivided into a number of longitudinal strips, whose displacement field is defined by simple polynomials in the transverse direction, and continuous harmonic functions in the longitudinal direction. As a result, the degrees of freedom significantly reduce due to the semi-analytical nature. The philosophy of the finite strip method is similar to Kantorovich method, which is used for the purpose of reducing the partial differential equations to a lower order or ordinary equations. In the finite strip method, the order reduction from a three-dimensional (3D) to a two-dimensional (2D) problem is achieved either by using the separation of variable approach or by the transformation approach.

The finite strip method (FSM) was created by Y. K. Cheung [3.9] in order to analyze the elastic plates with simply supported end conditions. The original idea for the FSM was to reduce the dimensions of a long span structure via the implementation of an analytical solution along the longitudinal direction. Powell et. al [3.10] further developed the finite strip method for modeling the rectangular slab bridges. Afterwards, the FSM methodology has been proposed for a variety of structures including plates, shells, laminated plates, bridges, tall buildings, etc [3.7, 3.1].

The nature of the finite strip concept is such that it deals well with the problems in which the structure has a known harmonic response under the applied loading. Among such kinds of problems, one can mention buckling and vibration of plates, plate-structures, and bridge structures. The classical finite strip method has some limitations. For instance, it can deal only with problems of simply supported end conditions, and it cannot handle shear forces and internal supports in the analysis.

In order to overcome the shortcomings of the conventional finite strip method with boundary conditions, concentrated loads, and continuous spans, spline finite strip method (SFSM) was

created by Cheung et al [3.11]. The spline finite strip method can be considered as a special form of the finite element method and in the same time represents an evolved version of the finite strip method. In addition to nearly as versatile as the standard finite element method, SFSM can achieve higher order continuity with the smaller number of degrees of freedom. In this technique, the displacement functions in the longitudinal directions are B3-splines, at the expense of more degrees of freedom in comparison with the conventional finite strip method. Among the characteristics of SFSM, one can mention dealing well with multi-span or column-supported structures.

The spline FSM has been successfully applied to the analyses of numerous types of structural problems such as box girder bridges, circular plates, skew plates and the plates of arbitrary shape [3.1, 3.7]. Chen et al. [3.12, 3.13] introduced the unequally spaced B3-spline functions in the analysis of stiffened plates and folded plate structures with intermediate supports. The method allows one to describe the accurate response in the region of high stress gradients, or at the locations of abrupt geometric changes, by spacing the knots more closely along the strips. Dawe [3.14] carried out an extensive research on the use of both conventional and spline finite strip methods in determining natural frequencies of single span and multi-span structures. The field of finite strip analysis in bridge engineering has been applied to bridges with different geometric and boundary conditions, such as hunched continues slab and box girder bridges [3.1, 3.15]. Static analysis of right box girder bridges with various types of end and interior supports by spline finite strip method were first carried out by Cheung et. al [3.16]. Afterwards, SFSM was extended to different applications in bridge structures like analyzing the hunched, continuous slab and box-girder bridges [3.17, 3.18], analysis of prestressed concrete box-girder bridges [3.19], and fatigue and fracture analyses [3.20].

The main disadvantage of the spline finite strip method in cable-stayed bridge analysis is that, until present, it could only model the deck while the towers and the cables are normally replaced by certain assumed boundary conditions applied to the deck strip model. This assumption is reasonable only when the stress distribution along the girders and slab of the bridge super-structure is required. Therefore, It will reduce the accuracy of the FSM in bridge analysis. Due to modeling by a continuously differentiable smooth series in the longitudinal direction in the finite strip analysis, difficulties are encountered in combining

different types of structural components in different directions. This is the reason why the analytical model developed using the finite strip method is still limited to bridge super-structure without piers and cables.

Cheung et al. [3.21, 3.22] has recently introduced an integrated finite strip method for analyzing multi-span, continuous slab-on- girder and box girder bridges, by modeling the bridge deck, the piers and the bearings together so that the interactions between piers and deck can be considered in the analysis. The objective of the current research is extending the integrated finite strip solution, based on the use of unequally spaced B3-spline functions, to analysis of long-span cable-stayed bridges by introducing different types of strips for modeling the cables and towers. The shell spline finite strip is proposed for modeling the deck. The Column Strip (CS) is developed to model the cantilever-behaved piers and towers as strip elements. A one dimensional spline strip is also proposed for modeling the cables. In addition, a special transition section is developed to combine the deck, piers, towers, and cables in the finite strip environment, and the bearings are modeled as special boundary conditions for the transition section.

By representing the entire cable-stayed bridge as a single integrated system the actual static and dynamic behavior of the bridge can be studied. Also, a great advantage is that the interactions between different structural components can be considered in the analysis, through the newly defined transition sections. Furthermore, the stresses and the displacements at not only the deck but also at other parts of the bridge, including piers and towers as well as cables can be calculated.

This paper is organized as follows. The development of the integrated finite strip method for modeling a long-span cable-stayed bridge is presented in section 3.2. The proposed solution is programmed on a desktop workstation and is used to study the static and free vibration analyses of Kap Shui Mun Bridge, an existent long-span cable-stayed bridge in Hong Kong. The displacements of the Kap Shui Mun Bridge under combination of various static loads are calculated and presented in section 3. In addition, the stiffness and the mass matrices derived from the integrated finite strip method can be used for free vibration analysis of long-span cable-stayed bridges. The natural frequencies of Kap Shui Mun Bridge for different modes are obtained through the eigenvalue analysis. Finally, the accuracy and

efficiency of the integrated finite strip program is verified against the finite element and field measurement results.

The results will demonstrate that the proposed framework and the associated computer program can efficiently predict the displacements and natural frequencies of long-span cable-stayed bridge systems. The simplicity of the input data, high convergence, and less degrees of freedoms are among the factors that make the proposed integrated finite strip method (IFSM) an efficient solution for analyzing long-span cable-stayed bridges.

3.2 Finite strip bridge model

The displacement of a strip in the integrated finite strip method is obtained by applying B3-spline functions in the longitudinal direction. For the transverse direction the idea is originated from the finite element method in which the cubic polynomials are used to represent the transverse shape function of the strip. This is exactly the same as spline finite strip method.

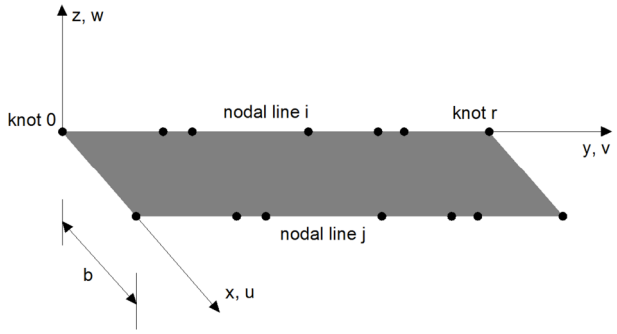

Fig. 3.1 Shell spline finite strip for deck modeling

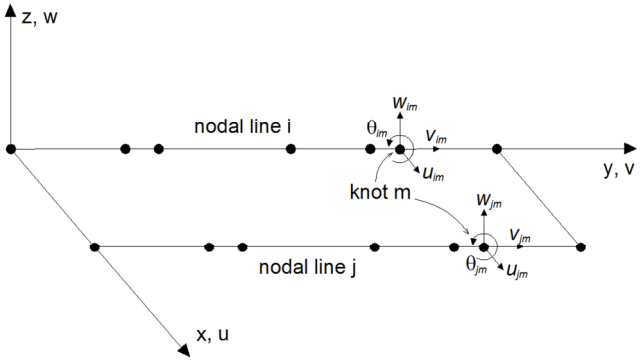

Fig. 3.2 Degrees of freedoms of on a knot

3.2.1 Bridge deck modeling

The bridge decks are mainly constructed by box girders or slab-girders that are considered in the category of plate and shell structures. As a result, the derivation of the stiffness and mass matrices of shells and plates can be generalized for bridge decks. The shell spline strip as shown in Fig. 3.1 is used for the deck modeling in which both in-plane and out-of-plane degrees of freedom are considered.

In analysis of flat shells, one can consider four degrees of freedom on each knot of a nodal line of a strip, three translational and one rotation as shown in Fig. 3.2. The total potential energy of a flat shell strip may be obtained from the algebraic summation of the membrane (in-plane) and bending (out-of-plane) deformations.

The displacement parameters vector of a shell spline strip centered at y_m is given by

$$\{\delta\}_m = \left[u_{im}, v_{im}, w_{im}, \theta_{im}, u_{jm}, v_{jm}, w_{jm}, \theta_{jm} \right]^T \tag{3-1}$$

The integrated finite strip method is based on the use of unequally spaced B3-spline functions. Actually, the concept of the transition section is originated from using unequal spaced functions in the displacement function of a strip. Moreover, in the formulation of the integrated and spline finite strip methods, it is better to have the locations of the supports and the concentrated load coinciding with the knots on the nodal lines, in order to obtain satisfactory results. The introduction of unequally spaced interior knots allows one to describe the accurate response in the region of high stress gradients, or at the locations of abrupt geometric changes, by spacing the knots more closely. In this case, the spline function centered at y_m can be expressed as

$$\Phi_m(y) = \begin{cases} 0 & y < y_{m-2} \\ A_m(y - y_{m-2})^3 & y_{m-2} \le y < y_{m-1} \\ A_m(y - y_{m-2})^3 + C_m(y - y_{m-1})^3 & y_{m-1} \le y < y_m \\ B_m(y_{m+2} - y)^3 + D_m(y_{m+1} - y)^3 & y_m \le y < y_{m+1} \\ B_m(y_{m+2} - y)^3 & y_{m+1} \le y < y_{m+2} \\ 0 & y_{m+2} \le y \end{cases} \tag{3-2}$$

in which

$$
\begin{aligned}
A_m &= \left[(y_{m+1} - y_{m-2})(y_m - y_{m-2})(y_{m-1} - y_{m-2}) \right]^{-1} \\
B_m &= \left[(y_{m+2} - y_{m-1})(y_{m+2} - y_m)(y_{m+2} - y_{m+1}) \right]^{-1} \\
C_m &= -(y_{m+2} - y_{m-2}) \left[(y_{m+2} - y_{m-1})(y_{m+1} - y_{m-1})(y_m - y_{m-1})(y_{m-1} - y_{m-2}) \right]^{-1} \\
D_m &= -(y_{m+2} - y_{m-2}) \left[(y_{m+1} - y_{m-2})(y_{m+1} - y_{m-1})(y_{m+1} - y_m)(y_{m+2} - y_{m+1}) \right]^{-1}
\end{aligned}
\tag{3-3}
$$

For the flat shell spline finite strip, the membrane displacement functions *u* and *v*, and the flexural displacement function *w* are expressed as the product of the transverse polynomials and longitudinal B3-splines as following

$$u = \sum_{m=-1}^{r+1} (N_1 \Phi_{1m}(y) u_{im} + N_2 \Phi_{5m}(y) u_{jm}) \tag{3-4}$$

$$v = \sum_{m=-1}^{r+1} (N_1 \Phi_{2m}(y) v_{im} + N_2 \Phi_{6m}(y) v_{jm}) \tag{3-5}$$

$$w = \sum_{m=-1}^{r+1} (N_3 \Phi_{3m}(y) w_{im} + N_4 \Phi_{4m}(y) \theta_{im} + N_5 \Phi_{7m}(y) w_{jm} + N_6 \Phi_{8m}(y) \theta_{jm}) \tag{3-6}$$

where r is the total number of longitudinal sections on a nodal line. In the matrix form Eqs. (3-4) to (3-6) can be rewritten as

$$
\{f\} = \begin{Bmatrix} u \\ v \\ w \end{Bmatrix} = \begin{bmatrix} N_1 & 0 & 0 & 0 & N_2 & 0 & 0 & 0 \\ 0 & N_1 & 0 & 0 & 0 & N_2 & 0 & 0 \\ 0 & 0 & N_3 & N_4 & 0 & 0 & N_5 & N_6 \end{bmatrix}
\begin{bmatrix}
[\Phi_{1m}] & & & & & & & \\
& [\Phi_{2m}] & & & & & & \\
& & [\Phi_{3m}] & & & & & \\
& & & [\Phi_{4m}] & & & & \\
& & & & [\Phi_{5m}] & & & \\
& & & & & [\Phi_{6m}] & & \\
& & & & & & [\Phi_{7m}] & \\
& & & & & & & [\Phi_{8m}]
\end{bmatrix}
\begin{Bmatrix} u_{im} \\ v_{im} \\ w_{im} \\ \theta_{im} \\ u_{jm} \\ v_{jm} \\ w_{jm} \\ \theta_{jm} \end{Bmatrix}
\tag{3-7}
$$

in which

$$N_1 = 1 - X$$

$$N_2 = X$$

$$N_3 = 1 - 3X^2 + 2X^3$$

$$N_4 = x(1 - 2X + X^2)$$

$$N_5 = (3X^2 - 2X^3)$$

$$N_6 = x(X^2 - X) \tag{3-8}$$

where $X = x/b$. $[\Phi_{1m}]$ to $[\Phi_{8m}]$are row matrices where each matrix has (m+3) local B3-splines. .$[\Phi_{1m}]$, $[\Phi_{2m}]$, $[\Phi_{5m}]$ and $[\Phi_{6m}]$are related to the displacements *u* and *v* of nodal lines *i* and *j* respectively, while $[\Phi_{3m}]$, $[\Phi_{4m}]$, $[\Phi_{7m}]$ and $[\Phi_{8m}]$ are related to the displacement *w*. Each longitudinal shape function has the following form

$$[\Phi] = \begin{bmatrix} \bar{\Phi}_{-1} & \bar{\Phi}_0 & \bar{\Phi}_1 & \Phi_2 & \ldots & \Phi_{m-2} & \bar{\Phi}_{m-1} & \bar{\Phi}_m & \bar{\Phi}_{m+1} \end{bmatrix} \tag{3-9}$$

where $\bar{\Phi}_i$ is an amended boundary local spline with regard to the end boundary conditions of the strip. In the short form, Eq. (3-7) is expressed as

$$\{f\} = [N][\Phi]\{\delta\} \tag{3-10}$$

3.2.2 Column strips for modeling piers and towers

The so-called Column Strip is proposed for modeling the cantilever-behaved piers and towers. The Column Strip (CS) is exactly similar to the flat shell spline finite strip, which was formerly proposed for deck modeling. However, CS is a vertical strip fixed at one end, for providing the support boundary conditions, and free at the other end, as shown in Fig. 3.3.

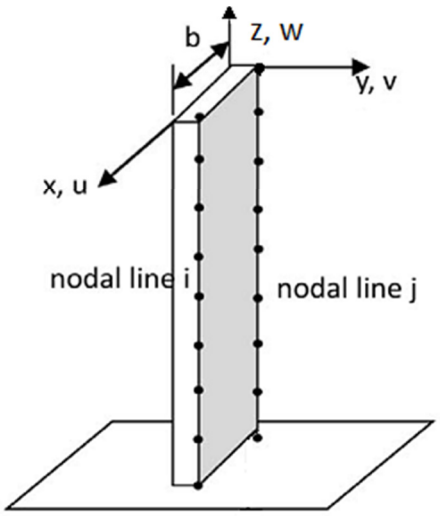

Fig. 3.3 Column Strip in local coordinate system (CS)

In fact, the global z direction of the column strip is similar to the local y direction in the flat shell spline finite strip, while the global v direction of the column strip is similar to local z direction of the shell spline finite strip. Therefore, the displacement function of CS is represented as

$$u = \sum_{m=-1}^{r+1} (N_1 \Phi_{1m}(z) u_{im} + N_2 \Phi_{5m}(z) u_{jm}) \tag{3-11}$$

$$v = \sum_{m=-1}^{r+1} (N_3 \Phi_{2m}(z) v_{im} + N_4 \Phi_{4m}(z) \theta_{im} + N_5 \Phi_{6m}(z) v_{jm} + N_6 \Phi_{8m}(z) \theta_{jm}) \tag{3-12}$$

$$w = \sum_{m=-1}^{r+1} (N_1 \Phi_{3m}(z) w_{im} + N_2 \Phi_{7m}(z) w_{jm}) \tag{3-13}$$

In a parametric study carried out by Cheung et al. [3.21], it has been demonstrated that CS can perfectly model almost all types of pier structures with different loading conditions. They compared the results obtained by both finite strip and finite element methods for top deflection of the piers in which the absolute differences were less than 2% for all trials.

Similar to the flat shell spline finite strip which is capable of modeling the box girder decks, the box section piers and towers can also be constructed by using column strips. In some cases, like the current case study, it is more convenient and efficient to use one-dimensional strips for modeling the piers and towers. This type of column strip has only one nodal line and is somehow similar to the beam element employed in finite element method. In order to achieve the compatibility with other strips in the bridge structure, B3-splines are also used in the displacement function of the one-dimensional column strip. However, each knot on the nodal line only has only three translational degrees of freedom. Consequently, the displacement function can be defined as

$$u = \sum_{m=-1}^{r+1} u_m \Phi_m(z) \tag{3-14}$$

$$v = \sum_{m=-1}^{r+1} v_m \Phi_m(z) \tag{3-15}$$

$$w = \sum_{m=-1}^{r+1} w_m \Phi_m(z) \tag{3-16}$$

In terms of displacement-strain relationships, the bending in the vertical and transverse directions and the axial stress are considered. Accordingly, the strain-displacement relationships are described as

$$\varepsilon = \frac{\partial w}{\partial z} \quad , \kappa_1 = -\frac{\partial^2 v}{\partial x^2} \quad , \kappa_2 = -\frac{\partial^2 v}{\partial z^2} \tag{3-17}$$

3.2.3 Cable strip model

In long-span cable-stayed and suspension bridges the cables are used which play an important role on the stability of the structure and in transferring the loading from the deck to the towers. In order to model the cables in the finite strip environment, the cable strip is developed, which is in fact a simplified version of the one-dimensional column strip.

In general, a cable can only resist against the axial tension stresses, while the other stresses including shear force, and bending and torsional moments are not taken into account in the analysis. Therefore, only the first term in Eq. (3-17) defines the strain-displacement relationship for a cable strip. It is worth to mention that the cables mostly have the geometric

nonlinear behavior due to the sag. There are different ways to consider the nonlinearity of the cables like adopting the equivalent modulus of elasticity for the linear cable stiffness but these are not discussed here.

3.2.4 Transition Section

The concept of the transition section comes from the finite element method and it can be used for assembling different structural components of a complicated structure, like a long-span cable-stayed bridge. In the past studies of bridge analysis by the finite strip method, the bridge model contained only the super-structure, while the effect of the sub-structures on the bridge is considered by other methods.

The transition section is developed based on unequal spaced B3-spline function and can be used to connect the strips located at different positions. Moreover, the bearings can be modeled as special boundary conditions for the transition section. A typical transition section connecting two different components is shown in Fig. 3.4. The width of the normal and the transitions sections are *H* and *h* respectively. One can call the vertical line as a nodal line on the pier strip and the horizontal line as a nodal line on the deck strip. The vertical and horizontal lines are crossed at points 3 and 8 of the deck and the pier strips. To model as a hinged bearing, which allows rotations but restricts translations, the knot 3 and knot 8 should have the same displacement value to achieve compatibility. Using the displacement functions defined in the previous sections, the displacements of knots 3 and 8 can be obtained. It should be noted that at these points only three spline functions have non-zero values.

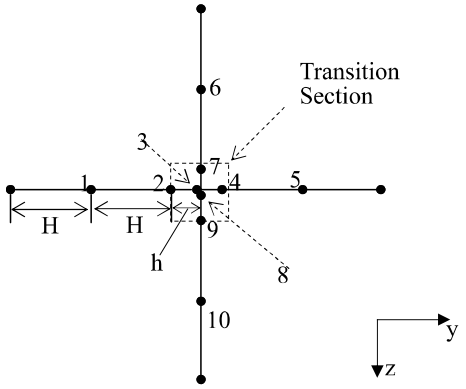

Fig. 3.4 Transition section

Consequently, three spline functions contribute in the displacement functions of knots 3 and 8 as given below

$$\{\Delta_3\} = \Phi_2(y_3)\{\delta_2\} + \Phi_3(y_3)\{\delta_3\} + \Phi_4(y_3)\{\delta_4\} \tag{3-18}$$

$$\{\Delta_8\} = \Phi_7(z_8)\{\delta_7\} + \Phi_8(z_8)\{\delta_8\} + \Phi_9(z_8)\{\delta_9\} \tag{3-19}$$

in which $\{\Delta_i\}$ and $\{\delta_i\}$ are the displacement vector and the displacement parameter vector of knot *i,* respectively while $\Phi_i(y_j)$ is the B3-spline function of knot *i* at knot *j.* The values of the spline functions can be easily obtained through Eqs. (3-2) and (3-3) as below

$$\Phi_2(y_3) = \Phi_4(y_3) = \Phi_7(y_8) = \Phi_9(y_8) = \frac{h}{2(2h+H)} \tag{3-20}$$

$$\Phi_3(y_3) = \Phi_8(y_8) = 1 - \frac{h}{(2h+H)} \tag{3-21}$$

According to the structural continuity condition, one can assume the following expressions

$$\begin{aligned} &\left|\{\delta_2\} - \{\delta_3\}\right| \le x \\ &\left|\{\delta_4\} - \{\delta_3\}\right| \le x \\ &\left|\{\delta_7\} - \{\delta_8\}\right| \le x \\ &\left|\{\delta_9\} - \{\delta_8\}\right| \le x \end{aligned} \tag{3-22}$$

where *x* is a positive real number with finite magnitude. If the translational displacement parameters vectors knots 3 and 8 are constrained, then

$$\{\delta_3\} = \{\delta_8\} \tag{3-23}$$

Therefore,

$$|\{\Delta_3\} - \{\Delta_8\}| = |(\Phi_2(y_3)\{\delta_2\} + \Phi_3(y_3)\{\delta_3\} + \Phi_4(y_3)\{\delta_4\}) - (\Phi_7(z_8)\{\delta_7\} + \Phi_8(z_8)\{\delta_8\} + \Phi_9(z_8)\{\delta_9\}|$$

$$= \frac{h}{2(2h+H)}\left|\{\delta_2\} + \{\delta_4\} - \{\delta_7\} - \{\delta_8\}\right| \tag{3-24}$$

From Eq. (3-22), it can be concluded that

$$\left|\{\Delta_3\}-\{\Delta_8\}\right| \le \frac{h}{2(2h+H)}4x = \frac{2xh}{(2h+H)} = \frac{2x(h/H)}{2(h/H)+1} \tag{3-25}$$

In order to have identical displacement at knots 3 and 8, it is obvious that the ratio of h/H should be infinitely small or mathematically

$$\lim_{h/H\to 0}\left|\{\Delta_3\}-\{\Delta_8\}\right| = 0 \tag{3-26}$$

Depending on the complexity of the structure, different values of *h* can meet the required accuracy. Numerical studies show that under normal circumstances with the ratio of *h/H*=0.001 a tolerance error smaller than 0.5% is achieved, which is acceptable for engineering analysis. Using the developed transition section in the spline finite strip procedure the compatibility for the displacements of different components of the structure is satisfied.

3.2.5 Boundary conditions

Due to the localization of B3-spline functions, only a few boundary local splines at each end have to be amended in order to apply the end boundary conditions. There are different methods for modifying the local B3-splines in order to satisfy the end and interior conditions. It should be noted that the elimination of a local spline means that a zero value is imposed on the displacement parameter vector for each restrained degree of freedom. In addition, the interior boundary conditions like point supports along the length of a member can be modeled [3.13]. In one technique, the degrees of freedom are restrained by the appropriate stiff springs [3.1]. A fictitious spring with a sufficiently large penalty parameter is introduced at the point.

After defining the displacement functions of all structural components of the long-span cable-stayed bridge in the environment of finite strip method, the stiffness and mass matrices as well as external load vectors of different components can be obtained using the

standard finite element procedure. The derived stiffness and mass matrices are assembled and make the global stiffness $[K]$ and mass $[M]$ matrices of the bridge.

3.2.6 Free vibration analysis

In order to evaluate the natural frequencies of the bridge, the free vibration analysis needs to be performed. According to the structural dynamics theory, the overall matrix equation for a bridge structure in free vibration at any instant of time is defined by

$$[K]\{\delta(t)\}+[M]\{\ddot{\delta}(t)\}=0 \tag{3.27}$$

in which $\delta(t)$ is the displacement vector of the entire bridge and is a function of time. It is assumed that the bridge structure has a sinusoidal vibration given by

$$\{\delta(t)\}=\{\delta\}\sin\omega t \tag{3.28}$$

where ω is defined as the natural frequency. Substituting Eqs.(3-28) into Eq. (3-27), the following equation is obtained

$$\left[[K]-\omega^2[M]\right]\{\delta\}=0 \tag{3-30}$$

Eq. (3-30) is a generalized eigenvalue problem in which the natural frequency ω and the displacement vector $\{\delta\}$ are referred to as eigenvalue and eigenvector respectively. Also, both $[K]$ and $[M]$ are symmetrical and positive definite matrices. The natural frequencies of the bridge structure and the corresponding mode shapes $\{\delta\}$ can be easily obtained by solving the eigenvalue problem of Eq. (3-30).

3.3 Finite strip analysis of Kap Shui Mun Bridge

The Kap Shui Mun Bridge, shown in Fig. 3.5, which is selected in this study, is a massive and complex double-deck long-span cable-stayed bridge structure is selected to study. The upper deck is targeted for highway traffic and the lower deck is mostly for railway traffic besides emergency lanes for vehicles. This bridge is located between the islands of Lantau

and Ma Wan in Hong Kong and is the world's longest cable-stayed bridge in terms of carrying both road and railway traffics. The bridge structure includes two concrete towers, four concrete piers, 176 cables, bearings, as well as a middle span deck of 430 m and 160 m side spans. Most of the main span, 387 m, is made of steel/concrete composite construction including steel frames and webs and concrete slabs. The rest of the main span and both side spans are constructed by prestressed concrete box girders. Four piers and two towers including Lantau and Ma Wan towers support the bridge deck in the vertical direction. Along the longitudinal direction, the deck is only fixed at the cross beam of the left tower while, it is unrestrained at the other supports. Along the transverse direction, the deck is fixed at all towers and piers. The bridge model has been simplified with a number of assumptions which will be explained in the following.

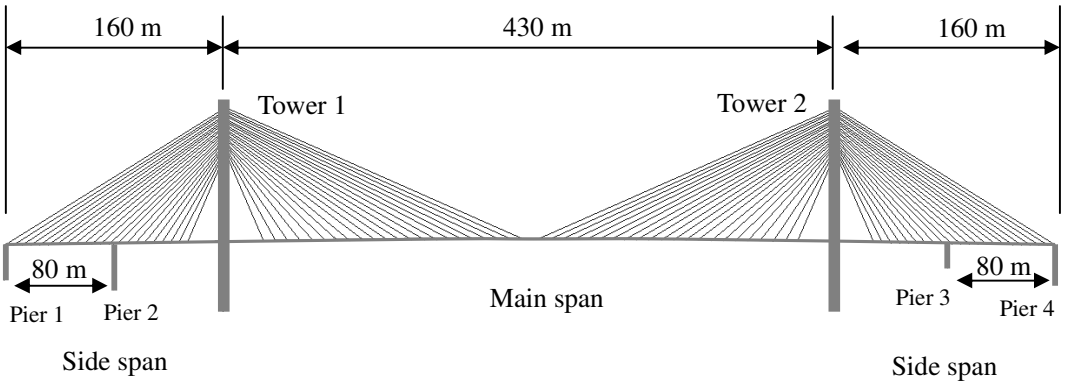

Fig. 3.5 Kap Shui Mun Bridge

3.3.1 Deck modeling

The deck of Kap Shui Mun Bridge consists of one main span and two side spans. The real cross section of the deck is shown in Fig. 3.6. The main span is made of a composite steel/concrete structure mainly. The side spans are made of concrete box-girders.

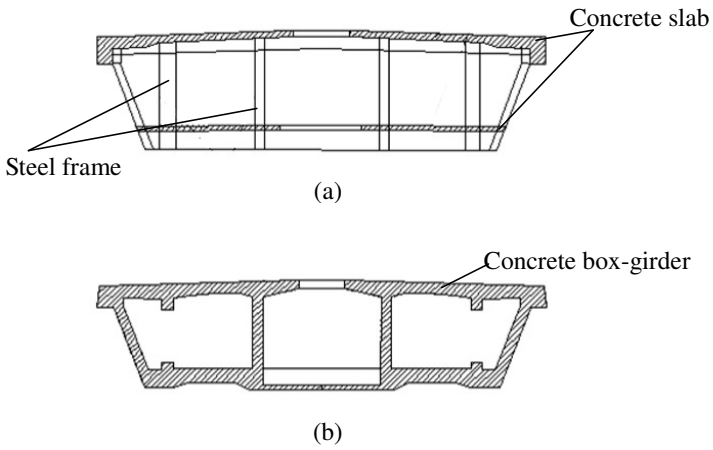

Fig. 3.6 Cross-section of the bridge deck [3.23] (a) main span; (b) side spans

Here, the deck is modeled as the flat shell in the integrated finite strip environment. The material properties calculated by Chang et al. [3.23] are shown in Table 3.1, and the geometrical properties are illustrated in Fig. 3.7. The deck is divided into four shell spline strips, and all the strips are divided into 292 sections so that the intersection points between deck with piers, towers, and cables can be modeled by transition section. The lengths of the sections vary along the deck so that the locations of the knots could match the ends of cables.

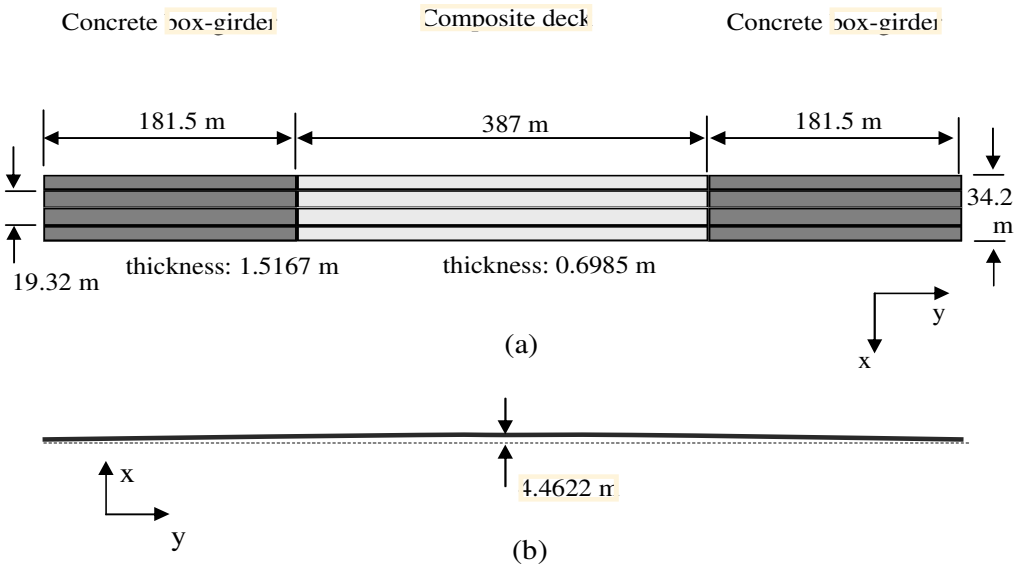

Fig. 3.7 Geometrical properties of the deck: (a) top view; (b) front view

Table 3.1 Material properties of deck [3.23]

Mechanical properties	Main span	Side spans
Modulus of elasticity (KPa)	2.00×10^{8}	3.00×10^{7}
Mass density (kg/m^{3})	3880	3630
Poisson's ratio	0.3	0.2
Moment of inertia (vertical) (m^{4})	191	363
Moment of inertia (transverse) (m^{4})	2530	5560

3.3.2 Towers and piers modeling

The strip meshing of the towers is shown in Fig. 3.8. The two H-shape concrete towers are placed on bedrock with a height of 150 m above the water level. As illustrated in Fig. 3.8, each tower consists of 2 shafts and 3 cross beams. The material properties of the concrete used for the towers and piers are $E = 3.5 \times 10^{7}\ KPa$ and $\upsilon = 0.2$, where E and υ are the modulus of elasticity and Poisson ratio respectively. The one-dimensional Column Strip introduced in the previous section is adopted for the tower structures in the finite strip model. In each tower, there are three struts linking the upper, intermediate and lower parts of the towers, respectively. The link beams are rigid and all six degrees of freedom of the joints should be restrained. However, in one dimensional column strip each knot has only three translational degrees of freedom and the rotational degrees of freedom are not taken into account. The four piers of the bridge are also modeled by one dimensional column strips in the finite strip model. The boundary conditions of towers and piers are all fixed at the ground.

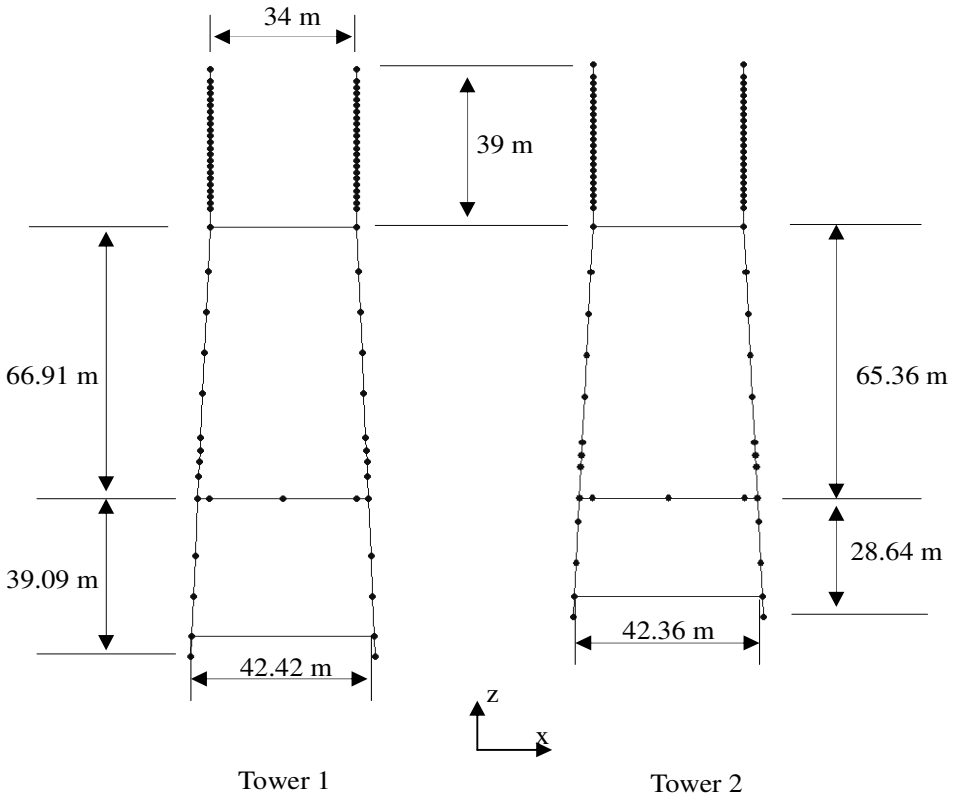

Fig. 3.8 Towers of the Kap Shui Mun Bridge

3.3.3 Cables modeling

The 176 cables are assumed to be linear elastic elements and are modeled by Cable Strip in the finite strip model. The material properties of the steel used for the cables are $E = 2.0 \times 10^8\ KPa$ and $\upsilon = 0.3$ in which E and υ are modulus of elasticity and Poisson ratio respectively. It should be noted that all the cables are prestressed which means that the thermal loads are converted to equivalent tension forces at the two ends of the strips. The initial prestress forces of the cables are listed in Appendix A.

3.3.4 Static analysis of Kap Shui Mun Bridge

Using the integrated finite strip method, the Kap Shui Mun Bridge has been modeled based on the assumptions introduced for the geometric and material properties. The complete

three-dimensional model is illustrated in Fig. 3.9. Several points in the long-span cable-stayed bridge are selected in Figs. 3.10 and the displacements corresponding to these points under static loads are calculated using both integrated finite strip and finite element methods. In the finite element model, the deck is modeled by thin shell elements while piers and towers are modeled as beam elements and cables are assigned truss elements.

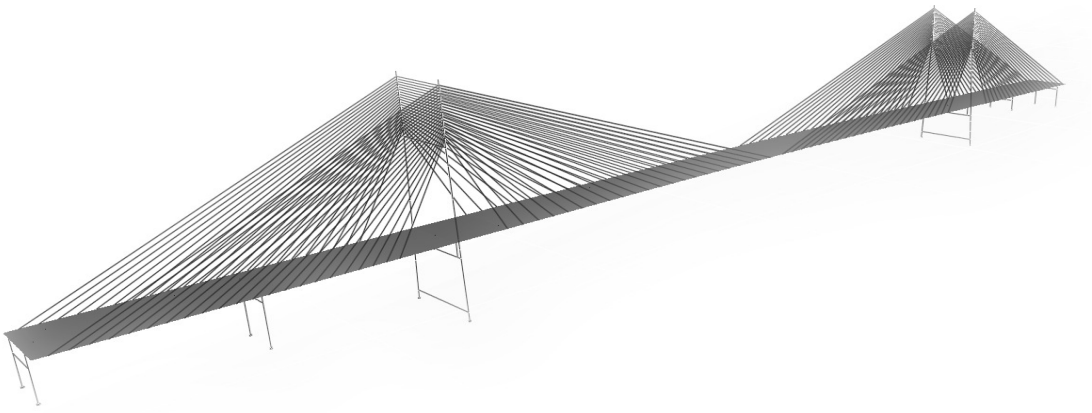

Fig. 3.9 Three-dimensional model of the Kap Shui Mun Bridge

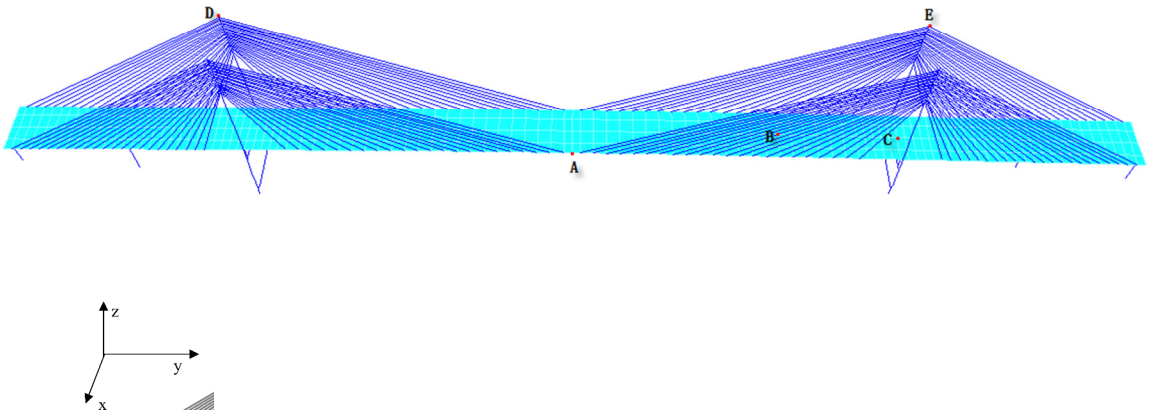

Fig. 3.10 Critical locations

The accuracy of the integrated finite strip model under static loads and the interactions between different bridge components are estimated. The external loads, such as wind load and vehicle load are mainly acting on the bridge deck, while some are acting on the sub-structure such as seismic load. For the same reason, two groups of external loads assigned to

the deck and towers are considered in the present study. The concentrated loads assigned to the bridge were Fe and Fd applied at the top of the towers in

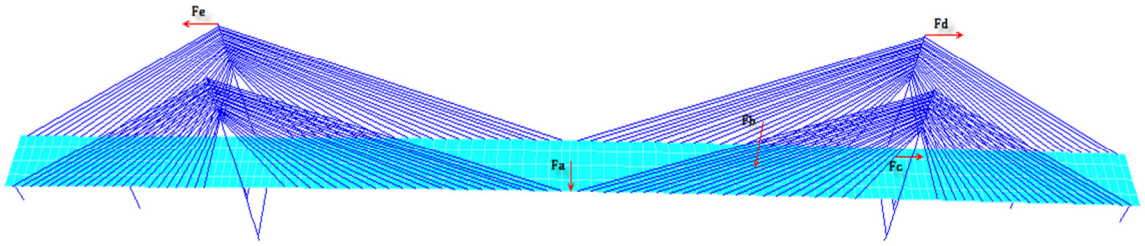

Fig. 3.11 Applied concentrated loads

opposite horizontal directions, Fa is a horizontal force applied at the middle of the main span towards the margin of the deck, Fb is applied downwards on vertical direction at the middle of the main span and at the middle point of the right half of the main span and Fc acting horizontally on the deck and on a section towards the right tower as shown in Fig. 3.11. The magnitude of the concentrated loads is assumed to be constant at 15,000 KN. The prestress condition in the cables is also considered for the analysis. As the temperature and the length of cables are different consequently the amount of tension load at the two ends of different cables is different.

The displacements of the selected points A to E (Fig. 3.10) under different combinations of static loads including Fa load only (Fig. 3.12), Fa and Fb loads (Fig. 3.13), Fa, Fb, and Fc loads (Fig. 3.14), Fa, Fb, Fc, and Fd loads (Fig. 3.15), and Fe load only (Fig. 3.16) were determined for horizontal (u), longitudinal (v) and vertical (w) directions. Moreover, the numerical finite strip results are compared with those obtained by finite element software SAP2000 and are summarized in Tables 3.2 to 6 for each loading combination. In the finite element model, the thin-shell finite element method is used for deck modeling. Similarly to IFSM, the cables are modeled as truss elements while the piers and towers are modeled by beam elements.

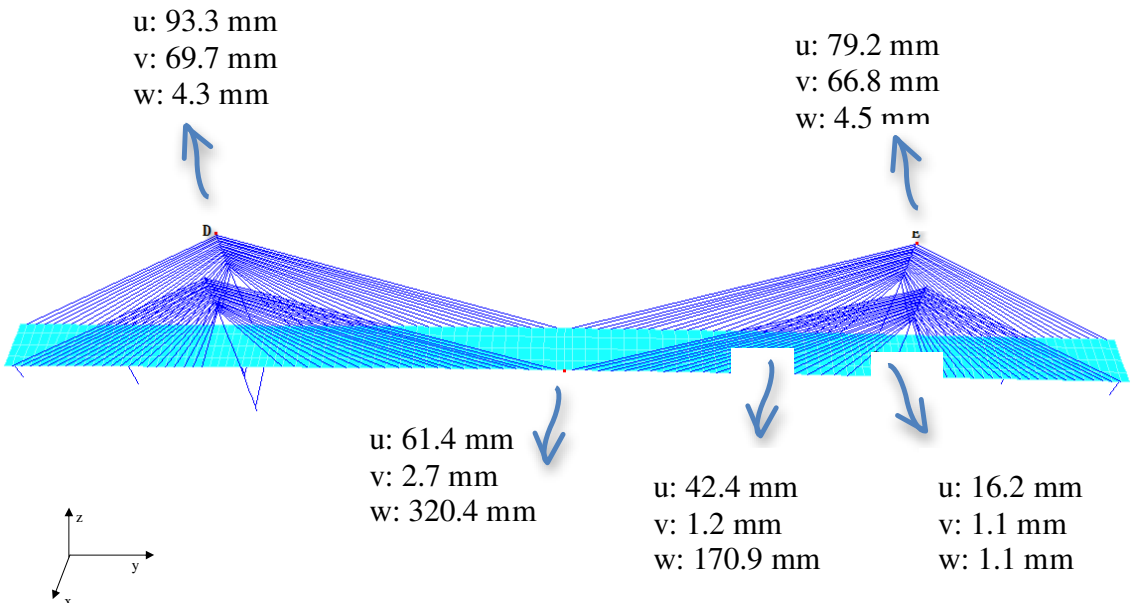

Fig. 3.12 Displacements under static load “Fa”

It is obvious that the maximum deflection is registered at the middle of the deck. When loading is applied at the towers, the displacements at the top of the towers in the longitudinal direction are considerable. A good agreement could be seen between the results of the finite strip and the finite element methods for different load combinations, considered at different locations. It can be concluded that by using the transition section in the integrated finite strip method the interactions between the towers and other sub-structures of the bridge can be considered. This achievement is valuable because the performance of the sub-structures strongly influences the whole bridge system. The deformed shape of the KSM Bridge under load case “Fa” is illustrated in Fig. 3.17.

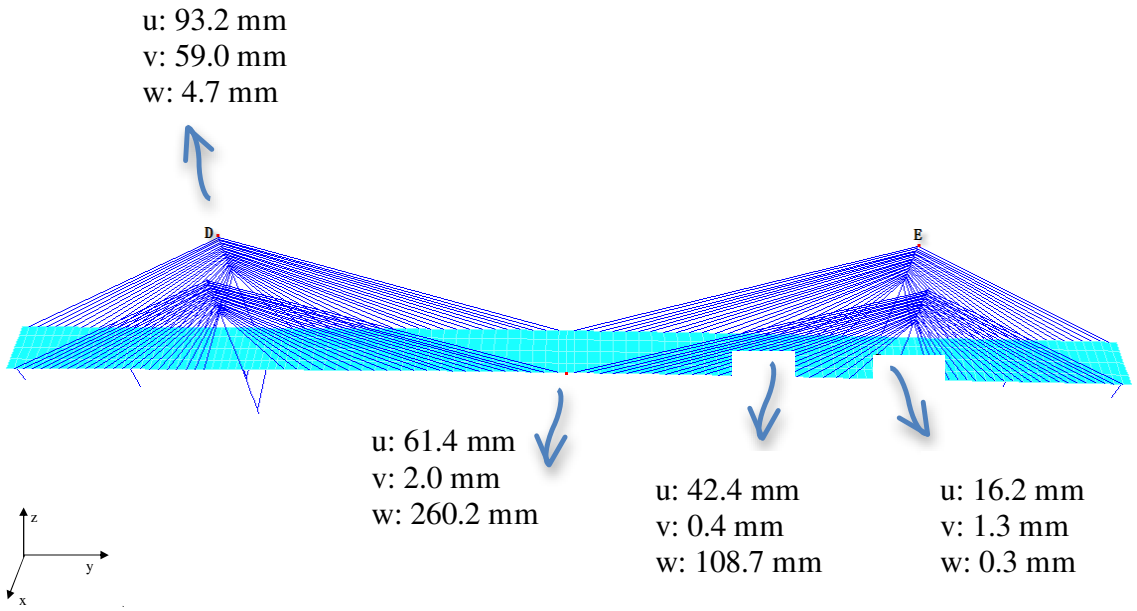

Fig. 3.13 Displacements under combination of static loads “Fa+Fb”

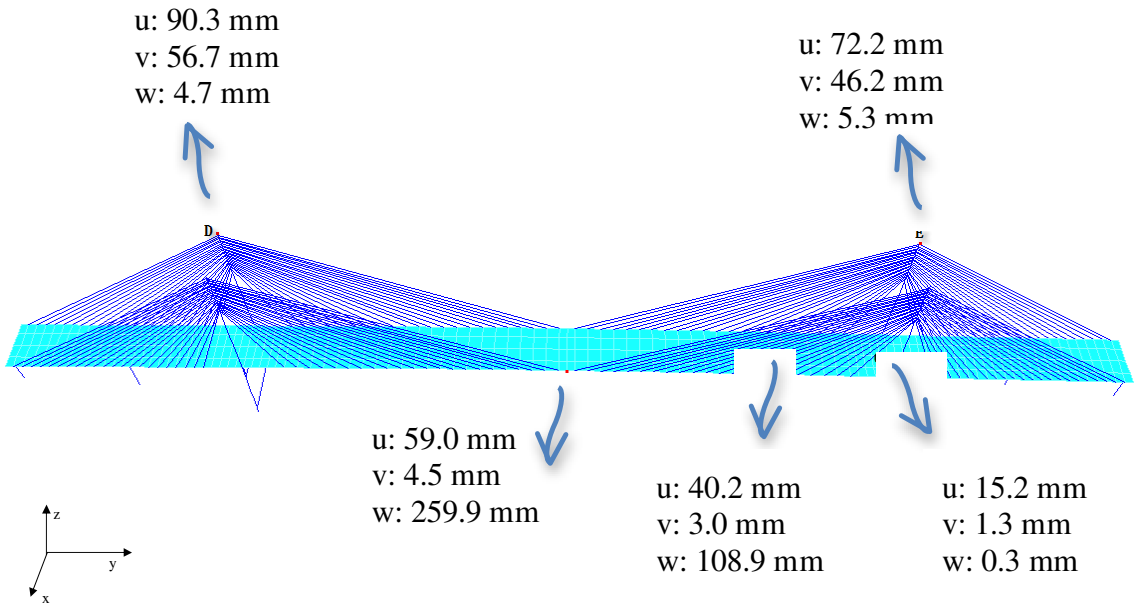

Fig. 3.14. Displacements under combination of static loads “Fa+Fb+Fc”

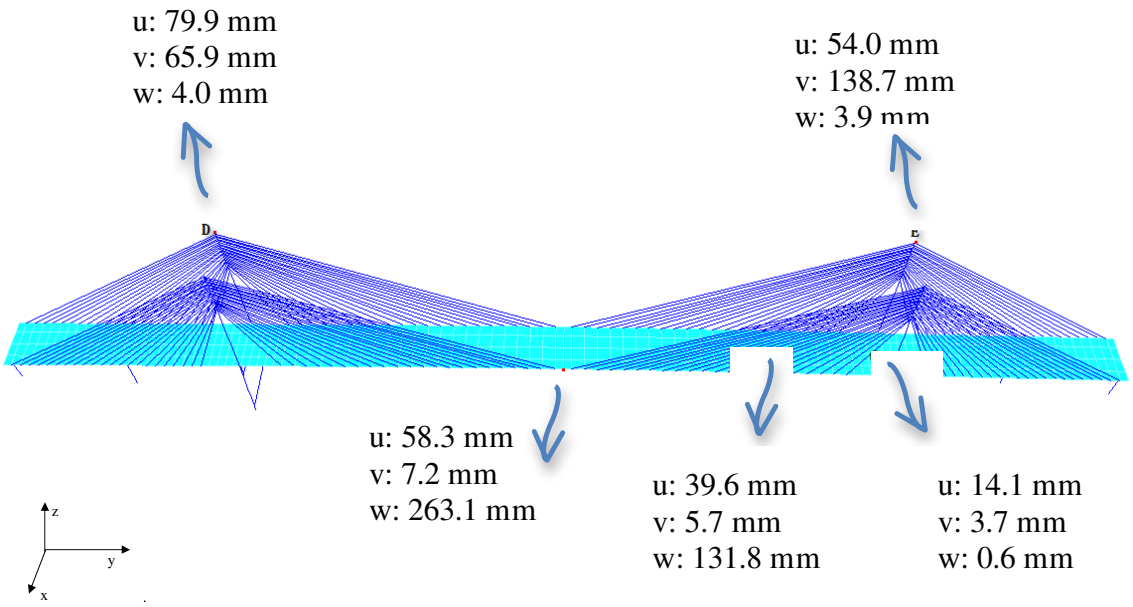

Fig. 3.15 Displacements under combination of static loads “Fa+Fb+Fc+Fd”

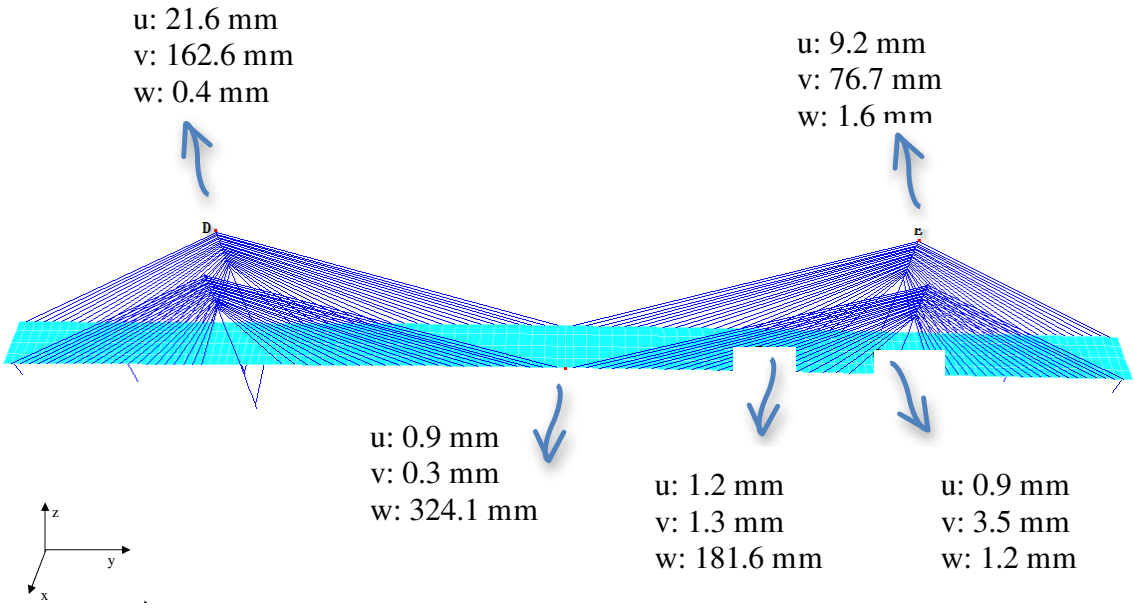

Fig. 3.16 Displacements under static load “Fe”

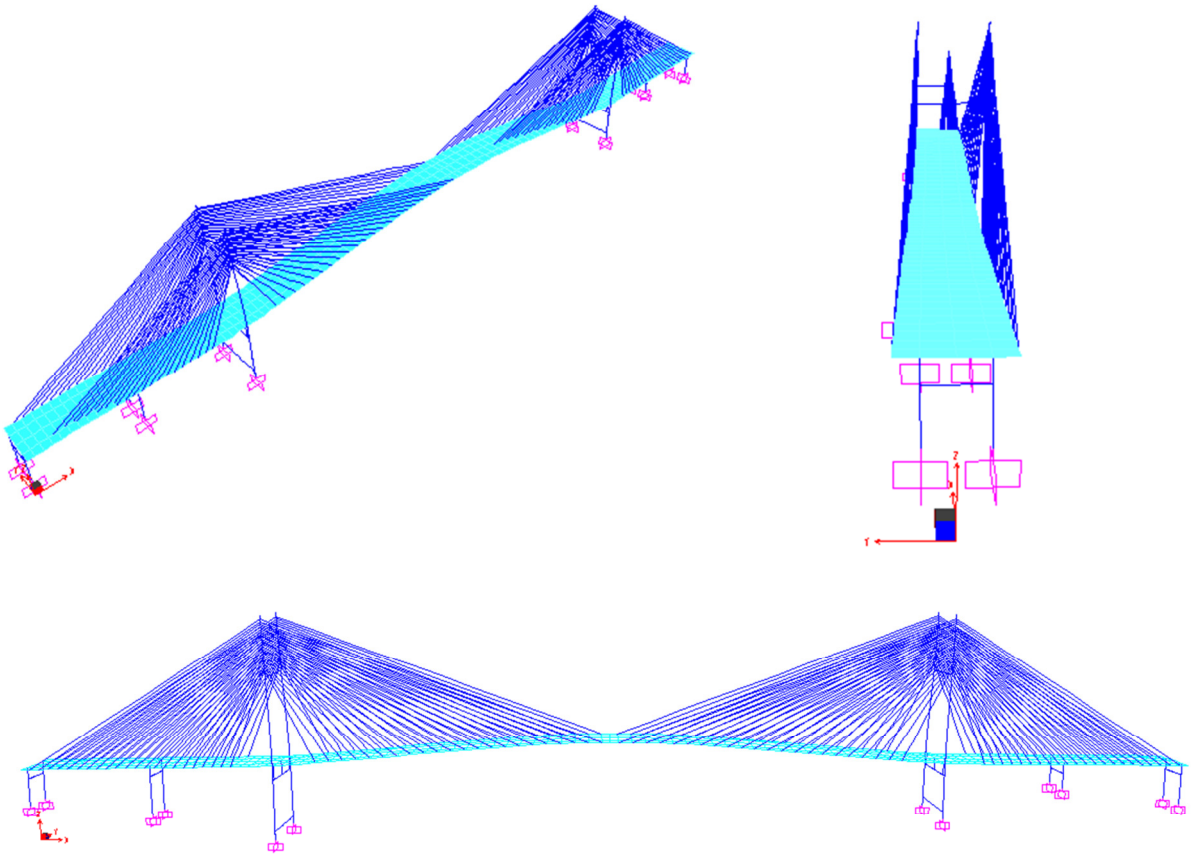

Fig. 3.17 Deformed shape of the bridge under load “Fa”

Table 3.2 Displacement under static load “Fa”

		Location	**A (375 m)**	**B (493.4 m)**	**C (590 m)**	**D (Tower 1 left - top)**	**E (Tower 2 left - top)**
Load “Fa”	u (mm)	IFSM	61.4	42.4	16.2	93.3	79.2
		FEM	61.3	42.6	16.4	92.4	76.8
	v (mm)	IFSM	2.7	1.2	1.1	69.7	66.8
		FEM	2.7	1.2	1.1	69.7	66.7
	w (mm)	IFSM	320.4	170.9	1.1	4.3	4.5
		FEM	318.1	169.9	1.1	4.2	4.4

Table 3.3 Displacement under static loads “Fa” and “Fb”

		Location	**A (375 m)**	**B (493.4 m)**	**C (590 m)**	**D (Tower 1 left - top)**
Load “Fa+Fb”	u (mm)	IFSM	61.4	42.4	16.2	93.2
		FEM	61.3	42.6	16.4	92.4
	v (mm)	IFSM	2.0	0.4	1.3	59.0
		FEM	1.9	0.4	1.3	59.1
	w (mm)	IFSM	260.2	108.7	0.3	4.7
		FEM	260.6	108.8	0.3	4.6

Table 3.4 Displacement under static loads “Fa”, “Fb” and “Fc”

		Location	**A (375m)**	**B (493.4m)**	**C (590m)**	**D (Tower 1 left - top)**	**E (Tower 2 left - top)**
Load “Fa+Fb+Fc”	u (mm)	IFSM	59.0	40.2	15.2	90.3	72.2
		FEM	58.9	40.3	15.4	89.4	74.4
	v (mm)	IFSM	4.5	3.0	1.3	56.7	46.2
		FEM	4.5	3.0	1.3	56.7	46.1
	w (mm)	IFSM	259.9	108.9	0.3	4.7	5.3
		FEM	260.2	109.0	0.3	4.6	5.4

Table 3.5 Displacement under static loads “Fa”, “Fb”, “Fc” and “Fd”

		Location	**A (375m)**	**B (493.4m)**	**C (590m)**	**D (Tower 1 left - top)**	**E (Tower 2 left - top)**
Load “Fa+Fb+Fc+ Fd”	u (mm)	IFSM	58.3	39.6	14.1	79.9	54.0
		FEM	58.1	39.7	14.3	79.2	56.0
	v (mm)	IFSM	7.2	5.7	3.7	65.9	138.7
		FEM	7.1	5.7	3.7	65.7	138.3
	w (mm)	IFSM	263.1	131.8	0.6	4.0	3.9
		FEM	264.6	131.9	0.6	3.9	4.0

Table 3.6 Displacement values under static load “Fe”

		Location	**A (375 m)**	**B (493.4 m)**	**C (590 m)**	**D (Tower 1 left - top)**	**E (Tower 2 left - top)**
Load “Fe”	u (mm)	IFSM	0.9	1.2	0.9	21.6	9.2
		FEM	1.0	1.3	0.9	21.3	9.4
	v (mm)	IFSM	0.3	1.3	3.5	162.6	76.7
		FEM	0.3	1.3	3.6	162.2	76.5
	w (mm)	IFSM	324.1	181.6	1.2	0.4	1.6
		FEM	325.4	181.5	1.2	0.4	1.6

3.3.5 Kap Shui Mun Bridge natural frequencies

Natural frequencies of the Kap Shui Mun Bridge are obtained from the integrated finite strip model and are categorized based on their mode shapes. These natural modes of vibrations are classified into four types including vertical-dominate modes, lateral-dominate modes, torsional-dominate modes and tower-dominate modes. The mode shapes can be assessed from the deflected shape of the bridge structure using the calculated displacements of the bridge structure. The first ten natural frequencies for different mode shapes are listed in Tables 3.7 to 3.10. The natural frequencies are compared with the ones obtained from the finite element of the Kap Shui Mun bridge model using SAP software. In general, there is a very good agreement between the results in all types of vibration modes. However, in the lateral mode, the differences between finite element and finite strip results in higher mode are a bit large. According to these results, the natural frequencies obtained through the finite strip method are generally higher than those obtained from finite element analysis for all types of mode shapes except for the lateral modes where in the higher modes the finite element frequencies are higher. Also, the deformed shape of the bridge for the first and second different dominant modes are plotted and shown in Figs. 3.18 to 3.25.

The comparison of the natural frequencies verifies the accuracy of the integrated finite strip solution for the modal analysis. Since the natural frequencies are important indicators of a structure dynamic performance, the high consistency of the natural frequencies shows that the proposed approach is capable of capturing the bridge dynamic characteristics. It makes the dynamic analysis of long-span cable-stayed bridges possible in a very efficient manner using integrated finite strip method.

Table 3.7 Natural frequencies for tower dominant modes

Mode number	**Natural frequency (Hz)**	
	IFSM	FEM
1	0.2113	0.2061
2	0.2409	0.2338
3	1.1381	1.1048
4	1.1391	1.1058
5	1.7369	1.7326
6	2.2547	2.2311
7	2.9212	2.8296
8	2.9946	2.8844
9	2.9995	2.9553
10	3.1087	3.0567

Table 3.8 Natural frequencies for vertical dominant modes

Mode number	**Natural frequency (Hz)**	
	IFSM	FEM
1	0.4250	0.4226
2	0.8523	0.8500
3	1.0032	1.0023
4	1.6523	1.6447
5	1.9097	1.8816
6	2.1625	2.0942
7	2.1734	2.1720
8	2.8199	2.8103
9	3.1381	3.1253
10	3.3502	3.2791

Table 3.9 Natural frequencies for lateral dominant modes

Mode number	**Natural frequency (Hz)**	
	IFSM	FEM
1	0.5217	0.5160
2	0.9305	0.9257
3	1.3537	1.3409
4	2.3504	2.3338
5	3.0212	2.9876
6	4.2623	4.3017
7	5.0318	5.0052
8	5.4121	5.9582
9	5.9974	7.9106
10	6.0846	8.0807

Table 3.10 Natural frequencies for torsional dominant modes

Mode number	**Natural frequency (Hz)**	
	IFSM	FEM
1	0.7526	0.7179
2	1.3419	1.2892
3	1.8928	1.8650
4	2.0027	1.9068
5	2.0977	2.0348
6	2.4899	2.3696
7	3.0853	3.0403
8	3.4545	3.3683
9	3.9164	3.7303
10	4.0698	3.8779

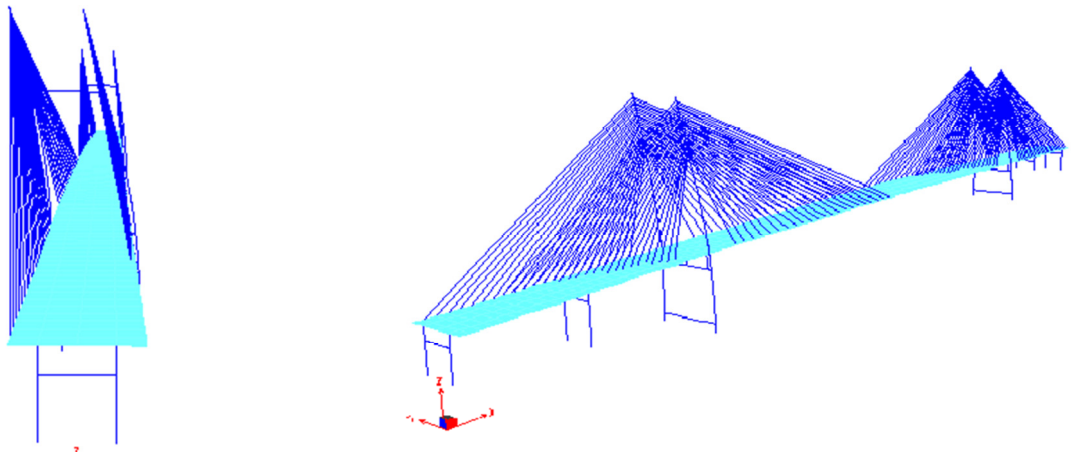

Fig. 3.18 Deformed shape of the bridge for first tower dominant mode (0.2113 Hz)

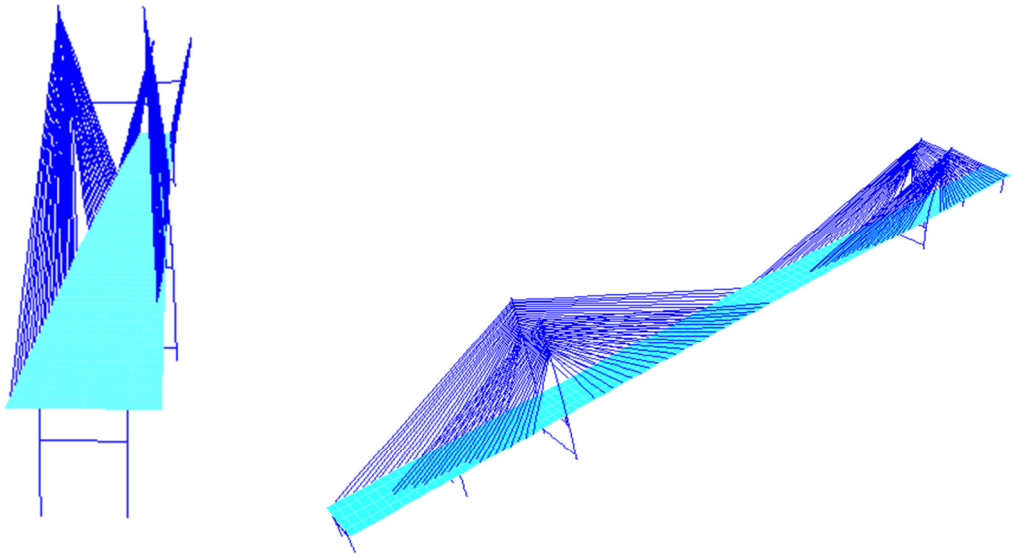

Fig. 3.19 Deformed shape of the bridge for second tower dominant mode (0.2409 Hz)

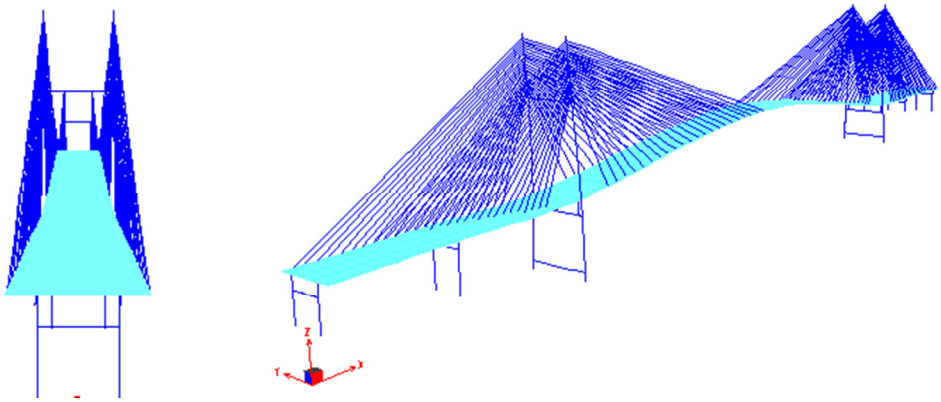

Fig. 3.20 Deformed shape of the bridge for first vertical dominant mode (0.4250 Hz)

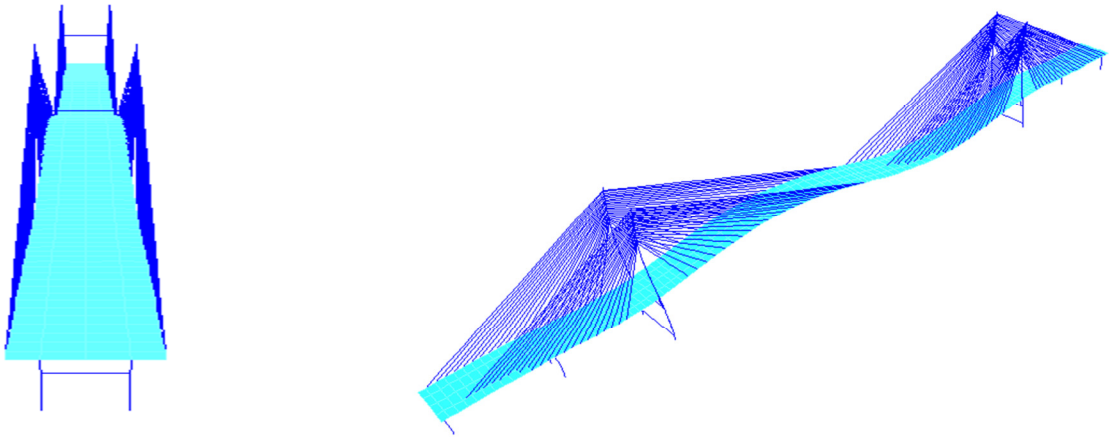

Fig. 3.21 Deformed shape of the bridge for second vertical dominant mode (0.8523 Hz)

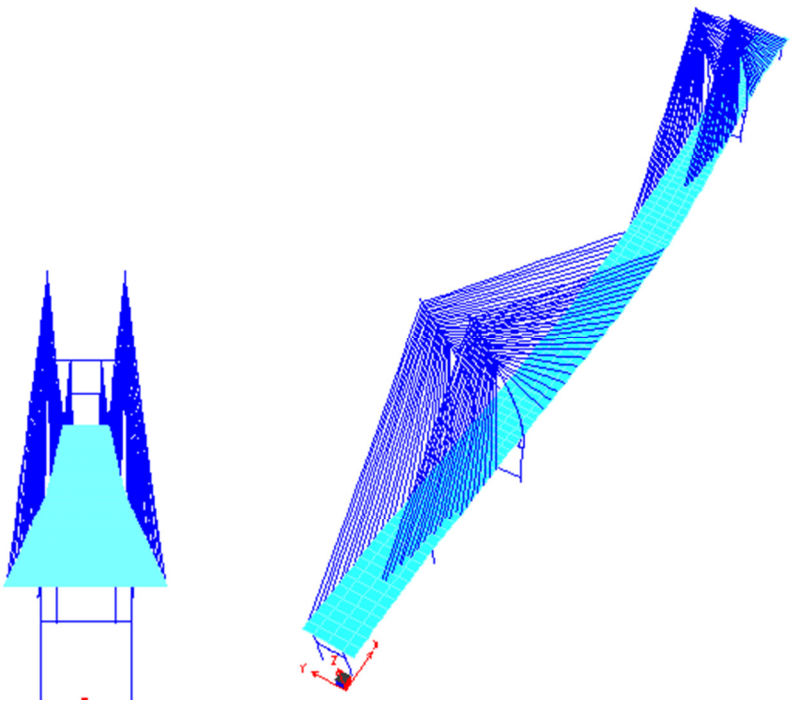

Fig. 3.22 Deformed shape of the bridge for first lateral dominant mode (0.5217 Hz)

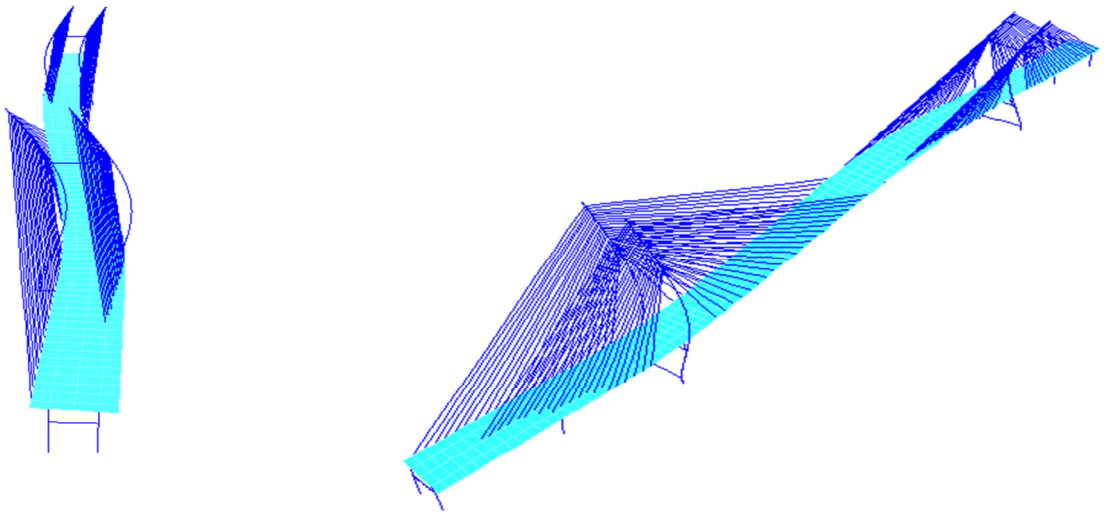

Fig. 3.23 Deformed shape of the bridge for second lateral dominant mode (0.9305 Hz)

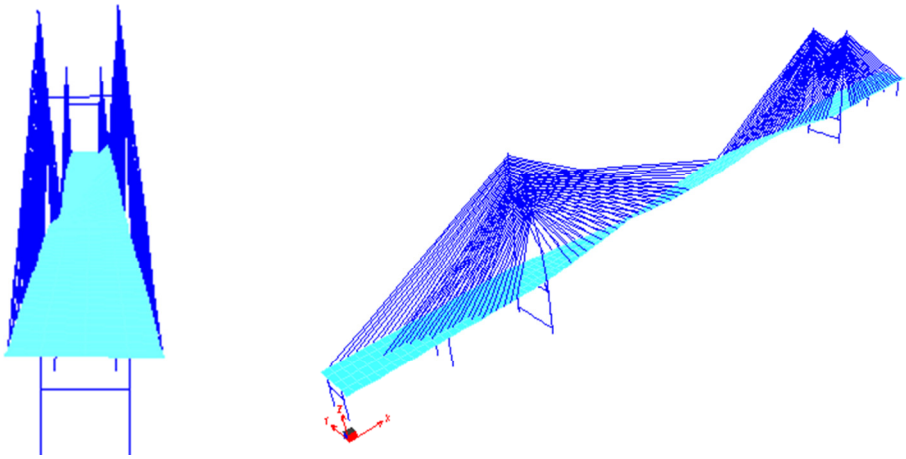

Fig. 3.24 Deformed shape of the bridge for first torsional dominant mode (0.7526 Hz)

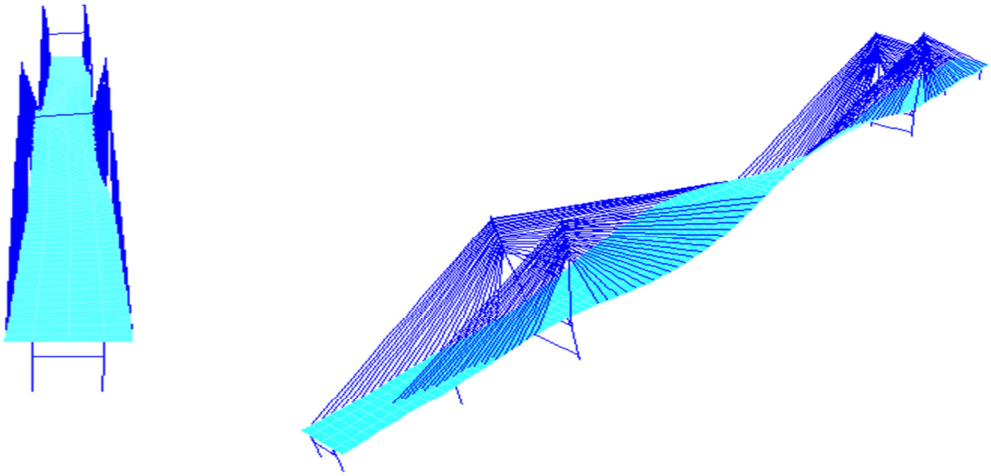

Fig. 3.25 Deformed shape of the bridge for second torsional dominant mode (1.3419 Hz)

3.3.6 Verification with experimental data

In order to further evaluate the accuracy of the integrated finite strip method for cable-stayed bridges, the finite strip natural frequencies of Kap Shui Mun Bridge are compared with those obtained from field measurements data as well as finite element modeling of the same bridge presented by other researchers. For this purpose, the natural frequencies of different

vibration modes including the first five vertical-dominant, three lateral-dominant, and three torsional-dominant modes of the deck are compared. The frequencies calculated from the

Table 3.11 Comparison of natural frequencies for different mode

Mode	Mode shape	Notation	Measured frequencies $f_{\exp}(Hz)$ [3.23]	FE Frequencies $f_{FEM}(Hz)$ [3.23]	FS frequencies $f_{FSM}(Hz)$	$\frac{(5)\_(3)}{(3)}$ %	$\frac{(5)\_(4)}{(4)}$ %
1	First vertical bending of deck	V1	0.39	0.41	0.42	7.6	2.4
2	Second vertical bending of deck	V2	0.66	0.58	0.85	28.8	46.5
3	Third vertical bending of deck	V3	1.07	0.93	1.00	-6.5	7.5
4	Fourth vertical bending of deck	V4	1.54	1.51	1.65	7.1	9.2
5	Fifth vertical bending of deck	V5	1.81	1.74	1.90	4.9	9.1
6	First lateral bending of deck	L1	0.49	0.49	0.52	6.1	6.1
7	Second lateral bending of deck	L2	1.25	1.15	0.93	-25.6	-19.1
8	Third lateral bending of deck	L3	2.12	2.45	1.35	-36.3	-44.9
9	First torsional mode of deck	T1	0.83	0.77	0.75	-9.6	-2.6
10	Second torsional mode of deck	T2	1.39	1.62	1.34	-3.6	-17.3
11	Third torsional mode of deck	T3	1.90	2.18	1.89	-0.5	-13.3

IFSM and their corresponding values obtained from the field vibration measurement and a finite-element modeling by Zhange et al [3.23] are summarized in Table 3.11. It is noticed that in most of the cases the differences between the IFSM and the measured frequencies as well as FE frequencies is below 10%. However, in some cases like second vertical mode (V2) or second and third lateral modes (L2, L3), the difference between the field measurements and both numerical methods is much higher.

According to Zhang et al. [3.23], in their finite element modeling, the geometric and material properties as well as the boundary conditions of the Kap Shui Mun Bridge are modeled based on the engineering drawings, which are highly idealized. It is worth noting that the finite strip modeling of KSM Bridge investigated in the current study is also based on the structural properties presented in the same reference [3.23]. However, in the FEM the deck is modeled using a single spine passing through the shear centers of the transverse beam elements, while in finite strip method the deck is modeled as a shell element. The discrepancies between the current numerical predictions and the measurements of the bridge vibration may be caused by a number of factors like inaccuracy in the analytical model discretization; uncertainties in the geometry and boundary conditions, and variations in the material properties of the bridge. Last but not least, in the finite strip the deck is modeled by flat shell strips, while in the FE the modeling is based on the use of beams elements. The three-dimensional finite element model as shown in Fig. 3.26 [3.23] was constructed using linear elastic beam elements for the towers and the deck, truss elements for the cables, and elastic or rigid links for the connections and the boundary constraints. The bridge deck originally consists of two parts including steel-concrete frames in the central portion of the main span and the trapezoidal box girders for the side segments. The calculated stiffness and masses are assigned to a single spine passing through the shear centers of the deck to better simulating the actual response of the deck.

The nonlinear effect due to cable tension and sagging is taken into account by linearizing the cable stiffness using the concept of an equivalent modulus of elasticity. On the other hand, the geometrically nonlinear behavior of the bridge structure, especially the cables, is not considered in the finite strip model. Nevertheless, the ambient vibration technique used for the experimental tests generally assumes that the structure behaves linearly.

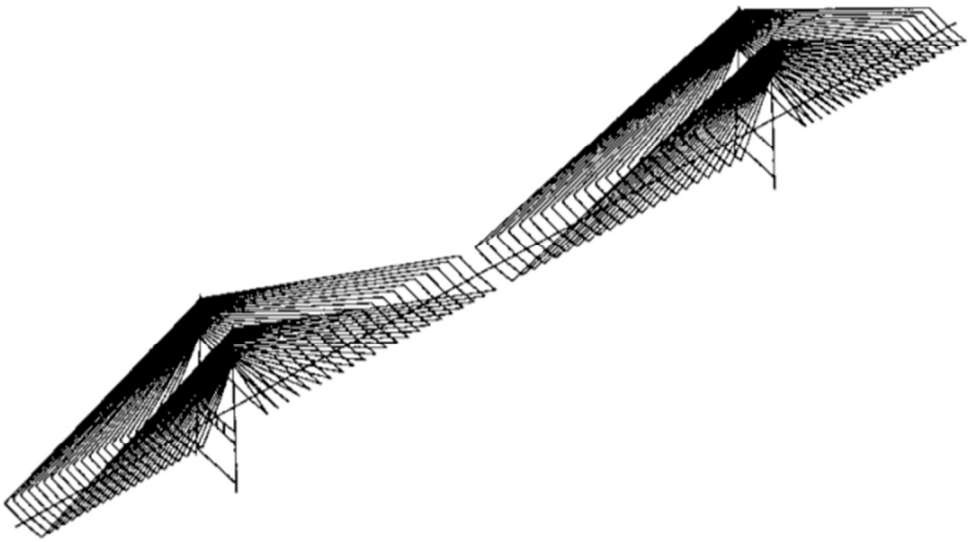

Fig. 3.26 Three-dimensional finite element model of the KSM bridge [3.23]

Zhang et al. [3.23] presented a finite element model updating for Kap Shui Mun Bridge in an iterative fashion so as to minimize the differences between the measured and numerical natural frequencies. The results for different natural frequencies are tabulated in Table 3.12, along with finite strip predictions. Comparing the numerical results with the measurement field data, it is obvious that in some cases the accuracy of the finite element predictions is still not only more but also less than the finite strip method even after six iterations. Finally, the finite strip results and the field vibration test show reasonable correlation in terms of the natural frequencies and the mode shapes of the bridge. However, significant discrepancies can still be witnessed between the predicted and the measured frequencies for some modes. Even the updated finite element solution is unable to remove the frequency differences completely. There are usually some errors associated with the measurement data and the postprocessing techniques. Also, the inherent assumptions and limitations of both finite element and finite strip method have considerable effect on the accuracy and convergence of the results.

Table 3.12 Comparison of natural frequencies with updating FEM results

Mode	Measured frequencies $f_{\exp}(Hz)$	FE frequencies $f_{FEM}(Hz)$	Updated FE frequencies (Hz)	FS frequencies $f_{FSM}(Hz)$
V1	0.39	0.41	0.40	0.42
V2	0.66	0.58	0.66	0.85
V3	1.07	0.93	0.97	1.00
V4	1.54	1.51	1.53	1.65
V5	1.81	1.74	1.82	1.90
L1	0.49	0.49	0.48	0.52
L2	1.25	1.15	1.21	0.93
L3	2.12	2.45	2.26	1.35
T1	0.83	0.77	0.81	0.75
T2	1.39	1.62	1.50	1.34
T3	1.90	2.18	1.91	1.89

3.4 Concluding remarks

In this paper, an integrated finite strip method is proposed for modeling long-span cable-stayed bridges. The method is applied to study of the static and free vibration analyses of cable-stayed bridges. The natural frequencies of the bridge structure can be obtained by solving an eigenvalue problem.

In spite of the large number of publications on the use of finite strip method in long-span cable-stayed bridge analysis, the application of existing methods for the static and dynamic analyses is restricted to the bridge super-structures or bridges with assumed pier and cable conditions only. To overcome this drawback, in this paper, the entire long-span cable-stayed bridge system is modeled by using the integrated finite strip method. For this purpose, different types of strips are introduced including flat shell spline strip, column strip, and cable strip which are able to model the deck, towers and piers, and cables respectively. Unequally spaced B3-spline functions are the base for creating the integrated finite strip

method. Using the latter concept, so called transition section is developed for modeling the joint points of different structural components. Consequently, the cables as well as piers and towers can be connected to the bridge deck in the simulation model, and the interactions between them can be considered in the analysis.

A series of computer programs are developed using C++ and MATLAB, and are used for analysis purposes. The Kap Shui Mun Bridge in Hong Kong is selected as the case study. The displacements under a combination of static loads, as well as the natural frequencies of the Kap Shui Mun Bridge are investigated and the results are confirmed by comparing them with other methods. A good agreement is witnessed between the integrated finite strip solutions with those obtained from finite element method as well as field measurements data.

The numerical results demonstrate that the convergence and efficiency of the proposed method is very high. According to the time required for running the analysis, it can be observed that the computational costs for the finite strip method are better than the finite element method. Therefore, the methodology can be efficiently used for analysis of long-span cable-stayed bridges. When it comes to the dynamic analysis, in which the structure has an impressive number of degrees of freedom, the integrated finite strip method becomes more efficient and more economic. In addition, the simplicity of the input data in the finite strip environment is highly appreciated when comparing it with finite element method, in which a lot of parameters and criteria need to be controlled.

The following points should be emphasized on to highlight the novelty and contribution of the present paper (i) An integrated finite strip discretization is proposed for long-span cable-stayed bridges. (ii) Finite strip analysis of cable-stayed bridges is no longer restricted to the bridge deck modeling. (iii) The interactions between different components can be considered in the analysis, e.g. structural interactions between cables and towers and deck can be taken into account. (iv) The advantages of the method are simplicity of input data and high efficiency because the computational effort required for structural analysis of long-span cable-stayed bridges significantly reduces. (v) The method is employed for static and free vibration analyses of bridges. A case study was performed for the Kap Shui Mun Bridge.

After the invention of integrated finite strip method for long-span cable-stayed bridges new opportunities are opened for applying this numerical technique. There is a high potential of

broadening the solution to dynamic and aerodynamic problems, composite hybrid bridges, and non-linear analysis.

References

[3.1] Cheung, M.S., Li, W., Chidiac, S. E., (1996) Finite strip analysis of bridges, 1st Edition. London: E & FN Spon

[3.2] Zhang , Wei., Cai, C.S., Pan, Fang., (2013), Finite element modeling of bridges with equivalent orthotropic material method for multi-scale dynamic loads, Engineering Structures, Volume 54, September 2013, Pages 82–93

[3.3] Ni, Y. Q., Zhou, H. F., Chan, K. C., Ko, J. M., (2008) Modal Flexibility Analysis of Cable-Stayed Ting Kau Bridge for Damage Identification, Computer-Aided Civil and Infrastructure Engineering, Volume 23, Issue 3, pages 223–236, April 2008

[3.4] Daniell, Wendy E., Macdonald, John H.G., (2007) Improved finite element modelling of a cable-stayed bridge through systematic manual tuning, Engineering Structures, Volume 29, Issue 3, March 2007, Pages 358–371

[3.5] Ren, Wei-Xin., Peng, Xue-Lin., (2005) Baseline finite element modeling of a large span cable-stayed bridge through field ambient vibration tests, Computers & Structures, Volume 83, Issues 8–9, March 2005, Pages 536–550

[3.6] Ren, Wei-Xin., Peng, Xue-Lin., Lin, You-Qin., (2005) Experimental and analytical studies on dynamic characteristics of a large span cable-stayed bridge, Engineering Structures, Volume 27, Issue 4, March 2005, Pages 535–548

[3.7] Cheung Y. K., Tham L. G. (1998) The finite strip method, USA: CRC Press.

[3.8] L. C. Wrobel; M. H. Aliabadi (2002) The Boundary Element Method. New Jersey: Wiley.

[3.9] Cheung, Y. K., (1968) The finite strip method in the analysis of elastic plates with two opposite simply supported ends, Proc. Inst. Civ. Eng., 40, 1-7

[3.10] Powell, G. H., Ogden, D. W., (1969) Analysis of orthotropic steel plate bridge decks, Proc. ASCE, 95 (ST5), 909-922

[3.11] Cheung, Y.K., Fan, S.C., Wu, C.Q., (1982) Spline finite strip in structural analysis, Proc. Int. Conf. Fin. Elem. Meth., Shanghai, 704-709.

[3.12] Chen CJ, Gutkowski RM, Puckett JA. (1991) B-Spline compound strip analysis of stiffened plates under transverse loading. Computers and Structures; 34(2):337–347.

[3.13] Chen CJ, Gutkowski RM, Puckett JA. (1991) Spline compound strip analysis of folded plate structures with intermediate supports. Computers and Structures; 39(3/4):369–379.

[3.14] Dawe, D.J., (2002) Use of the finite strip method in predicting the behaviour of composite laminated structures, ompositeStructures57, 11–36

[3.15] Cheung, M. S., Li, W., (1988) Analysis of haunched bridges by finite strip method, Computers and Structures, 28 (5), 621-626

[3.16] Y. K. Cheung, *S.* C. Fan, (1983) Static analysis of right box girder bridges by spline finite strip method, *Proc. Instn Ciu. Engrs,* Part 2, 75, June, 311-323

[3.17] Cheung, M.S., Li, W., (1990) Analysis of haunched, continuous bridges by spline finite strips, Comput. Struct;36(2), 287-300.

[3.18] Cheung, M. S., Li, W., (1992) Spline finite strip analysis of continuous haunched box-girder bridges, Canadian Journal of Civil Engineering

[3.19] Choi, C. K., Kim, K. H., Hong, H. S., (2002) Spline finite strip analysis of prestressed concrete box-girder bridges, Engineering Structures, Volume 24, Issue 12, December 2002, Pages 1575–1586

[3.20] Cheung, M.S., Li , W.C., (2003) Probabilistic fatigue and fracture analyses of steel bridges, Structural Safety, Volume 25, Issue 3, July 2003, Pages 245–262

[3.21] Cheung, Moe M. S., Shen, Zhenyuan., Chan, Ben Y.B., (2009) Integrated Finite Strip Solution for Box Girder Bridges and Slab-on-girder Bridges, Journal of Computer Modeling in Engineering and Science, vol.45, no.2, pp.155-177

[3.22] Shen, Zhenyuan., Cheung, Moe M. S., Naderian, Hamidreza., Dragomirescu, Elena., (2013), An Integrated Finite Strip Solution for Dynamic Analysis of Continuous Multi-span Bridges, Proceedings of the 3rd Specialty Conference on Mechanics and Materials, Montreal, Canada

[3.23] Zhang, Q. W., Chang, T. Y. P., Chang, C. C., (2001) Finite element model updating for the Kap Shui Mun cable-staed bridge, Journal of Bridge Engineering, Vol. 6, No. 4, July/ August

Chapter 4

Seismic Analysis of Long-Span Cable-Stayed Bridges by an Integrated Finite Strip Method*

*This chapter has been published in ASCE Journal of Bridge Engineering as "Naderian, Hamidreza., Cheung, Moe M. S., Shen, Zhenyuan., Dragomirescu, Elena., (2015) Seismic analysis of long-span cable-stayed bridges by an integrated finite strip method, ASCE Journal of Bridge Engineering, ISSN 1084-0702"

Abstract_This paper provides a very efficient, integrated framework for seismic analyses of long-span cable-stayed bridges. The efficiency comes from the dramatic reduction in formation time and the degrees-of-freedom associated with the structure, using the integrated finite strip method along with the application of a very robust and efficient time history method using Newmark scheme for dynamic analysis of the bridge structure. The previous versions of the finite strip method are limited to modeling the bridge deck only, while other structural components are replaced by assumed boundary conditions. Using the integrated finite strip method, all components of the long-span cable-stayed bridge can be modelled in a unified system, and consequently the real dynamic behaviour including the interactions between deck, piers and cables can be perfectly considered. In order to verify the solution, the geometric and dynamic properties of the Kap Shui Mun bridge, as a real example of a long-span cable-stayed bridge, are derived by the proposed finite strip method. Then, the seismic response of Kap Shui Mun bridge under uniform and nonuniform earthquake loadings is investigated by using the time history method. The results show that integrated finite strip method can be applied successfully for seismic analysis of long-span cable-stayed bridges where the analysis is performed in a minimal time.

Keywords: Seismic analysis, time history method, Newmark's method, long-span bridge, cable-stayed bridge, dynamic, integrated finite strip method.

4.1 Introduction

To meet the economic, social and recreational needs of the community for safe and efficient transportation systems, long-span bridges have been built throughout the world. These bridges represent some of the most challenging kinds of structures designed in civil engineering. Nowadays, long-span cable-stayed bridges are of great interest, mainly as an alternative and a more economic solution than the one provided by the suspension bridges. Because of their great flexibility, modern long-span cable-stayed bridges are usually very susceptible to dynamic loads. Therefore, the wind-resistant and earthquake-resistant designs become key issues for successful construction of these bridges.

The structural response of long-span bridges under dynamic and aerodynamic loads is very complicated, and powerful computational techniques are required, which can accurately analyze and predict the structural behavior of these massive structures. This is a major point in successful and optimized design of long-span cable-stayed bridges. Most of the bridge structural analyses are performed by the aid of the well-known finite element method (FEM). Quasi-static numerical analysis using FEM has been one of the most widely adopted approaches for the study and design of long-span bridges in the past few decades [4.1]. With increasing the span lengths and successful application of the light-weight composite materials for bridges, the dynamic characteristics of these structures have become more complex, and the conventional FEM approach might not always be sufficient. On the other hand, the formulation of a FEM model and setting up of the boundary conditions of a three dimensional (3D) bridge structure for dynamic analysis is very complicated and time consuming, especially for long-span cable-stayed bridges, where because of the extremely high number of degrees of freedom (DOF) involved, such procedure becomes inconvenient in practice. Besides, the convergence rate of the conventional FEM in dynamic problems is usually slow, since the nonlinearities associated with the flexible bridge structures lead to significant redistribution of the internal forces. One of the solutions for improving the convergence rate is to use very small size elements throughout the structure, resulting in a large number of degrees of freedom. Therefore, in the case of long-span cable-stayed bridges, with thousands of degrees of freedom, and in the same time with high nonlinear behavior under dynamic and aerodynamic forces, the finite element analysis seems to be not efficient enough.

Finite strip method, as a semi-analytical numerical analysis pioneered by Y. K. Cheung in 1970's, has shown a great potential for analyzing bridge structures. However, because of some limitations, this method is not as popular as the finite element method. For instance, the ordinary finite strip method can only deal with prismatic members with simply supported end conditions. Moreover, the method cannot handle shear forces, as well as internal supports and concentrated loads. In spite of the large number of references on the use of finite strip method in structural analysis, the application of the existing finite strip methods in seismic analysis is restricted to the bridge super-structures or bridges with assumed pier conditions only. In the conventional finite strip methods, the piers and the cables of the bridge are normally replaced by certain boundary conditions, and this assumption is reasonable only when the stress distribution along the girders and the slabs of the bridge super-structures is required. An alternative solution in considering the pier and the cable effects is to combine the finite strip bridge deck with piers and cables modeled by other types of elements, such as the boundary element, and thus the interactions between the bridge deck and the piers can be obtained via an iterative process. Nevertheless, this approach can be effective only for static and quasi-static analysis. When a complicated dynamic analysis, like the non-uniform seismic analysis is being considered, the ground excitations are transmitted from the piers and the cables to the super-structure, thus the dynamic characteristics of the these structural components play an important role in the prediction of the overall dynamic response of the bridge. With the recent developments in the formulation of the finite strip method, which is achieved through the so-called Integrated Finite Strip Method (IFSM) [4.2-4.4], it is suggested that this method can be employed for complete dynamic analysis of long-span cable-stayed bridges. In a recent study [4.3], the authors compared the computational times required by IFSM and FEM analyses. For similar modeling and mesh conditions, a 10% (around 24 minutes) time saving was determined when performing the dynamic analysis of a medium-span slab-girder bridge by IFSM (274 minutes) compared with conducting a finite element analysis (298 minutes). However, the number of sections for each strip in the integrated finite strip mesh could be even further reduced and consequently the computational time saving will be greater. The reason for such low computational time can be attributed to the semi-analytical nature of the IFSM model in the longitudinal direction, through which the number of sections for each strip can be

considerably reduced, without losing the accuracy of the outcomes. Moreover, the finite strip method can be easily programmed, such that only a limited amount of the input data is needed. Considering that it was only a simple case study, there is no doubt that in the case of long-span cable-stayed bridges, with an impressive number of degrees of freedom, the amount of computational time saving is much more significant comparing with the FE dynamic analysis. Therefore, IFSM can provide simple means for a rapid and accurate seismic analysis of long-span cable-stayed bridges, with various types of end and interior supports. It is worth to mention that when applied to most structural problems, it yields a relatively narrow band matrix of a small to moderate size, and thus it requires little computational effort. In IFSM, the different structural elements of a long-span cable-stayed bridge, such as the bridge deck, the piers, the towers and the cables, are represented by different types of strips, and a perfect connection between them is needed to be defined in order to model the entire bridge as an integrated system. In the current research, the flat shell spline finite strip is used for modeling the deck, while the column strip has been developed for modeling the piers, as well as the towers (pylons). Based on the column strip, the so-called cable strip is proposed for modeling the cables. Last but not least, a so-called transition section has been developed, so that different structural components can be connected together. The IFSM has the order continuity C2 because it uses B3-splines which are piecewise cubic polynomials with continuity over the entire interval up to the second derivative. It should be noted the same order continuity C2 in FEM can be achieved only if a fifth order polynomial is introduced for the interpolation. In common FE methods, the order continuity is usually C0 or C1. It means that more grid points and consequently more iterations are needed to ensure about the convergence of the results for the nonlinear terms in FEM.

In terms of dynamic analysis and design of long-span bridges, particular considerations should be made with regard to the safety criteria during extreme earthquakes and wind events. In recent decades, many researchers have achieved great fundamental progress in promoting the seismic random analysis of long-span structures and its engineering applications [4.5-4.10]. In the area of finite strip dynamic analysis, Cheung and Cheung [4.11] first proposed the finite strip solution for the free vibration analysis of thin-walled structures with different boundary conditions. Dawe [4.12] carried out an extensive research

on the use of both conventional and spline finite strip methods, for determining the behavior of composite laminated, prismatic plate and shell structures, based on the thin plate theory. The same study used the finite strip method for analyzing natural frequencies of single span and multi-span structures, and to estimate the transient response to dynamic loading for flat plates. Wang and Zhang [4.13] introduced a layerwise B-spline finite strip method for free vibration analysis of both thick and thin composite laminated plates. In this method, the composite laminated plates are divided into a number of layers along the thickness direction. In the area of aerodynamics, the finite strip method has been extended to flutter analysis of long-span cable-stayed bridges by Cheung and his colleagues [4.14, 4.15]. However, the extension is not a pure finite strip solution, but a combination with the finite element method. Free vibration analysis of arbitrarily shaped plates and shells has been carried out by Li [4.16] and Cheung et al. [4.17]. Cheung et al. [4.2, 4.3] introduced the integrated finite strip solution for dynamic analysis of slab-girder and box-girder bridges in the framework of frequency domain method.

In the environment of integrated finite strip method, this paper deals with time history analysis of long-span cable-stayed bridges under seismic load effects. First, the derivation of the dynamic properties of a long-span cable-stayed bridge, including stiffness, mass, and damping matrices, by integrated finite strip method (IFSM), is briefly presented. Using the stiffness and mass matrices derived from IFSM, the time history analysis of cable-stayed bridges is carried out by employing the Newmark's scheme. The Newmark's method is a powerful technique for solving the dynamic problems within the time history environment, which is used and explained in this paper.

The accuracy of the integrated finite strip solution in dynamic analysis of long-span cable-stayed bridges is evaluated by comparing the natural frequencies of the Kap Shui Mun Bridge with those obtained by finite element method and with the natural frequencies reported from the field-test measurements [4.18]. In addition, the effects of uniform, non-uniform, and varying seismic excitations on structural behavior of Kap Shui Mun Bridge are investigated. The numerical results show that the convergence and accuracy of the integrated finite strip method in dynamic analysis of long-span cable-stayed bridges is very high, which confirms the efficiency and capability of this numerical technique.

4.2 Dynamic properties estimation using integrated finite strip method

For extensive structural systems with numerous degrees of freedom, the finite strip method is one of the most efficient methods for structural analysis of bridges, reporting a reduced computational time required for the analysis, without affecting the degree of accuracy. Finite strip method is therefore an ideal platform for the traditional time-consuming dynamic analysis of long-span bridges. Cheung and his research group [4.2, 4.3] have recently introduced an integrated finite strip method for analyzing multi-span, continuous slab-on-girder and box girder bridges, by modeling the bridge deck, the piers and the bearings together so that the interactions between piers and deck can be considered in the analysis. The method has been extended to analysis of long-span cable-stayed bridges by developing other types of strips as well. The integrated finite strip method has been successfully applied for static and free vibration analysis of long-span cable-stayed bridges [4.4].

By representing the entire bridge as a single integrated system, the actual dynamic behavior of the bridge can be studied, in which the interactions between different structural components are also considered. In the following sub-section, the development of the dynamic properties of the long-span cable-stayed bridge using integrated finite strip method will be briefly presented.

4.2.1 Displacement functions

The displacement of a strip in the integrated finite strip method is obtained by applying B3-spline functions [4.19] in the longitudinal direction. For the transverse direction, the concept was adapted from the finite element method, in which the cubic polynomials are used to represent the transverse shape function of the strip. The same approach is utilized by the spline finite strip method.

Assuming the bridge deck as a shell structure, both in-plane and out-of-plane degrees of freedom are included in the analysis. A flat shell spline strip is shown in Fig. 4.1, in which each knot of a nodal line has four degrees of freedom, three translational *u, v, w* and one rotation θ. The total potential energy of a flat shell strip may be obtained from algebraic summation of the in-plane and out-of-plane deformations.

The displacement parameters vector of a shell spline strip centered at y_m is given by

$$\{\delta\}_m = \left[u_{im}, v_{im}, w_{im}, \theta_{im}, u_{jm}, v_{jm}, w_{jm}, \theta_{jm} \right]^T \tag{4-1}$$

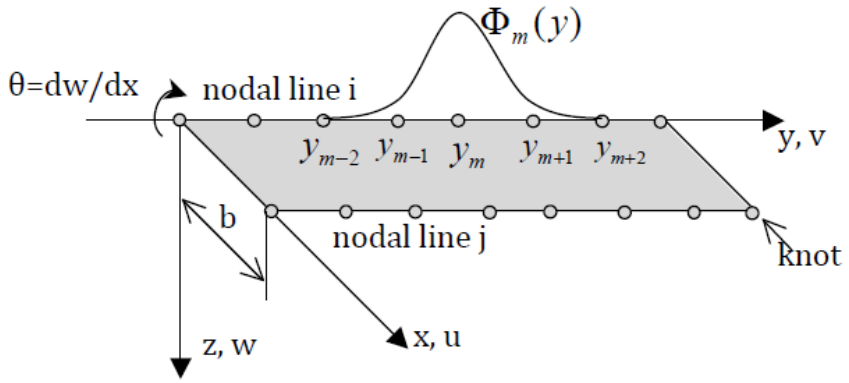

Fig. 4.1 Flat shell spline finite strip

The integrated finite strip method is based on the use of unequally spaced B3-spline functions, through which the transition section is developed for connecting different structural components together. Moreover, it allows the locations of the supports and the concentrated load to coincide with the knots on the nodal lines, thus leading to more accurate results. Besides, the introduction of unequally spaced interior knots allows one to describe the accurate response in the region of high stress gradients, or at the locations of abrupt geometric changes, by spacing the knots more closely. The unequally spaced B3-spline function centered at y_m can be expressed as

$$\Phi_m(y) = \begin{cases} 0 & y < y_{m-2} \\ A_m(y - y_{m-2})^3 & y_{m-2} \le y < y_{m-1} \\ A_m(y - y_{m-2})^3 + C_m(y - y_{m-1})^3 & y_{m-1} \le y < y_m \\ B_m(y_{m+2} - y)^3 + D_m(y_{m+1} - y)^3 & y_m \le y < y_{m+1} \\ B_m(y_{m+2} - y)^3 & y_{m+1} \le y < y_{m+2} \\ 0 & y_{m+2} \le y \end{cases} \tag{4-2}$$

in which

$$
\begin{aligned}
A_m &= \left[(y_{m+1}-y_{m-2})(y_m-y_{m-2})(y_{m-1}-y_{m-2})\right]^{-1} \\
B_m &= \left[(y_{m+2}-y_{m-1})(y_{m+2}-y_m)(y_{m+2}-y_{m+1})\right]^{-1} \\
C_m &= -(y_{m+2}-y_{m-2})\left[(y_{m+2}-y_{m-1})(y_{m+1}-y_{m-1})(y_m-y_{m-1})(y_{m-1}-y_{m-2})\right]^{-1} \\
D_m &= -(y_{m+2}-y_{m-2})\left[(y_{m+1}-y_{m-2})(y_{m+1}-y_{m-1})(y_{m+1}-y_m)(y_{m+2}-y_{m+1})\right]^{-1}
\end{aligned}
\tag{4-3}
$$

The membrane displacement functions *u* and *v*, and the flexural displacement function *w* are expressed as the product of transverse polynomials and longitudinal B3-splines as following

$$u = \sum_{m=-1}^{r+1} (N_1 \Phi_{1m}(y) u_{im} + N_2 \Phi_{5m}(y) u_{jm}) \tag{4-4}$$

$$v = \sum_{m=-1}^{r+1} (N_1 \Phi_{2m}(y) v_{im} + N_2 \Phi_{6m}(y) v_{jm}) \tag{4-5}$$

$$w = \sum_{m=-1}^{r+1} (N_3 \Phi_{3m}(y) w_{im} + N_4 \Phi_{4m}(y) \theta_{im} + N_5 \Phi_{7m}(y) w_{jm} + N_6 \Phi_{8m}(y) \theta_{jm}) \tag{4-6}$$

where r is the total number of longitudinal sections on a nodal line. Transverse shape functions adopted in above equations are cubic Hermite polynomial functions used for vertical displacement variation and linear interpolation for in-plane displacements as below

$$
\begin{aligned}
&N_1 = 1-X, N_2 = X, N_3 = 1-3X^2+2X^3, N_4 = x(1-2X+X^2), N_5 = (3X^2-2X^3) \\
&N_6 = x(X^2-X)
\end{aligned}
\tag{4-7}
$$

where $X = x/b$. $[\Phi_{1m}]$ to $[\Phi_{8m}]$ are row matrices and each matrix has (m+3) local B3-splines. $[\Phi_{1m}]$, $[\Phi_{2m}]$, $[\Phi_{5m}]$ and $[\Phi_{6m}]$ are related to displacements *u* and *v* of nodal lines *i* and *j* respectively, while $[\Phi_{3m}]$, $[\Phi_{4m}]$, $[\Phi_{7m}]$ and $[\Phi_{8m}]$ are related to displacement *w*.

The cantilever behavior of the piers and the towers is modeled by using the so-called column strip, which is similar to the flat shell spline finite strip. However, this is modeled as a vertical strip fixed at one end, for providing the support boundary conditions, and free at the other end, as shown in Fig. 4.2. In fact, the global *z* direction of the column strip is similar to the local *y* direction in the flat shell spline finite strip, which is controlled by the in-plane stiffness, in the corresponding direction while the global *v* direction of the column strip is similar to local *z* direction of the shell spline finite strip. With the assumed displacement

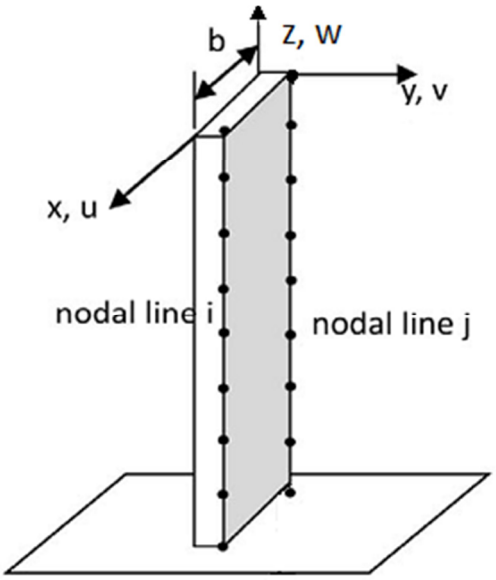

Fig. 4.2 Column Strip in local coordinate system (CS)

functions and the preset boundary conditions, the shape function of the column strip can be developed using the traditional finite element concepts.

Sometimes one-dimensional column strip is more applicable in modeling of piers and towers because this has only one nodal line and is rather similar to the beam element used in the finite element method. Each knot belonging to the nodal line has three translational degrees of freedom. Consequently, the displacement function can be defined as

$$u = \sum_{m=-1}^{r+1} u_m \Phi_m(z) \tag{4-8}$$

$$w = \sum_{m=-1}^{r+1} w_m \Phi_m(z) \tag{4-9}$$

$$v = \sum_{m=-1}^{r+1} v_m \Phi_m(z) \tag{4-10}$$

For the displacement-strain relationships, only the bending in the vertical and transverse directions, and the axial stress are considered, while the shear stress and torsional moment are assumed to be negligible as the amount of these forces are very low in a one-dimensional column strip.

In order to model the cables in the finite strip environment, the cable strip is developed, which is in fact a simplified version of the one-dimensional column strip. In general, a cable can only resist against the axial tension stresses. Therefore, only the axial stress defines the strain-displacement relationship for a cable strip.

It should be noted that all the strips in the finite strip method must come with the preset boundary conditions. There are some techniques like penalty method to consider the end boundary conditions of the strips, that can be simply applied to the finite strip modeling [4.20].

4.2.2 Modeling the transition section

With the concept of elements and nodes in the finite element method, there is no particular difficulty to add other elements to the bridge deck and to connect them together. However, the concept "element" in the longitudinal direction is not defined neither in the ordinary finite strip method, nor in spline the finite strip method. In order to solve this problem, a special transition section has been developed within the IFSM, which is applied to connect different components of a complicated structure, like a long-span cable-stayed bridge. As previously mentioned, the transition section is developed by using unequal spaced B3-spline functions. Moreover, the bearings can be modeled as special boundary conditions for the transition section. A typical transition section connecting two different components is shown in Fig. 4.3. Not losing generalization, it is assumed that the width of the normal and the transition sections are *H* and *h* respectively. For instance, one can call the vertical line as a

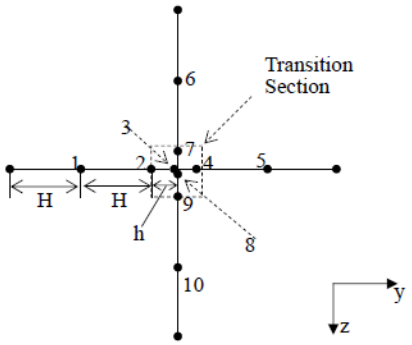

Fig. 4.3 Transition section

nodal line on the pier strip and the horizontal line as a nodal line on the deck strip. The vertical and horizontal lines overlap at knots 3 and 8 of the deck and the pier strips, respectively. To model a fixed bearing, which allows rotations but restricts translations, for example, the knot 3 and knot 8 should have the same displacement value to achieve compatibility. In order to have identical displacement at knots 3 and 8, it is obvious that the ratio of h/H should be infinitely small. Using the developed transition section in the spline finite strip procedure, the compatibility for the displacements of different components of the structure is satisfied.

4.2.3 Stiffness, mass, and damping matrices

After defining the displacement functions for all the structural members of the long-span cable-stayed bridge, in the environment of integrated finite strip method, the stiffness [k] and mass [m] matrices of different components can be calculated using the standard finite element procedure, which will be applied in the following form

$$\left[k\right] = \int \left[B\right]_i^T \left[D\right]\left[B\right]_j dA \tag{4-11}$$

$$\left[m\right] = \int \rho t \left[N\right]_i^T \left[N\right]_j dA \tag{4-12}$$

in which ρ is the density of the strip and t is the thickness of the strip; [D] and [B] are the elastic matrix and the strain matrix respectively; [N] is the shape function matrix. Similar to the FEM, the IFSM strip properties are converted to nodal properties during the model formulation process, although the amount of nodes required are significantly reduced due to the semi-analytical nature of the IFSM method. Thus, the derived matrices can be assembled using the standard assembling techniques and these can make the global stiffness matrix [K] and the global mass matrix [M] of the bridge.

There are different methods for evaluating the damping matrix [C] [4.21]. In this research, the classic Rayleigh damping is adopted, in which the damping matrix of the bridge [C] is a function of stiffness and mass matrices of the bridge as below

$$\left[C\right] = \alpha\left[M\right] + \beta\left[K\right] \tag{4-13}$$

where α and β are the Rayleigh damping factors, which can be investigated by having two structural damping ratios ξ associated with two specific frequencies. The damping ratio of ξ the nth mode of a structure is given by

$$\xi_n = \frac{1}{2\omega_n}\alpha + \frac{\omega_n}{2}\beta \tag{4-14}$$

Assuming the same damping ratio ξ for two different modes, α and β can be calculated.

4.3 Time history analysis

There are two groups of numerical methods employed for dynamic and seismic analysis of long-span bridges subjected to spatially varying earthquake ground motion. The first group is called stochastic methods, and includes the random vibration method (RVM) and the response spectrum method (RSM). Random vibration approach is based on a statistical characterization of the set of motions at the supports. The Response Spectrum Method is widely known for seismic analysis of short-span bridges as they are assumed to be under uniform excitations [4.22]. It has been further extended for the seismic analysis of long-span structures. Nevertheless, the RSM needs more improvements to reach a good accuracy and efficiency.

The second group is named the deterministic methods, like the time-history method (THM). The time history method is the most popular method for dynamic analysis of complex bridge structures and can be applied for the seismic analysis of long-span bridges without theoretical difficulties. However, it requires a suitable selection of the ground acceleration record samples for solving the dynamic equations. The numerical results are then processed statistically to produce the quantities required by the design requirements [4.22]. The computational cost is very high for the THM, especially if it is performed in the environment of the finite element method. Using the finite strip method, it is believed that time history analysis costs much less.

The dynamic motion equation of a discrete bridge structure is written as

$$[M]\{\ddot{\delta}(t)\} + [C]\{\dot{\delta}(t)\} + [K]\{\delta(t)\} = \{P(t)\} \tag{4-15}$$

where $\{\delta(t)\}$ is the relative displacement parameter vector, [C] is the damping matrix, and $\{P(t)\}$ is the external force vector. For a linear multi-degrees of freedom structure subjected to uniform ground acceleration excitation $\ddot{x}_g(t)$, the equation of motion is expressed as

$$[M]\{\ddot{\delta}(t)\} + [C]\{\dot{\delta}(t)\} + [K]\{\delta(t)\} = -[M]e\ddot{x}_g(t) \tag{4-16}$$

where *e* is a vector indicating the degrees of freedom influenced by the ground motion. For a long-span bridge discretized by the integrated finite strip method and subjected to differential ground motions, the dynamic equation of motion in the global coordinate system is given by the following formulation

$$\begin{bmatrix} M_s & M_{sb} \\ M_{sb}^T & M_b \end{bmatrix} \begin{Bmatrix} \ddot{\delta}_s(t) \\ \ddot{\delta}_b(t) \end{Bmatrix} + \begin{bmatrix} C_s & C_{sb} \\ C_{sb}^T & C_b \end{bmatrix} \begin{Bmatrix} \dot{\delta}_s(t) \\ \dot{\delta}_b(t) \end{Bmatrix} + \begin{bmatrix} K_s & K_{sb} \\ K_{sb}^T & K_b \end{bmatrix} \begin{Bmatrix} \delta_s(t) \\ \delta_b(t) \end{Bmatrix} = \begin{Bmatrix} 0 \\ P_b(t) \end{Bmatrix} \tag{4-17}$$

in which the subscripts *b* and *s* represent the master (support displacements) and slave degrees of freedom of the long-span structure respectively, and $P_b(t)$ is the reaction force vector. M_s, C_s, and K_s are the mass, damping, and stiffness matrices, associated with the unrestrained degrees of freedom δ_s; M_b, C_b, and K_b are mass, damping, and stiffness matrices associated with the restrained (support displacements) degrees of freedom δ_b; and M_{sb}, C_{sb}, and K_{sb} are coupling mass, damping, and stiffness matrices. Moreover, δ_s, $\dot{\delta}_s$ and $\ddot{\delta}_s$ are absolute displacement, velocity and acceleration vectors of unrestrained degrees of freedom respectively, while δ_b, $\dot{\delta}_b$, and $\ddot{\delta}_b$ are absolute displacement, velocity and acceleration vectors of restrained (support) degrees of freedom respectively. It is worth to mention that in the case of a lumped-mass model, M_{sb} is equal to zero in Eq. (4-17).

In the case of non-uniform excitation, the absolute displacement vector δ_s is decomposed into dynamic displacement and pseudo-static displacement as below

$$\delta_s = y_s + y_r \tag{4-18}$$

where y_s and y_r are pseudo-static and dynamic displacement vectors of δ_s. Moreover, y_s satisfies the following relationship

$$y_s = -K_s^{-1} K_{sb} \delta_b \tag{4-19}$$

Substituting Equation (18) and Equation (19) into Equation (17) leads to

$$M_s \ddot{y}_r + C_s \dot{y}_r + K_s y_r = M_s K_s^{-1} K_{sb} \ddot{\delta}_b + (C_s K_s^{-1} K_{sb} - C_{sb}) \dot{\delta}_b \tag{4-20}$$

It should be noted that Eq. (4-20) cannot be reduced to the conventional Eq. (4-16) when δ_b represents uniform ground displacements [4.23]. In fact, in Eq. (4-20) it is assumed that the damping forces are dependent of the absolute velocity vector. To eliminate this

inconsistency, the damping forces should be assumed to be dependent of the relative velocity vector $\{y_r'^T, 0\}^T$ in Eq. (4-20), which leads to the following equation [4.22]

$$M_s \ddot{y}_r + C_s \dot{y}_r + K_s y_r = M_s K_s^{-1} K_{sb} \ddot{\delta}_b \tag{4-21}$$

or

$$M_s \ddot{y}_r + C_s \dot{y}_r + K_s y_r = M_s r \ddot{\delta}_b \tag{4-22}$$

where

$$[r] = K_s^{-1} K_{sb} \tag{4-23}$$

The matrix [r] is, in fact, the influence matrix describing the effect of the sub-structure on the super-structure.

There are different schemes for solving Eq. (4-16), the Newmark method, the Wilson-u method [4.23], and the precise integration method [4.24]. In this research, the time-stepping analysis in the framework of Newmark's method was applied, which is described in the following section.

4.3.1 Newmark scheme for numeral integration

Assuming that at $t = t_i$ and $t = t_{i+1}$, the equations of motion can be written as

$$[M]\{\ddot{\delta}_i\} + [C]\{\dot{\delta}_i\} + [K]\{\delta_i\} = \{P_i\} \tag{4-24}$$

$$[M]\{\ddot{\delta}_{i+1}\} + [C]\{\dot{\delta}_{i+1}\} + [K]\{\delta_{i+1}\} = \{P_{i+1}\} \tag{4-25}$$

Using the Newmark method, similar to other types of time-stepping methods, the bridge responses at $t = t_{i+1}$ can be predicted under the condition that the responses at $t = t_i$ and the loading at both times are known.

The responses at $t = t_{i+2}, t_{i+3}, t_{i+4}, \cdots$ can be calculated using an iteration process. As a result, the time history response of the bridge is obtained. According to Eqs. (4-24) and (4-25), the number of unknowns are more than the number of equations. For that reason, further assumptions must be introduced, so that the all the unknown responses can be solved.

As previously mentioned, there are a number of approximate methods, such as the excitation interpolation method, the central difference method, the Newmark's method and the

Wilson's θ method, that can be used for this purpose. In the present study, the Newmark's method is used, being considered as the most popular method due to its ability to deal with nonlinear structures, as well as structures with multiple degrees of freedom [4.25].

The assumption that $\dot{\delta}_{i+1}$ and δ_{i+1} are related to $\ddot{\delta}_{i+1}, \delta_i, \dot{\delta}_i$ and $\ddot{\delta}_i$ is made, as below

$$\dot{\delta}_{i+1} = \dot{\delta}_i + \left[(1-\gamma)\Delta t\right]\ddot{\delta}_i + (\gamma\Delta t)\ddot{\delta}_{i+1}$$

$$\delta_{i+1} = \delta_i + \Delta t\dot{\delta}_i + \left[(\frac{1}{2}-\lambda)\Delta t^2\right]\ddot{\delta}_i + (\lambda\Delta t^2)\ddot{\delta}_{i+1} \tag{4-26}$$

where Δt is the time increment, which is usually assumed to be a constant from step to step as $\Delta t = t_{i+1} - t_i$. The time increment Δt is generally assumed to be less than 1% of the period of the system. In Eq. (4-26) γ and λ are Newmark's parameters, which define the variation of the acceleration over a time step and determine the accuracy and stability of the method [4.25]. For the Newmark's parameters, $\gamma = 0.5$ and $1/6 < \lambda < 1/4$ are the typical values. Mathematically different set of parameters is assigned, depending on the various physical interpretations. Some examples are introduced in the following lines.

In the case of the average acceleration, in which the acceleration between t_i and t_{i+1} is considered as the average of $\ddot{\delta}_i$ and $\ddot{\delta}_{i+1}$, the Newmark's parameters are $\gamma = 0.5$ and $\lambda = 0.25$. In the linear acceleration, the acceleration between t_i and t_{i+1} varies linearly between $\ddot{\delta}_i$ and $\ddot{\delta}_{i+1}$, and the Newmark's parameters are $\gamma = 0.5$ and $\lambda = 1/6$. The Newmark's time history analysis has an incremental form. Subtracting Eq. (4-25) from Eq. (4-24) leads to

$$M\Delta\ddot{\delta}_i + C\Delta\dot{\delta}_i + K\Delta\delta_i = \Delta P_i \tag{4-27}$$

in which the response and the force increments are given by

$$\Delta\ddot{\delta}_i = \ddot{\delta}_{i+1} - \ddot{\delta}_i,\ \Delta\dot{\delta}_i = \dot{\delta}_{i+1} - \dot{\delta}_i,\ \Delta\delta_i = \delta_{i+1} - \delta_i, \tag{4-28}$$

Using the defined increments, Eq. (4-26) can be rewritten as

$$\Delta\dot{\delta}_i = \Delta t\ddot{\delta}_i + (\gamma\Delta t)\Delta\ddot{\delta}_i$$

$$\Delta\delta_i = \Delta t\dot{\delta}_i + \frac{1}{2}\Delta t^2\ddot{\delta}_i + (\lambda\Delta t^2)\Delta\ddot{\delta}_i \tag{4-29}$$

or

$$\Delta\ddot{\delta}_i = \frac{1}{\lambda\Delta t^2}\Delta\delta_i - \frac{1}{\lambda\Delta t}\dot{\delta}_i - \frac{1}{2\lambda}\ddot{\delta}_i$$

$$\Delta\dot{\delta}_i = \frac{\gamma}{\lambda\Delta t}\Delta\delta_i - \frac{\gamma}{\lambda}\dot{\delta}_i + \Delta t(1-\frac{\gamma}{2\lambda})\ddot{\delta}_i \tag{4-30}$$

Substituting Eq. (30) into (27) leads to

$$\hat{K}\Delta\delta_i = \Delta\hat{P}_i \tag{4-31}$$

in which

$$\hat{K} = K + \frac{\gamma}{\lambda\Delta t}C + \frac{1}{\lambda\Delta t^2}M \tag{4-32}$$

$$\Delta\hat{P}_i = \Delta P_i + (\frac{M}{\lambda\Delta t} + \frac{\gamma C}{\lambda})\dot{\delta}_i + \left[\frac{M}{2\lambda} + \Delta t(\frac{\gamma}{2\lambda} - 1)\right]\ddot{\delta}_i \tag{4-33}$$

The displacement increment $\Delta\delta_i$ can be obtained through Eq. (4-31) while the acceleration and velocity increments are obtained from Eq. (4-30) respectively.

The time history response of the bridge estimated by the Newmark's method can be programmed using programming languages or technical software. In the present research, MATLAB software was used as it has numerous mathematical subroutines for scientific computation including the present problem [4.25].

4.4 Numerical studies

4.4.1 General

As a case study, the Kap Shui Mun Bridge in Hong Kong has been selected as shown in Fig. 4.4, which is a massive long-span cable-stayed bridge structure, with the total length of 750 m and the main span of 430 m. The Kap Shui Mun Bridge is located between the islands of Lantau and Mawan, and is the world's longest cable-stayed bridge, which carries both road and railway traffics. The bridge structure includes two concrete towers of 145 m and 133 m height, four concrete piers, namely, piers 1, 2, 3, 4 with the lengths of 24.8 m, 32.9 m, 16.9 m, and 26.8 m respectively, 176 cables, bearings, as well as one deck. In order to investigate the response of the bridge under seismic loading, in the current research, the bridge model has been simplified with a number of assumptions, which will be explained in the following sections.

4.4.2 Finite strip modeling of the bridge

The main span of the Kap Shui Mun Bridge consists of a composite steel/concrete structure. The side spans are made of concrete box-girders. Here, the deck is modeled as the flat shell in the integrated finite strip environment. The material properties considered for the bridge model were employed as reported by Zhang et al. [4.26], which are shown in Table 4.1, and the geometrical properties are illustrated in Fig. 4.5. The deck is divided into four shell

Table 4.1 Material Properties of the Bridge Deck [4.4]

Properties	Main Span	Side Spans
Modulus of elasticity (kPa)	2.00×10^{8}	3.00×10^{7}
Mass density (kg/m^3)	3880	3630
Poisson's ratios	0.3	0.2
Moment of inertia (vertical) (m^4)	191	363
Moment of inertia (transverse) (m^4)	2530	5560

spline strips, and all the strips are divided into several sections. The lengths of the sections vary along the deck so that the locations of the knots could match the ends of cables.

The strip meshing of the towers is shown in Fig. 4.6. The one-dimensional Column Strip is adopted for the tower structures in the finite strip model. In each tower, there are three struts linking the upper, intermediate and lower parts of the towers, respectively. The link beams are rigid and all six degrees of freedom of the joints should be restrained. However, in one dimensional column strip, each knot has only three translational degrees of freedom and the rotational degrees of freedom are not taken into account. The four piers of the bridge are also modeled by one-dimensional column strips. The boundary conditions for the towers and the piers are all fixed at the connection with the ground. The 176 cables are assumed to be linear elastic elements and are modeled by cable strip in the finite strip model. It should be noted that all the cables are prestressed, by converting the thermal loads into equivalent tension forces applied at the two ends of the strips.

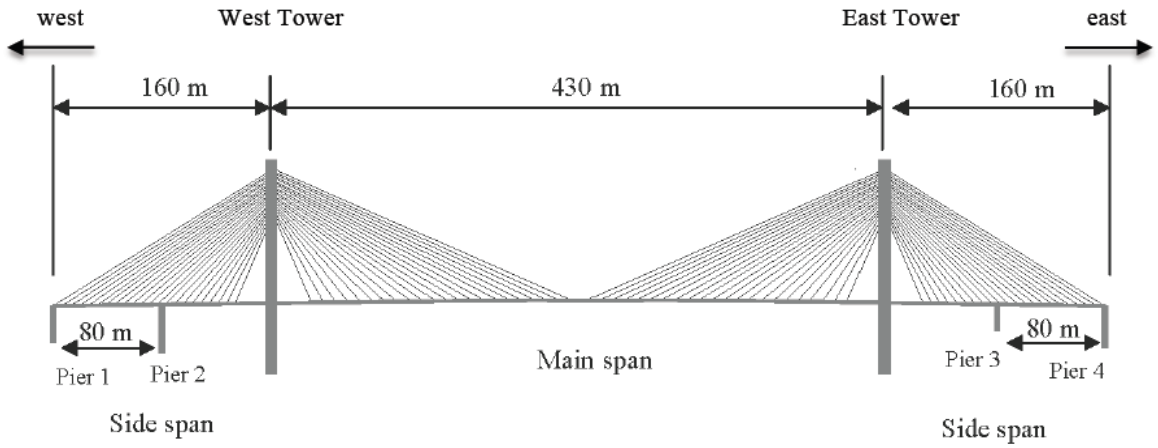

Fig. 4.4 Kap Shui Mun Bridge (Naderian et al. 2014)

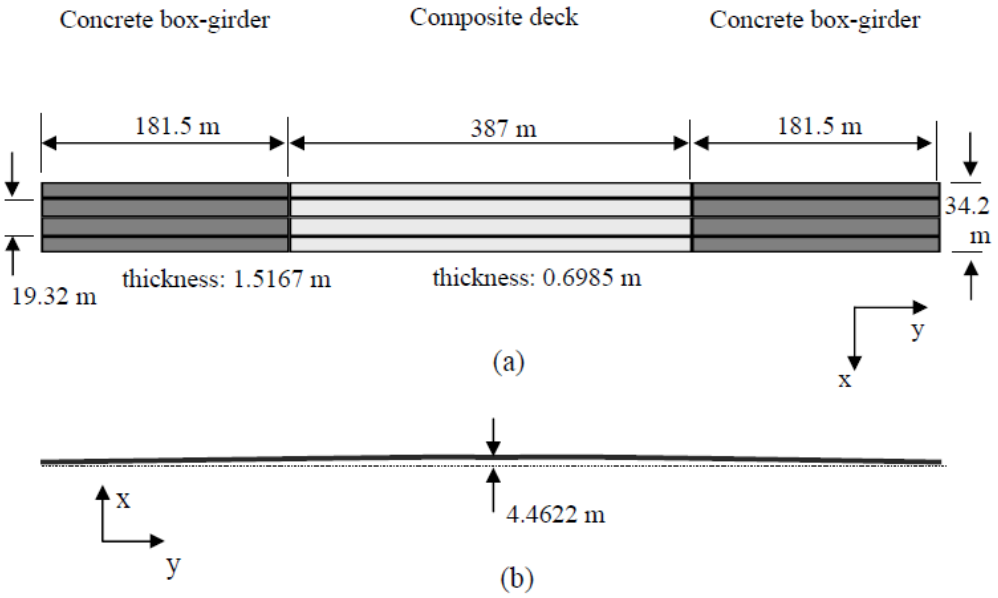

Fig. 4.5 Geometrical Properties of the deck: (a) Top view; (b) Front view

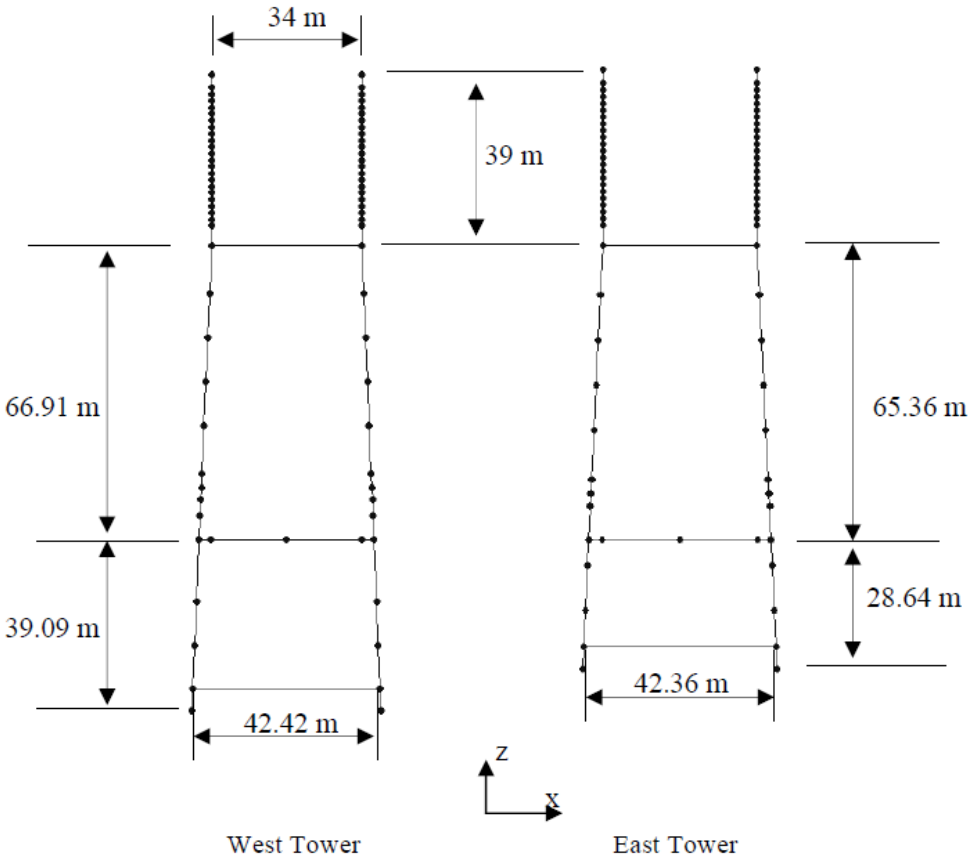

Fig. 4.6 The towers of the KSM Bridge

4.4.3 Verification of the integrated approach

In order to validate the integrated finite strip method for the dynamic analysis of long-span cable-stayed bridge, the first ten natural frequencies of the Kap Shui Mun Bridge are obtained and listed in Table 4.2. The first two vibration modes of the bridge occur in the towers; while the next modes are vertical bending of the deck, lateral bending of the deck, and torsional mode respectively. The finite strip results are compared with those obtained by finite element method as well as field measurement tests for vibration of deck [4.18]. The FE analysis has been performed by SAP2000 software. In the SAP model, the deck is modeled as thin shell elements, while the piers and the towers are modeled as beam elements; for the cables, truss elements are assigned. As it can be clearly noticed in Table

Table 4.2 Natural frequencies of the Kap Shui Mun Bridge

Mode number	**Natural frequency (Hz)**			**Nature of mode shape**	**Error %**	
	IFSM (1)	FEM (2)	Field tests [4.18] (3)		**[(1)-(2)/(2)]**	**[(1)-(3)/(3)]**
1	0.2113	0.2061	---	First mode of the tower	2.5	---
2	0.2409	0.2338	---	Second mode of the tower	3.0	---
3	0.4250	0.4226	0.39	First vertical bending of the deck	0.5	8.9
4	0.5217	0.5160	0.49	First lateral bending of the deck	2.1	6.4
5	0.7526	0.7179	0.83	First torsional mode of the deck	4.8	-9.3
6	0.8523	0.8500	0.66	Second vertical bending of the deck	0.2	29.1
7	0.9305	0.9257	0.90	Second lateral bending of the deck	0.5	3.3
8	1.0032	1.0023	1.07	Third vertical bending of the deck	0.0	-6.2
9	1.1381	1.1048	---	Third mode of the tower	3.0	---
10	1.1391	1.1058	---	Fourth mode of the tower	3.0	---

4.2, there is a very good agreement between the results, which confirms the accuracy of the integrated finite strip method in terms of dynamic analysis. Slightly higher values for the natural frequencies were found when employing the integrated finite strip method, especially for two mode shapes, the first lateral mode and the first torsional mode of the deck. The maximum error percentage when comparing the natural frequencies obtained

from the integrated finite strip method with those from the finite element analysis was 4.8 %, while comparing the same results with the field measurement tests data, the maximum error percentage was below 10 %, except for the second vertical bending mode of the deck, for which the measurements showed considerable difference between the results, thus the registered data being questionable [4.18]. In general, the field measurements reported slightly lower values for the natural frequencies of the Kap Shui Mun Bridge [4.18], when compared with both numerical methods, the IFSM and the FEM. The first two modes reported by the IFSM and the FEM, were bending tower modes, therefore these were not reflected in the field measurements data, which considered only the deck vibration measurements.

Natural frequencies of long-span cable-stayed bridges have major effect on the bridge dynamic performance. Therefore, high consistency of the natural frequencies is very important; moreover the good agreement between results confirms that the integrated finite strip method is capable of capturing the bridge dynamic characteristics. Consequently, the seismic analysis of long-span cable-stayed bridges can be performed in a very efficient manner.

4.4.4 Seismic analysis

Several case studies are performed for the seismic analysis of the Kap Shui Mun (KSM) Bridge using the time domain method within the integrated finite strip method environment. Moreover, the results are validated against finite element analysis for some of the cases analyzed. In order to investigate the seismic response of KSM Bridge, certain critical points for which the displacements and stresses can be problematic for the structure, are selected as shown in Fig. 4.7. The dynamic analysis results for these locations are evaluated and plotted in the following sub-sections.

In the finite element SAP model, the direct integration method was adopted, when performing the dynamic analysis.

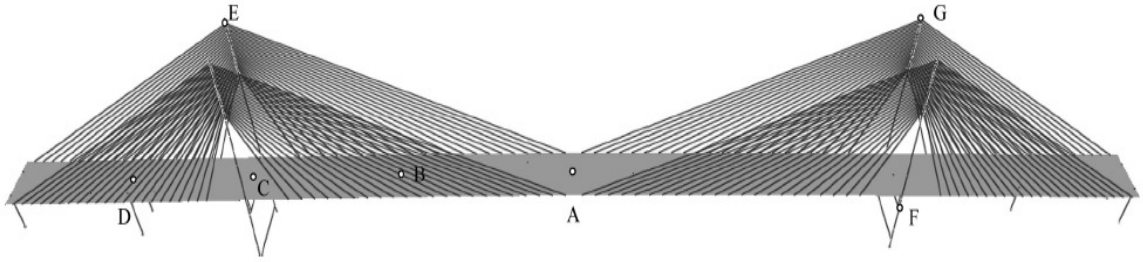

Fig. 4.7. Some critical points for seismic response investigation

4.4.4.1 Seismic wave effect on long-span cable-stayed bridge

In the category of short-span bridges, all supports can be assumed to move uniformly (uniform excitation) under seismic loads. On the other hand, various spatial effects such as the wave-passage effect, the incoherence effect, and the local site effect may play an important role in the seismic response of the long-span bridges. Wave-passage effect is a dynamic phenomenon in which seismic waves arrive at different supports at different times. Incoherence effect refers to the loss of coherence of seismic waves due to multiple reflection and refraction waves, as they propagate through the highly inhomogeneous soil medium. Also the change in the amplitude and frequency content of seismic ground motion, owing to different local soil conditions is known as local effect [4.27]. The wave-passage effect is of particular importance for the seismic response of long-span bridges, while the incoherence effect is of comparatively less importance [4.22].

4.4.4.2 Seismic behavior under uniform excitation

As the simplest case, all the degrees of freedom in the corresponding direction vibrate under the same ground motion. An artificial sine wave, as well as a real seismic wave, are selected and applied to the bridge structure, and their effects are investigated using the integrated finite strip method.

Under the effect of the sine wave ground acceleration with the amplitude of one, the longitudinal acceleration and the displacement output results at point F, in the east tower of the KSM Bridge are obtained and shown in Figs. 4.8 and 4.9, respectively, and these are compared with the finite element time-history analysis. A good agreement can be seen

between the results of IFSM and FEM for the time-history analysis under uniform excitation. As it can be seen from the curves, the amplitude of both displacements and accelerations are increasing, and the rate of the increase in the first ten seconds is higher than for the following time intervals. However, the amplitude of accelerations and displacements responses obtained from the finite strip time-history analysis are slightly higher than the finite element results.

As further research, the Chichi earthquake, a real earthquake wave as plotted in Fig. 4.10, is assigned to all degrees of freedom of the KSM Bridge, in the transverse direction. The same analysis approach is performed by both IFSM and FEM, and the transverse acceleration and displacement results at point B in the deck of the Kap Shui Mun Bridge are calculated and

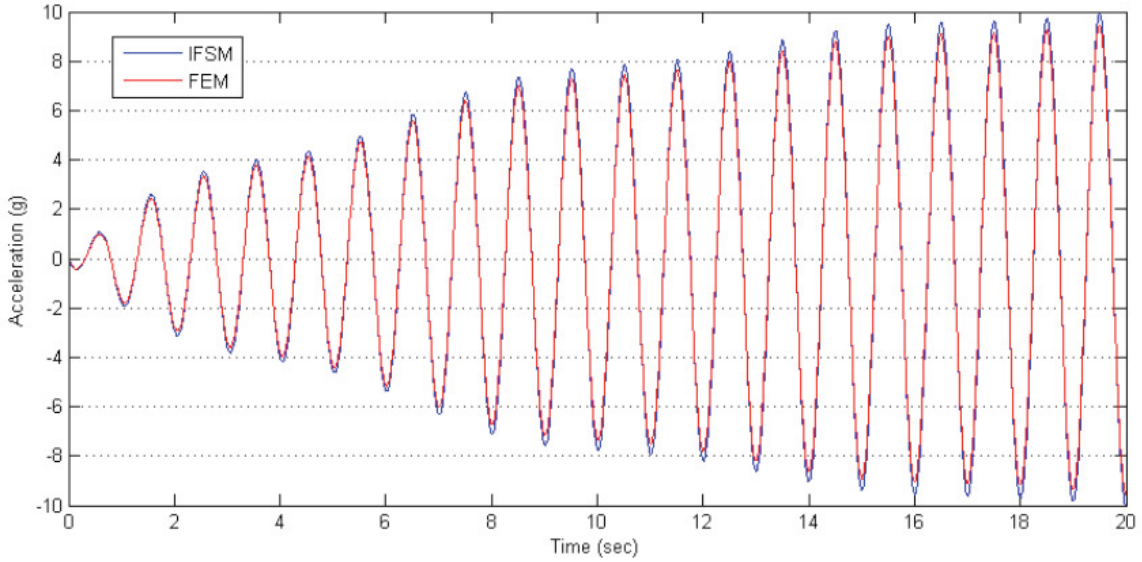

Fig. 4.8 Longitudinal acceleration responses under uniform sine waves excitation at point F (see Fig. 4.7) at the top of the East Tower

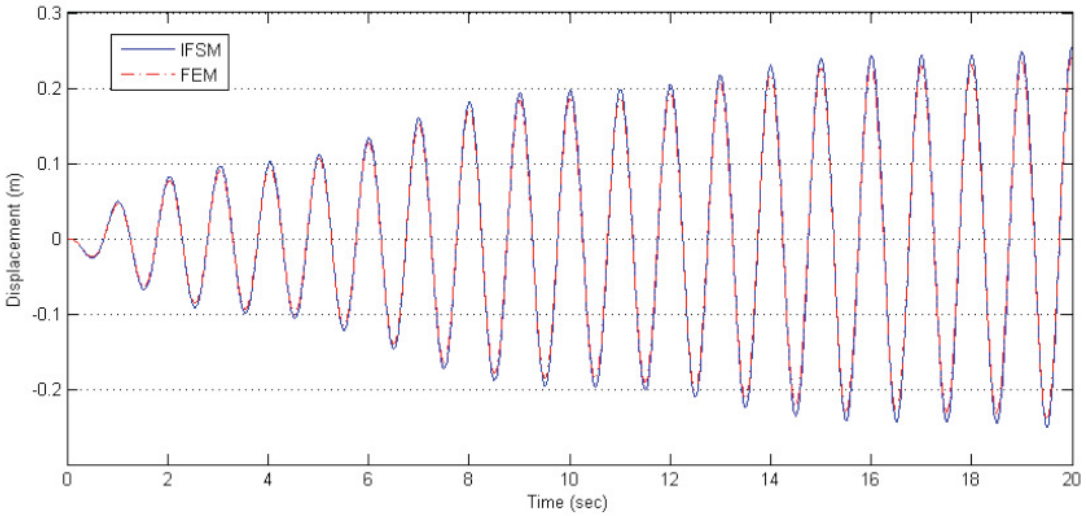

Fig. 4.9 longitudinal displacement responses under uniform sine waves excitation at point F (see Fig. 4.7) at the top of the East Tower

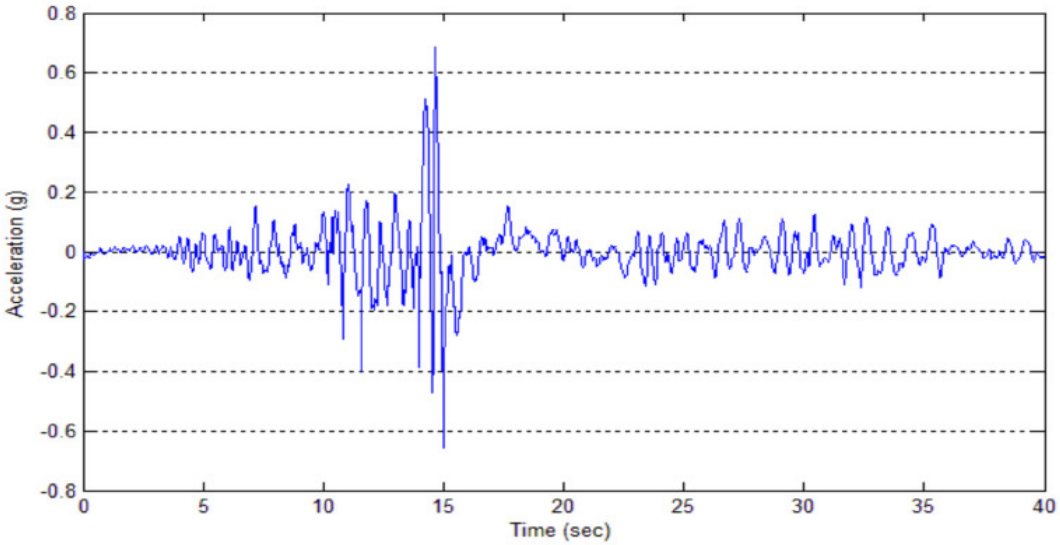

Fig. 4.10 The acceleration record of Chichi earthquake

shown in Figs. 4.11 and 4.12, respectively. In contrast with the sine wave excitation (Figs. 4.8 and 4.9), the seismic responses under Chichi earthquake are not uniform. According to Figs. 4.11 and 4.12, the maximum displacements and the maximum accelerations are

encountered in the period between 15 to 20 seconds. It is worth noting that the amount of displacement registered before this period is very low, being consistent with the low acceleration input of the Chichi earthquake for the same time interval. Again, the numerical results from both FEM and IFSM for time-history analysis are in very good agreement.

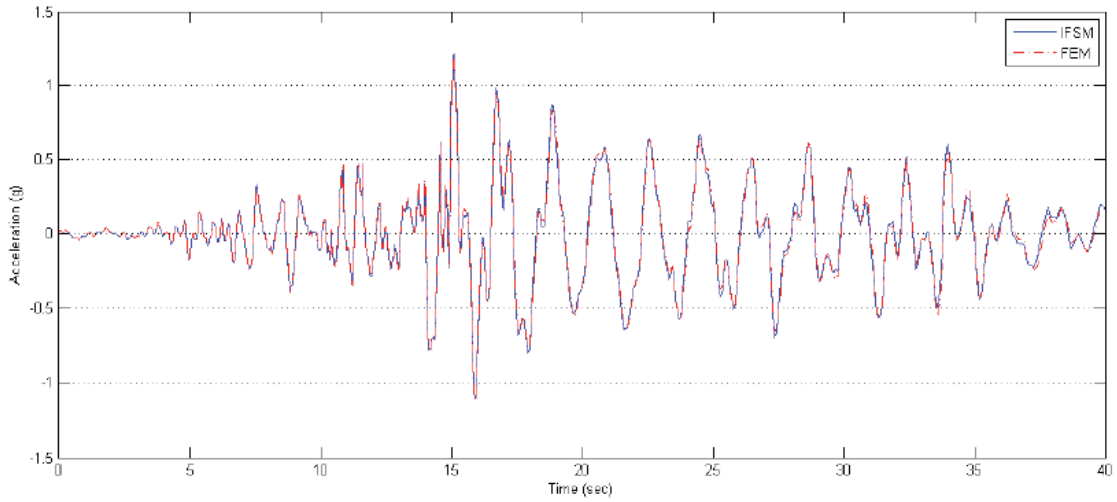

Fig. 4.11. Transverse acceleration responses under uniform Chichi earthquake excitation at point B (see Fig. 4.7) on the deck

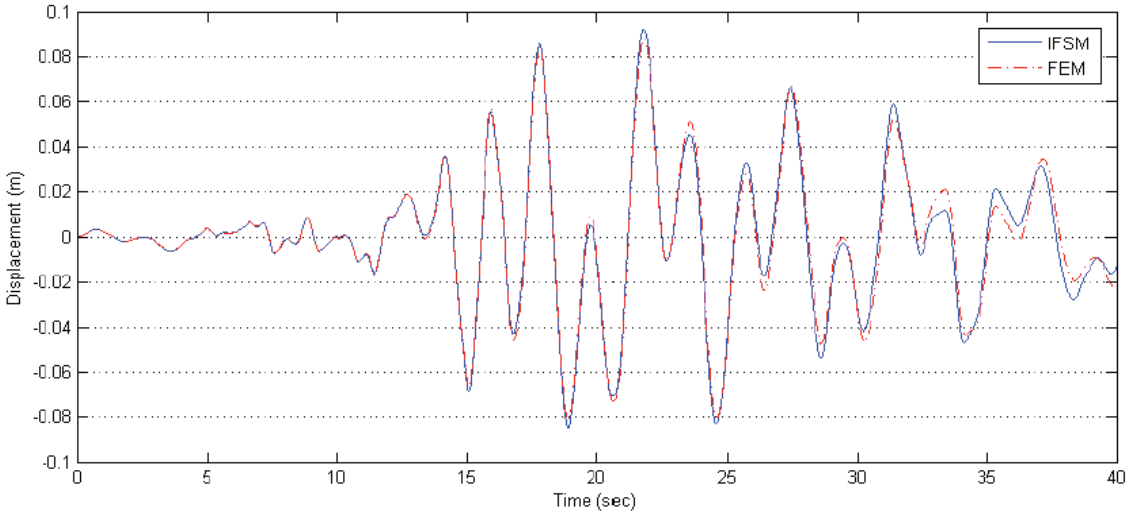

Fig. 4.12.Transverse displacement responses under uniform Chichi earthquake excitation at point B (see Fig. 4.7) on the deck

4.4.4.3 Seismic behavior under non-uniform excitation

When considering non-uniform excitation of long span bridges, different motions should be prescribed at different supports. Using the integrated finite strip and time domain methods, the effects of wave passage and varying seismic excitations as the samples of non-uniform excitations applied to Kap Shui Mun Bridge model are studied.

4.4.4.3.1 Wave passage effect

Wave passage effect accounts for the time delay in ground motions, as the seismic waves do not arrive at bridge foundations at the same time, especially for massive structures, such as long-span bridge, in which the distance between the piers and the towers is long. Wave passage or out-of-phase effects, where non-vertical waves reaching different points at the ground surface, at different times, and producing a time shift between the motions at these points.

The Chichi earthquake wave is adopted as the input source, however, for the parametric study, the velocities of the earthquake waves are assumed to be 500 m/s and 1000 m/s, in the longitudinal direction. The earthquake wave is assumed to start propagating from the first west pier, and afterwards the ground motion will be transmitted to the following towers and piers one by one. In the finite strip model, this is achieved by inputting the seismic waves with different time lags, at the various supports. An earthquake wave with infinite velocity is also adopted, which means that there is no time lag when transmitting the seismic wave between different supports. This is equivalent to the uniform excitation.

After applying the non-uniform excitation from Chichi earthquake in the longitudinal direction, but with different wave velocities, the acceleration and displacement responses of point E, situated at top of the west tower are determined as depicted through Figs. 4.13 to 4.18. Looking at seismic curves, it can be noticed that the maximum responses were encountered when the bridge is under the effect of the uniform excitation (Figs. 4.15 and 4.18). Furthermore, the maximum amplitudes of displacement and acceleration are identified in the period between 15 to 20 seconds for all the velocities investigated. It can be concluded that under uniform excitation the displacements and the accelerations of the bridge are higher than that of non-uniform excitation. As the velocity of the earthquake waves

increases, the amplitude of the accelerations increases. According to Figs. 4.16 and 4.17, the maximum displacement recorded at point E decreases when the velocity increases from 500 m/s to 1,000 m/s.

4.4.4.4 Varying seismic excitation

In the time history method, the numerical results are highly dependent on the selected ground acceleration sample records. To investigate the dynamic behavior of a long span

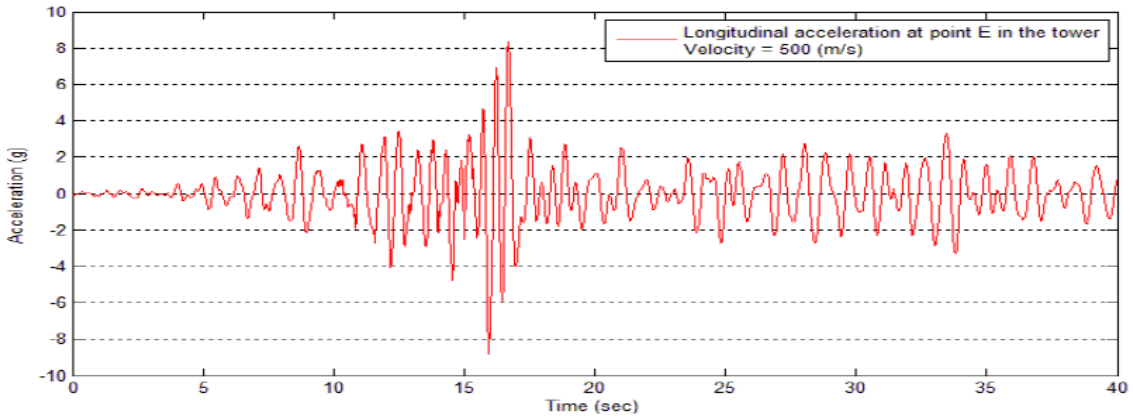

Fig. 4.13 Longitudinal acceleration at point E (see Fig. 4.7) at the West Tower for velocity = 500 m/s

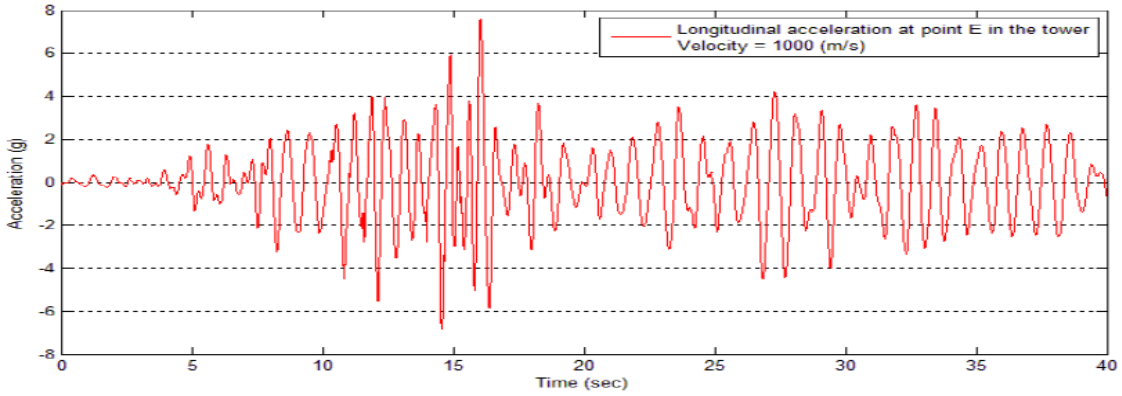

Fig. 4.14 Longitudinal acceleration at point E (see Fig. 4.7) at the West Tower for velocity = 1000 m/s

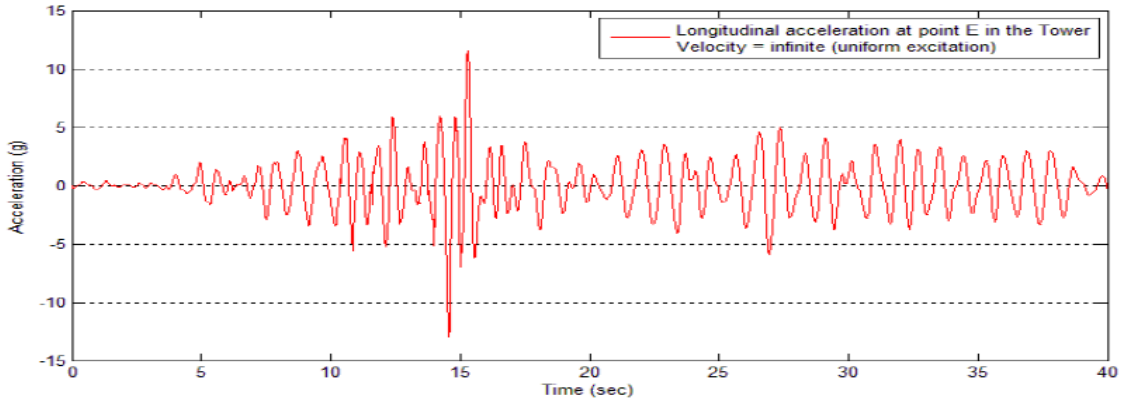

Fig. 4.15 Longitudinal acceleration at point E (see Fig. 4.7) at the West Tower for velocity = infinite

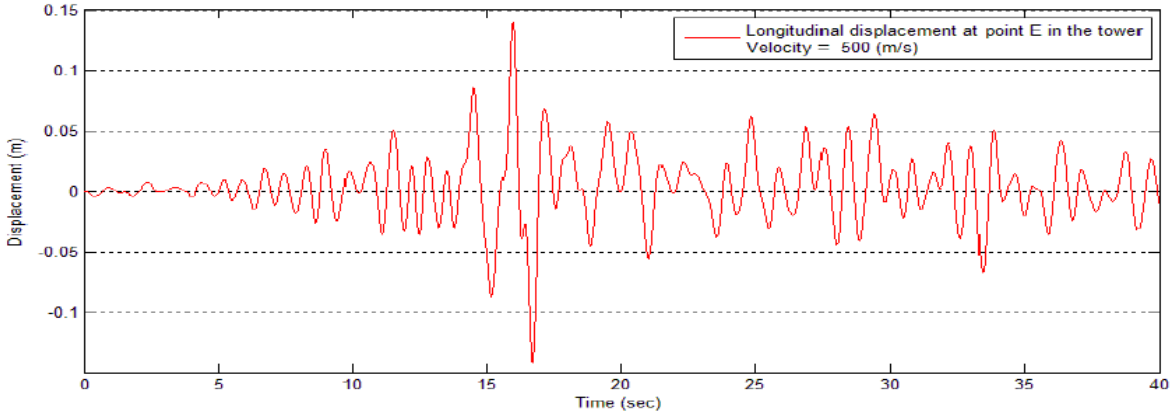

Fig. 4.16 Longitudinal displacement at point E (see Fig. 4.7) at the West Tower for velocity = 500 m/s

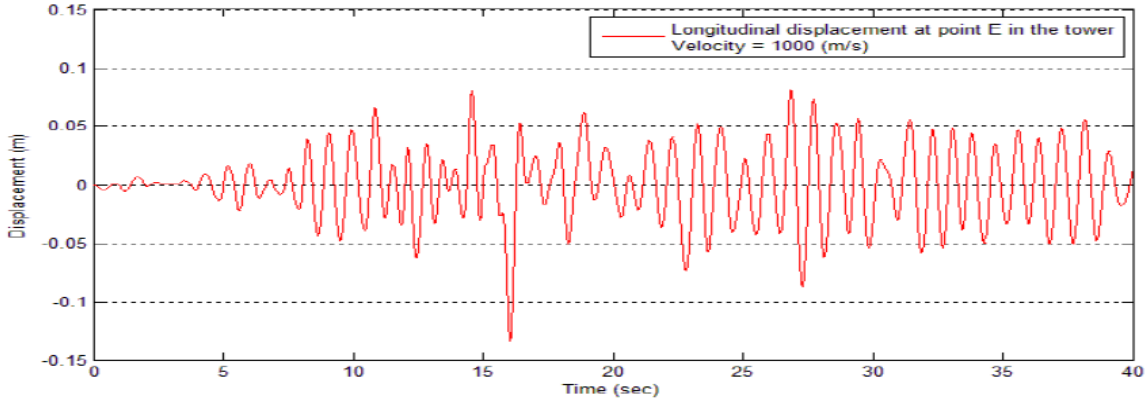

Fig. 4.17 Longitudinal displacement at point E (see Fig. 4.7) at the West Tower for velocity = 1,000 m/s

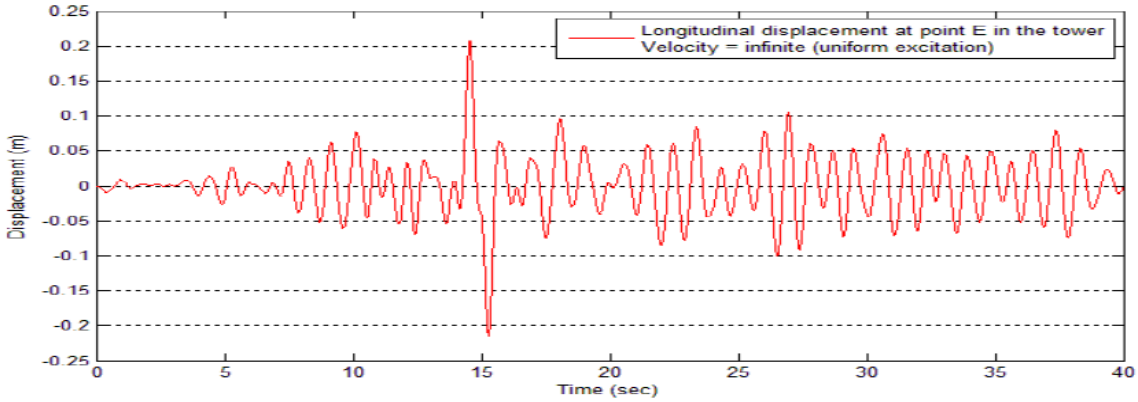

Fig. 4.18 Longitudinal displacement at point E (see Fig. 7) at the West Tower for velocity = infinite

cable-stayed bridge under varying seismic excitation at the supports, the earthquake records from SMART-1 (Strong Motion Array in Taiwan, phase I) is used. SMART-1 is a dense digital array of strong motion seismographs built by the Institute of Earth Sciences (Taiwan) and the University of California at Berkeley. The earthquake records in SMART-1 are the raw data observed at different places during an earthquake event. Therefore, the records have already included the influence of the incoherence effect, attenuation effect and site effect. Two acceleration records, Input-1 and Input-2, observed at two places at distance 1,000 m apart are used. The vertical and longitudinal components of both acceleration records are illustrated in Figs. 4.19 and 4.20 respectively.

(a)

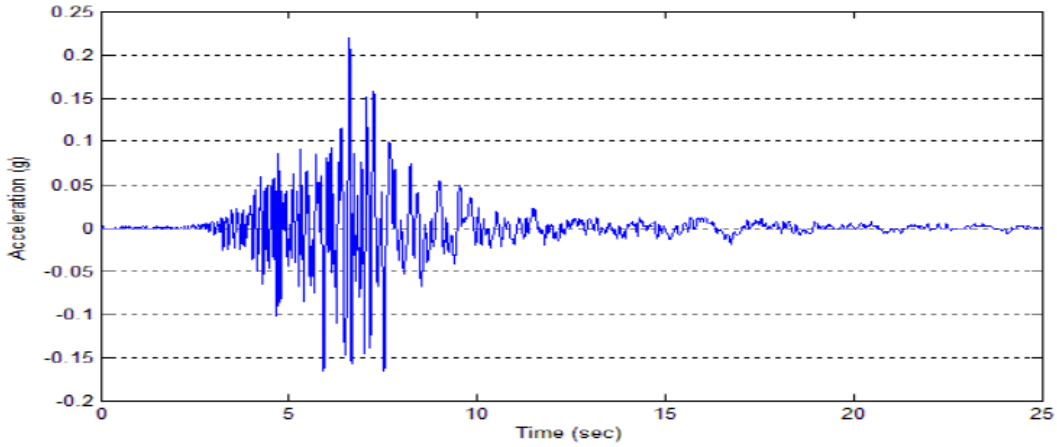

(b)

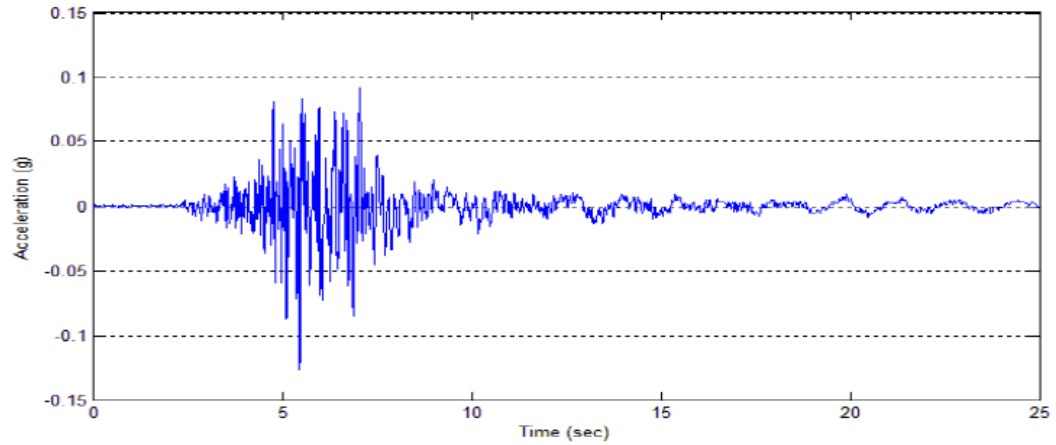

Fig. 4.19 Vertical components of seismic waves: (a) Input-1; (b) Input-2

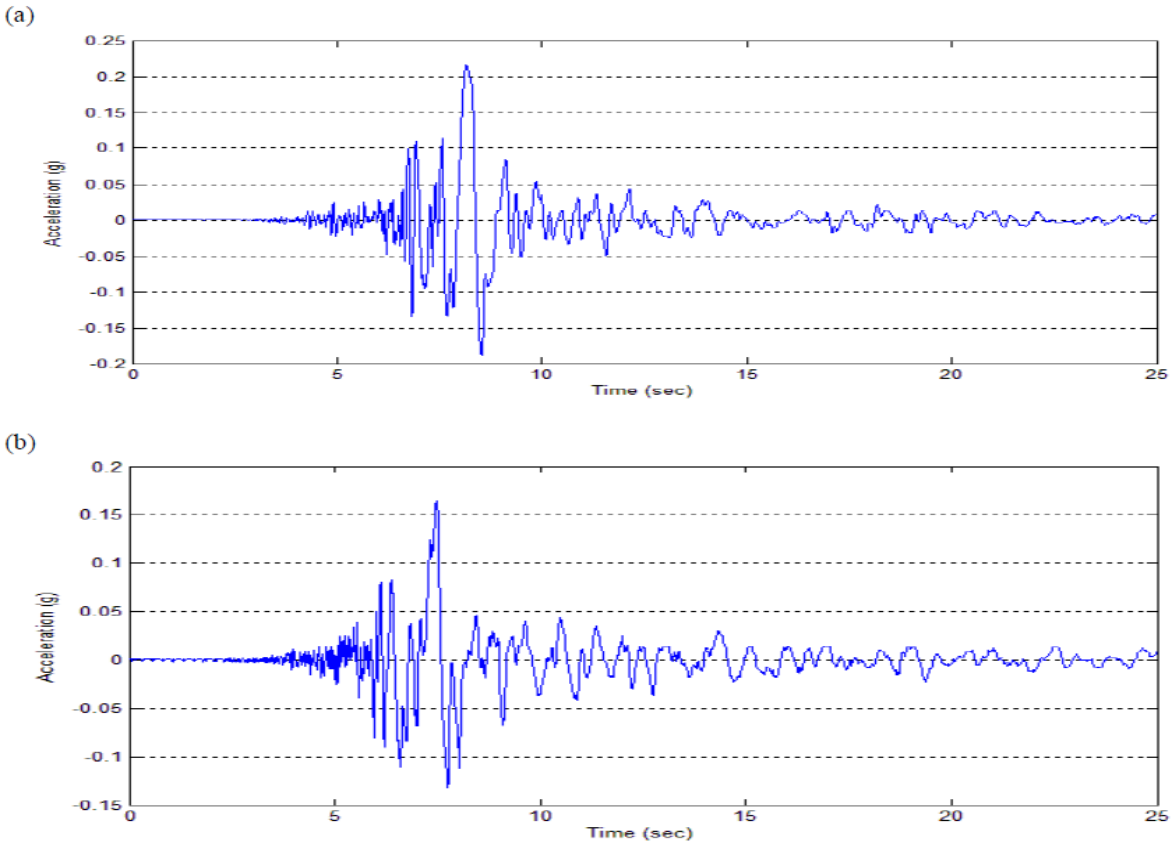

Fig. 4.20 Longitudinal components of seismic waves: (a) Input-1; (b) Input-2

Three analysis cases are undertaken: for the first and second cases, Input-1 and Input-2 are assigned to the entire bridge at the supports respectively. Thus, these two cases correspond to the uniform excitation. In the third case, Input-1 is applied to the two west piers and west tower of the Kap Shui Mun Bridge, while Input-2 is applied to two east piers and east tower. The vertical displacement response at point A, in the middle of the deck and the longitudinal displacement response at point G, at the top of the east tower are obtained and presented in Figs. 4.21 to 4.23 and Figs. 4.24 to 4.26 respectively. The seismic response in different case studies can be thus compared, and it can be witnessed that under uniform excitations (Figs. 4.21, 4.22, 4.24, and 4.25), the amount of displacements at points A and G are higher than those obtained from non-uniform excitation (Figs. 4.23 and 4.26). In almost all cases, the displacement is zero at the targeted points from the start time to t = 5 sec. Also, the maximum displacements occur in the period between 10 and 15 seconds. It seems that in all three cases the displacement curves are converging to zero.

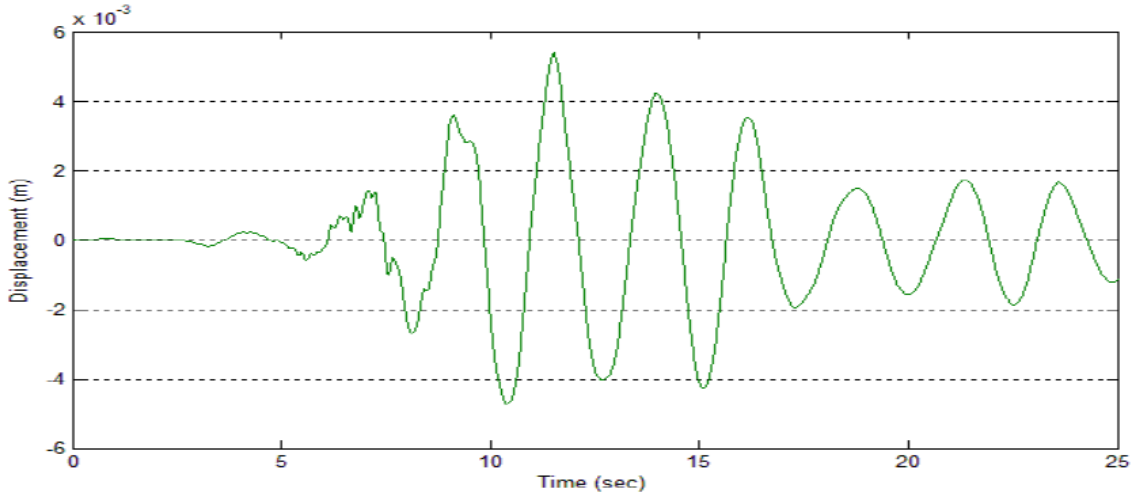

Fig. 4.21 Vertical displacement responses at point A (see Fig. 4.7) on the deck: Input-1 + Input-1 (see Fig. 4.19)

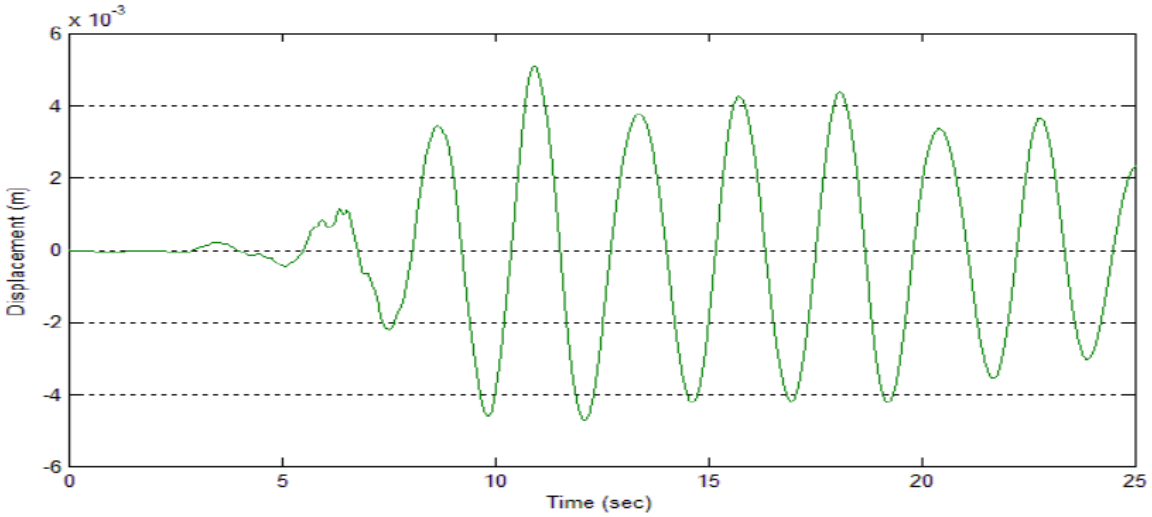

Fig. 4.22 Vertical displacement responses at point A (see Fig. 4.7) on the deck: Input-2 + Input-2 (see Fig. 4.19)

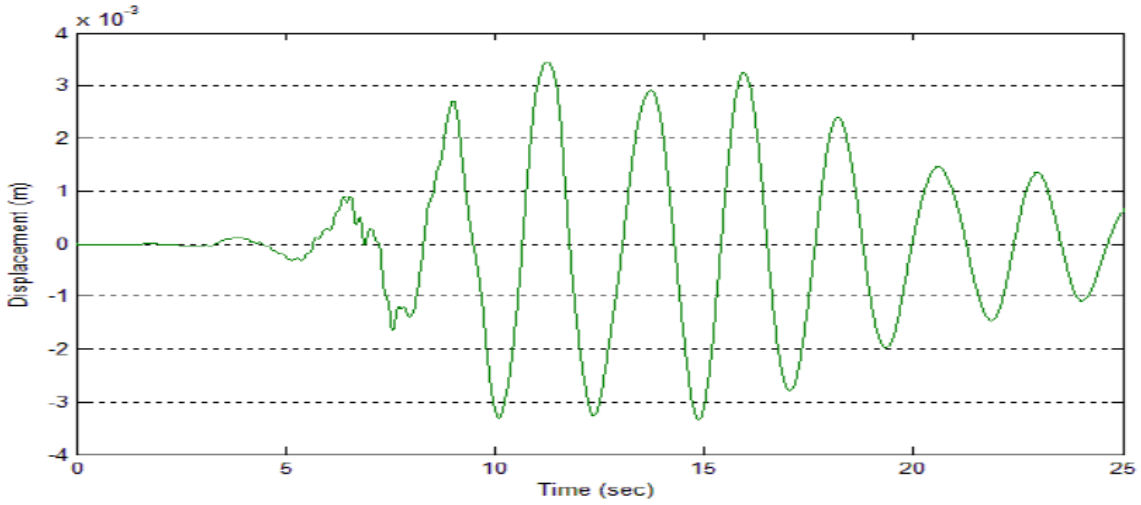

Fig. 4.23 Vertical displacement responses at point A (see Fig. 4.7) on the deck: Input-1 + Input-2 (see Fig. 4.19)

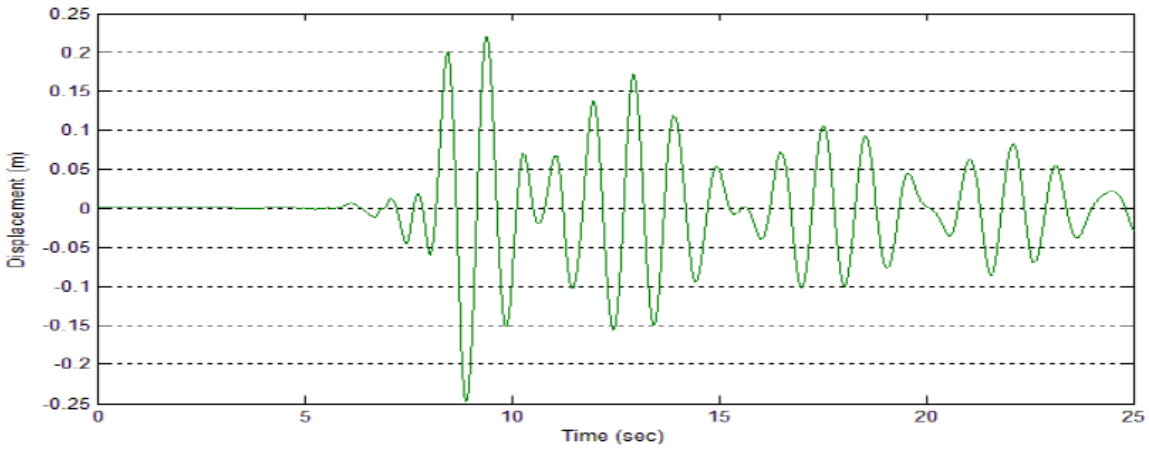

Fig. 4.24 Longitudinal displacement responses at point G (see Fig. 4.7) on the East Tower: Input-1 + Input-1 (see Fig. 4.20)

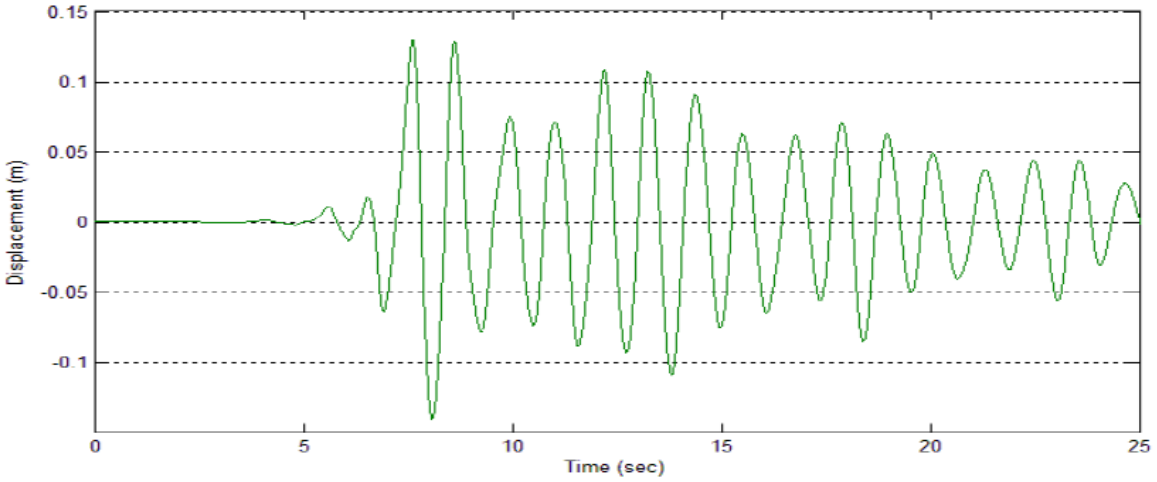

Fig. 4.25 Longitudinal displacement responses at point G (see Fig. 4.7) at the East Tower: Input-2 + Input-2 (see Fig. 4.20)

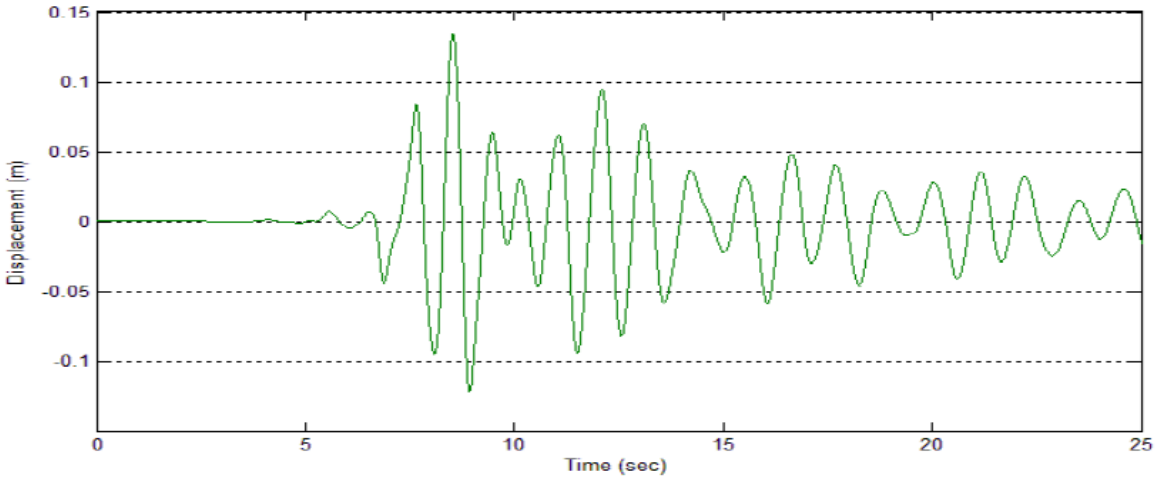

Fig. 4.26 Longitudinal displacement responses at point G (see Fig. 4.7) at the East Tower: Input-1 + Input-2 (see Fig. 4.20)

4.5 Conclusions

The present research was carried out in the environment of the integrated finite strip method, on seismic analysis of long-span cable-stayed bridges. Using the integrated system, the dynamic properties of the whole bridge can be derived by employing the finite strip method. Current practice of using the finite strip methods for performing dynamic analysis is limited

to investigation of the bridge super-structure, subjected to simulated boundary conditions over the pier supports and cables. Subsequently, the interactions between the bridge deck (super-structure) and the other components could not be considered using the conventional finite strip methods. Using the finite strip solution proposed in the current research, the entire bridge can be modeled as an integrated system, in which the structural interactions between the structural elements can be considered as well.

In the present study, the development of the integrated finite strip method (IFSM) was briefly presented. Using the stiffness and mass matrices derived from IFSM, the time history analysis of cable-stayed bridges was performed by the Newmark's method. The proposed dynamic finite strip analysis was formulated and programmed by a comprehensive computer programs including C++ and MATLAB. The accuracy of the proposed technique was evaluated by comparing the natural frequencies of the Kap Shui Mun bridge obtained by finite strip method, with those obtained by finite element method, and reported from the field test measurements, and were found to be in very good agreement, the difference in values being lower than 4.8% and 10%, respectively. The seismic analysis of the Kap Shui Mun Bridge, under uninform and nonuniform excitations, employed within the IFSM, showed that the displacement and acceleration responses at different locations along the bridge were higher for uniform earthquake excitations, which was also consistent with the results obtained from the FEM analysis of the same bridge.

The computational time is a very important factor in seismic analysis of long-span bridges. Due to the considerable reduction in the degrees of freedom, the developed code for the IFS method is efficient enough in complicated analyses of massive structures, like the dynamic analysis of Kap Shui Mun Bridge. The complete modeling of a long-span cable-stayed bridge using integrated finite strip method and the application of time domain method suggest that, the seismic analysis of a complicated structure can be performed in minimal time. The numerical results demonstrate that the convergence and efficiency of the IFS method is very high in comparison with other numerical methods.

References

[4.1] Cook, R. D., Malkus, D. S. and Plesha, M. E. (1989), Concepts and applications of finite element analysis.3rd Ed., Wiley, New York, NY, USA.

[4.2] Cheung, Moe M. S., Shen, Zhenyuan., Chan, Ben Y.B., (2009) Integrated Finite Strip Solution for Box Girder Bridges and Slab-on-girder Bridges, Journal of Computer Modeling in Engineering and Science, vol.45, no.2, pp.155-177

[4.3] Shen, Zhenyuan., Cheung, Moe M. S., Naderian, Hamidreza., Dragomirescu, Elena., (2013), An Integrated Finite Strip Solution for Dynamic Analysis of Continuous Multi-span Bridges, Proceedings of the 3rd Specialty Conference on Mechanics and Materials, Montreal, Canada

[4.4] Naderian, Hamidreza., Cheung, Moe M. S., Shen, Zhenyuan., Dragomirescu, Elena., (2015), Integrated Finite Strip Analysis for Long-span Cable-stayed Bridges, Computers & Structures, Volume 158, 1 October 2015, Pages 82-97

[4.5] Lee, M. and Penzien, J., (1983) Stochastic analysis of structures and piping systems subjected

to stationary multiple support excitations, Earthquake Eng. Struct. Dyn., 11, 91–110

[4.6] Dumanoglu, A. and Severn, R.T., (1990) Stochastic response of suspension bridges to earthquake forces, Earthquake Eng. Struct. Dyn., 19, 133–152

[4.7] Lin, Y.K., Zhang, R., and Yong, Y., (1990) Multiply supported pipeline under seismic wave excitations, J. Eng. Mech., 116, 1094–1108

[4.8] Berrah, M. and Kausel, E., (1992) Response spectrum analysis of structures subjected to spatially varying motions, Earthquake Eng. Struct. Dyn., 21, 461–470

[4.9] Kiureghian, A.D. and Neuenhofer, A., (1992) Response spectrum method for multi-support seismic excitations, Earthquake Eng. Struct. Dyn., 21, 713–740

[4.10] Ernesto, H.Z. and Vanmarcke, E.H., (1994) Seismic random vibration analysis of multi-support structural systems, J. Eng. Mech., ASCE, 120, 1107–1128

[4.11] Cheung, M. S., Cheung, Y. K., (1971) Natural vibrations of thin flat-walled structures with different boundary conditions, J Sound Vibr ;18:325–37

[4.12] Dawe, D.J., (2002) Use of the finite strip method in predicting the behaviour of composite laminated structures, ompositeStructures57, 11–36

[4.13] Wang, S., Zhang, Y., (2004) Vibration analysis of rectangular composite laminated plates using layerwise B-spline finite strip method, Composite structures,;(68), 349-358.

[4.14] Lau, David T., Cheung, M. S., Cheng, S. H., (2000) 3D Flutter analysis of bridges by spline finite strip method, Journal of Structural Engineering, Vol. 126, No. 10, October

[4.15] Cheng, S. H., Lau, David T., Cheung, M. S., (2003) Comparison of numerical techniques for 3D flutter analysis of cable-stayed bridges, Computers and Structures 81 2811–2822

[4.16] Li, W. Y. (1988), Spline finite strip analysis of arbitrarily shaped plates and shells, PhD thesis, Univ. of Hong Kong.

[4.17] Cheung, Y. K., Tham, L. G., and Li, W. Y. (1988), Free vibration and static analysis of general plate by spline finite strip, Computational Mechanics, 3(3), 187-197.

[4.18] Lau, C. K.; Mak, W. P.; Wong, K. Y.; Man, K. L.; Chan, W. Y.; Wong, K. F. (1999) Structural Performance Measurement and Design Parameter Validation for Kap Shui Mun Cable-Stayed Bridge, ADVANCES IN STEEL STRUCTURES, Vol.2, No.1

[4.19] Prenter, P. M., (1975) Splines and Variational Methods, New York: Wiley

[4.20] Cheung, M.S., Li, W., Chidiac, S. E., (1996) Finite strip analysis of bridges, 1st Edition. London: E & FN Spon,

[4.21] Humar, J., (2012) Dynamics of Structures, Third edition, CRC Press

[4.22] Clarence W. de Silva, (2005) Vibration and Shock Handbook, CRC Press Taylor & Francis Group

[4.23] Clough, R.W. and Penzien, J., (1993) Dynamics of Structures, McGraw-Hill, New York

[4.24] Zhong, W.X. and Williams, F.W., (1995) A precise time step integration method, Proc. Inst. Mech. Engrs, 208C, 6, 427–430

[4.25] Chang, C. C., (2004) Earthquake Engineering, Lecture Notes, Department of Civil and Environmental Engineering, HKUST

[4.26] Zhang, Q. W., Chang, T. Y. P., Chang, C. C., (2001) Finite element model updating for the Kap Shui Mun cable-staed bridge, Journal of Bridge Engineering, Vol. 6, No. 4, July/ August

[4.27] Saxena V., Deodatis G., Shinozuk M., (2000) EFFECT OF SPATIAL VARIATION OF EARTHQUAKE GROUND MOTION ON THE NONLINEAR DYNAMIC RESPONSE OF HIGHWAY BRIDGES, 12th World Conference on Earthquake Engineering, Auckland, New Zealand

Chapter 5

An optimal numerical scheme for composite laminated FRP plates and plate-assemblies with different boundary conditions

Abstract_ Fiber reinforced polymers, which are nowadays widely used as composite construction materials, are difficult to model due to their complicated mechanical and chemical properties. This paper proposes an optimal discretization scheme in the environment of the spline finite strip method for composite FRP laminates. The accuracy and convergence of the employed method is very high. Consequently, the computational time is very low, which makes the spline finite strip method an efficient tool for analysing composite laminated FRP structures. The proposed scheme is applied for linear elastic bending and stress analyses of laminated FRP plate structures. Unequally spaced B3-spline functions are augmented to the ordinary spline finite strip method. The coupling effects between the flexural and membrane degrees of freedom of the FRP laminate are considered in the finite strip solution. General boundary and loading conditions can be handled. The accuracy of the laminate spline approach for different boundary conditions as well as stiffened FRP plates and highly asymmetric laminates are verified through comparing with finite element results. A number of case studies are performed to prove that the developed spline finite strip technique can be effectively applied for numerical modeling of composite FRP laminated plate structures.

Keywords: Fiber-reinforced polymer (FRP)**;** composite laminated plate; spline finite strip method; bending analysis; stress analysis; linear elastic

5.1 Introduction

Composite structures are usually constructed in the form of laminates consisting of multiple laminas oriented in the desired directions and perfectly bonded together. Composite laminated plates, such as fiber reinforced polymer (FRP) composites, have been successfully used in aerospace and marine applications for over 50 years and are now increasingly employed for different civil engineering, mechanical engineering, and aerospace engineering structures around the world. FRP composite materials have shown great potential as alternative construction materials to conventional ones. It has been proved that FRP composites have the potential to revolutionize the construction of structures, producing more efficient and cost- effective structures.

Advanced composite laminated FRP plates have many advantages, among which the most significant are the high stiffness and the strength to weight ratios, the durability, and the fatigue resistance. For example, in civil engineering, FRP plates can be used in strengthening, retrofitting and reinforcing of concrete structures and bridges. In such applications, the FRP plates are usually assumed to act as isotropic or orthotropic materials [5.1, 5.2]. However, the real nature of the laminates is generally anisotropic which needs to be considered into the structural analysis in order to obtain more accurate results. One of the obstacles to the extensive use of advanced FRP composites in construction is the lack of simplified and practical design approaches and guidelines. Unlike the standard construction materials, structural analysis and design of advanced composites is very complicated, since the material properties are coupled with the structural geometry and with the deformations. Therefore, an optimal numerical technique for modeling the structural behavior of FRP laminated structures is impetuously needed. Different methodologies have been developed for bending and stress analyses of composite laminated structures, including laminated FRP plates, such as mesh-free methods [5.3], finite element methods [5.4-5.10], and other analytical techniques [5.11-5.13].

The spline finite strip method (SFSM), as a special form of FEM, can be efficiently used for composite FRP laminates because of its analytical merits. In this technique, the

displacement functions in the longitudinal directions are B3-spline, while the degrees of freedom in comparison with conventional finite strip method are higher. The advantage of latter method over the conventional one is the ability of handling more complex types of loadings (such as concentrated loads), geometries (such as continuous span bridges), and boundary conditions. When applied to most structural problems, SFSM yields a relatively small size band stiffness matrix, and thus it requires little computational effort. Furthermore, the SFSM has the high continuity properties due to the use of B3-splines which are piecewise cubic polynomial with continuity over the entire interval, up to the second derivative. The same order continuity C2 in the standard FEM can be achieved only if a fifth order polynomial is introduced with Hermit polynomials with three degrees of freedom per node, which leads to a much larger matrix. In the commonly used FE methods, the order of continuity is usually C0 or C1, which means more grid points are needed to ensure the convergence of the results. Consequently, higher number of iterations will be needed for the convergence of the nonlinear terms as well. Not only the computational time but also the simplicity of the input data as well as the ease of programming are among the factors that can make SFSM highly efficient for spatial discretization of FRP laminated plates and shells.

The spline FSM has been successfully extended to the analysis of different types of structural problems including box girder bridges, circular plates, skew plates and the plates of arbitrary shapes [5.14, 5.15]. Chen et al. [5.16, 5.17] introduced the unequally spaced B3-spline functions in the analysis of stiffened plates and folded plate structures with intermediate supports. Using unequal B3 splines, the accurate response in the region of high stress gradients or at the locations of abrupt geometric changes can be evaluated, or by spacing knots more closely in these regions. Dawe et al, [5.18-5.22] carried out an extensive research on the use of spline finite strip methods in determining the behavior of composite laminated, prismatic plate and shell structures based on the thin plate theory. He used the method for analyzing a variety of problems including buckling stresses and natural frequencies of single span and multi-span structures, and for investigating the post-buckling response of plate structures [5.23-5.25], thermal buckling [5.26] and the transient response to dynamic loading of flat plates. Wang and Zhang [5.27] introduced a layerwise B-spline finite strip method for free vibration analysis of both thick and thin composite laminated

plates. In this method, the composite laminated plates are divided into a number of numerical layers in the thickness direction. Recently, Beena et. al [5.28] used the means of spline finite strip method for modeling and conducting the linear static analysis of functionally graded plates. However, his study is limited to simply supported boundary conditions. Qiao et al. [5.29] used FSM for post-buckling analysis of composite plates under shear and compression.

Although a considerable research has been carried out on the use of spline finite strip method for composite laminated plates, the elastic bending and stress analyses of laminated FRP plates has not yet been addressed in the literature, to the best knowledge of the authors. In this paper, the spline finite strip method is extended for elastic bending analysis of composite laminated FRP plates with different boundary conditions. The coupling effects between out of plane and in plane degrees of freedom of the FRP plate is considered by introducing the relative constitutive equations in the spline finite strip formulation. The low computational time, simplicity of the input data, as well as high efficiency and accuracy are the highlights of the proposed method. Besides, the method is able to easily handle a variety of boundary conditions as well as dealing with composite FRP folded plates.

The present study is organized as follows. First, the extension of the spline finite strip method for elastic bending and stress analyses of composite laminated FRP plates with different boundary conditions is formulated and presented in Section 5.2. The developed solution is programmed on a desktop workstation and is used to study of the laminated FRP plates and plate assemblies. The deflections and stresses of FRP laminated flat shells under bending loads are calculated and reported in Section 5.3. The spline finite strip results are validated against standard finite element method through performing a number of case studies for the bending analysis of composite FRP laminates and of the asymmetric FRP aluminum plates under static and wind loadings respectively. In addition, the resultant stresses of the composite AL-FRP building envelopes will be investigated. Finally, it will be demonstrated that the application of spline finite strip method on FRP laminated plates can open new doors for extending the methodology to more complicated types of problems in the field of composite FRP structures such as dynamics and aerodynamics of laminated FRP structural systems like hybrid multi-span FRP bridges.

5.2 Theoretical approach

5.2.1 Background

A composite laminated FRP plate is a collection of FRP lamina arranged in a specified order. Adjacent lamina may be of the same or different materials, and their fiber orientations with respect to a reference axis may be arbitrary. In Fig. 5.1, a rectangular flat multi-layer composite laminated FRP plate is shown.

The classical lamination theory is used in the present study to derive the stiffness matrix of a composite laminated FRP plate. In contrast with the simplified theory of laminated beams which is restricted to symmetric laminates without coupling, the classical lamination theory can be applied for analysis of different types of laminated FRP plates, including nonsymmetric laminates with arbitrary orientated plies where coupling effects result in complex combinations of extensional, flexural, and torsional deformations. In the lamination theory, it is assumed that each lamina is in a state of plane stress while the interlaminar stresses are neglected. In addition, a perfect bonding between different laminas is assumed, which means that the laminated FRP plate behaves as a unity, homogenous, anisotropic plate. Therefore, the deformation hypothesis of classical homogeneous plate theory can be used for derivation of FRP laminate stiffness matrix. The main difference between lamination theory and theory of homogeneous, isotropic plates [5.30] appears in lamina constitutive relationships.

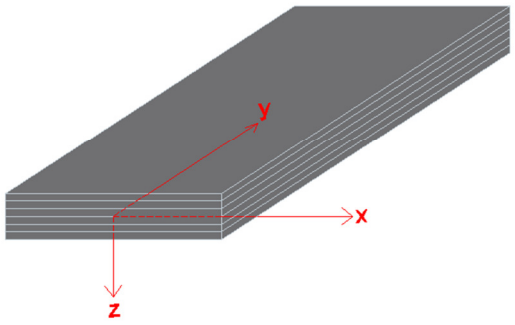

Fig. 5.1 Multi-layer composite laminated plate

5.2.2 Displacement functions

The displacement of an FRP laminate strip in the spline finite strip method can be obtained by applying B3-spline functions in the longitudinal direction and the polynomials in the transverse direction of the strip. Fig. 5.2 defines the coordinate system where its origin is assumed to be on the middle surface of the FRP laminated plate. As a result of assuming plane stress condition in each lamina, transverse shear strains are neglected. In addition, in-plane displacements are linear functions of the z coordinate and transverse normal strain is negligible. Considering these assumptions, the displacements of the FRP laminate at a general point can be expressed in terms of

$$\bar{u}(x,y,z) = u(x,y) + z\psi_x(x,y) \tag{5-1}$$

$$\bar{v}(x,y,z) = v(x,y) + z\psi_y(x,y) \tag{5-2}$$

$$\bar{w}(x,y,z) = w(x,y) \tag{5-3}$$

where ψ_x and ψ_y are independent rotations while *u*, *v,* and *w* are displacements at the middle surface of the laminate along x, y, and z axes respectively.

5.2.3 Discretization by spline strips

In the environment of the spline finite strip method, each laminated FRP plate can be discretized into a number of strips. Shell spline strip as shown in Fig. 5.2, can be used for modeling the composite laminate in which both in-plane and out-of-plane degrees of freedom are considered. The parameters in Fig. 5.2 are defined in the following lines. In contrast with isotropic shell strip [5.1], the coupling effects need to be investigated in analyzing the laminate shell strip.

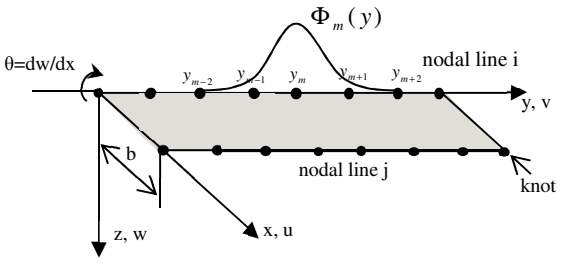

Fig. 5.2 Flat shell spline finite strip

In the case of flat laminates, one can consider four degrees of freedom on each knot of a nodal line of a strip, three translational and one rotation. The total potential energy of a flat laminate strip is obtained from algebraic summing the membrane (in-plane) and bending (out-of-plane) deformations.

The displacement parameters vector of a laminate spline strip centered at y_m is given by

$$\{\delta\}_m = \left[u_{im}, v_{im}, w_{im}, \theta_{im}, u_{jm}, v_{jm}, w_{jm}, \theta_{jm} \right]^T \tag{5-4}$$

In the formulation of the spline finite strip method it is better to have the locations of the supports and the concentrated load coinciding with the knots on the nodal lines, in order to obtain acceptable results. To reach this goal, unequally spaced B3-spline functions are used in the present study. Moreover, the introduction of unequally spaced interior knots allows one to describe the accurate response in the region of high stress gradients, or at the locations of abrupt geometric changes, by spacing knots more closely. In this case, the spline function centered at y_m can be expressed as

$$\Phi_m(y) = \begin{cases} 0 & y < y_{m-2} \\ A_m(y - y_{m-2})^3 & y_{m-2} \le y < y_{m-1} \\ A_m(y - y_{m-2})^3 + C_m(y - y_{m-1})^3 & y_{m-1} \le y < y_m \\ B_m(y_{m+2} - y)^3 + D_m(y_{m+1} - y)^3 & y_m \le y < y_{m+1} \\ B_m(y_{m+2} - y)^3 & y_{m+1} \le y < y_{m+2} \\ 0 & y_{m+2} \le y \end{cases} \tag{5-5}$$

in which

$$
\begin{aligned}
A_m &= \left[(y_{m+1} - y_{m-2})(y_m - y_{m-2})(y_{m-1} - y_{m-2}) \right]^{-1} \\
B_m &= \left[(y_{m+2} - y_{m-1})(y_{m+2} - y_m)(y_{m+2} - y_{m+1}) \right]^{-1} \\
C_m &= -(y_{m+2} - y_{m-2}) \left[(y_{m+2} - y_{m-1})(y_{m+1} - y_{m-1})(y_m - y_{m-1})(y_{m-1} - y_{m-2}) \right]^{-1} \\
D_m &= -(y_{m+2} - y_{m-2}) \left[(y_{m+1} - y_{m-2})(y_{m+1} - y_{m-1})(y_{m+1} - y_m)(y_{m+2} - y_{m+1}) \right]^{-1}
\end{aligned}
\tag{5-6}
$$

The membrane displacement functions *u* and *v*, and the flexural displacement function *w* at the middle surface of the FRP laminate can be expressed as the product of transverse polynomials and longitudinal B3-splines as following

$$u = \sum_{m=-1}^{r+1} (N_1 \Phi_{1m}(y) u_{im} + N_2 \Phi_{5m}(y) u_{jm}) \tag{5-7}$$

$$v = \sum_{m=-1}^{r+1} (N_1 \Phi_{2m}(y) v_{im} + N_2 \Phi_{6m}(y) v_{jm}) \tag{5-8}$$

$$w = \sum_{m=-1}^{r+1} (N_3 \Phi_{3m}(y) w_{im} + N_4 \Phi_{4m}(y) \theta_{im} + N_5 \Phi_{7m}(y) w_{jm} + N_6 \Phi_{8m}(y) \theta_{jm}) \tag{5-9}$$

where r is the total number of longitudinal sections on a nodal line and

$$
\begin{aligned}
N_1 &= 1 - X \\
N_2 &= X \\
N_3 &= 1 - 3X^2 + 2X^3 \\
N_4 &= x(1 - 2X + X^2) \\
N_5 &= (3X^2 - 2X^3) \\
N_6 &= x(X^2 - X)
\end{aligned}
\tag{5-10}
$$

in which $X = x/b$, and Φ_{1m} to Φ_{8m} are the longitudinal shape functions; Φ_{1m}, Φ_{2m}, Φ_{5m} and Φ_{6m} are related to displacements *u* and *v* of nodal lines *i* and *j* respectively while Φ_{3m}, Φ_{4m},

Φ_{7m} and Φ_{8m} are related to displacement *w*. The longitudinal shape functions consist of (m+3) local B3-splines. Each longitudinal shape function has the following form

$$[\Phi]=\begin{bmatrix} \bar{\Phi}_{-1} & \bar{\Phi}_0 & \bar{\Phi}_1 & \Phi_2 & \cdots & \Phi_{m-2} & \bar{\Phi}_{m-1} & \bar{\Phi}_m & \bar{\Phi}_{m+1} \end{bmatrix} \tag{5-11}$$

where $\bar{\Phi}_i$ is an amended local boundary spline with regard to the end boundary conditions of the strip.

5.2.4 Strain-displacement relations

Analysis of flat laminates under in-plane loads and bending loads are based on the Kirchhoff-Love hypothesis. Assuming that all layers are perfectly bonded (no slippage between the layers), Kirchhoff hypothesis state that a line perpendicular to geometric mid-surface (reference plane) remains straight and does not change its length while the laminate is deforming under the applied loading. This hypothesis results in $\varepsilon_{zz} = 0, \gamma_{xz} = \gamma_{yz} = 0$. Then the strain distribution at a general point in the laminate is expressed by

$$\begin{Bmatrix} \bar{\varepsilon}_x \\ \bar{\varepsilon}_y \\ \bar{\gamma}_{xy} \end{Bmatrix} = \begin{Bmatrix} \varepsilon_x \\ \varepsilon_y \\ \gamma_{xy} \end{Bmatrix} + z \begin{Bmatrix} \kappa_x \\ \kappa_y \\ \kappa_{xy} \end{Bmatrix} \tag{5-12}$$

or

$$\{\bar{\varepsilon}\} = \{\varepsilon\} + z\{\kappa\} \tag{5-13}$$

in which $\varepsilon_x, \varepsilon_y, \gamma_{xy}$ and $\kappa_x, \kappa_y, \kappa_{xy}$ are mid-surface strains and curvatures respectively, and are defined by

$$\varepsilon_x = u_{,x} \quad \varepsilon_y = v_{,y} \quad \gamma_{xy} = u_{,y} + v_{,x} \tag{5-14}$$

$$\kappa_x = w_{,x} \quad \kappa_y = w_{,y} \quad \kappa_{xy} = 2w_{,x}w_{,y} \tag{5-15}$$

5.2.5 Constitutive equations

The following constitutive equations can relate the stresses to the strains in an arbitrary lay-up laminate strip

$$\begin{Bmatrix} N_x \\ N_y \\ N_{xy} \\ M_x \\ M_y \\ M_{xy} \end{Bmatrix} = \begin{bmatrix} A_{11} & & & & & \\ A_{12} & A_{22} & & Sym & & \\ A_{16} & A_{26} & A_{66} & & & \\ B_{11} & B_{12} & B_{16} & D_{11} & & \\ B_{12} & B_{22} & B_{26} & D_{12} & D_{22} & \\ B_{16} & B_{26} & B_{66} & D_{16} & D_{26} & D_{66} \end{bmatrix} \begin{Bmatrix} \mathcal{E}_x \\ \mathcal{E}_y \\ \gamma_{xy} \\ \kappa_x \\ \kappa_y \\ \kappa_{xy} \end{Bmatrix} \tag{5-16}$$

or in a simplified form as

$$\begin{Bmatrix} N \\ M \end{Bmatrix} = \begin{bmatrix} A & B \\ B & D \end{bmatrix} \begin{Bmatrix} \varepsilon \\ \kappa \end{Bmatrix} \tag{5-17}$$

where N_x, N_y, N_{xy} are membrane and shear forces per unit length and M_x, M_y, M_{xy} are the bending and twisting moments per unit length in the middle surface of the laminate. A, B, and D are matrices of order 3 including laminate extensional stiffness, laminate-coupling stiffness, and laminate-bending stiffness matrices respectively and are obtained by the following integrations [5.30]

$$A_{ij} = \int_{-t/2}^{t/2} (\bar{Q}_{ij)_k}\, dz = \sum_{k=1}^{N} (\bar{Q}_{ij)_k} (z_k - z_{k-1}) \tag{5-18}$$

$$B_{ij} = \int_{-t/2}^{t/2} (\bar{Q}_{ij)_k} z\, dz = \frac{1}{2} \sum_{k=1}^{N} (\bar{Q}_{ij)_k} (z_k^2 - z_{k-1}^2) \tag{5-19}$$

$$D_{ij} = \int_{-t/2}^{t/2} (\bar{Q}_{ij)_k} z^2\, dz = \frac{1}{3} \sum_{k=1}^{N} (\bar{Q}_{ij)_k} (z_k^3 - z_{k-1}^3) \tag{5-20}$$

where the subscripts i, j=1,2, or 6; N is the number of laminas; t is the laminate thickness; z_k and z_{k-1} are distances from middle-surface to inner and outer surfaces of the k_{th} lamina respectively as illustrated in Fig. 5.3.

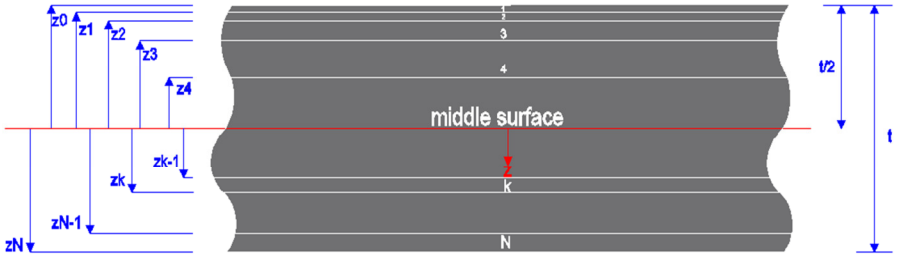

Fig. 5.3 Laminated plate cross-sectional geometry and ply numbering system

The extensional stiffness matrix [A] relates the in-plane forces {N} to the midplane strains $\{\varepsilon\}$, and the bending stiffness matrix [D] relates the moments {M} to the curvatures $\{\kappa\}$. Moreover, the coupling stiffness matrix [B] couples the in-plane forces {N} with the curvatures and the moments {M} with the mid-plane strains. Having nonzero B_{ij} terms implies that the laminated plate will bend or twist under in-plane forces, and will also exhibit mid-plane stretching under bending or twisting moment forces. It is worth noting that for a symmetric laminate with respect to the middle surface in terms of geometry and material property, the matrix [B] will be zero. On the other hand, for the asymmetric laminate about the middle surface, the matrix [B] will have nonzero elements. In fact, the coupling at laminate is not related to material anisotropy but is due to geometric and/or material property asymmetry with respect to the middle surface. In Eqs. (5-18) to (5-20), $(\bar{Q}_{ij})_k$ are the components of the transformed k^{th} lamina stiffness matrix as below [5.30]

$$\bar{Q} = \begin{bmatrix} \bar{Q}_{11} & \bar{Q}_{12} & \bar{Q}_{16} \\ \bar{Q}_{12} & \bar{Q}_{22} & \bar{Q}_{26} \\ \bar{Q}_{16} & \bar{Q}_{26} & \bar{Q}_{66} \end{bmatrix} \tag{5-21}$$

in which

$$\begin{aligned} \bar{Q}_{11} &= Q_{11}c^4 + Q_{22}s^4 + 2(Q_{12} + 2Q_{66})s^2c^2 \\ \bar{Q}_{12} &= (Q_{11} + Q_{22} - 4Q_{66})s^2c^2 + Q_{12}(c^4 + s^4) \\ \bar{Q}_{22} &= Q_{11}s^4 + Q_{22}c^4 + 2(Q_{12} + 2Q_{66})s^2c^2 \\ \bar{Q}_{16} &= (Q_{11} - Q_{12} - 2Q_{66})c^3s - (Q_{22} - Q_{12} - 2Q_{66})cs^3 \\ \bar{Q}_{26} &= (Q_{11} - Q_{12} - 2Q_{66})cs^3 - (Q_{22} - Q_{12} - 2Q_{66})c^3s \\ \bar{Q}_{66} &= (Q_{11} + Q_{22} - 2Q_{12} - 2Q_{66})s^2c^2 + Q_{66}(s^4 + c^4) \end{aligned} \tag{5-22}$$

where c=cos θ, s=sin θ, and θ is the lamina orientation angle while Q_{ij} are the components of the lamina stiffness matrix which are related to the engineering constants as follows

$$Q_{11} = \frac{E_1}{1-\nu_{12}\nu_{21}},\ Q_{12} = \frac{\nu_{12}E_2}{1-\nu_{12}\nu_{21}},\ Q_{22} = \frac{E_2}{1-\nu_{12}\nu_{21}},\ Q_{66} = G_{12} \quad (5\text{-}23)$$

in which E_1 and E_2 are modulus of elasticity of the lamina in longitudinal and transverse directions respectively, while ν_{12} and ν_{21} are the corresponding Poison's ratios respectively and G_{12} is the shear modulus of the lamina.

5.2.6 Boundary conditions

Due to the localization of unequally spaced B3-spline functions, only a few boundary local splines at each end need to be amended in order to model the end boundary conditions. There are a number of methods for modifying the local B3-splines in order to satisfy the end and interior boundary conditions. The elimination of a local spline means that a zero value is imposed on the displacement parameter vector for each restrained degree of freedom. The interior boundary conditions, such as point supports along the length of a member can be modeled as well [5-14].

After defining the displacement functions and constitutive equations in the environment of spline finite strip method, the stiffness matrix of the FRP laminate and the equivalent nodal forces of external loads can be obtained using the standard finite element procedure. The derived stiffness matrices and load vectors are assembled and make the global stiffness matrix $[K]$ and load vector $[P]$ of the FRP laminate.

5.3 Numerical examples

The unequally spaced B3-spline finite strip method, employing laminate constitutive equations with coupling effects, in the formulation of bending displacements of composite laminated FRP plates is implemented in MATLAB and Visual C++ programming languages. The developed code can model various types of plates and plate assemblies including isotropic plate with two independent engineering constants E and *v*, orthotropic plate with four independent engineering constants, E_x, E_y, ν_{xy} and G_{xy}, and composite

laminate with coupling effects in which [A], [B], and [D] matrices are used as the constitutive relations. In order to ascertain the validity of the spline finite strip treatment, the program is used to calculate the displacements of FRP laminates with different boundary conditions. Comparisons between finite strip and finite element analyses are made through which the accuracy of the spline method can be verified. Then, the method is used to investigate the bending deflections and stresses of composite AL-FRP building envelopes with different geometric shapes under uniform wind pressure.

5.3.1 FRP Laminates with different boundary conditions

Using the laminate strips, composite antisymmetric FRP laminated plates with different end conditions are modeled and their structural behavior is investigated in the following.

a) Simply supported FRP laminated plate

An extremely thin square antisymmetric FRP laminate with the length of 1 m and simple supports at the corners and under a concentrated static load applied at the center of the FRP laminate with the value of 10 N is studied. The composite plate is an [-45/45/-45/45] antisymmetric angle-ply laminate consisting of the same 0.25 mm thick unidirectional AS/3501 carbon/epoxy laminate. The lamina engineering constants are E_1=138 GPa, E_2 = 9 GPa, G_{12} = 6.9 GPa, ν_{12} = 0.3, and $\nu_{12} = \nu_{12}$.

Using Equivalent Single Layer (ESL) method, the same laminate is modeled by finite element method via ABAQUS software. Some other material properties are needed for a shell element in the finite element modeling including E2=E3, v12=v13, G12=G13, G23=E2/2(1+v23). Also, it is assumed that v23=v12=v13.

The maximum rotation of the laminate obtained by both SFSM and FEM using different meshes, are listed in Table 5.1. The finite strip discretization shows that using only four strips the results converged without any impediment, while in the finite element model 64 elements are required to achieve convergence under the same conditions. In all circumstances, the rotations of finite element are lower than those obtained by finite strip method.

Table 5.1 Maximum rotation of the composite FRP laminate with simple supports at the corners

SFSM				FEM		
4 strips 8 sections	8 strips 4 sections	4 strips 4 sections	8 strips 8 sections	400 8 node thick shell elm. DoFs 6	400 8 node thin shell elm. DoFs 5	64 4 node shell ele.
dw/dx = θ (rad)						
-0.16	-0.17	-0.17	-0.16	-0.15	NA	-0.15

b) Clamped supported FRP laminated plate

The same study is performed herewith on the same FRP laminate; however, different end conditions are employed, in which the clamped supports at the corners are applied as illustrated in Fig. 5.4(a). The deflections of the FRP laminate at three locations a, b, and c are listed in Table 5.2 for different spline strips and finite element discretizations. Comparing the laminate model of 8 strips with 4 sections against the one with 4 strips with 8 sections, it can be noticed that in the finite strip method increasing the number of section discretization in the longitudinal directions is more helpful in converging the results when compared with the strip discretization.

Similar to the previous case study, the deflections obtained through finite element method are higher than those obtained by finite strip method, which might be due to the shear effects. In fact, the thin-plate theory applied to the present finite strip formulation, omits the effect of the shear strains, while these effects are handled by thick shell theory. Nevertheless, the difference between FE and FS results is lower than 10 % for all investigated cases.

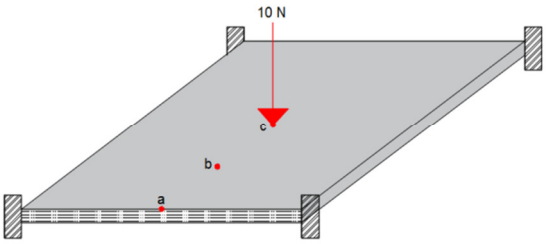

(a)

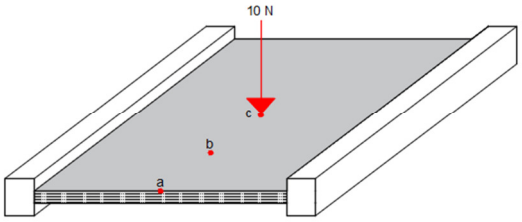

(b)

Fig. 5.4 FRP Laminated plate under concentrated bending load (a) clamped supports at the corners (b) two ends free and two ends clamped

Table 5.2 Deflections of composite FRP laminate with corner clamped supports

Node	SFSM				FEM		
	4 strips 8 sections	8 strips 4 sections	4 strips 4 sections	8 strips 8 sections	400 8 node thick shell elm. DoFs 6	400 8 node thin shell elm. DoFs 5	64 4 node shell elm.
Deflection w (cm)							
a	3.0	2.6	2.6	3.0	3.3	4.2	3.4
b	4.6	4.5	4.3	4.8	5.2	6.4	5.3
c	5.9	5.8	5.6	6.1	6.6	7.9	6.6

c) FRP Laminated plate with two ends free, two ends clamped

In the third case study, the same laminated FRP square plate is considered as free support at two ends and clamped at the other two ends as illustrated in Fig. 5.4 (b). The deflections at three locations under the concentrated load are listed in Table 5.3.

Table 5.3 confirms that using only four strips, the spline finite strip method again gives very accurate results while the same mesh in the finite element method cannot converge the results in a similar manner. The same accuracy in the finite element method can be achieved by using at least 64 four-node thin shell elements, or elements with more nodes and degrees of freedom. The finite element results indicate that the use of thick shell elements does not change the accuracy of the results. Surprisingly, the shear effects are negligible in this case.

Table 5.3 Deflections of composite FRP laminate with two ends free, two ends clamped

Node	SFSM		FEM				
	4 strips 8 sections	4 strips 4 sections	16 8-node thin shell elm. DoFs 5	16 4- node shell elm.	400 8-node thick shell elm. DoFs 6	400 8-node thin shell elm. DoFs 5	64 4- node shell elm.
Deflection w (cm)							
A	1.3	1.3	1.3	0.6	1.3	1.3	1.1
B	1.5	1.5	1.5	1.2	1.6	1.6	1.4
c	2.0	1.9	2.1	1.6	2.1	2.1	1.9

d) FRP laminated plate with two ends clamped and one pin support at the middle of the lateral edge under uniformly distributed loading

The proposed spline finite strip method can handle not only concentrated forces but also line and uniform loads. Herein, the FRP laminate is loaded by a uniform bending load with the value of 50 N/m^2. The laminate is clamped at two ends and there is a pin support at the middle of one lateral edge as illustrated in Fig. 5.5. The bending displacements along the middle line of the plate, which connects the pin supported edge to the free edge, are obtained by using different finite strip and finite element meshes, and are listed in Table 5.4.

Discretizing by only four strips and four sections, the finite strip analysis converged while in the finite element method 8-node rectangular thin shell elements are required to converge the results appropriately. In addition, the finite element method is more conservative in predicting the bending displacements.

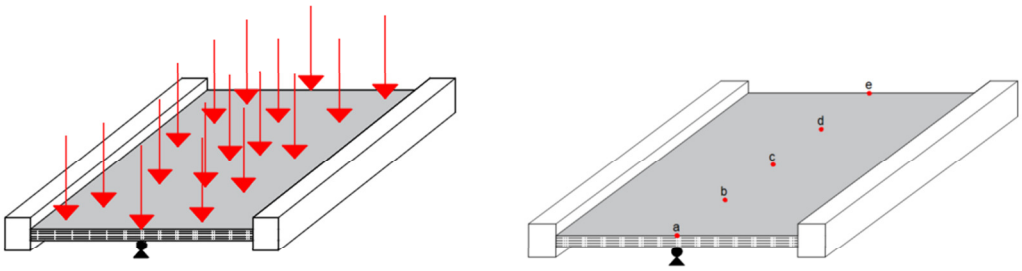

Fig. 5.5 FRP laminated plate with two ends clamped and one pin support at the middle of the lateral edge under uniform loading

Table 5.4 Deflections of composite FRP laminate with two ends clamped and one pin support at the middle of one end

Node	SFSM		FEM	
	4 strips 8 sections	4 strips 4 sections	16 8-node thin shell elm. DoFs 5	16 4- node Shell elm.
Deflection w (cm)				
a	0	0	0	0
b	1.9	1.9	2.0	1.6
c	2.9	2.9	3.0	2.5
d	3.4	3.4	3.6	2.8
e	4.3	4.2	4.4	3.4

5.3.2 Asymmetric composite AL-FRP envelops

In order to prove the capability of the proposed finite strip solution of modeling highly asymmetric laminates, the structural behavior of the composite aluminum FRP (AL-FRP) envelopes under wind loading is investigated. Composite AL-FRP plates are usually employed in construction of high-rise buildings as envelopes and curtain walls. However, as an example of highly asymmetric laminated plate owing to different layers of different thickness and material, and to investigate the potential of the spline finite strip solution for

considering the asymmetric conditions, this study is presented in the current chapter. A composite AL-FRP building envelope consists of adjacent layers of materials with different properties. Herein, the aluminum plate, BFRP plate, PVC foam, and gypsum as illustrated in Fig. 5.6. are assembled to make the composite plate. The material and thickness properties of the composite envelope are listed in Table 5.5. In the following case studies the building envelope has a square geometry with the length of 3 meters. Each layer is assumed to behave as an isotropic material but they make an anisotropic composite laminate because of the asymmetric geometric properties with regard to the middle surface of the laminate. Therefore, the coupling effects play an important role in the structural response of these plates. In the following case studies, boundary conditions, the value of wind loading, and the foam thickness are varied. An equivalent uniform static load as the wind force is distributed along the entire surface of the first layer of the AL-FRP laminated plate.

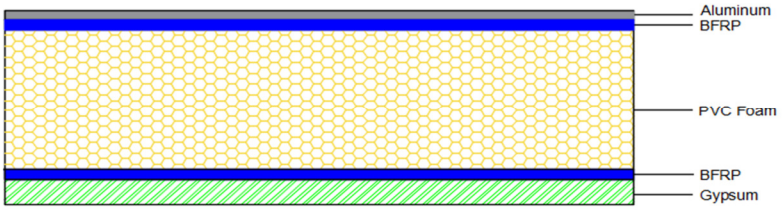

Fig. 5.6 AL-FRP composite plate cross-sectional geometry

Table 5.5 Material properties of the composite AL-FRP plate

Material	Thickness (mm)	E (GPa)	v
Aluminum	3	68.90	0.33
BFRP	2	21.50	0.10
PVC Foam	Varied	0.065	0
BFRP	2	21.50	0.10
Gypsum	12	3.00	0.23

A composite AL-FRP plate with the foam thickness of 10 mm under uniform pressure with the value of 3 KPa, as shown in Fig. 5.7, is modeled by spline strips. Four pin supports are applied at the corners of the plate as the boundary conditions. For the finite element method, shell composite section has been used in ABAQUS to represent the composite AL-FRP plate as this section has the ability to model adjacent layers within the same shell element. The deflections along the middle line of the plate are listed and plotted in Table 5.6 and Fig. 5.8 respectively. Using only 12 strips, the finite strip results converged and a good agreement is witnessed between the FS and FE results. According to the error percentage, the difference between the results of FE and FS is on the increase when the deflections decrease. Nonetheless, the maximum error is 12% which is reasonable.

As the further study, the foam thickness and the wind pressure increased to 80 mm and 10 KPa respectively. Additionally, the plate is modeled by SAP2000 using shell composite section elements in which no de-bonding is assumed between different layers. The numerical results of bending analysis are listed in Table 5.7 and are plotted in Fig. 5.9. In contrast with the previous case study, the deflections obtained from ABAQUS are much higher than the finite strip responses. Nevertheless, the finite strip results are still very close to the finite element results of SAP2000, as shown in Fig. 5.9. In this case, one can call the composite plate in the category of thick plate. In the ABAQUS model, the shear effects have been considered while they are not handled in the SAP and finite strip models. The latter is the reason for the considerable difference between the ABAQUS and FS results.

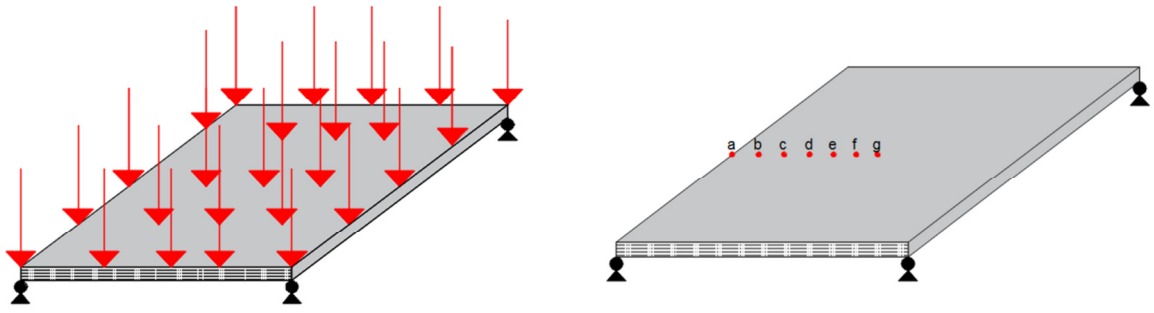

Fig. 5.7 Composite AL-FRP plate with pin supports at the corners and under uniformly distributed wind loading

Table 5.6 Deflections of the corner simply supported asymmetric composite AL-FRP plate under uniform wind pressure of 3 KPa (foam thickness: 10 mm)

Node	Deflections (cm)		Error %
	FEM (Abaqus) 144, 8 node 5 DOFs shell element	SFSM 12 strips 12 sections	
a	19.0	16.7	12.1
b	20.9	18.8	10.0
c	22.9	21.0	8.3
d	24.7	23.0	6.8
e	26.2	24.6	6.1
f	27.1	25.7	5.1
g	27.4	26.1	4.7

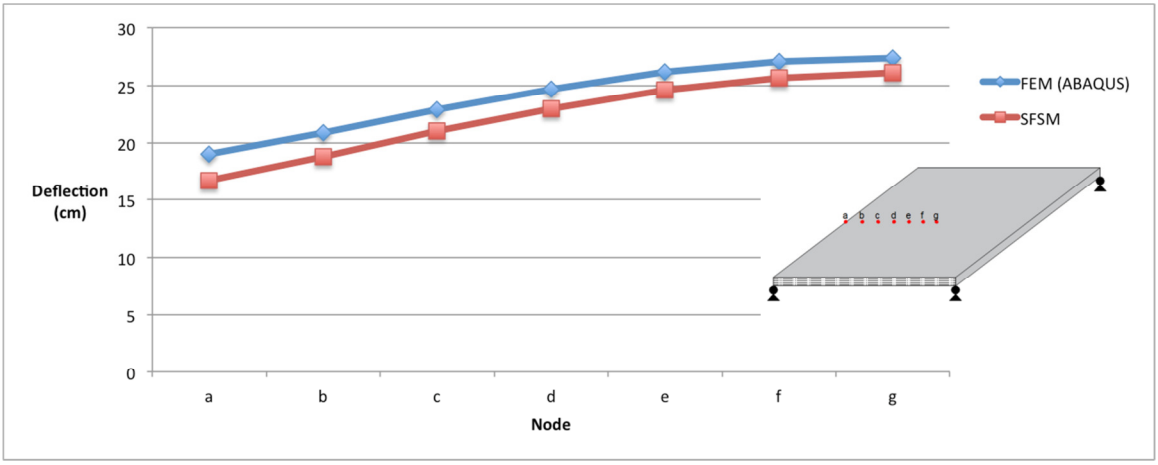

Fig. 5.8 Deflections of the corner simply supported asymmetric composite AL-FRP plate along the middle line under uniform wind pressure of 3 KPa

Table 5.7 Deflections of the corner simply supported asymmetric composite AL-FRP plate under uniform wind pressure of 10 KPa (foam thickness: 80 mm)

Node	Deflections (cm)		
	FEM (Abaqus), 144 8-node 5 DOFs shell element	FEM (SAP2000)	SFSM 12 strip 12 sections
a	4.8	2.4	2.6
b	5.1	2.7	3.0
c	5.4	3.0	3.2
d	5.9	3.3	3.6
e	5.9	3.5	3.8
f	6.0	3.6	3.9
g	6.1	3.7	4.0

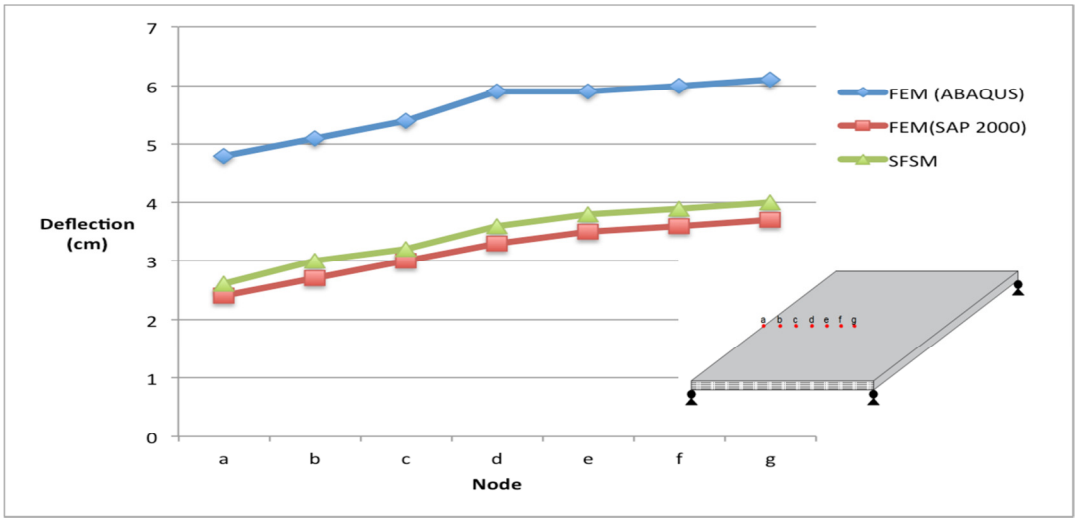

Fig. 5.9 Deflections of the corner simply supported asymmetric composite AL-FRP plate under uniform wind pressure of 10 KPa

Comparing the bending deflections of the previous two case studies, it can be concluded that thickening of the foam increases the bending capacity of the building envelope. Nonetheless, the accuracy of the finite strip analysis decreases because of the lack of handling the shear effects.

To investigate more complex boundary conditions, the square composite AL-FRP plate is considered to be simply supported at two parallel edges while free to rotate but restrained against displacements along x and y axes at the other two ends. The foam thickness is 80 mm and the AL-FRP laminate is under uniform wind load with the value of 10 KPa. The deflections obtained by both FS and FE methods along the middle lines of the laminate in two directions are presented in Tables 5.8 and 5.9 as well as Figs. 5.10 and 5.11. The deflections of both spline finite strip and SAP2000 models are almost the same while those obtained by ABAQUS are higher than finite strip results, which is again because of the shear effects. The deflections in this example are lower comparing with the previous example (Table 5.7) in which under the same wind pressure and thickness, the displacements were much higher due to the boundary conditions.

Looking at the displacement curves of Figs. 5.10 and 5.11 and comparing the FE SAP analysis results with SFSM, it can be concluded that when the shear effects are omitted, the spline finite strip method is more conservative than the finite element method in elastic bending analysis of composite FRP laminated plates.

5.3.2.1. Stiffened composite AL-FRP Plate

The proposed spline finite strip method is capable of modeling not only laminated plates but also laminated plate-assemblies. A composite AL-FRP plate-structure stiffened by two ribs at the two edges of the laminate as illustrated in Fig. 5.12 is investigated in this section. The stiffened plate is under uniform wind pressure of 10 KPa and the foam thinness is 80 mm. The other two edges of the square stiffened plate are simply supported. The deflections along the middle line of the stiffened-plate are calculated by both spline finite strip and finite element methods. The bending analysis results are listed in Table 5.10. A good agreement can be noticed between the obtained deflections. It is obvious that stiffening the plates by the ribs will result in decreasing the bending deflections.

It is worth noting that the same analyses were carried out for composite AL-FRP plates under wind suction and the similar results were obtained. One reason for the similarity of the results is that the laminate is modeled as a unified shell section in the spline finite strip method.

Table 5.8 Deflections of asymmetric composite AL-FRP plate (simply supported at two parallel edges and free to rotate but restrained against displacements along x and y axes at the other two ends) along node g to m

Node 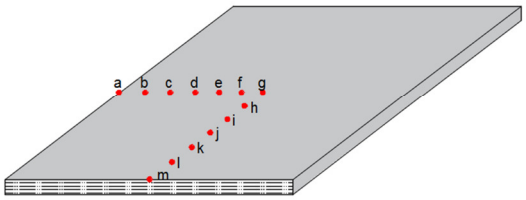	Deflections (cm)		
	FEM (Abaqus) 144, 4 node shell element	FEM (SAP2000)	SFSM 12 strip 12 sections
g	1.9	1.5	1.5
h	1.9	1.5	1.5
i	1.9	1.5	1.5
j	1.9	1.5	1.6
k	2.0	1.5	1.6
l	2.0	1.6	1.6
m	2.1	1.6	1.7

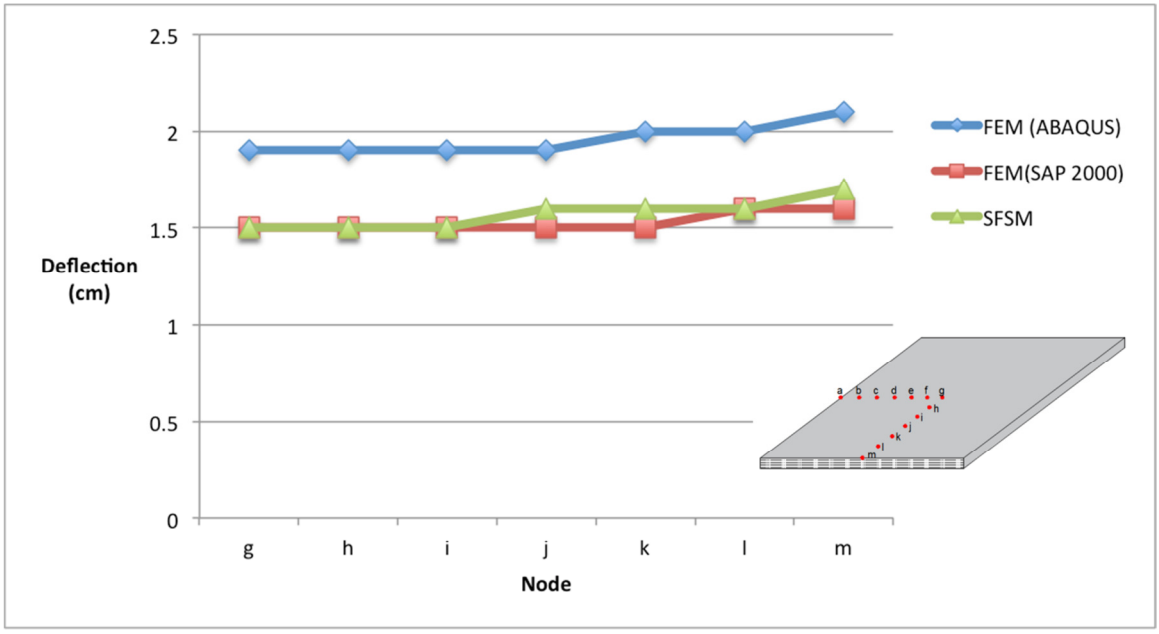

Fig. 5.10 Deflections of asymmetric composite AL-FRP plate along node g to m

Table 5.9 Deflections of asymmetric composite AL-FRP plate (simply supported at two parallel edges and free to rotate but restrained against displacements along x and y axes at the other two ends) along node a to g

Node 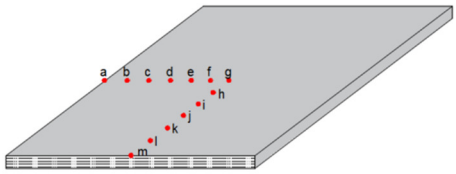	Deflections (cm)	
	FEM (SAP2000)	SFSM 12 strip 12 sections
a	1.5	1.7
b	1.5	1.7
c	1.5	1.6
d	1.4	1.6
e	1.4	1.6
f	1.4	1.6
g	1.4	1.6

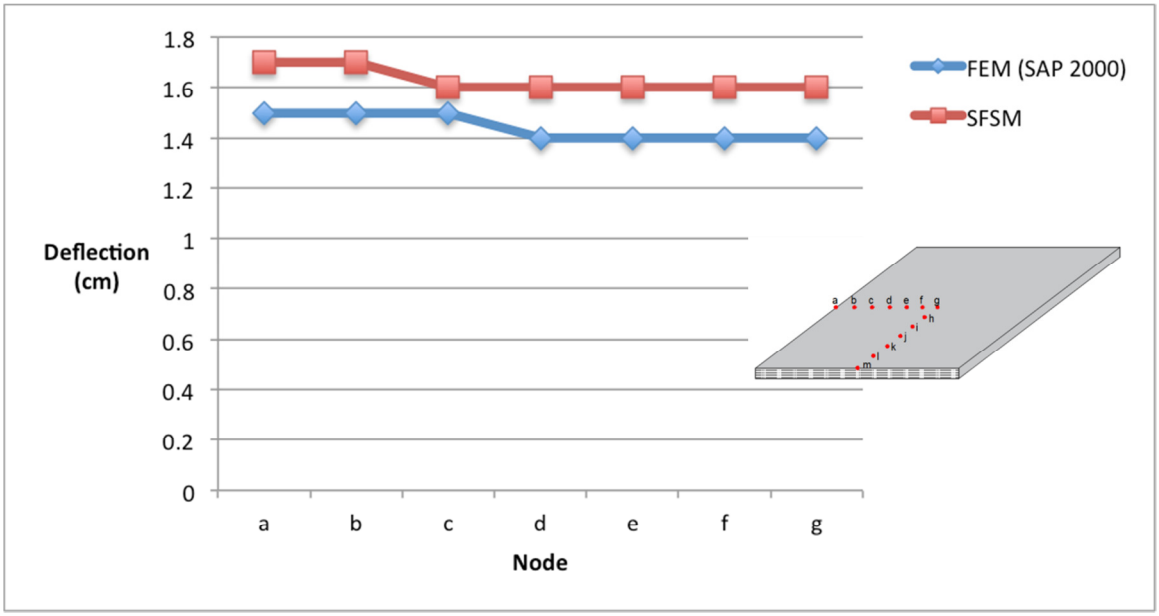

Fig. 5.11 Deflections of asymmetric composite AL-FRP plate along node a to g

5.3.3 Stress analysis

After obtaining the displacements by spline finite strip method, the strains and consequently the stresses of the composite laminated FRP plate can be easily evaluated. Here, the bending moments M_x, M_y as well as the axial stresses σ_x and σ_y in the center of the composite AL-FRP plates with three different boundary conditions were calculated and are presented in Table 5.11. The material and geometric properties of the plates are the same as Table 5.5. In all case studies, the foam thickness is 80 mm and the applied uniform wind load on the building envelope is 10 KPa. Comparing the resultant stresses of Table 5.11, it is obvious that the clamped supports at the corners of the AL-FRP plate increase the stress capacity of the building envelope with the percentage of more than 30 % comparing with the simple supported plates. Furthermore, the drastic reduction of resultant axial stresses in the building envelope with clamped supports along two opposite edges shows that the membrane capacity of the plate significantly increased under this type of support condition.

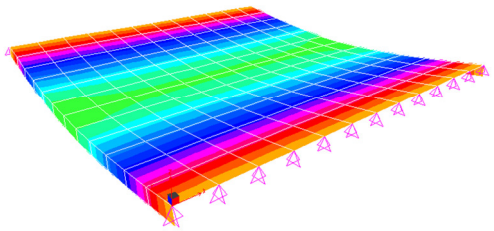

Fig. 5.12 Deformed shape of the stiffened composite AL-FRP plate under uniform wind pressure (FE model)

Table 5.10 Deflections of the asymmetric stiffened composite AL-FRP plate under uniform wind pressure

Node 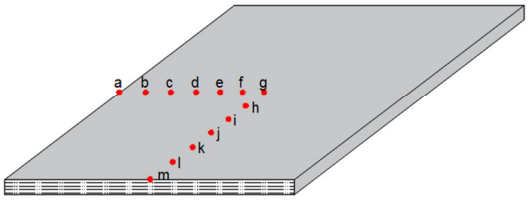	Deflections (cm)		
	FEM (Abaqus) 144, 4 node shell element	FEM (SAP2000)	SFSM 12 strip 12 sections
A	0	0	0
B	0.5	0.4	0.4
C	0.9	0.7	0.7
D	1.3	1.1	1.1
E	1.6	1.3	1.3
F	1.8	1.5	1.5
G	1.9	1.5	1.5

Table 5.11 Spline finite strip stress resultants in the middle line of the plate

Stress resultants	σ_x (KPa)	σ_y (KPa)	M_x (KN.m)	M_y (KN. m)
Corner simple supported AL-FRP plate	96.9	67.3	3.6	5.7
Corner clamped supported AL-FRP plate	68.3	44.2	2.5	4.4
Clamped edge supported AL-FRP plate	5.2	0.9	0.9	3.7

5.4 Conclusion

In the context of spline finite strip method, an optimal special discretization scheme was developed for elastic bending and stress analyses of composite FRP laminated plates. The method is able to handle different boundary conditions. Due to the semi-analytical property employed in the longitudinal direction, the number of sections for each strip in the SFSM model can be largely reduced without losing the accuracy of the outcomes. Therefore, the results converge using lower number of degrees of freedom. Consequently, the computational time could be significantly reduced by using a much coarser grid while preserving same accuracy compared with standard FEM, and thus greater efficiency could

be achieved. In the case of asymmetric composite FRP laminates, the coupling effects between membrane and flexural displacements can be handled in the proposed finite strip solution. The method was used for calculating elastic bending displacements and stresses of composite FRP flat shells and composite AL-FRP building envelopes with different end conditions under static and wind loads. The results were compared and validated against standard finite element analyses. Furthermore, the stiffened AL-FRP plate was studied to illustrate the capability of the method in dealing with laminated FRP folded plates.

The following points should be emphasized on to highlight the novelty and contribution of the present paper: (i) An optimal finite strip discretization scheme is proposed for FRP laminated plates and plate assemblies. (ii) The proposed scheme is applied for elastic bending and stress analyses of laminated FRP plates in which the coupling effects between membrane and flexural displacements can be considered in the analysis. (iii) General boundary conditions can be handled. (iv) The main features of the proposed method are simplicity of the input data as well as boundary conditions, low computational time and high efficiency and accuracy. (v) The finite element results are generally more conservative than SFSM in predicting the displacements of the FRP laminated plates. It is concluded that the effects of the shear deformations in relatively thick composite AL-FRP laminated plates are considerable. (vi) The numerical results showed that the finite element method needs finer mesh in complex boundary conditions while the accuracy of the spline finite strip method does not change.

The current research dealt with regular composite FRP plates and plate-structures. In the case of complicated applications of laminated FRP structures like hybrid composite FRP bridges, the efficiency of the proposed spline finite strip solution in terms of computational time could be more significant. Nevertheless, the current versions of the finite strip methods have important limitations especially in complicated analyses of massive structures. For instance, in the area of bridge engineering, the finite strip method is limited to model the bridge deck only while other components like piers and cables are replaced by pre-assumed boundary conditions. This reduces the accuracy of the finite strip analysis especially for the dynamic and aerodynamic analyses where the interactions between different structural components play an important role in the structural response. Moe Cheung and his research group have recently developed an integrated finite strip solution [5.31] which is able to

model all components of the bridge structure using spline finite strip method. Consequently, the structural interactions are considered in the analysis as well. Taking into account of all these features, the proposed methodology in this paper can be effectively applied for more complicated types of FRP laminated structures, like composite hybrid FRP decks in bridge engineering. In the case of a huge structure with thousands of degrees of freedoms and in complex analyses like dynamic and aerodynamic analyses of structures, the proposed solution can provide an efficient and accurate scheme. The latter will be the subject of the future studies.

References

[5.1] Naderian, H. R., Ronagh, H. R., Azhari, M., (2011) Torsional and flexural buckling of composite FRP columns with cruciform sections considering local instabilities, Composite Structures 93 (10), 2575-2586

[5.2] Naderian, H. R., Ronagh, H. R., Azhari, M., (2012), Global Buckling Behavior of Composite FRP Cruciform Section Columns by Complex Finite Strip Method, Proceedings of the 6th International Conference on Advanced Composite Materials in Bridges and Structures, Kingston, Ontario, Canada, 22 – 25 May 2012.

[5.3] Peng, L.X. , Liew K.M. , Kitipornchai S. , (2011) Bending Analysis of Folded Laminated Plates by the FSDT Meshfree Method, Procedia Engineering, Volume 14, 2011, Pages 2714-2721

[5.4] Yingqing Huang, Shenglin Di, Changchun Wu, Huiyu Sun, (2002) Bending analysis of composite laminated plates using a partially hybrid stress element with interlaminar continuity, Computers & Structures, Volume 80, Issues 5–6, March 2002, Pages 403–410

[5.5] Nguyen Duc Thai, Michele D'Ottavio, Jean-François Caron, (2013) Bending analysis of laminated and sandwich plates using a layer-wise stress model, Composite Structures, Volume 96, February 2013, Pages 135–142

[5.6] Amale Mahi, El Abbas Adda Bedia, Abdelouahed Tounsi, (2015) A new hyperbolic shear deformation theory for bending and free vibration analysis of isotropic, functionally graded, sandwich and laminated composite plates, Applied Mathematical Modelling, Volume 39, Issue 9, 1 May 2015, Pages 2489–2508

[5.7] Xiaodan Teng, Y.X. Zhang, (2014) Nonlinear finite element analyses of FRP-

strengthened reinforced concrete slabs using a new layered composite plate element, Composite Structures, Volume 114, August 2014, Pages 20–29

[5.8] Aysun Baltaci, Mehmet Sarikanat, Hasan Yildiz, (2007) Static stability of laminated composite circular plates with holes using shear deformation theory, Finite Elements in Analysis and Design, Volume 43, Issues 11–12, August 2007, Pages 839–846

[5.9] B. Saboori, S.M.R. Khalili, (2011) Static analysis of tapered FRP transmission poles using finite element method, Finite Elements in Analysis and Design, Volume 47, Issue 3, March 2011, Pages 247–255

[5.10] Yin Fan, Hai Wang,(2016) Nonlinear bending and postbuckling analysis of matrix cracked hybrid laminated plates containing carbon nanotube reinforced composite layers in thermal environments, Composites Part B: Engineering, Volume 86, 1 February 2016, Pages 1–16

[5.11] M.M. Alipour, (2016) An analytical approach for bending and stress analysis of cross/angle-ply laminated composite plates under arbitrary non-uniform loads and elastic foundations, Archives of Civil and Mechanical Engineering, Volume 16, Issue 2, February 2016, Pages 193–210

[5.12] M. Filippi, E. Carrera, (2016) Bending and vibrations analyses of laminated beams by using a zig-zag-layer-wise theory, Composites Part B: Engineering, Volume 98, 1 August 2016, Pages 269–280

[5.13] J.L. Mantari, F.G. Canales, (2016) A unified quasi-3D HSDT for the bending analysis of laminated beams, Aerospace Science and Technology, Volume 54, July 2016, Pages 267–275

[5.14] Cheung, M.S., Li, W., Chidiac, S. E., (1996), Finite strip analysis of bridges, 1st Edition. London: E &

FN Spon

[5.15] Cheung Y. K., Tham L. G. (1998), The finite strip method, USA: CRC Press; 1998

[5.16] Chen CJ, Gutkowski RM, Puckett JA. (1991), B-Spline compound strip analysis of stiffened plates under transverse loading. Computers and Structures; 34(2):337–347.

[5.17] Chen CJ, Gutkowski RM, Puckett JA. (1991), Spline compound strip analysis of folded plate structures with intermediate supports. Computers and Structures; 39(3/4):369–379.

[5.18] Wang, S., Dawe, D.J., (1997) Spline finite strip analysis of the buckling and vibration of composite prismatic plate, International Journal of Mechanical Sciences, Volume 39, Issue 10, October 1997, Pages 1161–1180

[5.19] Dawe, D.J., (2002) Use of the finite strip method in predicting the behaviour of composite laminated structures, Composite Structures 57, 11–36

[5.20] Wang S, Dawe DJ. (1999) Buckling of composite shell structures using the spline finite strip method. Compos Part B 1999;30B:351–64.

[5.21] Tan D, Dawe DJ. (1998) Buckling and vibration analysis of composite laminated plates and shells using general spline function. Compos Struct 1998;40:25–42.

[5.22] Dawe DJ, Tan D. (1999) Finite strip buckling and free vibration analysis of stepped rectangular composite laminated plates. Int J Numer Meth Engng 1999;46:1313–34.

[5.23] Dawe DJ, Wang S. (1998) Postbuckling analysis of thin rectangular laminated plates by spline FSM. Thin-Walled Struct 1998;30:159– 79.

[5.24] Wang S, Dawe DJ. (1999) Spline FSM postbuckling analysis of shear deformable rectangular laminates. Thin-Walled Struct 1999;34: 163–78.

[5.25] Dawe DJ, Wang S. (2000) Postbuckling analysis of composite laminated panels. AIAA J 2000;38:2160–70.

[5.26] Dawe DJ, Ge S. (2000) Thermal buckling of shear-deformable composite laminated plates by the spline finite strip method. Comput Meth Appl Mech Engng 2000;185:347–66. 312.

[5.27] Wang, S., Zhang, Y., (2004) Vibration analysis of rectangular composite laminated plates using layerwise B-spline finite strip method, Composite structures,;(68), 349-358

[5.28] Beena, K.P., Parvathy, U., (2014) Linear static analysis of Functionally Graded Plate using Spline Finite Strip Method, Composite Structures 117 (2014) 309–315

[5.29] Qingyuan Chen, Pizhong Qiao, (2014) Post-buckling analysis of composite plates under combined compression and shear loading using finite strip method, Finite Elements in Analysis and Design, Volume 83, June 2014, Pages 33–42

[5.30] Gibson, Ronald. F., (2012) Principles of Composite Material Mechanics, CRC Press

[5.31] Naderian, H., Cheung, Moe M. S., Shen, Z., Dragomirescu, E., (2015), Integrated Finite Strip Analysis of Long-span Cable-stayed Bridges, Computers and Structures, Volume 158, 1 October 2015, Pages 82–97

Chapter 6

On the use of integrated finite strip method for vibration analysis of continuous multi-span and cable-stayed hybrid FRP bridge systems

Abstract_ This research proposes a very efficient numerical technique for simulating hybrid FRP bridge systems. An Integrated Finite Strip Method (IFSM) is employed in order to evaluate the bending, vibration, and seismic performance of continuous multi-span and long-span cable-stayed FRP bridges. With the rapid development of FRP materials in bridge construction industry, hybrid FRP bridge decks are replacing the traditional steel and concrete decks. The use of FRP materials leads to significant reduction of the deck weight and consequently provides the opportunity for designing and building Ultra-Long Cable-stayed Bridge (ULSCSB) structures. The application of FRP decks could cover a variety of bridge systems from short and medium span bridges to long-span cable-stayed bridges. However, the structural performance of hybrid FRP bridges is totally different with steel and concrete bridge structures due to the complexity of the mechanical behavior of the FRP deck. The anisotropy nature of the FRP laminated deck is considered into the analysis by introducing so-called laminate spline strip in the environment of integrated finite strip solution. In addition, the structural interactions between all the components of the bridge can be handled into the structural

analysis by introducing the so-called transition section elements. The so-called column strip and cable strip are used to model the towers and cables respectively. Two case studies are presented, through which the accuracy and efficiency of the IFSM in modelling such structures, as well as performing the bending, frequency, and earthquake analysis of slab-girder and long-span cable-stayed FRP bridges are investigated. The finite strip results are validated against the finite element analysis results. The developed IFSM solution provides the opportunity for analysis and design of hybrid FRP bridge structures in a very efficient way, where the coupling effects of the FRP laminated deck and the structural interactions of bridge components are fully handled.

Keywords: Fiber reinforced polymer, Hybrid bridge, FRP deck, cable-stayed bridge, integrated finite strip method, laminate strip, free vibration, earthquake loading

6.1 Introduction

The Finite Strip Method (FSM) provides an attractive numerical solution for analysing bridge structures. High accuracy and efficiency due to its semi-analytical nature as well as rapid convergence owing to the small bandwidth elastic matrices, along with the simplicity of the input data and simulation have made FSM outstanding among conventional numerical techniques of bridge analysis. Despites the merits of the FSM, this method is only applicable for structural elements with simple shapes, like plates and shells and folded-plate structures. When it comes to a more complicated system, such as a cable-stayed bridge with numerous structural elements attached together under different orientations, the FSM is no longer a powerful tool for the 3D modelling and solving the structure. Therefore, until present, the application of FSM was limited to model the bridge deck only, while other structural components like piers, towers, and cables were modeled as special boundary conditions of the deck [6.1]. Alternatively, a combination of FSM and other numerical solutions like

FEM, and Boundary Element Method (BEM) can model the entire bridge system. However, only an iterative process can provide the compatibility and model the interactions between the displacements of the joint knots. This technique is only effective for structures with simple geometric shape and under static or quasi-static forces. In the cases of complex structures and structures under dynamic or aerodynamic excitations, such as non-uniform seismic waves and self-excited wind forces, the iterative process is no longer efficient. When external forces are applied to the bridge, the internal forces are transmitted between structural elements. Particularly, in dynamic phenomena like earthquake, the effects of seismic waves are transmitted from the foundation of the bridge to the piers and towers, and then to the deck and cables. Therefore, handling structural interactions of all elements of the bridge system is a necessary step in performing an accurate dynamic analysis and design of bridges. For all these reasons, the application of FSM in bridge analysis had almost reached the technical limit for more than a decade. After a number of years of research on developing and by trying different solutions, M. S. Cheung and his colleagues [6.1] created an innovative integrated framework that is capable of 3D modelling of an entire bridge system in the environment of spline finite strip method, where the effects of structural interactions between different segments of the bridge are also handled.

FRP materials have superior structural specifications over the traditional steel and concrete materials, such as high strength and stiffness to the mass ratios, high resistance to corrosion and favorable fatigue characteristics. This encourages the use of advanced composite materials in multi-span and cable-stayed bridges. Among the important factors employed in designing, maintaining, and constructing of long-span cable-stayed bridges, one can mention lengthening the bridge span, life cycle effectiveness, as well as earthquake and aerodynamic stability**.** With the rapid development of using advanced new hybrid fiber reinforced polymer (FRP) materials in the construction of cable-stayed bridges, some of these criteria, including the increase in the main span of the bridge as well as providing better structural health conditions of the super structure, can be achieved. Nevertheless, the dynamic and aerodynamic instability becomes a critical issue because of the significant reduction in the weight of the structure which makes the bridge more sensitive under the vibration of extreme natural hazards like earthquake and typhoons. Research shows the stiffness of advanced composite materials, including FRP, is coupled to the geometry of the structure

[6.2, 6.3]. The latter indicates the importance of the accurate simulation of the composite structure geometry although it is a very expensive computational process.

Despites the great potential for popularizing the FRP materials in ultra-long span cable-stayed bridges, conventional design methods are not properly meshed with hybrid FRP cable-stayed bridges due to the complexity of the failure mechanism and due to the anisotropic nature of FRP laminate. In contrast with traditional steel and concrete materials which are typically modelled as isotropic materials, FRP composites are highly anisotropic depending on the type of fibers, the matrix, and the orientation of each lamina. Taking into account the above features, the structural performance of long-span cable-stayed FRP bridges, especially the dynamic and aerodynamic characteristics, is totally different from the conventional cable-stayed bridges due to the longer span, lighter weight and more flexible structural system. In addition, the highly non-linear material properties coupled with the geometrical complexity, cause the structural analysis and design of cable-stayed FRP bridges extremely more challenging.

To the knowledge of authors, the first all composite cable-stayed bridge is the Aberfeldy Footbridge, in the UK, where the main structure is a cable-stayed bridge made by glass fiber reinforced polymer (GFRP) deck, and is suspended by Parafil-Aramid ropes and GFRP towers. Salim et al [6.4] carried out research on the analysis and design of the FRP composite deck-and-stringer bridges. By the means of pultruded FRP shapes, Qiao et al [6.5] suggested a systematic approach for analysis of FRP deck bridges. Bridge engineering researchers in the University of California, San Diego in collaboration with the Federal Highway Administration built a 4-lane traffic way composite cable-stayed bridge with the length of 137.2 m and the A-frame pylon of 57.9 m [6.6]. In spite of the state of the art research reports on the application of FRP materials in short span bridges, there is still lack of research on the FRP based long span cable-stayed bridges. Almansour and Cheung [6.7-6.10] proposed a comprehensive multi-scale design approach of hybrid FRP bridge in the frameworks of both micro and macro levels. They performed a number of case studies which resulted in developing different types of FRP deck sections for long-span cable-stayed bridges. The studies by Virlogeux showed that a very thin FRP deck section can support the static and traffic loads applied to a cable-stayed bridge [6.11]. Through experimental tests, Burgueno et. al [6.12] investigated the dynamic characteristics of FRP

composite bridges. M. S. Cheung and his research group in Hong Kong University of Science and Technology and Sichuan University, carried out extensive analytical and experimental research on micro-scale and macro-scale design of the FRP bridge decks for a number of existing bridges [6.13-6.15]. The design process is based on the multi-scale design approach introduced by Cheung and Almansour [6.9, 6.10], considering the FRP laminated material configuration and micro-material properties.

Integrated finite strip method as a very accurate and user friendly technique has the great potential to be extended for modelling of hybrid FRP deck bridges. The laminate spline strip developed in the previous chapter can perfectly model the anisotropic laminated FRP deck considering the coupling effects between flexural and membrane displacements of the FRP deck while the rapid convergence rate of the numerical results is still guaranteed. Integrating the laminate strips with the column strips, cable strips, and transition section elements will provide the opportunity to model an FRP bridge in the environment of finite strip method. In the following the numerical procedure will be explained. The developed methodology will be examined through performing two case studies including a continuous multi-span FRP bridge and a long-span cable-stayed hybrid FRP bridge system. The accuracy and efficiency of the proposed models in analyzing the bending, free vibration, seismic performances of the FRP bridge will be investigated through the comparison with the finite element analysis.

6.2 Integrated finite strip analysis of hybrid FRP bridges

So-called laminate spline strip, developed in the previous chapter, can be employed for modelling an FRP deck system which is generally made by of FRP laminates. The material properties of each layer including engineering constants as well as the FRP ply angle for each layer are modelled by laminate spline strips. The coupling effects between flexural and membrane degrees of freedoms of the composite FRP deck are considered in the integrated finite strip solution through the relevant constitutive equations as addressed in Eq. (5-16) in chapter 5. The column strip (three-dimensional and one-dimensional column strips), presented in chapter 3, model the piers and towers of the hybrid FRP bridge. The cable strip proposed in chapter 3 is used for simulating the cables. The connectivity between FRP deck, cables, piers, and towers is provided by transition section elements as described in chapter 2.

Eventually, the overall hybrid FRP bridge can be modelled in the environment of the integrated finite strip method.

The principle of the minimum potential energy following the standard finite element procedure can be used to derive the bending and dynamic properties of the laminate strips, column strips, and cable strips. For instance, the stiffness matrix $[k_{FRP}]$ and the force vector $\{f_{FRP}\}$ of a laminate FRP strip *i* are given by

$$[k_{FRP}] = \int [B]_i^T [D_{FRP}][B]_i dV \tag{6-1}$$

$$\{f_{FRP}\} = \int [N]_i^T q dA \tag{6-2}$$

in which $[N]$ and $[B]$ are the shape function matrix and the strain matrix of the laminate strip respectively, while $[D_{FRP}]$ and q are the material property matrix of the laminate and the magnitude of external forces respectively. In a similar manner, the mass matrix of a laminate FRP strip $[m_{FRP}]$ is presented by

$$[m_{FRP}] = \int [N]_i^T \rho [N]_i dV \tag{6-3}$$

in which ρ is the mass density of the strip and *t* is the thickness of the strip.

In the IFSM, the strip properties are converted to knots along the nodal lines during the simulating process. However, the number of required knots is significantly reduced comparing to FEM due to the semi-analytical nature of the IFSM. The stiffness and mass matrices as well as the force vectors of all the strips are assembled using conventional assembling procedure. Thereafter the entire 3D model of the hybrid FRP bridge is built using IFSM. When assembling the entire FRP Bridge model, the connectivity between different components (cable-deck connectivity, pier-deck connectivity, tower-deck connectivity, etc.) is provided by transition section elements which have already been defined in the formulation of each individual strip.

6.3 Bending analysis of FRP Bridge using IFSM

After simulating the entire 3D model of the hybrid FRP bridge system using IFSM and defining the global stiffness matrix $[K]$ and force vector $\{F\}$, the displacements $\{\delta\}$ not only

at the FRP deck structure but also for other locations of the bridge, like towers and cables can be estimated by

$$\{F\} = [K]\{\delta\} \tag{6-4}$$

6.4 Frequency analysis of FRP Bridge using IFSM

A standard eigenvalue analysis between mass matrix $[M]$ and stiffness matrix $[K]$ of the FRP bridge provides the natural frequencies and mode shapes of the structure

$$[M]\{\ddot{\delta}\} + [K]\{\delta\} = 0 \tag{6-5}$$

where $\{\ddot{\delta}\}$ is the vector of the second derivative of the displacements. The eigenvalues and eigenvectors of the Eq. (6-5) are corresponding to the natural frequency and the mode shapes of the FRP bridge. Accurate free vibration estimation is an essential factor in complicated dynamic analyses of bridge structures like earthquake resistant design and aerodynamic flutter design. The dynamic characteristics are highly influenced by the free vibration behaviour of the hybrid FRP bridge. In bridge structures especially in long-span cable-stayed and suspension bridges, in some cases the dominant mode shape can occur in the towers instead of the deck [6.1]. The IFSM is capable of considering the vibration mode shapes not only of the deck but also the tower dominant modes. This is another advantage of using the IFSM in bridge analysis, including the FRP bridge systems.

6.5 Seismic analysis of FRP Bridge using IFSM

Using the dynamic properties of the IFSM, the seismic analysis of an FRP bridge can be performed in minimal time. Seismic analysis of bridge structures against earthquake effects can be performed by both time domain and frequency domain methods. Herein, the Newmark scheme previously presented in chapter 4 is employed for the time history analysis of the FRP bridge model. The seismic equation of motion of an FRP bridge system is defined as

$$[M]\{\ddot{\delta}\} + [C]\{\dot{\delta}\} + [K]\{\delta\} = -[M]a_g \tag{6-6}$$

where $\{\dot{\delta}\}$ is the velocity vector or the vector of the first derivative of displacements, and a_g is the ground acceleration of the earthquake. The classic Rayleigh damping can be adopted to form the damping matrix of the FRP bridge as below

$$[C]=\alpha[M]+\beta[K] \tag{6-7}$$

in which α and β are the Rayleigh damping factors, which are obtained from the structural damping ratios ξ of two specific frequencies. The damping ratio ξ of the *n*th mode of the structure is given by

$$\xi_n=\frac{1}{2\omega_n}\alpha+\frac{\omega_n}{2}\beta \tag{6-8}$$

where ω_n is the angular natural frequency of the *n*th mode of the FRP bridge. The detailed explanation of the seismic analysis using IFSM can be found in chapter 4.

6.6 Numerical examples

The integrated finite strip method augmenting the material properties of the FRP laminated deck has been formulated and programmed on a desktop workstation. The C++ programming language was employed for IFSM discretization while MATLAB was used for temporal discretization. The IFSM has been used to study the bending and vibration performance of a continuous multi-span FRP deck bridge and a long-span cable-stayed hybrid FRP bridge. Bending analysis as well as the free vibration and time-history seismic analysis in the environment of IFSM will examine the vibration performance of the selected case studies. In addition, both FRP bridges have been modelled by FEM using SAP2000 in order to validate the accuracy of the IFSM results.

6.6.1 Integrated finite strip analysis of continuous multi-span FRP Bridge

In the first case study, a multi-span continuous FRP bridge deck is investigated. To verify the accuracy and efficiency of the proposed integrated finite strip solution for both static and free vibration analysis, a short span hybrid FRP slab-girder bridge model, as shown in Figure 6.1 (a), is presented. The layout of the FRP laminated deck and the configurations of

different layers are listed in Table 6.1. Each ply is made by CFRP (IM6G/3501-6) with the following properties: mass density $\rho = 1600\ (kg/m^3)$, modulus of elasticity along the longitudinal direction $E_{11} = 147\ GPa$, modulus of elasticity along the transverse direction $E_{11} = 10\ GPa$, Shear modulus $G_{12} = 7\ GPa$, and Poisson ratio ν_{12}=0.25. The pier is made from concrete with the modulus of elasticity $E = 3.0\times10^4\ \text{MPa}$, the Poisson's ratio of 0.2, and the material density is 2,500 kg/m^3. Both IFSM and FEM are adopted to model the static and dynamic behavior of the structure, and the results are compared.

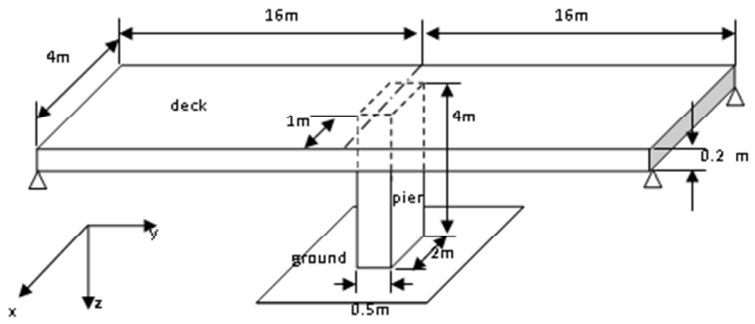

(a)

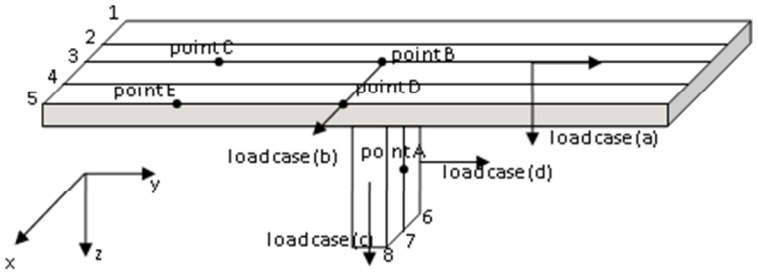

(b)

Figure 6.1 An FRP slab girder bridge (a) geometry; (b) IFSM model and forces

A full bridge model is constructed using the laminate strip for the FRP deck, 3D column strip (CS) for the pier and the transition section elements for the bearings. The deck is divided into four equal strips, and the pier is divided into two column strips. Each deck strip is composed of 32 sections as well as two additional transition sections where they connect to the piers. Each pier strip is composed of 4 sections, as well as one transition section, at the connection with the deck. For FEM model, the mass and stiffness of the bridges is

constructed with five degrees-of-freedom shell elements throughout the structure. A shell element is derived from a combination of an in-plane element with translation in the x and y directions, and a bending element with translation in the z direction, plus bending along the x and y directions. The deck is meshed with 32 by 4 elements, and the pier is meshed with 4 by 2 elements.

Table 6.1 Layout of the FRP deck

FRP slab-girder bridge deck (Thickness: 0.20m)		
Ply number	Angle (degrees)	Thickness (mm)
1	0	20
2	90	20
3	0	20
4	90	20
5	0	20
6	0	20
7	90	20
8	0	20
9	90	20
10	0	20
Total		200

6.6.1.1 Bending performance of the FRP slab girder bridge

For the static analysis, the ability of the transition element to transfer loading between the laminated FRP deck strip and the column strip is assessed. Four load cases, with constant 1,000 KN point forces acting on different components and in different directions, are assigned to the bridge model as shown in Figure 6.1(b). The vertical and horizontal drifts along different nodal lines, determined from both numerical methods, are summarized in Tables 6.2 to 6.5. It was noticed that the displacement calculated from the integrated finite strip approach agrees well with the FEM results, for all loading conditions, which indicates

that the proposed approach can successfully model a hybrid FRP bridge structure in the FS environment, taking the pier-bearing-deck interaction into consideration.

Table 6.2: Load Case (a)

Case a	Deck-modal line 3						Pier-nodal line 7		
	Y (m)	0 (left)	8	16	24	32 (right)	z (m)	0 (top)	2
v (mm)	IFSM	0.072	0.105	0.156	0.275	0.145	IFSM	0.149	0.048
	FEM	0.073	0.110	0.166	0.302	0.149	FEM	0.166	0.052
w (mm)	IFSM	-1.696	-150.121	0.060	470.458	6.705	IFSM	0.071	0.046
	FEM	-1.580	-174.372	0.068	450.783	6.856	FEM	0.068	0.046

Table 6.3: Load Case (b)

Case b	Deck-modal line 3						Pier-nodal line 7		
	Y (m)	0	8	16	24	32	z (m)	0	2
u (mm)	IFSM	0.001	0.832	1.813	0.983	0.004	IFSM	1.486	0.598
	FEM	0.003	0.832	1.605	0.832	0.003	FEM	1.605	0.527

Table 6.4: Load Case (c)

Case c	Deck-modal line 4						Pier-nodal line 8		
	Y (m)	0	8	16	24	32	z (m)	0	2
w (mm)	IFSM	0.000	0.123	0.193	0.112	0.000	IFSM	0.198	0.219
	FEM	0.000	0.118	0.197	0.118	0.000	FEM	0.197	0.236

Table 6.5: Load Case (d)

Case d	Deck-modal line 2						Pier-nodal line 6		
	Y (m)	0	8	16	24	32	z (m)	0	2
v (mm)	IFSM	0.034	0.055	0.089	0.048	0.030	IFSM	0.139	1.836
	FEM	0.031	0.053	0.115	0.062	0.010	FEM	0.115	1.733

6.6.1.2 Frequency analysis of FRP slab girder bridge

The accuracy of the dynamic analysis highly depends on the free vibration natural frequencies of the bridge model. Table 6.6 compares the first 7 natural bending frequencies of the models. The very small deviation of the modal frequencies between the two methods demonstrates that the integrated approach is capable of capturing the free vibration characteristics of a bridge and both two methods should have similar dynamic behaviour, whereas the minor deviation is likely to be caused by the slight differences in mass distribution within different elements. The deformed shape of the FRP slab girder bridge for the first seven natural modes are illustareted in Fig. 6.2.

Table 6.6 Natural Frequency of the FRP slab Bridge

Mode Number	Frequency (Hz)		Mode Shape
	Integrated FSM	FEM	
1	2.08	2.00	Heave (deck) antisymmetrical
2	3.38	3.11	Heave (deck) symmetrical
3	8.08	7.90	Heave (deck) antisymmetrical
4	10.78	9.90	Heave (deck) symmetrical
5	17.59	17.33	Torsional (deck) antisymmetrical
6	19.60	19.96	Torsional (deck) symmetrical
7	29.47	29.38	Heave (deck) antisymmetrical

(a) First mode (2.08 Hz)

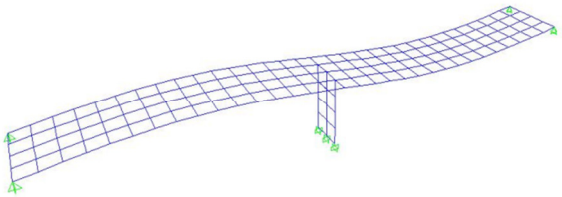

(b) Second mode (3.38 Hz)

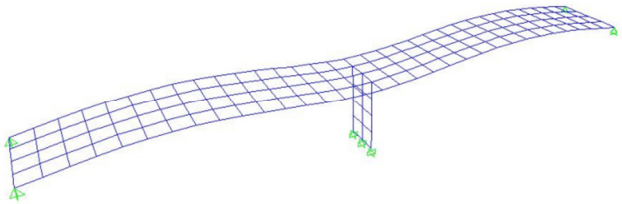

(c) Third mode (8.08 Hz)

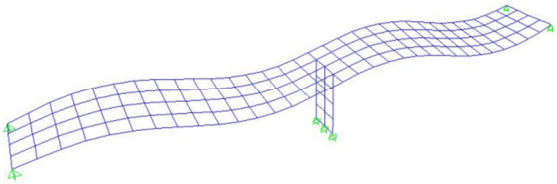

(d) Fourth mode (10.78 Hz)

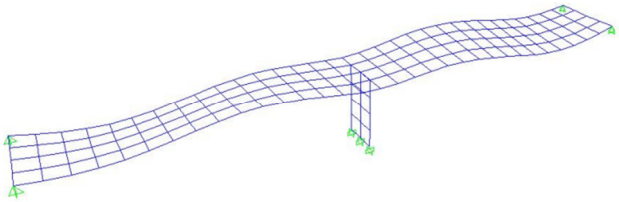

(e) Fifth mode (17.59 Hz)

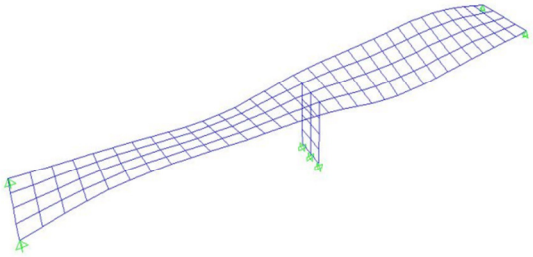

(f) Sixth mode (19.60 Hz)

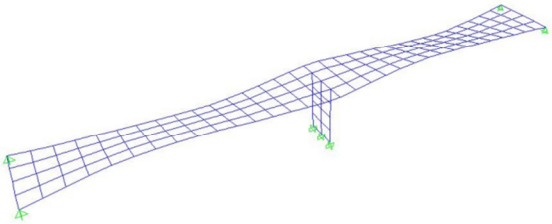

(g) Seventh mode (29.47 Hz)

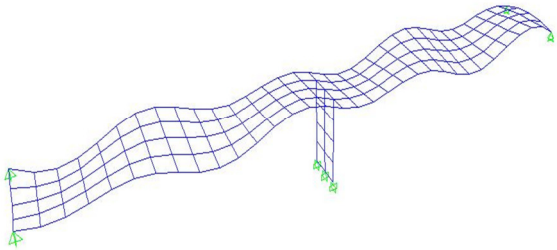

Fig. 6.2 Mode shapes of the hybrid FRP slab-girder Bridge

As further studies, and in order to compare the free vibration performance of an FRP deck bridge with a concrete deck bridge [6.16], the natural frequencies of both systems were compared in Table 6.7. The material properties of the deck are the same as for the pier, while the thickness of the concrete deck is 25 cm. The integrated finite strip results show that the natural frequencies of the FRP bridge are higher than those of the concrete bridge because the total weight of the FRP deck is reduced due to the use of the FRP material instead of concrete. In other words, the stiffness to mass ratio has increased in FRP bridge comparted to the concrete bridge. Comparing the mode shapes of the two bridges, it can be concluded that the torsional mode is more likely to occur in the FRP bridge model. Therefore, special attention needs to be paid to investigating the torsional instability in FRP bridges. The latter proves that the dynamic behaviour of the FRP bridge is totally different from the concrete bridge one.

Table 6.7 Comparison of natural frequencies of FRP and concrete bridges

Mode	Frequency (Hz)		Mode Shape	
	FRP bridge	Concrete bridge [6.16]	FRP bridge	Concrete bridge [6.16]
1	2.08	1.53	Heave (deck) antisymmetrical	Heave (deck) antisymmetrical
2	3.38	2.40	Heave (deck) symmetrical	Heave (deck) symmetrical
3	8.08	6.11	Heave (deck) antisymmetrical	Heave (deck) antisymmetrical
4	10.78	7.73	Heave (deck) symmetrical	Heave (deck) symmetrical
5	17.59	13.57	Torsional (deck) antisymmetrical	Heave (deck) antisymmetrical
6	19.60	15.77	Torsional (deck) symmetrical	Heave (deck) symmetrical
7	29.47	22.45	Heave (deck) antisymmetrical	Heave (deck) antisymmetrical

6.6.2 Long-span cable-stayed hybrid FRP Bridge

In order to evaluate the accuracy of the laminate spline strip in the environment of integrated finite strip method for free vibration and seismic analysis of hybrid FRP deck long-span cable-stayed bridges, the Kap Shui Mun Bridge, shown in Fig. 6.3 is taken as the reference model. Also, to examine the integrated finite strip results and the performance of the proposed system, a 3D finite element model is constructed by SAP 2000. The composite laminated FRP deck is modelled by shell layered linear finite elements. The seismic performance of the cable-stayed FRP Bridge is investigated under uniform and non-uniform seismic excitations. Therefore, the feasibility of applying such FRP deck system in ultra-long span cable-stayed bridges can be discussed.

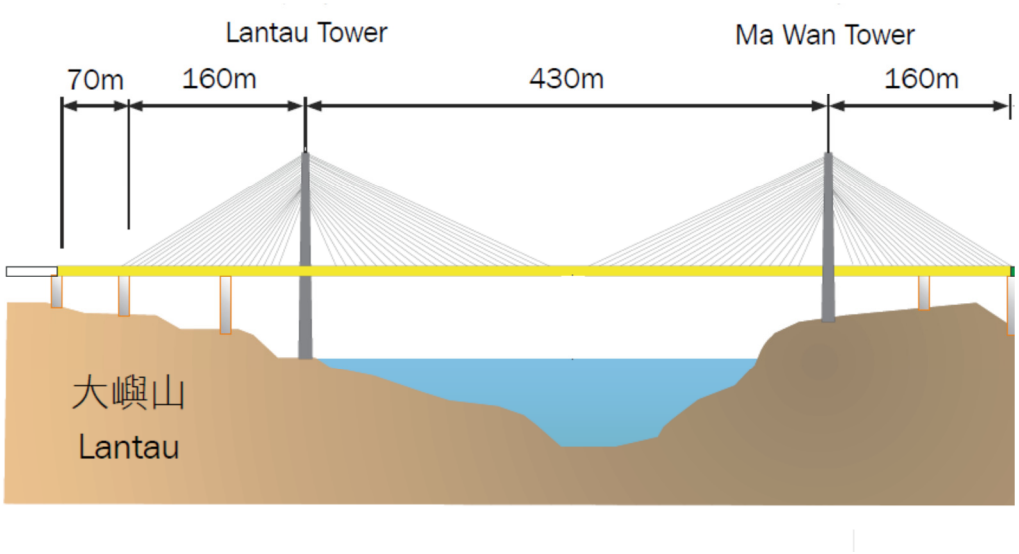

Fig. 6.3 Kap Shui Mun Bridge [6.17]

The Kap Shui Mun Bridge, located in the Lantau Link, provides a direct access to the Hong Kong International Airport. The total length of the bridge is 820 m which classifies the Kap Shui Mun as the world's second longest cable-stayed bridge carrying both road and rail traffic. It is a double decked bridge including a dual three lane expressway at the upper deck while two railway tracks and two single lane sheltered carriageways within the lower deck. The bridge is supported by two concrete pylons with the heights of 145 m and 133 m in the west and east sides respectively. The legs of each tower were constructed by a jump-form process and were joined together by post-tensioned struts [6.17]. The tops of the towers

were also post-tensioned to resist the bursting forces caused by the stay cable anchorages. The entire bridge is supported by 176 stay cables made up of 51 to 102 high tensile steel strands. The Bridge was opened to traffic in May 1997 after 54 months of construction. The IFSM and FEM models of the original Kap Shui Mun Bridge have been constructed and calibrated using site experiment data which are highly idealized [6.1].

6.6.2.1 Specifications of carbon fiber reinforced plastic (CFRP) deck system

The design of the cross-section of the laminated FRP deck is influenced by some major considerations including the long span cable stayed bridge requirements, and the advanced material properties and macro/structural design requirements. Although the glass fiber reinforced polymer (GFRP) can satisfy the strength requirement with much lower costs, the deflection of the middle span is too large for its low Young's modulus, as reported in [6.13]. After testing different types of FRP materials, carbon fiber reinforced polymer with the following properties has been proposed by Cheung et al. [6.14] as the core material of the deck section: CFRP (IM6G/3501-6) with the mass density of $\rho = 1600\ (kg/m^3)$, modules of elasticity along the longitudinal direction $E_{11} = 147\ GPa$, modules of elasticity along the transverse direction $E_{11} = 10\ GPa$, Shear modules $G_{12} = 7\ GPa$, and Poisson ratio ν_{12}=0.25. A square tube based FRP box girder deck system, as illustrated in Fig. 6.4, is suggested to replace the steel-concrete deck [6.13].

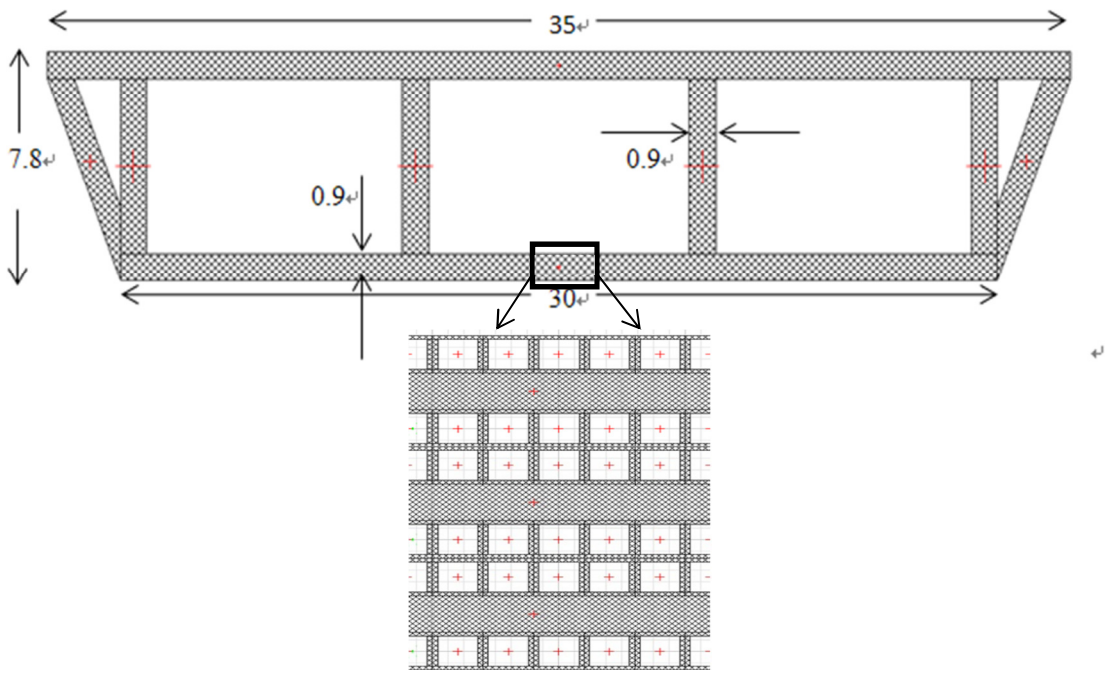

Fig. 6.4 The design of the FRP bridge deck system [6.13]

6.6.2.2 Integrated finite strip modelling of FRP cable-stayed Bridge

Herein, a thin laminated flat FRP deck has been chosen for the bridge composite deck, which has been modeled such that it has properties compatible with the deck designed by Chaw [6.13] in terms of cross-section area, FRP material properties and the angle of lamina orientations in the FRP laminated deck system. The composite hybrid FRP deck is modelled by using laminate spline strips developed in chapter 5. There are 38 layers of 1.0 cm thickness CFRP lamina, introduced in the previous section, with the orientation configuration in the sequences of 0, 90, 0 degrees.

The two concrete pylons and other piers and linked beams are modelled by one-dimensional column strips, while the cables are modelled by one-dimensional cable strips. The pre-stress condition in the cables is also included in the current analysis. All the interaction points between different structural elements, including hybrid FRP deck, pylons, piers, and link beam are modelled by transition section elements. More detailed information about the geometry of the Kap Shui Mun Bridge, as well as the finite strip discretization were addressed in chapter 3. Therefore, a fully 3D finite strip simulation of the hybrid FRP cable stayed bridge is made in the environment of IFSM.

6.6.2.3 Free vibration analysis of the FRP cable-stayed bridge

One of the most important factors in the dynamic and aerodynamic performance of cable-stayed bridge is originated from the free vibration and natural frequency properties of the bridge. For instance, the identification of dominant mode shape of the cable-stayed bridge can predict the aeroelastic behavior of the bridge in flutter or buffering responses. In this section, the free vibration analysis of the selected long-span cable-stayed FRP bridge in the environment of IFSM is performed through which the natural frequencies as well as dominant mode shapes of the FRP structure are identified. Using the overall mass and stiffness matrices, an eigenvalue analysis can estimate the natural frequency of the FRP bridge system as well as the deformed shape of the bridge structure thorough the eigenvalue and eigenvectors respectively. The first ten dominant frequency of each mode shape, including tower, lateral, vertical, and torsional modes are classified and presented in Tables 6.8 to 6.11 respectively. The frequencies obtained by the integrated finite strip method are compared with the free vibration finite element analysis and the percentage of the difference between the results is listed in the tables. In all cases, a good agreement is witnessed between the results, while the natural frequencies of IFSM are slightly higher than those obtained by the FE analysis except in the case of lateral mode shapes in which in higher modes the finite element frequencies are higher and the difference between the results are significantly more which is questionable. The reason for the difference between the results could be because of the different distribution of the mass properties between the elements of the FE model. In general, the percentage of error in most cases is less than 10 %. According to the results, the best agreement between the results is observed in the cases of vertical bending mode and tower modes. It can be concluded that the tower dominant modes are well predicted in the environment of IFSM. The deformed shapes of the first symmetric and antisymmetric mode shapes of each specific vibration mode of FRP cable-stayed bridge are displayed in Figs. 6.8 to 6.12.

Table 6.8, Natural frequencies of the tower dominant modes

Mode Number	IFSM (Hz)	FEM (Hz)	Error %
1	0.19	0.19	0.0
2	0.22	0.21	4.5
3	1.13	1.10	2.6
4	1.13	1.10	2.6
5	1.33	1.27	4.5
6	1.88	1.77	5.8
7	2.23	2.12	4.9
8	3.15	3.00	4.7
9	3.22	3.09	4.0
10	3.31	3.11	6.0

Table 6.9, Natural frequencies of the deck lateral dominant modes

Mode Number	IFSM (Hz)	FEM (Hz)	Error %
1	0.57	0.55	3.5
2	1.00	0.98	2.0
3	3.92	3.70	5.6
4	5.62	5.30	5.6
5	5.97	5.73	4.0
6	6.29	6.46	-2.7
7	6.93	7.74	-11.6
8	7.13	8.12	-13.8
9	7.28	8.40	-15.3
10	7.46	8.88	-19.0

Table 6.10, Natural frequencies of the deck vertical dominant modes

Mode Number	IFSM (Hz)	FEM (Hz)	Error %
1	0.33	0.32	3.0
2	0.40	0.38	5.0
3	0.67	0.66	1.4
4	0.79	0.77	2.5
5	0.88	0.87	1.1
6	0.93	0.91	2.1
7	0.99	0.97	2.0
8	1.04	1.02	1.9
9	1.14	1.12	1.7
10	1.17	1.16	0.8

Table 6.11, Natural frequencies of the deck torsional dominant modes

Mode Number	IFSM (Hz)	FEM (Hz)	Error %
1	0.50	0.45	10.0
2	0.62	0.57	8.0
3	1.13	1.05	7.0
4	1.29	1.23	4.6
5	1.43	1.35	5.5
6	1.46	1.43	2.0
7	1.64	1.54	6.0
8	1.73	1.63	5.7
9	1.79	1.73	3.3
10	1.99	1.84	7.5

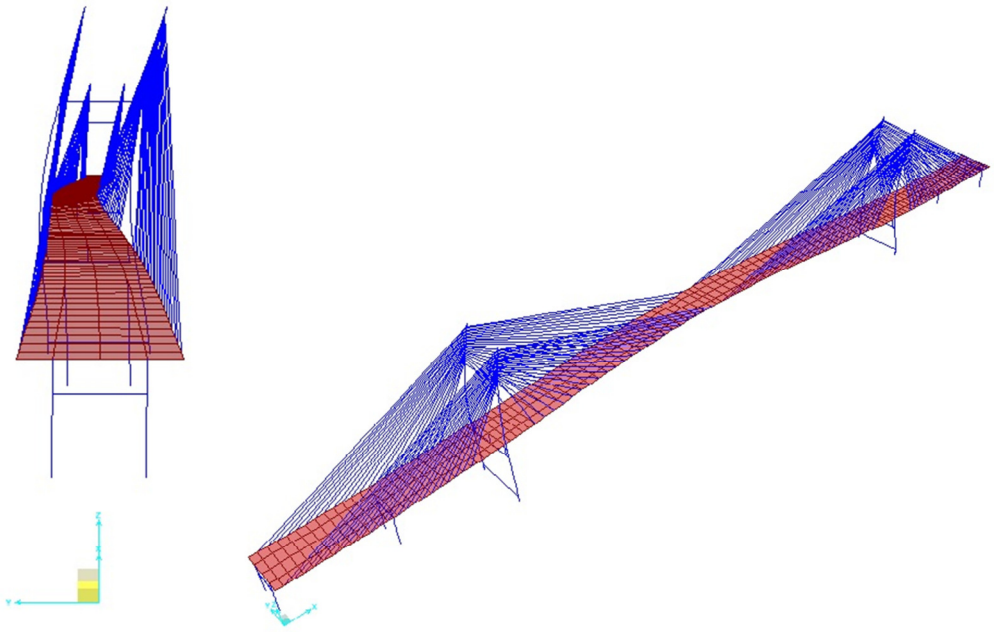

Fig. 6.5 First symmetric lateral mode shape of the FRP cable-stayed bridge (0.5725 Hz)

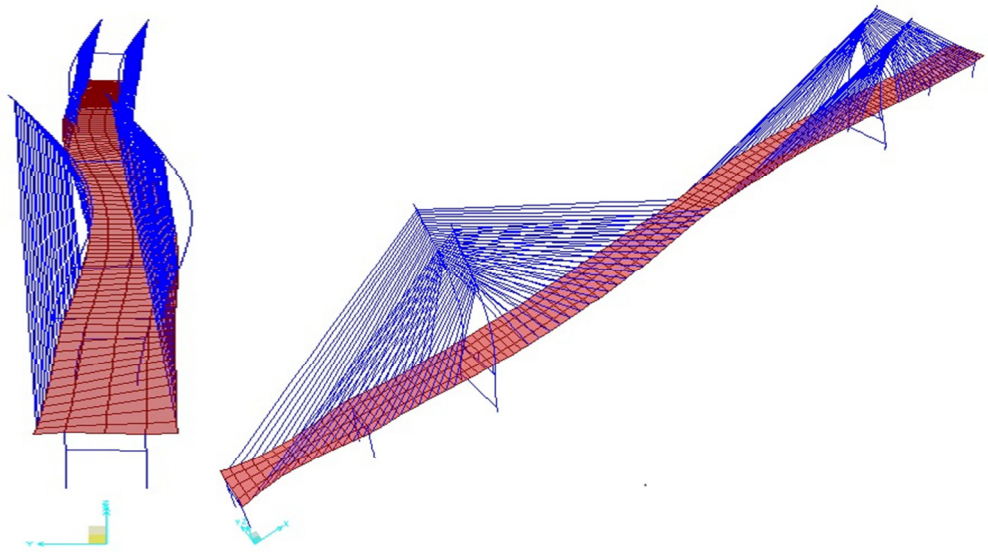

Fig. 6.6 First antisymmetric lateral mode shape of the FRP cable-stayed bridge (1.003 Hz)

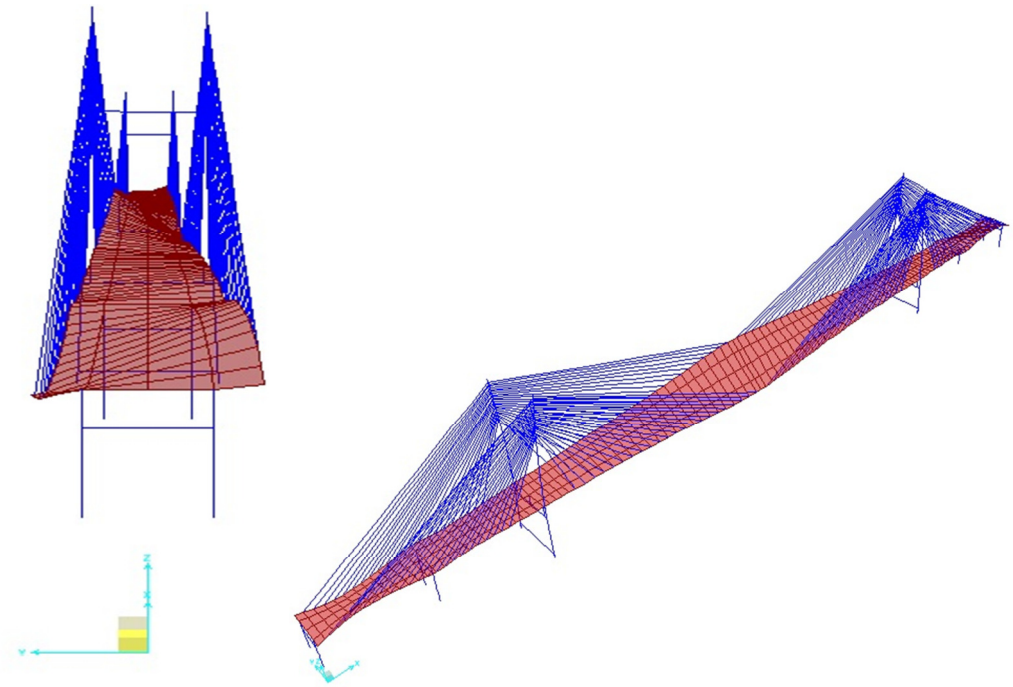

Fig. 6.7 First symmetric torsional mode shape of the FRP cable-stayed bridge (0.5027 Hz)

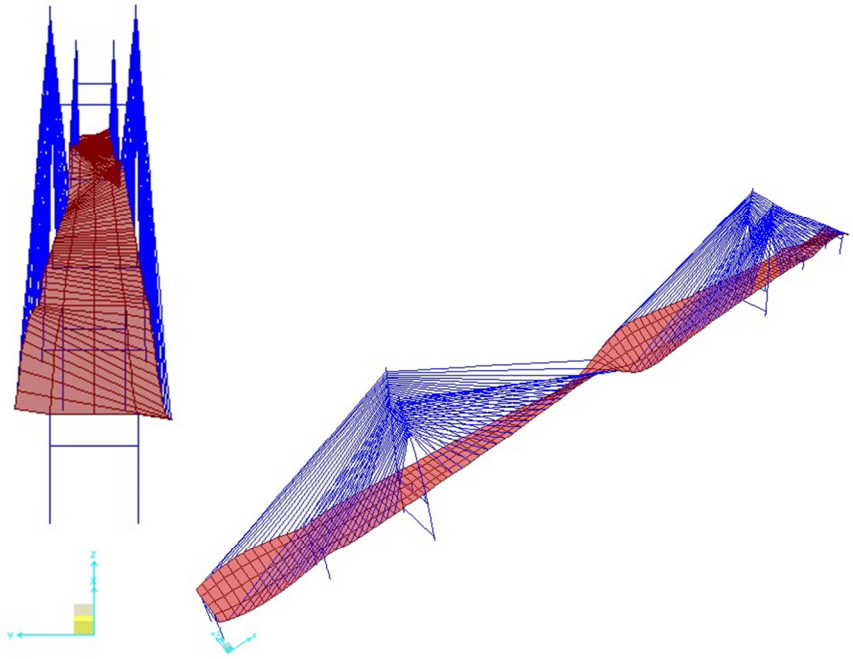

Fig. 6.8 First antisymmetric torsional mode shape of the FRP cable-stayed bridge (0.6290 Hz)

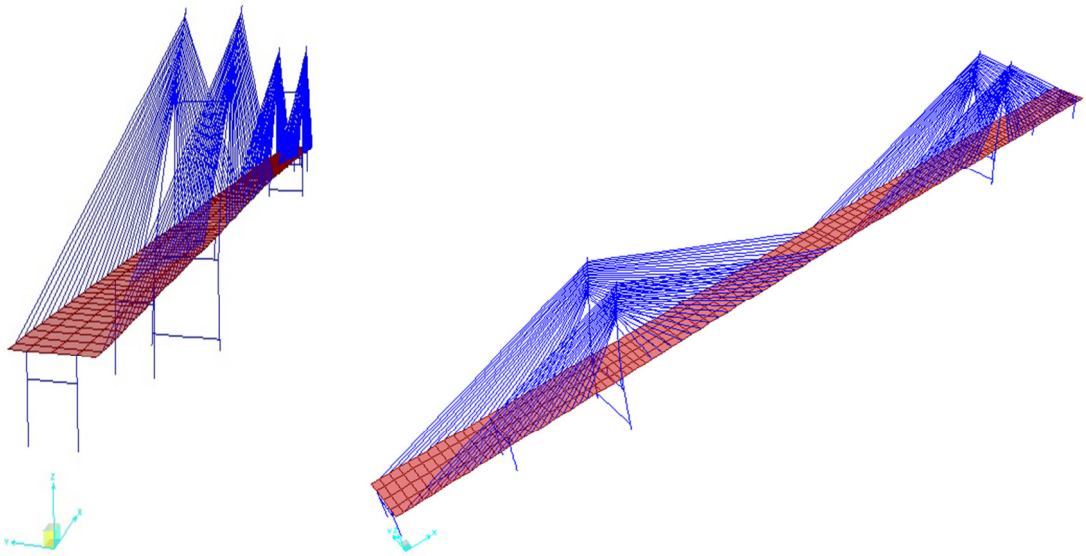

Fig. 6.9 First symmetric tower dominant mode shape of the FRP cable-stayed bridge (0.1986 Hz)

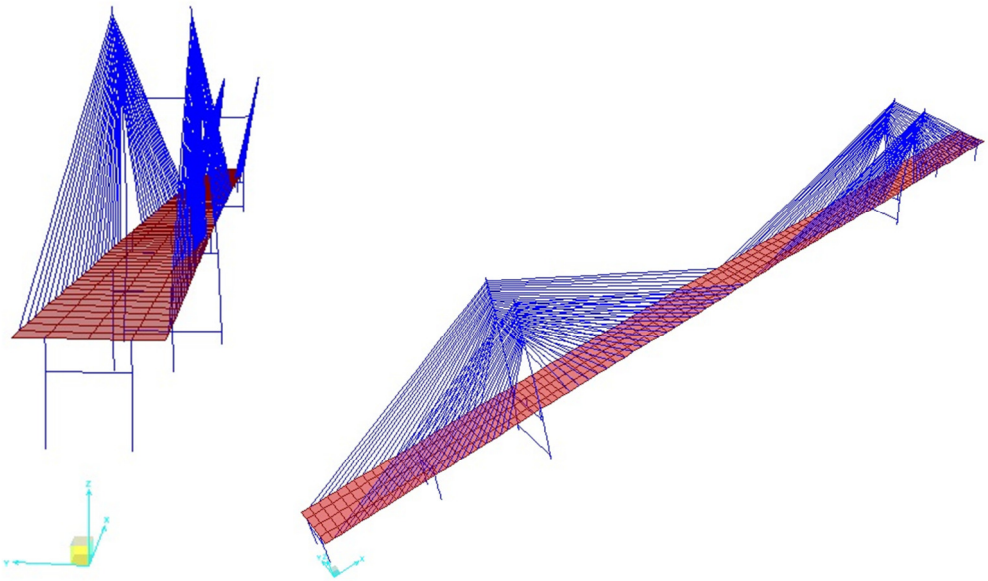

Fig. 6.10 First antisymmetric tower dominant mode shape of the FRP cable-stayed bridge (0.2245 Hz)

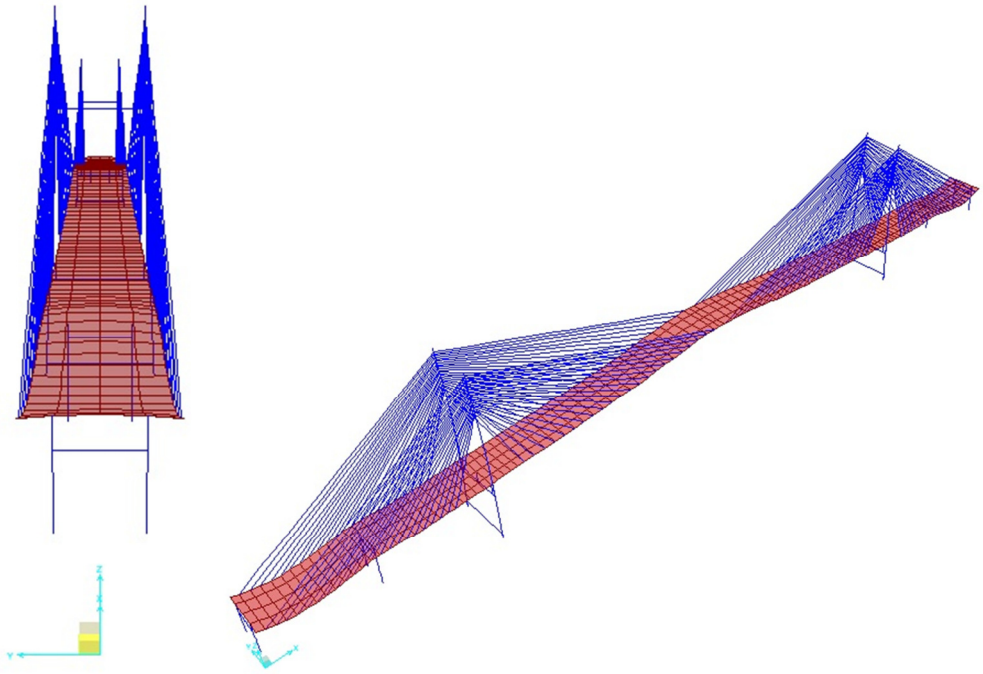

Fig. 6.11 First symmetric bending mode shape of the FRP cable-stayed bridge (0.3354 Hz)

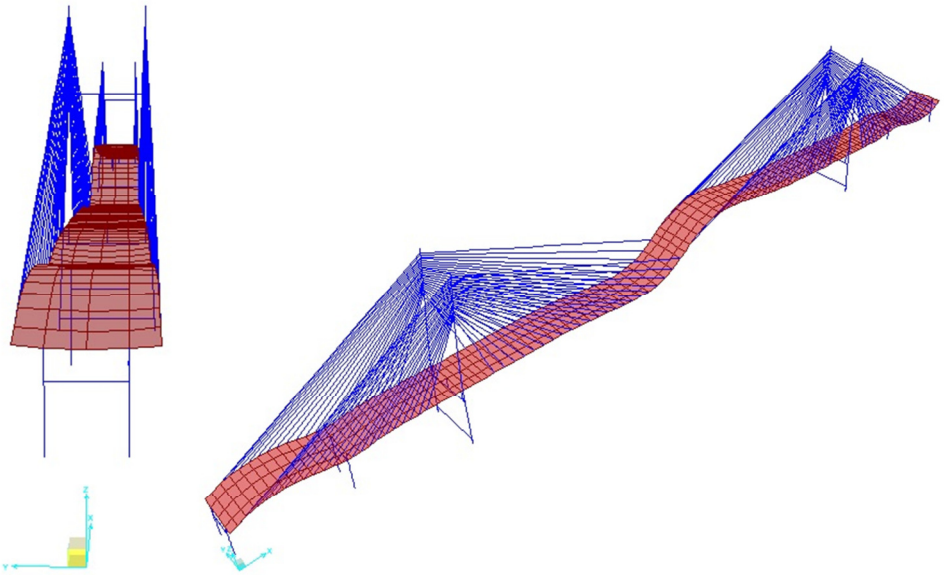

Fig. 6.12 First antisymmetric bending mode shape of the FRP cable-stayed bridge (0.4009 Hz)

In order to investigate the effects of FRP deck in the vibration behavior of the long-span cable-stayed bridge, a comparison study is made between the natural frequencies and mode shapes of the original model of the Kap Shui Mun Bridge with those of the FRP bridge model. The first ten mode shapes and the corresponding natural frequencies of the original Kap Shui Mun Bridge and the hybrid FRP version are presented in Table 6.12. As can be seen, the dominant mode in both cases is the tower (pylon) swaying mode. Also, it seems that torsional mode is more likely to occur at lower frequencies in the hybrid FRP bridge than the original Kap Shun Mun Bridge. Torsional free vibration mode is an important factor in aerodynamic flutter stability of long-span cable-stayed bridges. Therefore, special considerations need to be provided in the design of the hybrid FRP cable-stayed bridges for flutter phenomenon. Herein, the natural frequencies of the hybrid FRP cable-stayed bridge are generally lower than those of original Kap Shui Mun Bridge which is questionable. The total weight of the bridge deck is reduced due to the use of FRP materials instead of the steel-concrete, while it is expected to provide a relatively high stiffness in a FRP bridge which is compatible with a conventional concrete-steel cable-stayed bridge. Therefore, the stiffness to mass ratio and subsequently the natural frequencies are expected to be higher in the case of FRP bridge. It can be concluded that the stiffness of the proposed FRP deck needs to be modified by increasing the thickness of the laminated FRP deck, or by considering alternative sequences of ply angles, or by adopting another type of FRP material. Regardless of the concluding remarks of the results, the latter study proves that the dynamic behavior of the cable-stayed FRP bridge is different from the original one.

Table 6.12 Vibration specifications of original and FRP Bridges

Mode number	FRP Bridge	Mode shape	Original Bridge [6.1]	Mode shape [6.1]
1	0.19	tow1	0.21	tow1
2	0.22	tow2	0.24	tow2
3	0.33	V1	0.42	V1
4	0.40	V2	0.52	L1
5	0.50	T1	0.75	T1
6	0.57	T2	0.85	V2
7	0.62	L1	0.93	L2
8	0.67	V3	1.00	V3
9	0.79	V4	1.13	tow 3
10	0.88	V5	1.14	tow 4

6.6.3 Seismic analysis of hybrid FRP long-span cable-stayed bridge

In the previous section, it was shown that the vibration characteristics of the FRP cable-stayed bridge system are entirely different from the original Kap Shui Mun Bridge. This brings the need to investigate the dynamic performance of the cable-stayed FRP bridges more deeply. The integrated finite strip method was successfully extended to model and to analyze the hybrid FRP long-span cable-stayed bridges, as a very efficient and straightforward numerical technique. The methodology will be further extended in this section in order to investigate the performance of hybrid FRP cable-stayed bridge under uniform and nonuniform earthquake excitations. In the environment of IFSM, the Newmark Scheme is deployed for time history analysis of the FRP cable-stayed bridge. More details on the time history scheme of finite strip seismic analysis can be found in chapter 4.

6.6.3.1 Time history analysis of cable-stayed FRP bridge under earthquake load

Using the dynamic properties of the hybrid FRP cable-stayed bridge by IFSM, the damping matrix can also be calculated using the Rayleigh Ritz relationships (Eq. (6-7)). Similar steps as the ones presented in chapter 4 can be followed in order to perform the time domain

analysis of hybrid FRP cable-stayed bridge. As previously mentioned, various spatial effects such as the wave-passage effect, the incoherence effect, and the local site effect, must be considered in the design of the long-span cable-stayed bridges against the earthquake loading. In the following, the seismic performance of hybrid FRP under different types of uniform and non-uniform seismic excitations will be studied. A finite strip time domain analysis is performed through which the acceleration and the displacement responses of the FRP Kap Shui Mun Bridge at different locations of the bridge can be determined. Some critical locations are targeted in the bridge structure as illustrated in Fig. 6.13.

Also, a FE time history analysis is performed using SAP 2000 in order to validate the IFSM for seismic analysis of hybrid FRP cable-stayed bridges. In the finite element model, the direct integration method has been adopted, when performing the dynamic analysis.

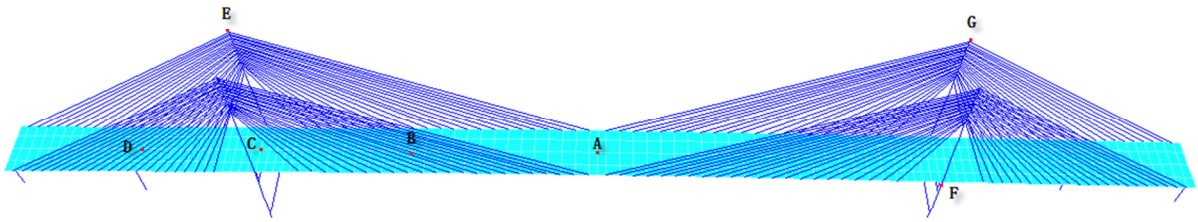

Fig. 6.13 Critical points for seismic response investigation

6.6.3.2 Seismic performance under uniform sine waves

In the first case study, a uniform sine wave earthquake is applied to the hybrid FRP cable-stayed bridge. In uniform excitation, all the degrees of freedom in the corresponding direction vibrate under the same ground acceleration. The IFSM and FE longitudinal acceleration and the displacement output curves at point F, in the east tower of the bridge are obtained and illustrated in Figs. 6.14 and 6.15, respectively. A good agreement is witnessed between the results of the integrated finite strip and finite element solutions. Despite the sharp jump in the first few seconds of the responses, the amplitude of both displacements and accelerations almost remain constant in the next time intervals which means the bridge

is stable under the applied earthquake wave. The amplitude of accelerations and displacements responses obtained from the finite strip time-history analysis are generally slightly higher than the finite element results which shows IFSM is more conservative but in the same time more accurate than FEM because it has less numerical damping. The small longitudinal displacement at point F might be because of the very low weight of the FRP deck through which the magnitude of the transmitted internal forces from the deck to the tower decreases.

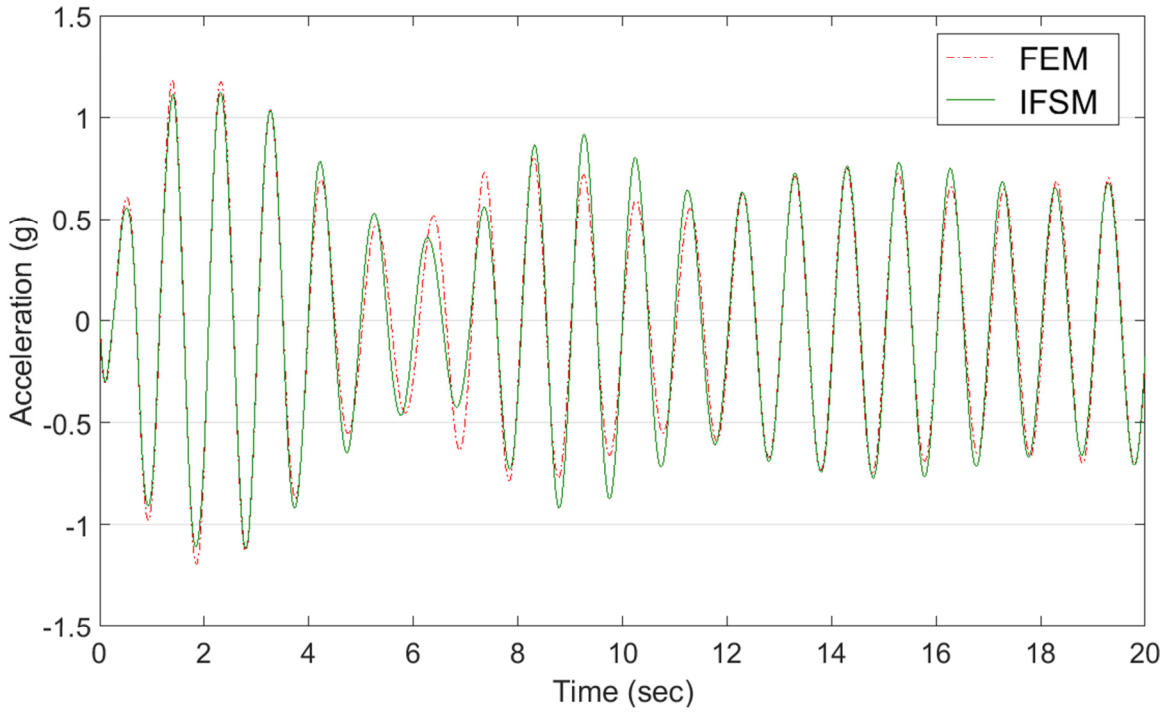

Fig. 6.14 Longitudinal acceleration responses of FRP bridge under uniform sine wave excitation at Point F in the east tower

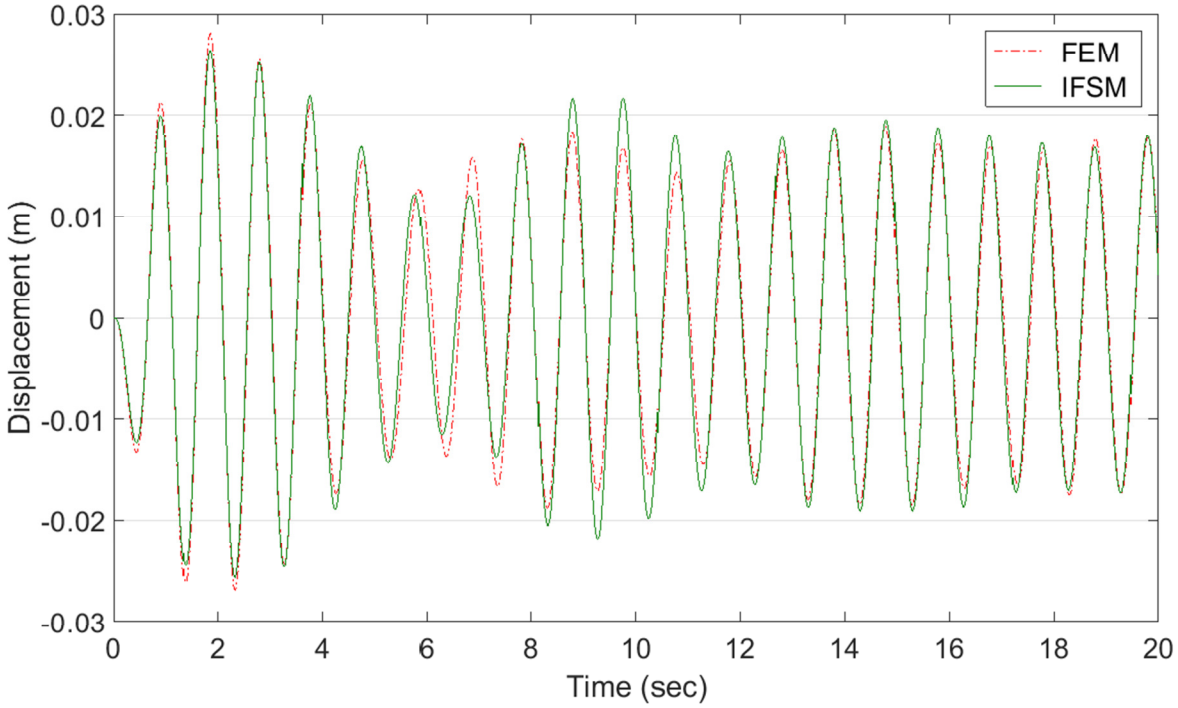

Fig. 6.15 Longitudinal displacement responses of FRP bridge under uniform sine wave excitation at Point F in the east tower

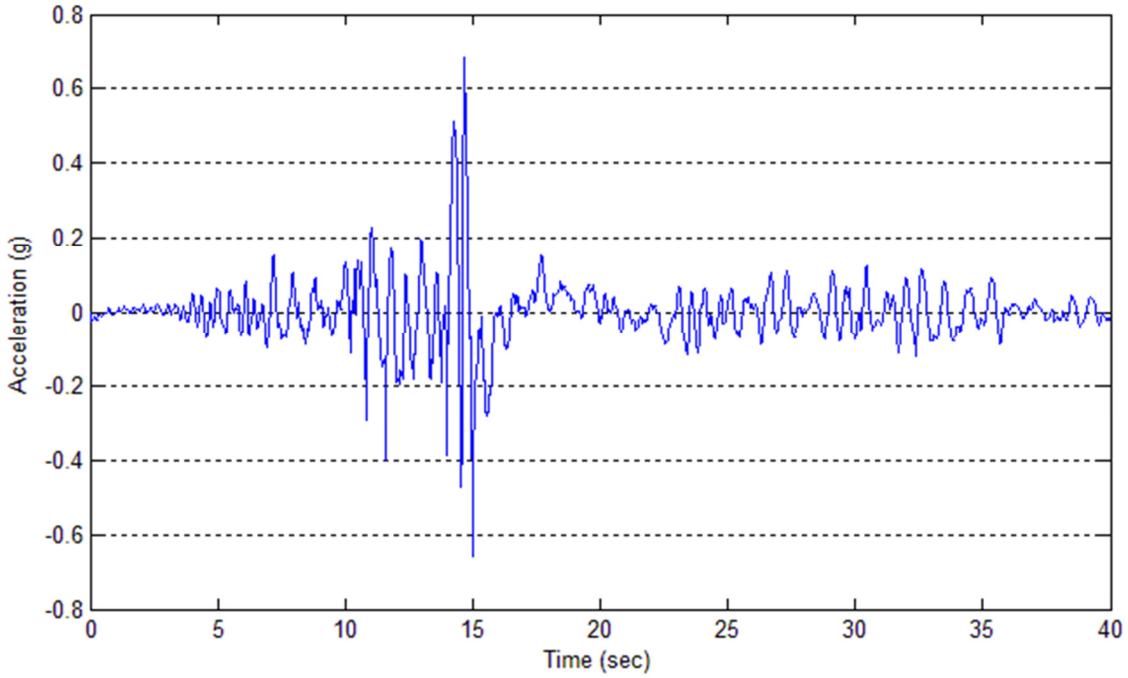

Fig. 6.16 Acceleration record of Chichi Earthquake

6.6.3.2 Seismic performance under uniform Chichi earthquake

As an example of a real earthquake wave, the acceleration records of Chichi earthquake, as shown in Fig. 6.16, is assigned to all degrees of freedom of the FRP cable-stayed bridge in the transverse direction. The acceleration and displacement curves at point B on the deck of the FRP Bridge are calculated and plotted in Figs. 6.17 and 6.18, respectively. It can be seen that the seismic responses under Chichi earthquake are not uniform. The maximum displacements and accelerations are registered between 15 to 20 seconds which is naturally owing to the maximum applied ground acceleration at the same time step (Fig. (6.16)). The displacements and accelerations registered before the occurrence of the maximum amplitude are very low, being consistent with the low acceleration input of the Chichi earthquake for the same time interval. The seismic performance of the bridge after the critical period of 15 to 20 seconds shows that the bridge system will remain stable due to the decreasing displacements and acceleration curves. The numerical results of both FEM and IFSM for time-history analysis are in very good agreement which confirms the accuracy of the IFSM in seismic analysis of FRP bridges.

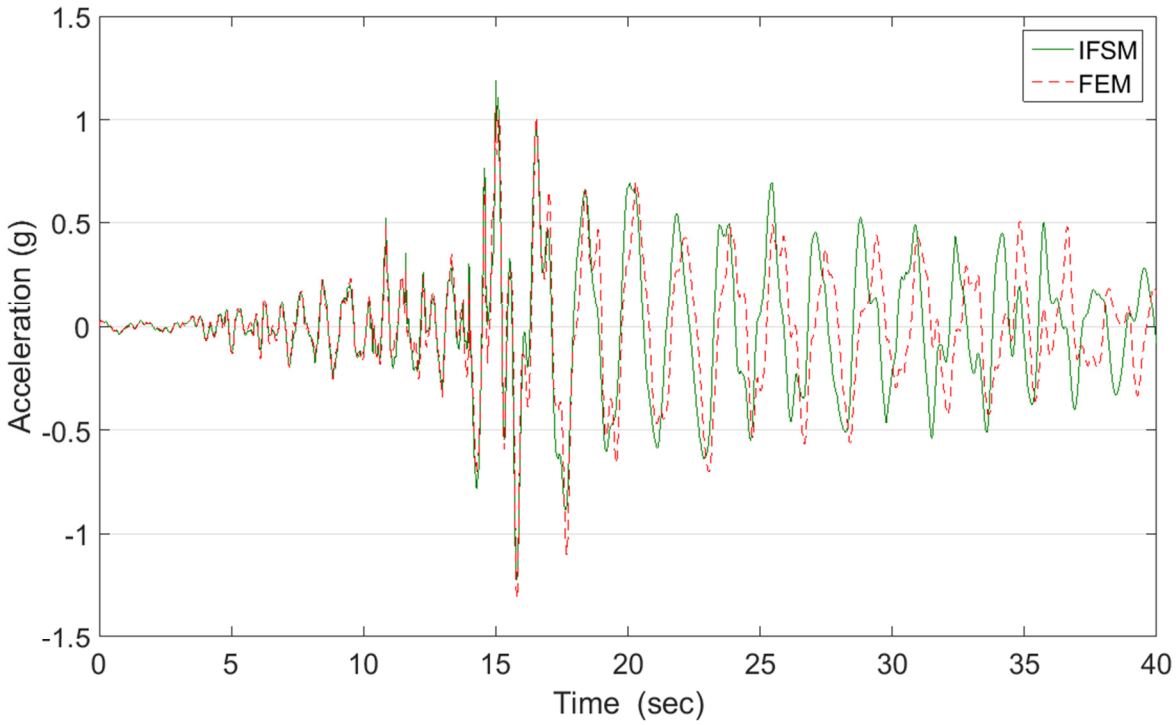

Fig. 6.17 Transverse acceleration responses of FRP bridge under uniform Chichi earthquake excitation at Point B on the deck

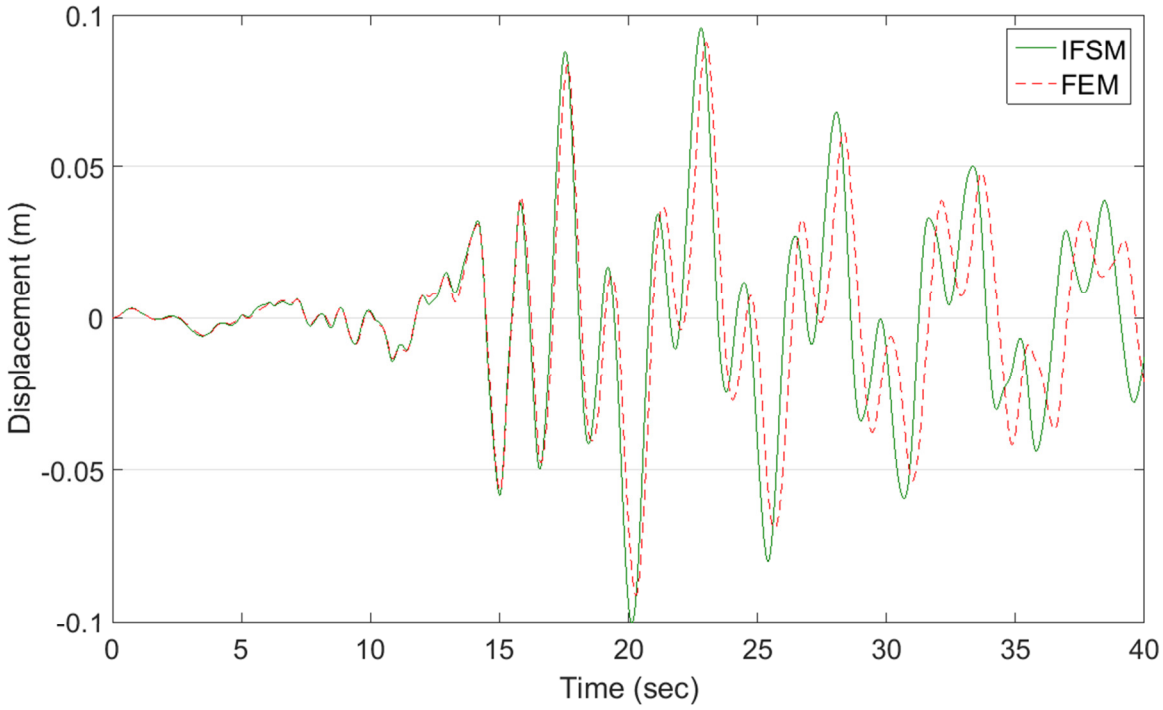

Fig. 6.18 Transverse displacement responses of FRP bridge under uniform Chichi earthquake excitation at Point B on the deck

6.6.3.3 Seismic performance under non-uniform Chichi earthquake

The real nature of the earthquake excitation effects on long span bridges is essentially non-uniform, in which different motions are prescribed at different supports of the bridge structure. Integrated finite strip time domain method is employed in this section to study the effects of the wave passage and varying seismic excitations, as the examples of non-uniform excitations. Wave passage effect accounts for the time delay in ground motions, as the seismic waves do not arrive at bridge foundations at the same time, especially for massive structures, such as long-span bridges, in which the distance between the piers and the pylons is very long.

Herein, the non-uniform excitation of the Kap Shui Mun FRP Bridge is studied under the Chichi earthquake wave record which is adopted as the input source. The velocities of the seismic waves are considered to be 500 m/s and 1000 m/s, in the longitudinal direction. The seismic wave is assumed to start propagating from the first west pier, and afterwards the ground motion will be transmitted to the following towers and piers one by one. In the finite

strip model, the time delay is simulated by inputting the seismic waves with different time lags, at the various supports. A seismic wave with the infinite velocity is also adopted which is in fact equivalent to the uniform excitation.

The IFSM acceleration and displacement responses of point E, located at the top of the west tower, are depicted through Figs. 6.19 to 6.24. For all the cases, it can be noticed that the maximum amplitudes of the displacements are identified slightly after the occurrence of the maximum applied ground acceleration. After this critical period, the amplitude of the responses starts to decrease gradually. In other words, the effects of the earthquake excitations are damped which is a positive sign about the stability of the investigated FRP bridge structure. Looking at the response curves, it can be also concluded that under uniform excitation the displacements and the accelerations of the bridge are generally higher than those obtained under non-uniform excitations. According to Figs. 6.22 and 6.23, the maximum displacement recorded at point E increases when the velocity increases from 500 m/s to 1,000 m/s. It seems that the amount of seismic forces transmitted to the tower is significant which might be due to the higher ratio of the tower stiffness to the deck stiffness.

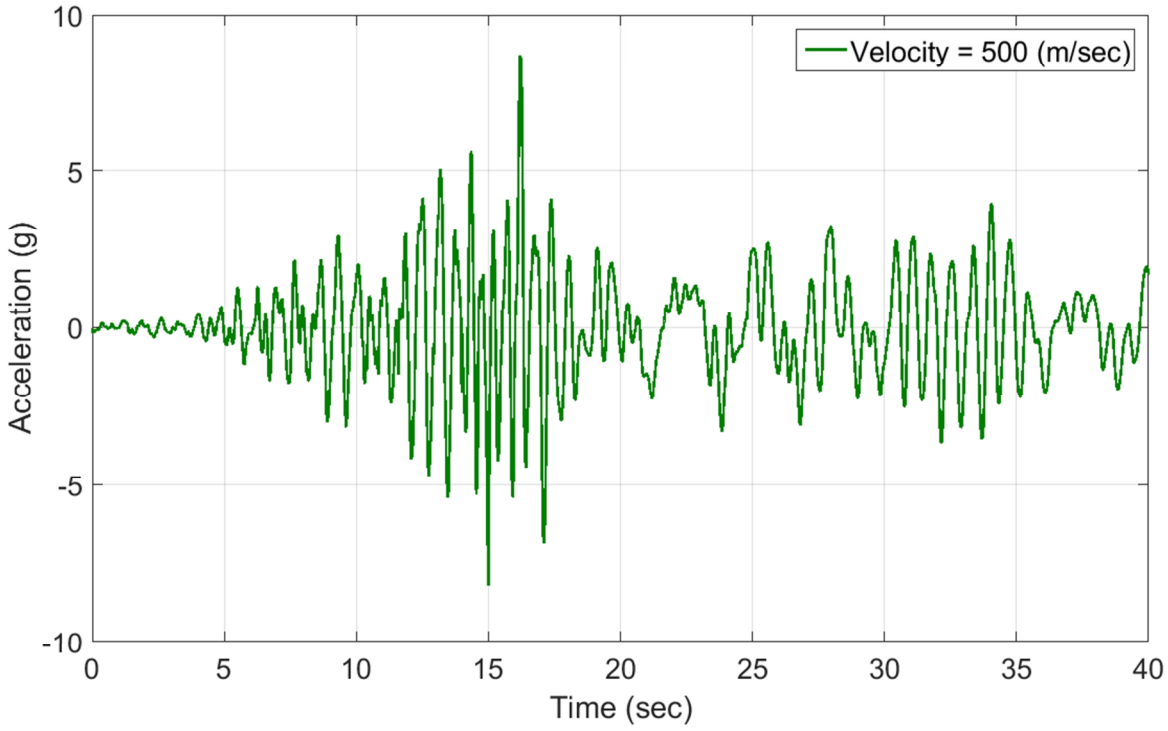

Fig. 6.19 Longitudinal acceleration response of FRP bridge at Point E at the west tower for velocity = 500 m/s

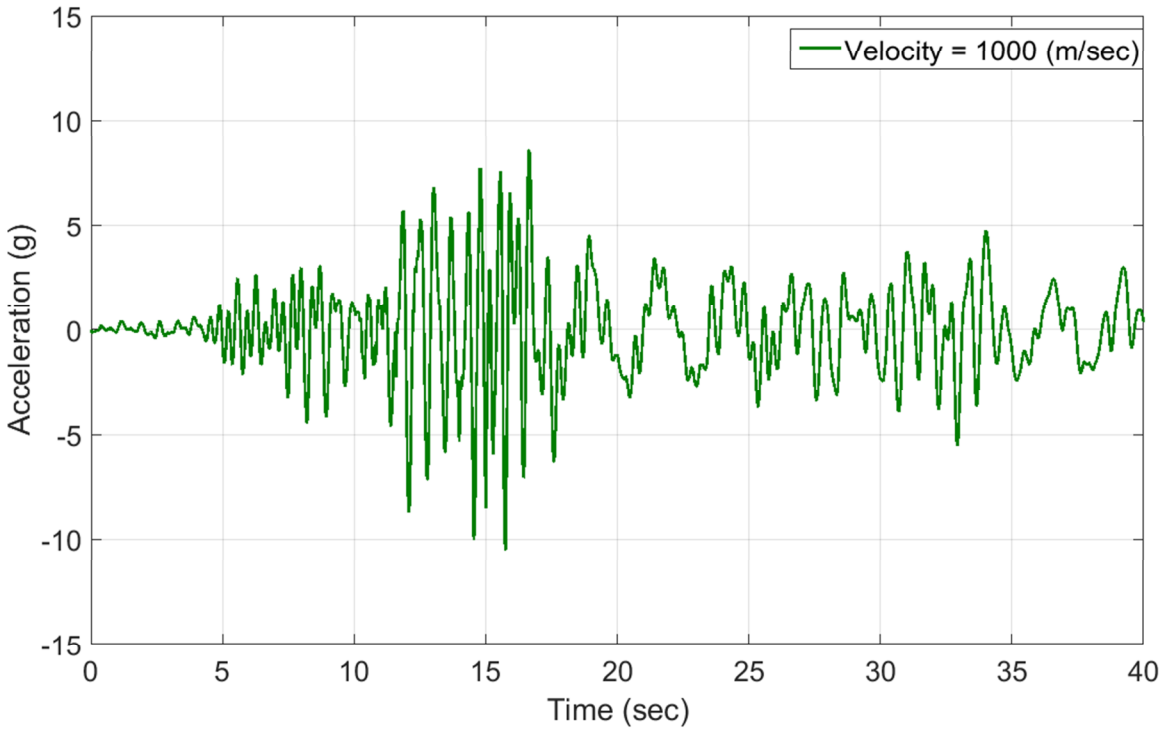

Fig. 6.20 Longitudinal acceleration response at Point E of FRP bridge at the west tower for velocity = 1,000 m/s

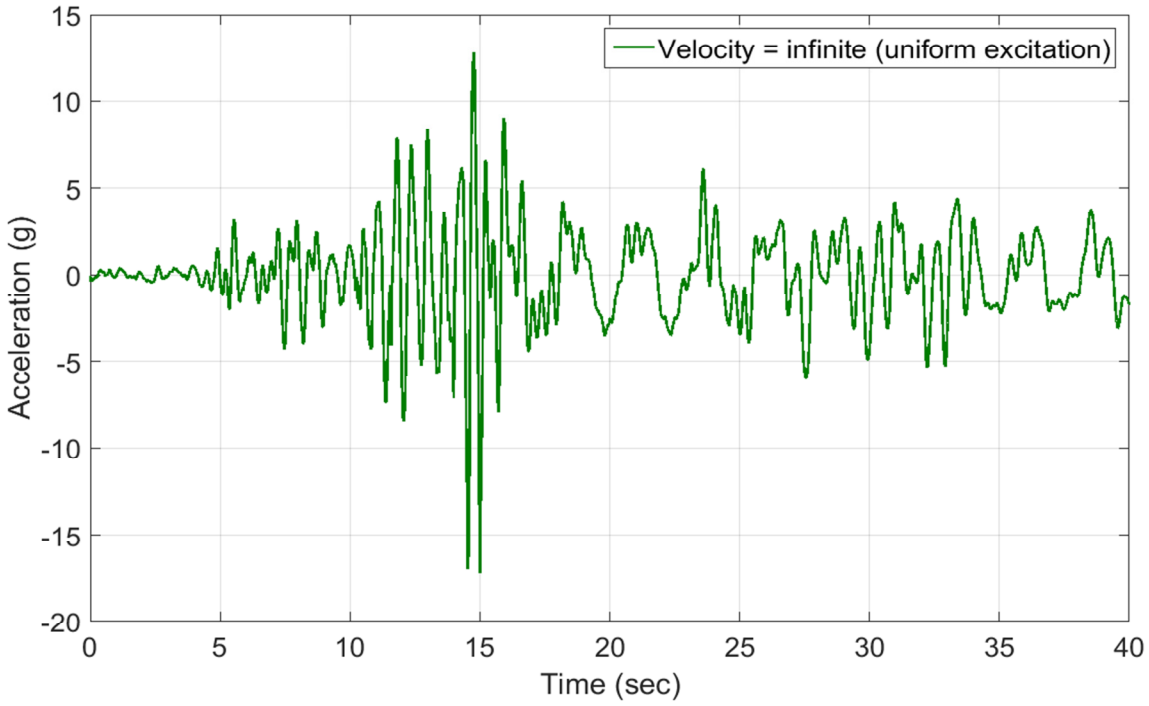

Fig. 6.21 Longitudinal acceleration response of FRP bridge at Point E at the west tower for velocity = infinite

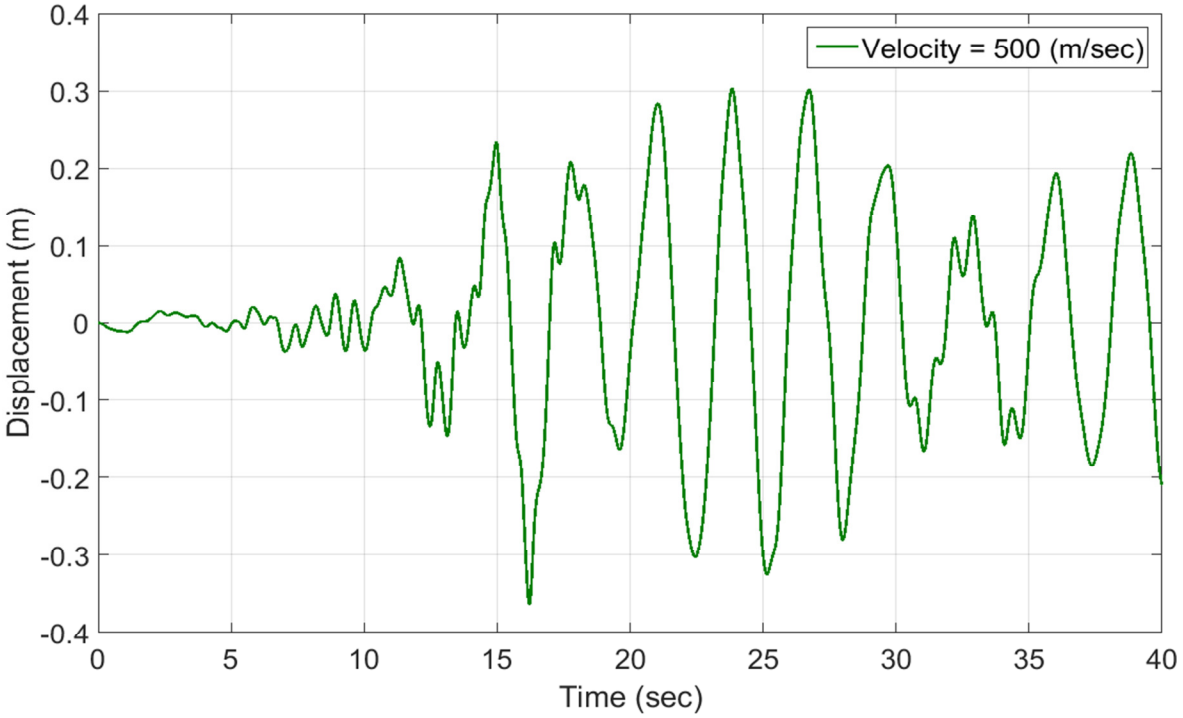

Fig. 6.22 Longitudinal displacement response of FRP bridge at Point E at the west tower for velocity = 500 m/s

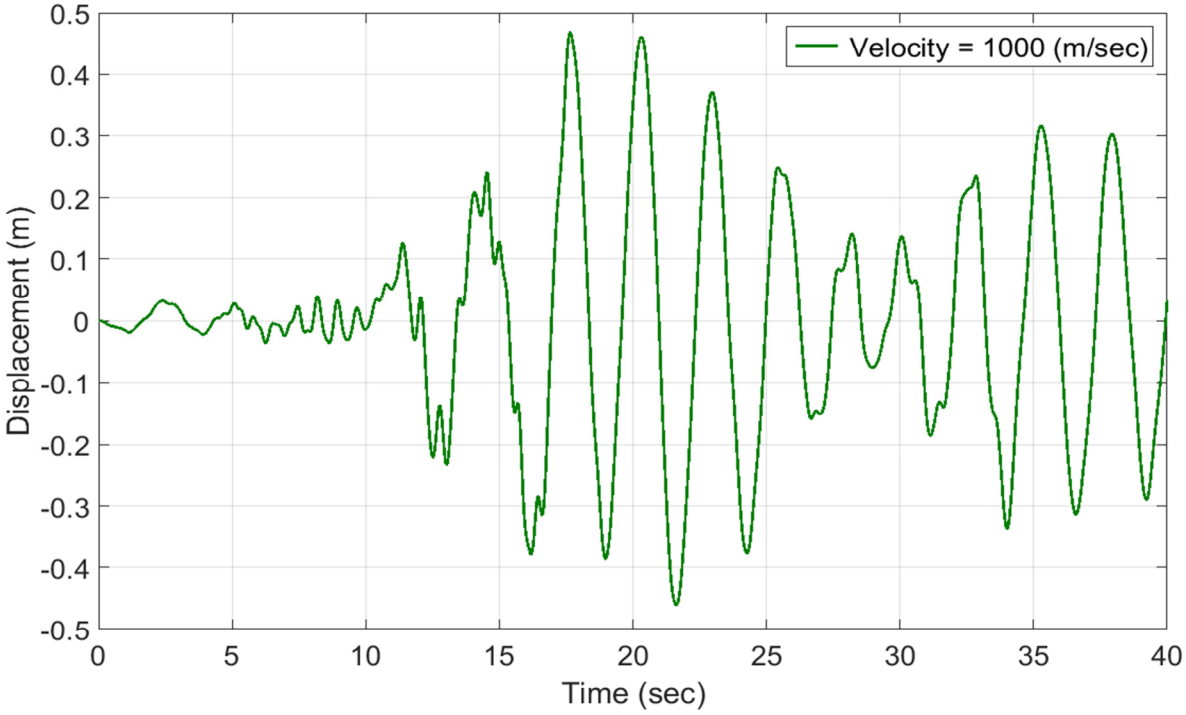

Fig. 6.23 Longitudinal displacement response of FRP bridge at Point E at the west tower for velocity = 1000 m/s

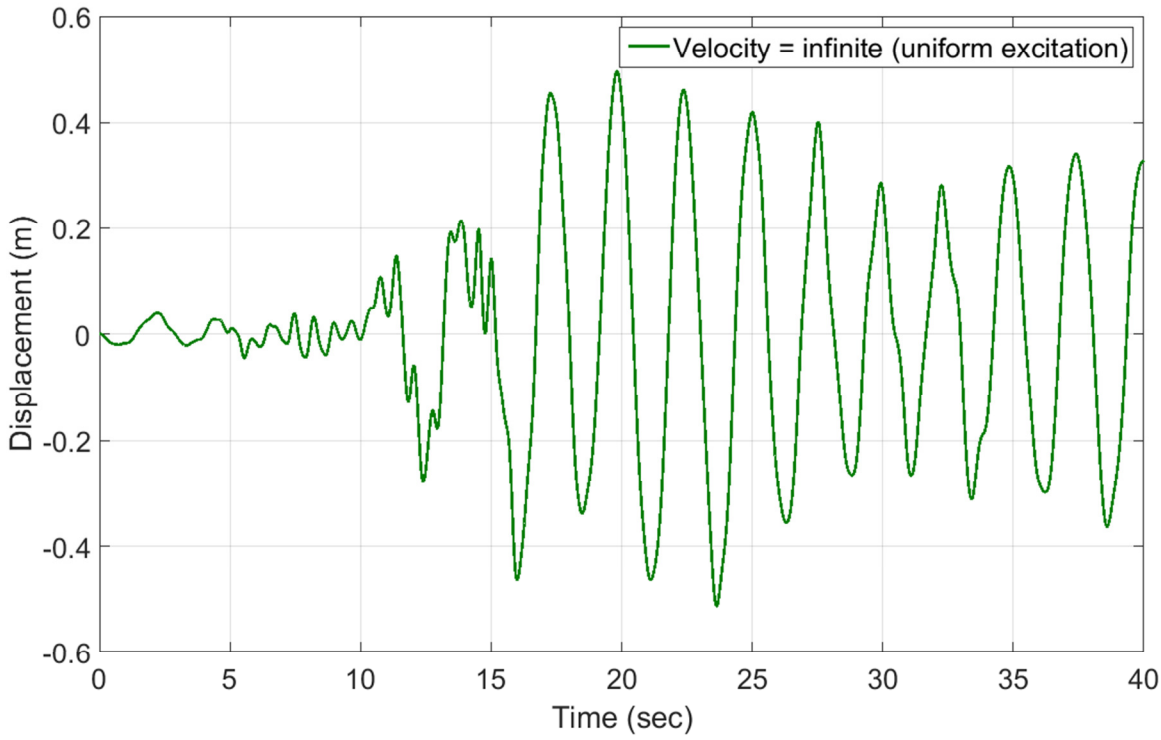

Fig. 6.24 Longitudinal displacement response of FRP bridge at Point E at the west tower for velocity = infinite

6.6.3.4 Seismic performance under varying seismic excitation

To investigate the dynamic behavior of an FRP long span cable-stayed bridge under varying seismic excitation at the supports, the earthquake records from SMART-1 (Strong Motion Array in Taiwan, phase I) is used. SMART-1 is a dense digital array of strong motion seismographs built by the Institute of Earth Sciences (Taiwan) and the University of California at Berkeley. The earthquake records in SMART-1 are the raw data observed at different places during an earthquake event. Therefore, the records have already included the influence of the incoherence effect, the attenuation effect and the site effect. Two acceleration records, Input-1 and Input-2, observed at two places at distance 1,000 m apart are used. The vertical and longitudinal components of both acceleration records are illustrated in Figs. 6.25 and 6.26 respectively.

(a)

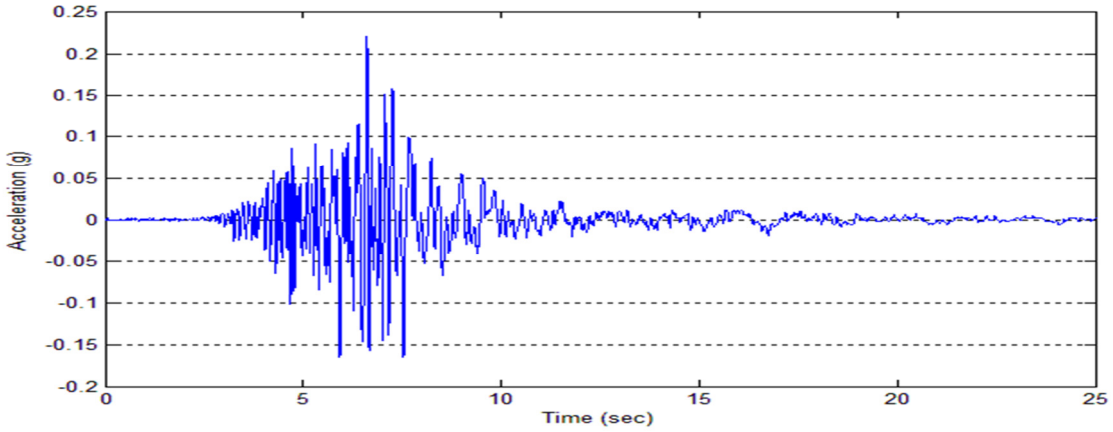

(b)

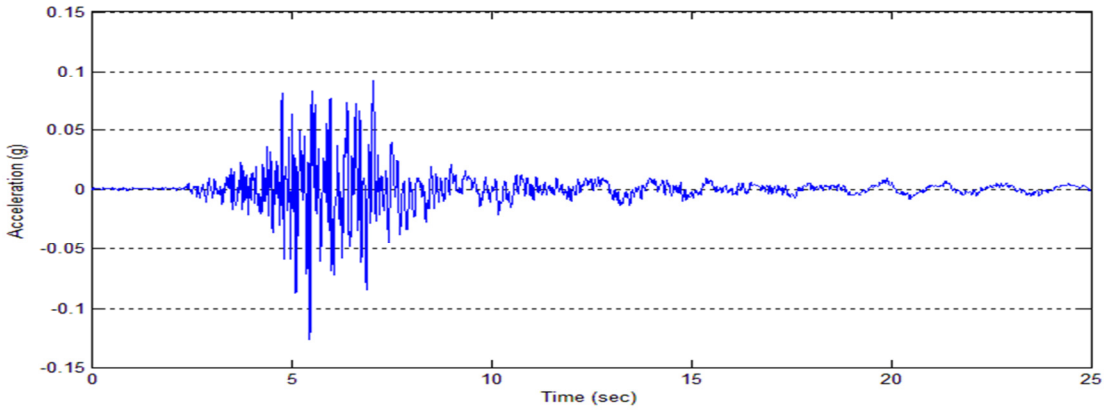

Fig. 6.25 Vertical components of seismic waves: (a) Input-1; (b) Input-2

(a)

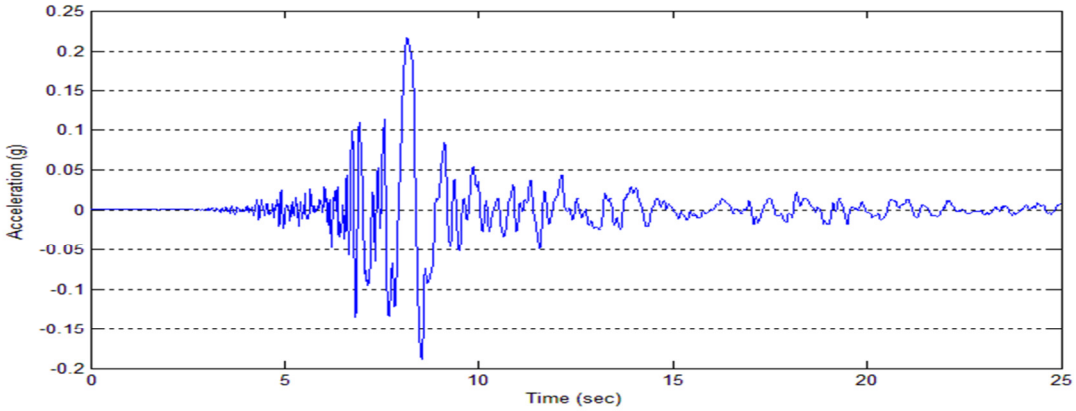

(b)

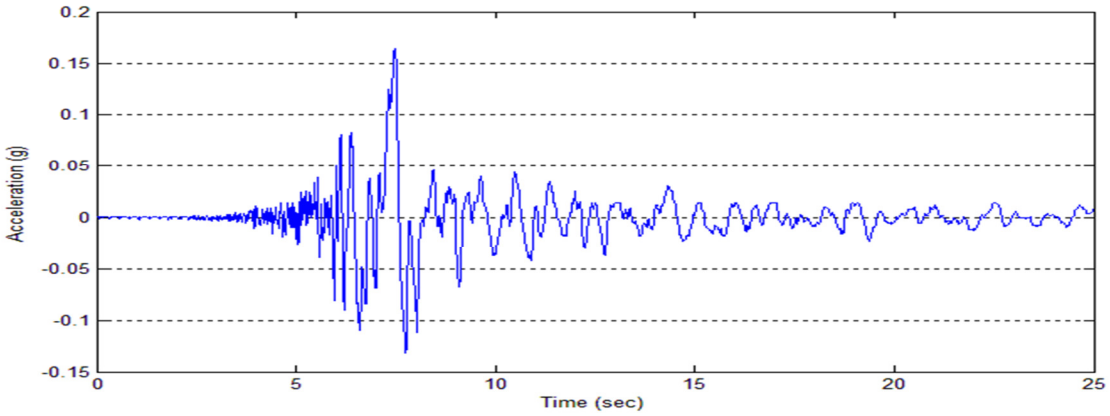

Fig. 6.26 Longitudinal components of seismic waves: (a) Input-1; (b) Input-2.

Three case studies are undertaken from which for the first and second cases, Input-1 and Input-2 are assigned to the entire FRP cable-stayed bridge. Therefore, the two cases are correspondent to the uniform excitation. In the third case, Input-1 is applied to the two west piers and to the west tower of the FRP cable-stayed bridge, while Input-2 is applied to the two east piers and the east tower. The vertical displacement response at point A, in the middle of the FRP deck and the longitudinal displacement response at point G, at the top of the east concrete tower are calculated using the time history integrated finite strip analysis and are presented in Figs. 6.27 to 6.29 and Figs. 6.30 to 6.32 respectively.

The integrated finite strip response curves show that under uniform excitations (Figs. 6.27, 6.28, 6.30, and 6.31), the maximum amplitude of the displacements recorded at points A and G are slightly higher than those from non-uniform excitation (Figs. 6.29 and 6.32). In some cases, the tendency of the displacement response curves of the FRP bridge to converge is very low. The latter indicates that the seismic stability of the FRP cable-stayed bridge is critical under varying seismic effects. The reason for very small values of the displacement responses at location A is because of the symmetric behavior of the cable-stayed FRP under earthquake loads where the displacements at the center of the deck are almost zero. Last but not least, it can be noticed that the concrete towers are more affected by the varying seismic excitation than the FRP deck. As a result, the seismic design of the concrete towers must be accurately taken into account as an important factor in seismic design of the entire FRP cable-stayed bridge system.

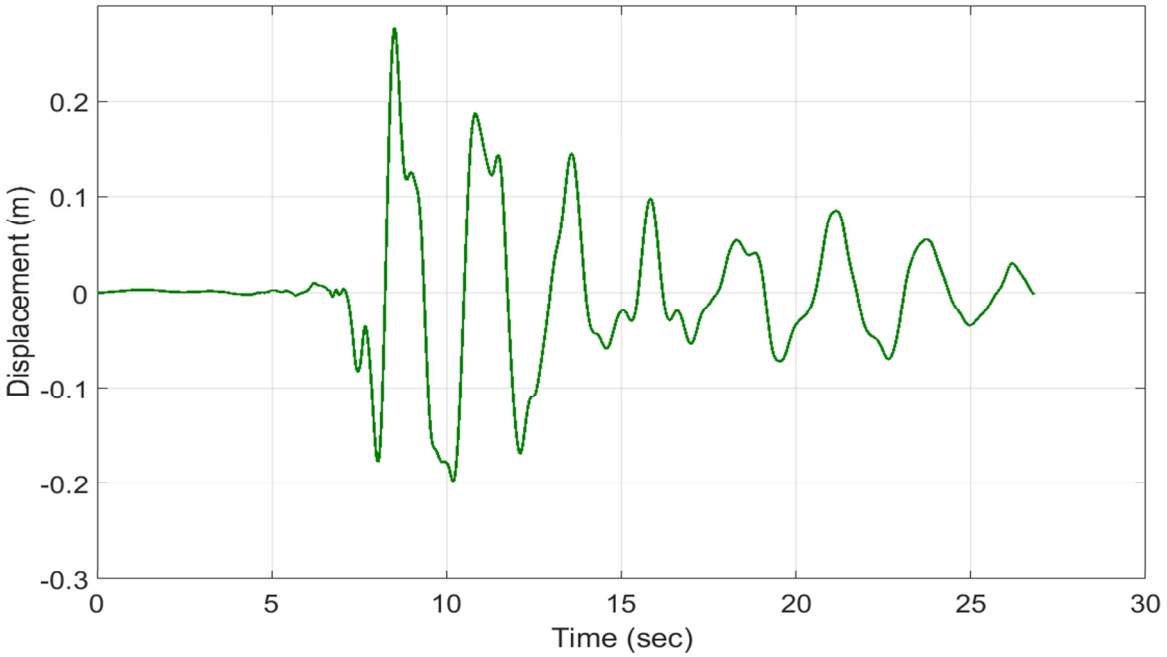

Fig. 6.27 Longitudinal displacement responses of FRP bridge at Point G at the east tower: Input 1 & Input 1

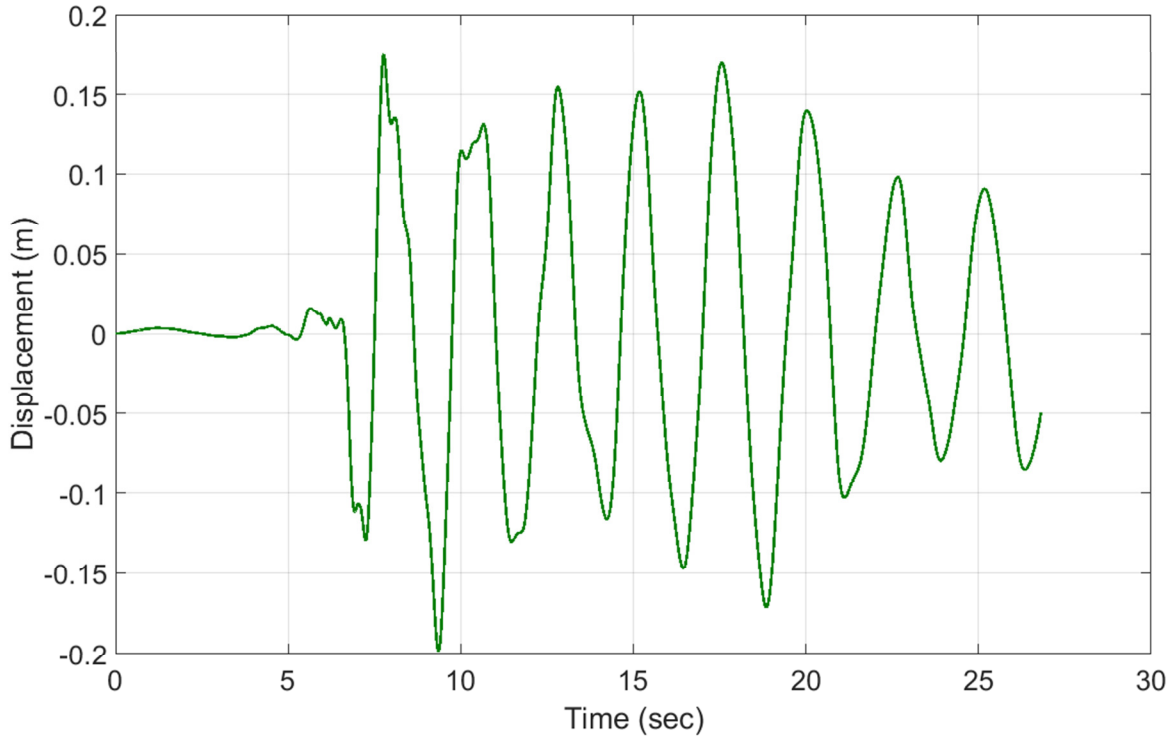

Fig. 6.28 Longitudinal displacement responses of FRP bridge at Point G at the east tower: Input 2 & Input 2

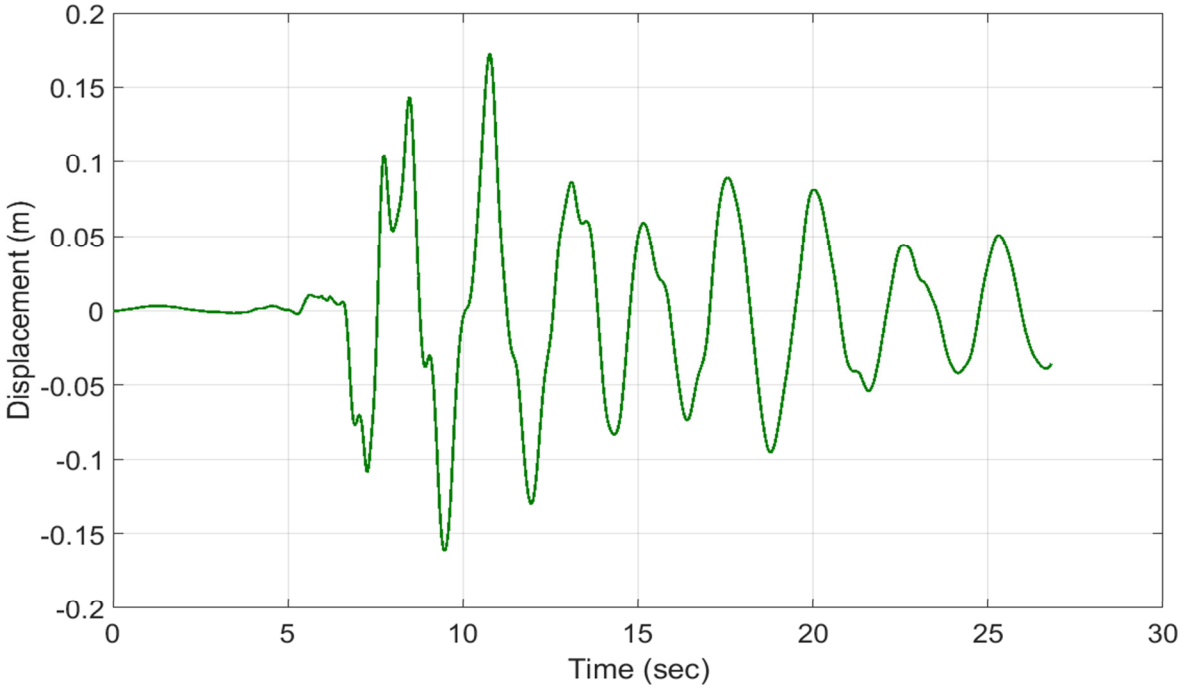

Fig. 6.29 Longitudinal displacement responses of FRP bridge at Point G at the east tower: Input 1 & Input 2

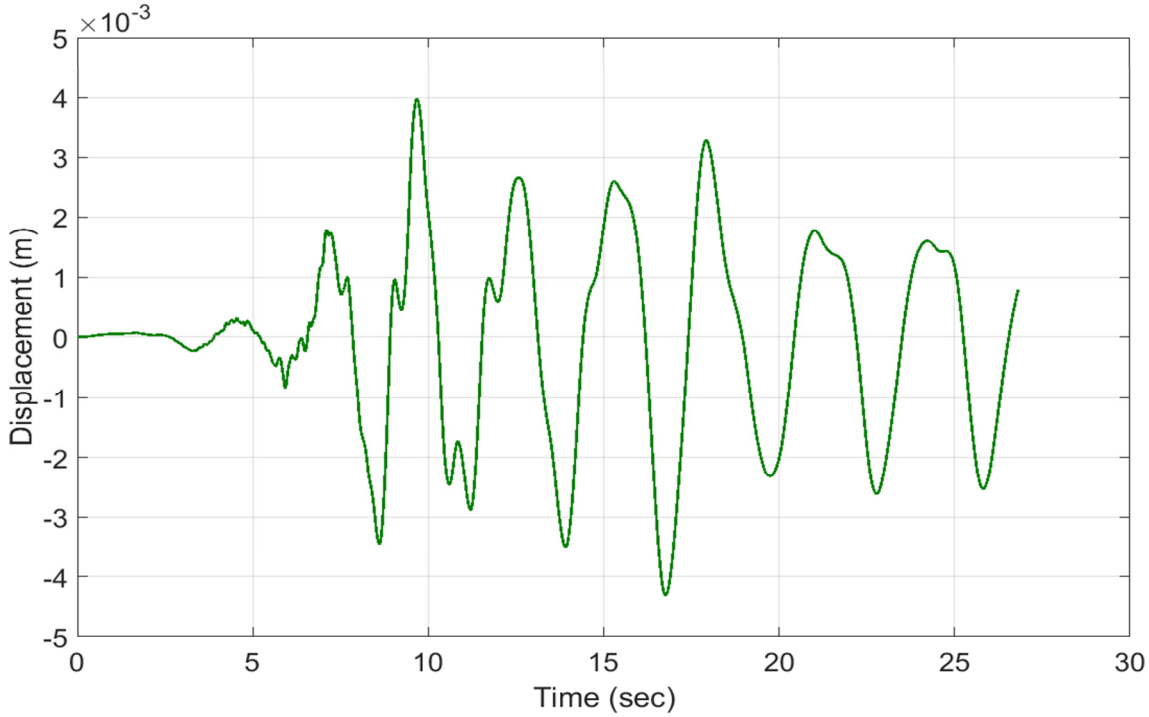

Fig. 6.30 Vertical displacement responses of FRP bridge at Point A on the deck: Input 1& Input 1

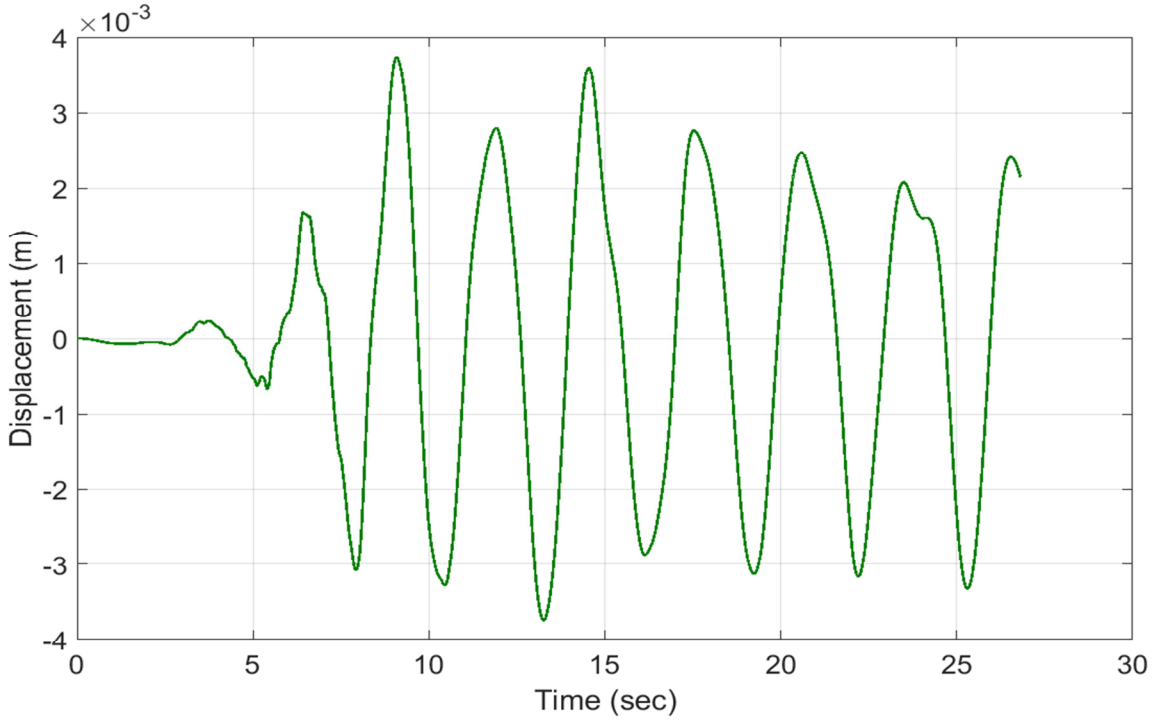

Fig. 6.31 Vertical displacement responses of FRP bridge at Point A on the deck: Input 2 & Input 2

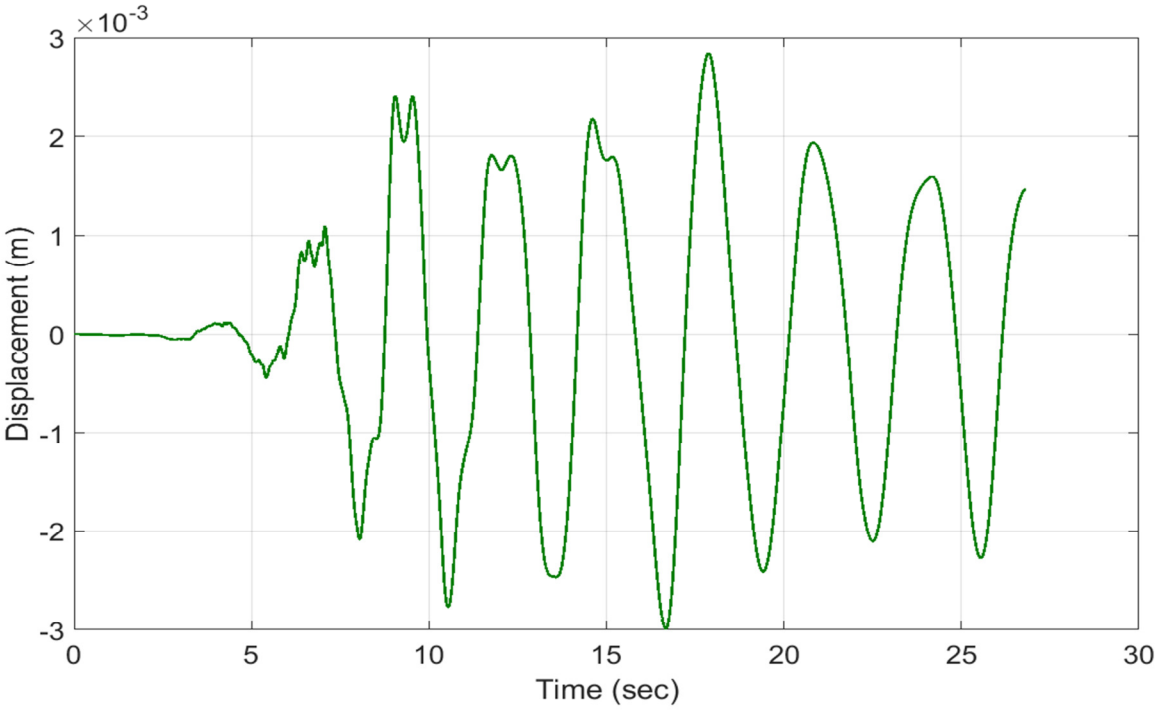

Fig. 6.32 Vertical displacement responses of FRP bridge at Point A on the deck: Input 1& Input 2

6.6.4 Efficiency

In order to determine the functionality of the IFSM, when comparing it with the FEM, the computational times for several simulations, performed, were recorded. Using a personal computer with an Intel Core2 Duo CPU (1.66 GHz) and 3GB physical memory, several dynamic analyses for different sampling frequencies were performed by MATLAB for IFSM. The computer times required by IFSM and FEM are compared and listed in Table 6.14. In order to achieve uniform preconditions for the dynamic analysis, similar meshes are chosen in both models. Nonetheless, due to the semi-analytical properties in the longitudinal direction, the number of sections for each strip in the IFSM model could be significantly reduced without losing accuracy. Consequently, the time for computation could also be reduced, and greater efficiency is achieved. It must be noted that this case study was performed on the simple bridge model presented in section 6.6.1 (Fig. 6.1). In the case of a hybrid long-span cable-stayed bridge, the efficiency of the proposed integrated finite strip solution will be more appreciated. For instance, when a continuous real time analysis is required in which a lot of iterative analyses are performed, the advantages of the proposed methodology in time saving will be more illustrated.

Table 6.14 Computational times for dynamic analysis

Method	Sampling frequency	
	262144	524288
IFSM	8000 sec	16400 sec
FEM	8800 sec	17800 sec

6.7 Concluding remarks

An efficient integrated finite strip framework is deployed for continuous multi-span and cable-stayed hybrid FRP bridges in the environment of the finite strip method. The so-called laminate strip can model the FRP deck considering the coupling effects between the in-plane and out-of-plane degrees of freedom as well as the anisotropic material properties of the laminated FRP deck. The other components of the bridge can also be modelled by spline based finite strips. 3D and 1D column strips model the piers and the towers, while cable strips model the cables. The transition section elements combine the strips of different

orientations. The application of the laminate strip along with the integrated finite strip method resulted in a very precise and efficient numerical technique for modelling the FRP based bridge structures. The application of the proposed finite scheme was extended for bending, free vibration, and seismic analysis of FRP bridges. The finite strip results of natural frequencies and mode shapes of an FRP slab-girder bridge and a cable-stayed FRP bridge were compared with those obtained by finite element method and a very good agreement was witnessed. In addition, a comprehensive study was performed on seismic performance of long-span cable-stayed FRP bridge under uniform and non-uniform earthquake excitations. A time history analysis using Newmark scheme was performed in the environment of IFSM where the effects of sine wave excitation, Chichi Earthquake, as well as varying seismic excitation were investigated. The numerical examples proved that the developed laminate spline strip is well meshed with IFSM.

Among the advantages of the proposed solution are the high efficiency and accuracy as well as minimal computational time and the simplicity of input data. Moreover, the structural interaction between different bridge components can be handled in the current analysis procedure. Consequently, the dynamic analysis results like seismic excitations in which there is significant structural interactions between towers, piers, linked beams, cables, and deck can be easily handed.

Last but not least, the numerical studies showed that the torsional mode is more likely to occur in FRP bridge than traditional concrete bridges. Therefore, special attention needs to be paid to the subject of torsional instability in the design of FRP bridges. Moreover, in the case of FRP cable-stayed bridge, the concrete towers are very sensitive to the earthquake excitations when comparing to the FRP bridge deck.

References

[6.1] Naderian, H., Cheung, M. S., Shen, Z., Dragomirescu, E., (2015) Integrated Finite Strip Analysis of long-span cable-stayed bridges, Computers and Structures 158 (2015) 82–97

[6.2] Jones, R.M., (1999), Mechanics of composite materials, Second Edition, Taylor & Francis, 1999.

[6.3] Reddy, J., (2004), Mechanics of Laminated Composite Plates and Shells: Theory and Analysis, CRC Press, New York.

[6.4] Salim, H.A., Davalos, J.F., Qiao, P., Kiger, S.A., (1997), Analysis and design of fiber reinforced plastic composite deck-and-stringer bridges, Composite Structures, 38(1), (1997), 295-307.

[6.5] Qiao, P., Julio, F., Davalos, B., Brown, B., (2000) A systematic analysis and design approach for single-span FRP deck/stringer bridges, Composites: Part B 31, (2000), 593 - 609.

[6.6] Zhang, Q.W., Chang, T.Y.P., Chang, C.C., (2001) Finite-Element Model Updating For The Kap Shui Mun Cable-Stayed Bridge, Journal Of Bridge Engineering, 6(4), (2001), 285-293

[6.7] Almansour, H., Cheung, M.S., (2010) Structural performance of laminated FRP box girder bridge deck compared to slab on prestressed concrete girder bridge, The 8th Canada Japan Joint Workshop on Composites, Montreal, Canada, July 26-29, (2010), 1-32

[6.8] Almansour, H.H., Cheung, M.S., Chan, Ben Y.B., (2010), Analysis and design of hybrid long span cable-stayed bridges using multi-scale modeling techniques, Proceedings of the International Conference on Computing in Civil and Building Engineering, the University of Nottingham

[6.9] Almansour, H.H., Cheung M.S., (2003), Finite element modeling of a CFRP composite deck for long span cable-stayed bridge. Proc. JCJC-III, Ueda, Nagano, Japan.

[6.10] Almansour, H.H., (2006), The performance of hybrid long-span cable-stayed bridges using advanced composites, department of civil and environmental engineering, the University of Ottawa

[6.11] Virlogeux, M., (1999), Recent evolution of cable-stayed bridges, Engineering Structures, 21(8) (1999), 737–755.

[6.12] Burgueno, R., Karbhari, V.M., Seible, F., Kolozes R.T., (2001) Experimental dynamic characterization of an FRP composite bridge, superstructure assembly, Composite Structures, 54, (2001),427 - 444.

[6.13] Chao, W., (2015), Damage modelling of FRP composite bridge decks, PhD thesis, department of civil and environmental engineering, Hong Kong University of Science and Technology

[6.14] Chan, Ben Y.B., Cheung, Moe M.S. Chao, Wang, (2013), Nonlinear dynamic analysis of fiber reinforced ultra-long span cable stayed bridges, Journal of Bridge Structures 9 (2013) 3–19

[6.15] Zhao P., Xie L., Cheung Moe M.S., (2015) Analysis and design procedure of hybrid long-span cable-stayed bridge using advanced composite material, Journal of Reinforced Plastics and Composites, 2015, 0(0) 1–24

[6.16] Shen Z., Cheung Moe M.S., Naderian H., Dragomirescu E., (2013) An integrated finite strip solution for dynamic analysis of continuous multispan bridges. In: Proceedings of the 3rd specialty conference on mechanics and materials. Montreal, Canada; 2013.

[6.17] Kap Shui Mun Bridge, Highways Department - The Government of the *Hong Kong* Special Administrative Region

Chapter 7

Integrated finite strip flutter analysis of bridges

Abstract Recently developed integrated finite strip method (IFSM) is a very efficient and accurate computational technique for modelling bridges and for performing the vibration analysis of bridges. This method is the sole existent finite strip solution capable of modelling the entire bridge system and considering the effects of structural interactions between different components. In this paper, IFSM is extended to the aerodynamic flutter analysis under wind effects. The developed methodology is capable to perform a three-dimensional (3D) flutter analysis in the environment of IFSM. The solution falls into the category of both multi-mode and full-mode flutter analysis. Aerodynamic stiffness and damping property matrices, as well as structural property matrices are derived by IFSM. In addition, an optimal scheme is proposed for solving the flutter eigenvalue problem using linearization of the flutter equation of motion. Furthermore, a simple technique has been proposed in order to handle different end boundary conditions. The critical flutter frequency and the respective critical wind speed can be obtained by solving an eigenvalue flutter analysis. The proposed finite strip solution is very straightforward in terms of amount of input data, boundary conditions, modelling, and flutter analysis process. Last but not least, the convergence rate of the

method is very high due to the semi-analytical and localization nature of IFSM which leads the band-width of the dynamic property matrices to be very narrow. The localised nature and the ability to reduce the computing time by bandwidth minimisation are the main advantages of B3-spline functions. The numerical results also show that IFSM improves significantly the convergence of the critical flutter frequencies, and therefore leads to smaller storage requirements for the global structural and aerodynamic matrices, and faster flutter eigenvalue extraction. Benchmark numerical investigations are presented including the study of a simply supported thin flat shell, and the model of the Kap Shui Mun Bridge, an existing long-span cable-stayed bridge.

Keywords: Flutter, plate, long-span, cable-stayed bridge, aerodynamic, self-excited, aeroelasticity, B3 spline, integrated finite strip method.

7.1 Introduction

One of the main challenges in structures surrounded by the wind flow is the aerodynamic instability due to effects of self-excited forces. If the wind-structure interaction leads to an increase in the magnitude of oscillatory motions, the aeroelastic instability occurs. It is caused by aerodynamic forces induced on the structure as a consequence of its motion. Such aerodynamic forces are called self- excited forces. This self-excited oscillatory instability phenomenon is called flutter. Some examples of structures critical against flutter are the airfoils in aerospace industry like the aircraft wings, and long-span cable-stayed bridges in civil engineering. In flutter, at a critical wind speed, the self-excited aerodynamic forces acting on an oscillatory system starts feeding the energy of the system, instead of dissipating it, which leads to destructive divergent vibrations of the structure. The aerodynamic behavior of the structures depends on the interaction between the aerodynamic forces, inertial and damping, and the stiffness properties of the structures.

Therefore, a multi-disciplinary study between solid-mechanics, dynamics, and fluid-dynamics can investigate the aeroelasticity of an airfoil or a long-span bridge.

Modern long-span bridges are usually constructed by very slender deck structures which results in increasing the risk of instability under extreme dynamic loads, like wind and earthquake loads. With the advent of new advanced materials such as composite fiber reinforced polymers (FRP), longer span bridges are built throughout the world. On the other hand, these types of materials are very lightweight; consequently, the stability of the bridge structures against the wind effects has become more critical. The nature of wind load is very complex and turbulent which means it is not easy to understand the structural behavior of the bridges under wind flow. Flutter, is one of the most important criteria in the analysis and design of long-span cable-stayed and suspension bridges. The determination of the dynamic and aerodynamic characteristics of the bridge is a crucial step in solving the flutter problem. Since 1960s, a number of publications have dealt with both analytical and experimental studies on flutter of long-span bridges. Tanaka et al. [7.1], and Ge. et al. [7.2] investigated the flutter of plates and bridges by multi-mode and full-mode approaches. Huang et al. [7.3] studied the aerodynamic behavior of bridges under skew wind by performing a series of section model tests. Dowell et al. [7.4] investigated the flutter of rectangular plates under the three-dimensional axial flow through numerical and experimental tests. Wu et al. [7.5] presented a framework for linear and nonlinear aeroelastic analysis of cable-supported bridges. The topic of the bridge flutter is still highly important and researchers try to develop different types of experimental and analytical techniques for better understanding the flutter phenomenon [7.6-7.12].

Finite strip method, pioneered by Y. K. Cheung and M. S. Cheung [7.13, 7.14], is one of the most efficient and accurate numerical techniques for modelling the long-span structures with highly harmonic behaviour along the longitudinal direction of the structure. Among them, one can mention buckling and free vibration of thin-walled structures as well as the structural investigation of long-span bridges. Despite the merits of finite strip method, its application to bridge engineering has been limited to model only the bridge deck, while other structural components of the structure, including piers, towers, cables, etc. were modeled as special boundary conditions of the deck [7.13]. For that reason and at the same time, with the advancement of other numerical techniques, the popularity of the finite strip

method among bridge engineers has declined in the recent decades. In order to overcome this obstacle, Naderian et al. [7.15, 7.16] developed the so called Integrated Finite Strip Method (IFSM), which is able to model the entire cable-stayed bridge system. IFSM is, in fact, an evolved version of Spline Finite Strip Method (SFSM) [7.17], which is itself a more comprehensive format of conventional Finite Strip Method (FSM), at the expense of incorporating more degrees of freedom. However, as a tool, this is more powerful than the ordinary finite strip method in terms of dealing with structures with complex geometry, boundary, and loading conditions. Moreover, SFSM is also capable of modelling multi-span bridges and structures subjected to not only uniformly distributed forces but also concentrated forces. In IFSM, the bridge deck is divided into a number of flat shell spline finite strips in the longitudinal direction and B3 spline functions define the longitudinal shape function of the displacement function. Using B3-splines, the continuity over the second derivative of the displacement function is achieved. Furthermore, the splines have localization properties through which the band-width of the global property matrices becomes very narrow. Subsequently, the computational time can dramatically decreases. When it comes to complicated analyses, for instance, vibration-based real time structural health monitoring of huge bridge structures under earthquake, typhoons, or high traffic loads, where numerous iterative dynamic analyses must be performed consistently, even a small percentage of the computational saving is highly appreciated. Therefore, IFSM can be a suitable platform for vibration investigation of modern bridge structures. Naderian et al. [7.16] have recently extended the finite strip method to seismic analysis of long-span cable-stayed bridges. In this paper, the IFSM is further extended to the aerodynamic flutter analysis.

It is worth mentioning that M. S. Cheung et al. [7.18] used a combination of spline finite strip method and finite element method for flutter analysis of long-span cable-stayed bridges. Despite the merits of their suggested method, there are still considerable concerns on efficiency and accuracy of the solution, that are addressed in the following: I. the aerodynamic stiffness and damping matrices are not derived by spline finite strip method but are derived based on lumped aerodynamic forces. The distribution of the aerodynamic forces along the nodal lines of the strip is based on the trapezoidal discretization while in the spline finite strip method it must be done by B3 spline discretization. II. Only the deck is modelled

by spline finite strips, while other components like piers, towers, and cables are simulated by equivalent beam finite elements. In other words, their numerical solution is a partially finite strip solution. III. The aerodynamic self-excited forces are spatially distributed on the deck of the bridge, while the general formulation of the self-excited flutter forces is based on applying the self-excited forces on the centre of elasticity of the deck [7.19]. According to the present research, the spatial distribution of self-excited aerodynamic forces is not only inefficient, but also it might be against general assumptions of the flutter formulation, which might lead to les accurate results. Although the idea behind the uniform distribution of wind loads is to consider the effects of the spatial distribution of aerodynamic forces over the cross section of the bridge deck, our recent studies indicate that the aerodynamic performance is not sensitive on this factor. Therefore, spatial discretization of aerodynamic loads on the entire deck system decreases the efficiency of the solution procedure. The latter will be discussed more in detail, later in this chapter, when providing the numerical examples. Last but not least, the proposed method by Cheung et al. [7.18] might not perfectly and efficiently consider the structural interactions between deck, piers, towers, and cables because the compatibility between displacements of the interaction joints is obtained through an iterative process. However, this technique could be effective for simple types of structures under static/quasi-static forces only. In the case of complex structures like long-span cable-stayed bridges or structures under dynamic and aerodynamic excitations, such as non-uniform seismic excitations or aerodynamic self-excited forces, such simplification can no longer be adopted.

All the above mentioned concerns have been eliminated in the present study by introducing the Integrated Finite Strip Flutter formulation. Shell spline finite strip models the bridge deck, one-dimensional column strip models the towers and piers, and the cable strip models the bridge cables. Transition section elements in each of the mentioned strips provide the connectivity and boundary conditions of bearings between different structural components of the cable-stayed bridge.

In this research, first the IFSM is briefly reviewed, then, the general formulation of the flutter equation of motion is presented. The integrated finite strip flutter formulation along with the derivation of the aerodynamic stiffness and damping matrices, as well as the structural property matrices are fully explained. In addition, a simplified method has been

developed in order to handle the boundary conditions corresponding to the flutter problem. Thirdly, multi-mode and full-mode aeroelastic approaches are integrated within the finite strip treatment. Finally, a simple eigenvalue analysis based on linearization of the flutter equation of motion is proposed, through which the critical flutter frequencies and consequently the critical wind speeds can be obtained, by solving a standard eigenvalue analysis. The proposed finite strip flutter solution is applied to two numerical examples where the flutter behavior of a thin-walled flat plate as well as long-span cable-stayed Kap Shui Mun Bridge is investigated. The accuracy of the method in predicting critical flutter speeds and frequencies, as well as the convergence of the currently developed finite strip method for the flutter analysis is examined. The results show that IFSM and the proposed flutter analysis scheme is a powerful efficient tool for the aerodynamic analysis of a plate in general and for the bridge structures as a system. Rapid convergence and small storage requirements are the highlights of the proposed method.

7.2 Review on integrated finite strip method

Integrated Finite Strip Method (IFSM) [7.15, 7.16] is the latest version of finite strip method which is able to fully simulate and analyze the bending and vibration of long-span cable-stayed bridges. Not only the bridge deck but also all other structural parts of a long-span cable-stayed bridge including towers, piers, linked beams, cables as well as bearings can be modeled in the environment of the spline finite strip method using different types of strips including shell spline strip, columns strips, and cable strip. The key parameter of the originality of the IFSM is the so-called transition section, which has been defined based on unequal spline strips. Transition sections provide the compatibility of displacements and vibrations in intersection points of different components and they also handle the boundary conditions of bearings. The compatibility can be achieved by selecting an extremely small length for the spline transition section [7.15]. Another important feature of the IFSM is that the structural interactions between different components, for example between towers and cables, can be modelled. This capability is very important especially for dynamic analyses of long-span bridges like seismic analysis and flutter analysis in which there is a considerable interaction and load effect transmission between different structural elements. More details on the development of the IFSM is addressed by Naderian et al. [7.15].

7.3 Aerodynamic flutter equation of motion

The self-excited aeroelastic forces acting on a plate or a bridge structure are originally caused by wind effects. This means that the flutter resultant forces can be considered as external forces. Similar to the general dynamic systems, the equilibrium of the effective forces including the inertia force, the damping force, the elastic force, and the applied flutter force will form the flutter equation of the motion. For a structure for which the displacements are defined by a vector $\{\delta\}$ including n degrees of freedom, the matrix analysis can be used to formulate the flutter equation of motion as

$$[M_s]\{\ddot{\delta}\} + [C_s]\{\dot{\delta}\} + [K_s]\{\delta\} = \{F_{aer}\} \tag{7-1}$$

where $[M_s]$, $[C_s]$, and $[K_s]$ are the global structural mass, damping, and stiffness matrices with the order of $n \times n$ while $\{F_{aer}\}$ is the global self-excited aerodynamic force vector. $\{\dot{\delta}\}$ and $\{\ddot{\delta}\}$ are the vectors of the first and second derivatives of displacements respectively. The self-exited forces $\{F_{aer}\}$ are dependent on the vertical (*w)*, lateral (*u)*, and rotation (θ) displacements of the structure and their first derivatives, and it can be expressed as

$$\{F_{aer}\} = [C_{aer}]\{\dot{\delta}\} + [K_{aer}]\{\delta\} \tag{7-2}$$

in which $[C_{aer}]$ and $[K_{aer}]$ are $n \times n$ global aerodynamic damping and stiffness matrices respectively. The self-exited aerodynamic force associated with the second derivative of the displacements, called aeroelastic inertial forces, is omitted as the air density is significantly lower than that of the structural materials. Substituting Eq. (7-2) into Eq. (7-1), yields the flutter equation of motion as

$$[M_s]\{\ddot{\delta}\} + [C_s]\{\dot{\delta}\} + [K_s]\{\delta\} = [C_{aer}]\{\dot{\delta}\} + [K_{aer}]\{\delta\} \tag{7-3}$$

or

$$[M]\{\ddot{\delta}\} + [C]\{\dot{\delta}\} + [K]\{\delta\} = 0 \tag{7-4}$$

in which $[M] = [M_s]$, $[C] = [C_s] - [C_{aer}]$, and $[K] = [K_s] - [K_{aer}]$, where $[M]$, $[C]$, $[K]$ are system mass, damping, and stiffness matrices respectively. The aerodynamic damping $[C_{aer}]$ and stiffness matrices $[K_{aer}]$ are not necessarily symmetric because of non-conservative nature of the aerodynamic forces. Therefore, the system stiffness $[K]$ and system damping $[C]$ matrices are both asymmetric, which results in coupling effects between the flutter response frequencies. In other words, the asymmetry of the aerodynamic properties enables the flutter response of the structures to be coupled between multiple mode shapes.

7.4 Integrated finite strip flutter formulation

7.4.1 General

Both structural and aerodynamic properties of different components of the bridge can be derived by integrated finite strip method. In the case of a long-span cable-stayed bridge, the self-excited flutter forces acting on the bridge deck are only considered in the analysis. In the following sub-section the integrated finite strip discretization as well as the derivation of the structural and aerodynamic matrices in the environment of IFSM are presented.

7.4.2 Integrated finite strip discretization

Considering the bridge deck as a shell structure, both in-plane and out-of-plane degrees of freedom need to be considered. A flat shell spline strip is shown in Fig. 7.1, where each knot of a nodal line has four degrees of freedom, three translational (u, v, w) and one rotation (θ).

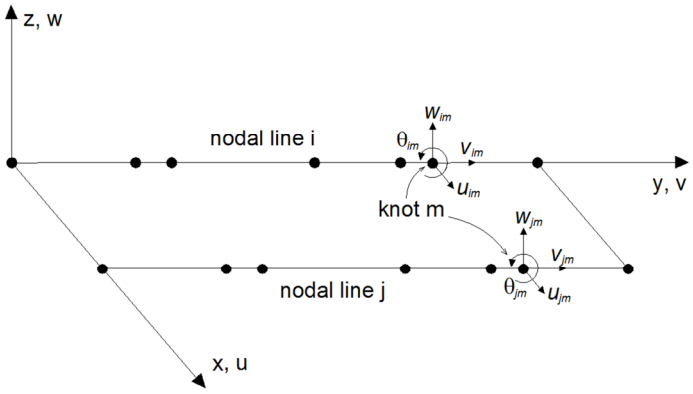

Fig. 7.1 Shell spline finite strip

The vector of displacement parameters of a shell spline strip centered at y_m is given by

$$\{\delta\}_m = \left[u_{im}, v_{im}, w_{im}, \theta_{im}, u_{jm}, v_{jm}, w_{jm}, \theta_{jm} \right]^T \tag{7-5}$$

It must be noted that the parameters of Eq. (7-5) are in fact spline coefficients not the physical degrees of freedom. The integrated finite strip method is based on the use of unequally spaced B3-spline functions, through which the transition section is developed for connecting different structural components together. Moreover, it allows the locations of the supports and the concentrated load to coincide with the knots on the nodal lines, thus leading to more accurate results. Moreover, the introduction of unequally spaced interior knots allows one to describe accurate response in the region of high stress gradients, or at the locations of abrupt geometric changes, by spacing the knots more closely.

In flutter analysis problem of a flat shell or a bridge deck, unequally spaced B3-spline function centered at y_m may define the longitudinal shape of function as

$$\Phi_m(y) = \begin{cases} 0 & y < y_{m-2} \\ A_m(y - y_{m-2})^3 & y_{m-2} \le y < y_{m-1} \\ A_m(y - y_{m-2})^3 + C_m(y - y_{m-1})^3 & y_{m-1} \le y < y_m \\ B_m(y_{m+2} - y)^3 + D_m(y_{m+1} - y)^3 & y_m \le y < y_{m+1} \\ B_m(y_{m+2} - y)^3 & y_{m+1} \le y < y_{m+2} \\ 0 & y_{m+2} \le y \end{cases} \tag{7-6}$$

in which

$$\begin{aligned} A_m &= \left[(y_{m+1} - y_{m-2})(y_m - y_{m-2})(y_{m-1} - y_{m-2}) \right]^{-1} \\ B_m &= \left[(y_{m+2} - y_{m-1})(y_{m+2} - y_m)(y_{m+2} - y_{m+1}) \right]^{-1} \\ C_m &= -(y_{m+2} - y_{m-2}) \left[(y_{m+2} - y_{m-1})(y_{m+1} - y_{m-1})(y_m - y_{m-1})(y_{m-1} - y_{m-2}) \right]^{-1} \\ D_m &= -(y_{m+2} - y_{m-2}) \left[(y_{m+1} - y_{m-2})(y_{m+1} - y_{m-1})(y_{m+1} - y_m)(y_{m+2} - y_{m+1}) \right]^{-1} \end{aligned} \tag{7-7}$$

The section lengths of B3 spline function can be chosen to be equal for flutter analysis of simple cases like a long-span flat shell where there is no need to employ unequally spaced splines. The length of the plate strip L is divided into m sections of equal length *h*. A typical local B3-spline function of equal spaced is defined as

$$\Phi_m(y)=\frac{1}{6h^3}\begin{cases}(y-y_{m-2})^3 & y_{m-2}\le y\le y-y_{m-1}\\ h^3+3h^2(y-y_{m-1})+3h(y-y_{m-1})^2-3(y-y_{m-1})^3 & y_{m-1}\le y\le y_m\\ h^3+3h^2(y_{m+1}-y)+3h(y_{m+1}-y)^2-3(y_{m+1}-y)^3 & y_m\le y\le y_{m+1}\\ (y_{m+2}-y)^3 & y_{m+1}\le y\le y_{m+2}\\ 0 & otherwise\end{cases} \tag{7-8}$$

The membrane displacement functions *u* and *v*, and the flexural displacement function *w* are expressed as the product of transverse polynomials and longitudinal B3-splines

$$u=\sum_{m=-1}^{r+1}(N_1\Phi_{1m}(y)u_{im}+N_2\Phi_{5m}(y)u_{jm}) \tag{7-9}$$

$$v=\sum_{m=-1}^{r+1}(N_1\Phi_{2m}(y)v_{im}+N_2\Phi_{6m}(y)v_{jm}) \tag{7-10}$$

$$w=\sum_{m=-1}^{r+1}(N_3\Phi_{3m}(y)w_{im}+N_4\Phi_{4m}(y)\theta_{im}+N_5\Phi_{7m}(y)w_{jm}+N_6\Phi_{8m}(y)\theta_{jm}) \tag{7-11}$$

where r is the total number of longitudinal sections on a nodal line. In the matrix form Eqs. (7-9) to (7-11) can be rewritten as:

$$\{f\}=\begin{Bmatrix}u\\ v\\ w\end{Bmatrix}=\begin{bmatrix}N_1&0&0&0&N_2&0&0&0\\ 0&N_1&0&0&0&N_2&0&0\\ 0&0&N_3&N_4&0&0&N_5&N_6\end{bmatrix}\begin{bmatrix}[\Phi_{1m}]&&&&&&&\\ &[\Phi_{2m}]&&&&&&\\ &&[\Phi_{3m}]&&&&&\\ &&&[\Phi_{4m}]&&&&\\ &&&&[\Phi_{5m}]&&&\\ &&&&&[\Phi_{6m}]&&\\ &&&&&&[\Phi_{7m}]&\\ &&&&&&&[\Phi_{8m}]\end{bmatrix}\begin{Bmatrix}u_{im}\\ v_{im}\\ w_{im}\\ \theta_{im}\\ u_{jm}\\ v_{jm}\\ w_{jm}\\ \theta_{jm}\end{Bmatrix} \tag{7-12}$$

Transverse shape functions adopted in Eq. (7-12) are cubic Hermite polynomial functions for vertical displacement variation and linear interpolation for in-plane displacements as

$$N_1 = 1 - X, N_2 = X, N_3 = 1 - 3X^2 + 2X^3, N_4 = x(1 - 2X + X^2), N_5 = (3X^2 - 2X^3)$$
$$N_6 = x(X^2 - X) \quad (7\text{-}13)$$

In Eq. (7-12), $[\Phi_{1m}]$ to $[\Phi_{8m}]$ are the row matrices and each of them includes (m+3) local B3-splines as

$$[\Phi_{im}]=[\Phi_{-1} \quad \Phi_0 \quad \Phi_1 \quad \Phi_2 \quad \ldots\ldots \quad \Phi_{m-2} \quad \Phi_{m-1} \quad \Phi_m \quad \Phi_{m+1}] \quad (7\text{-}14)$$

$[\Phi_{1m}]$, $[\Phi_{2m}]$, $[\Phi_{5m}]$ and $[\Phi_{6m}]$ are related to the displacements *u* and *v* of nodal lines i and j respectively, while $[\Phi_{3m}]$, $[\Phi_{4m}]$, $[\Phi_{7m}]$ and $[\Phi_{8m}]$ are related to the displacement *w*.
In the short form, Eq. (7-12) is expressed as

$$\{f\} = [N_t][\Phi]\{\delta\} \quad (7\text{-}15)$$

where $[N_t]$ is a 3×8 matrix and $[\Phi]$ is an $8 \times 8\ (m+3)$ matrix, while $\{\delta\}$ is an $8\ (m+3)\times 1$. Thus, $\{\delta\}$ is an $8\ (m+3)\times 1$ matrix.

7.4.2.1 Column strip

The cantilever behavior of the piers and the towers of a long-span cable-stayed bridge can be simulated by the so-called three-dimensional (3D) Column Strip (CS3) which is a vertical shell spline strip fixed at one end, for providing the support boundary conditions, and free at the other end, as shown in Fig. 4.2.

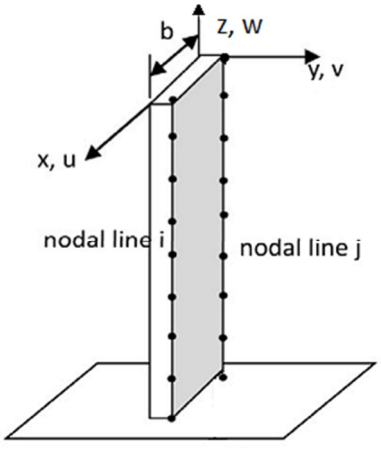

Fig. 7.2 Column Strip (CS3)

In some cases, one-dimensional (1D) column strip (CS1) is more applicable and is actually easier to be employed for modelling the piers and towers. In CS1 each knot belonging to the nodal line has three translational degrees of freedom. Consequently, the displacement function can be defined as

$$u = \sum_{m=-1}^{r+1} u_m \Phi_m(z) \tag{7-16}$$

$$w = \sum_{m=-1}^{r+1} w_m \Phi_m(z) \tag{7-17}$$

$$v = \sum_{m=-1}^{r+1} v_m \Phi_m(z) \tag{7-18}$$

For the displacement-strain relationships, only the bending in the vertical and transverse directions and the axial stress are considered, while the shear stress and torsional moment are assumed to be negligible as the amounts of these forces are very low in CS1.

7.4.2.2 Cable strip

In order to model the bridge cables in the finite strip environment, the cable strip is employed. The cable strip is a simplified version of the CS1. Generally, cables can resist only the axial tension stresses and not the compression. For this reason, in the cable strip model, only the axial stress defines the strain-displacement relationship.

7.4.2.3 Connectivity provisions

In contrast with the finite element method, in which the auxiliary bridge structural elements, like piers and cables can be easily connected to the bridge deck, the concept “element” in the longitudinal direction is not defined in the conventional finite strip methods. In other words, it is impossible to insert an extra component at an intermediate point within a spline strip, from the finite strip point of view. In order to eliminate this impediment, a special transition section has been developed within the IFSM [7.15]. The methodology has been applied to connect different components of complex structures, such as long-span cable-stayed bridges [7.15]. Therefore, deck-pier and deck-tower connectivity as well as cable-deck and cable-

tower connectivity are modelled by employing the newly developed transition section elements.

The transition section is created by using unequally spaced B3-spline functions. A typical transition section connecting two different components is shown in Fig. 4.3. Without losing generality, it is assumed that the width of the normal and the transition sections are H and h respectively. In Fig. 4.3, the vertical line is a nodal line on the column strip while the horizontal line is a nodal line on the shell spline strip of the deck. This schematic can also be applied to the cable strip and shell spline strip joints for ensuring the connectivity. The vertical and horizontal lines overlap at knots 3 and 8 of the shell and column strips, respectively. In order to achieve identical displacements at knots 3 and 8, the ratio of h/H should be infinitely small. Depending on the complexity of the structure, different values of h can meet the required accuracy. Numerical studies showed that a good accuracy can be obtained under normal circumstances with the ratio of h=H = 0.001 [7.15]. Using the developed transition section in the spline finite strip procedure, the compatibility for the displacements of different components of the structure is satisfied. It must be noted that the bearings can be modeled as special boundary conditions for the transition section. For example, in order to model a fixed bearing, which allows rotations but restricts translations, the displacements of knots 3 and 8 must be equal in order to achieve compatibility, which can be implemented through the transition section as detailed above.

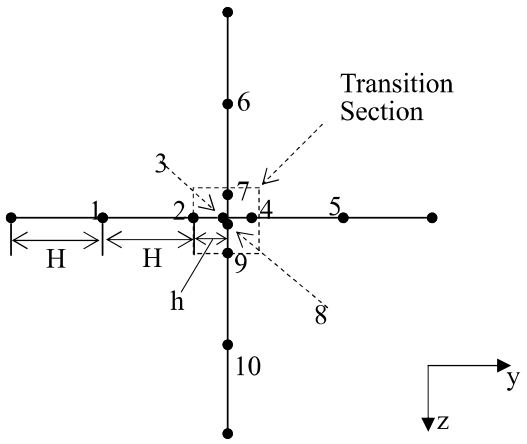

Fig. 7.3 Typical transition section element

7.4.3 Finite strip structural property matrices

After the discretization of the entire bridge system is performed using IFSM, the principle of minimum potential energy can be applied to derive the mass matrix $[m]$ and stiffness matrix $[k]$ of the shell strip, column strip, and cable strip as follows

$$[m] = \int [N]_i^T \rho [N]_i dV \tag{7-19}$$

$$[k] = \int [B]_i^T [D][B]_i dV \tag{7-20}$$

in which ρ is the density of the strip; [D] and [B] are the elastic matrix and the strain matrix respectively, and [N] is the shape function matrix, which is the multiplication of the transverse and the longitudinal spline functions as $[N_t][\Phi]$. It must be noted that in the case of one-dimensional column strip (CS1) and the cable strip the integral is performed over the length of the strip. Similar to the FEM, the IFSM strip properties are converted to the knots of the nodal lines along the strip during the model formulation process. However, the amount of knots required is significantly reduced due to the semi-analytical nature of the IFSM. The structural matrices of the strips can be assembled using the standard assembling techniques. The global structural stiffness matrix $[K_s]$ and the global structural mass matrix $[M_s]$ of the entire bridge system are formed after assembling all structural components.

The structural damping matrix $[C_s]$ is usually a function of the structural stiffness and mass matrices and it can be obtained from the following formula, referred to as the "classic Rayleigh damping"

$$[C_s] = \alpha [M_s] + \beta [K_s] \tag{7-21}$$

where α and β are the Rayleigh damping factors, which can be determined by having two structural damping ratios ξ associated with two specific frequencies. The damping ratio ξ of the n^{th} free vibration mode of a structure is given by

$$\xi_n = \frac{1}{2\omega_n}\alpha + \frac{\omega_n}{2}\beta \tag{7-22}$$

where ω_n is the angular frequency of the n^{th} mode. Assuming the same damping ratio ξ for two different modes, α and β can be calculated.

7.4.4 Finite strip aerodynamic property matrices

7.4.4.1 Aerodynamic self-excited forces

In order to derive the aerodynamic damping and stiffness matrices of a flat shell or a bridge deck using finite strip method, first, the self-excited flutter forces need to be recognized. According to the linear aerodynamics, three types of uniformly distributed line loads acting along the centre of elasticity of a moving structure, including lift force L_f , drag force D_f, and pitching moments M_f, as illustrated in Fig. 7.4, define the self-excited flutter forces per unit length of the structure as

$$L_f = \frac{1}{2}\rho_{air}U^2B(K_wH_1^*\frac{w'}{U} + K_wH_2^*\frac{B\theta'}{U} + {K_w}^2H_3^*\theta + {K_w}^2H_4^*\frac{w}{B} + K_wH_5^*\frac{Bu'}{U} + {K_w}^2H_6^*\frac{u}{B}) \quad (7\text{-}23)$$

$$D_f = \frac{1}{2}\rho_{air}U^2B(K_wP_1^*\frac{u'}{U} + K_wP_2^*\frac{B\theta'}{U} + {K_w}^2P_3^*\theta + {K_w}^2P_4^*\frac{u}{B} + K_wP_5^*\frac{w'}{U} + {K_w}^2P_6^*\frac{w}{B}) \quad (7\text{-}24)$$

$$M_f = \frac{1}{2}\rho_{air}U^2B^2(K_wA_1^*\frac{w'}{U} + K_wA_2^*\frac{B\theta'}{U} + {K_w}^2A_3^*\theta + {K_w}^2A_4^*\frac{w}{B} + K_wA_5^*\frac{u'}{U} + {K_w}^2A_6^*\frac{u}{B}) \quad (7\text{-}25)$$

where u, w, θ are the vertical bending, lateral bending, and torsional displacements, as shown in Fig. 7.5, while u', w', θ' are the first derivatives of the corresponding displacements. K_w is the non-dimensional reduced frequency given by $K_w = B\omega_f/U$ where ω_f is the flutter angular frequency ω_f, B is the deck width, and U is the mean wind velocity. The terms H_i^*, P_i^*, A_i^* (i=1,2,3, …, 6) are the aerodynamic derivatives associated with the self-excited lift L_f, drag D_f, and moment M_f aerodynamic forces respectively. The flutter derivatives are all functions of reduced frequency K_w and are usually measured from experimental tests performed on the cross-section of the structure. Also, ρ_{air} is referred to the air density. When the cross-section of the deck is a slab girder, the centre of elasticity is equal to the geometric shear centre, while in the case of a box girder bridge, the aerodynamic forces need to be mapped on the nodal lines of the strip. This procedure however is out of the scope of the current research as the deck of the bridge is assumed to be a slab-girder. However, this can be achieved simply by adjusting the displacement functions. Also, it must be noted that the wind velocity acting on the cross-section of the plate (deck) might apply by different angles of attack. It is the responsibility of the aerodynamic design engineer to investigate which wind attack angle can cause the maximum aerodynamic force and subsequently the instability of the structure.

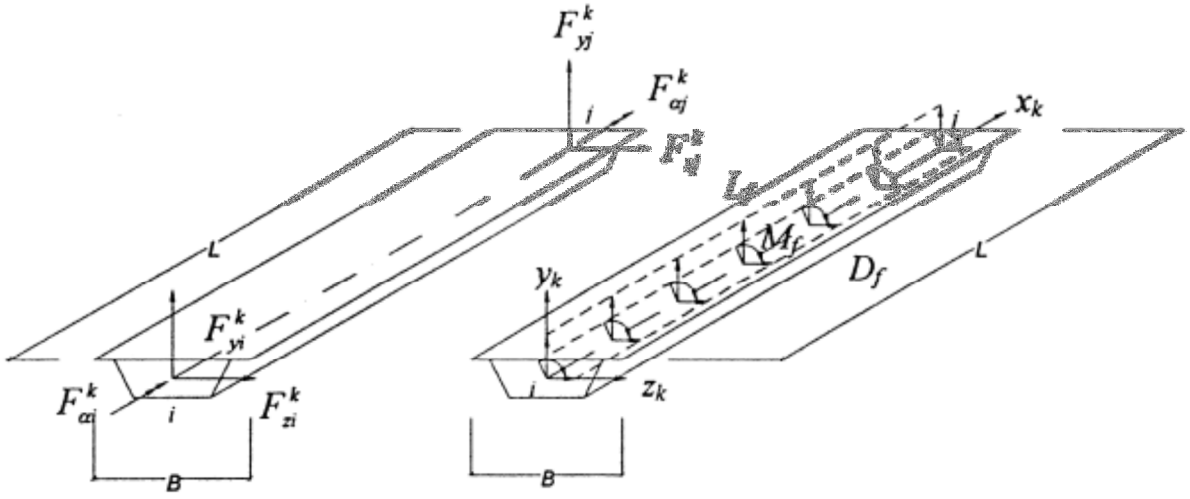

Fig. 7.4 Self-excited aerodynamic forces [7.1]

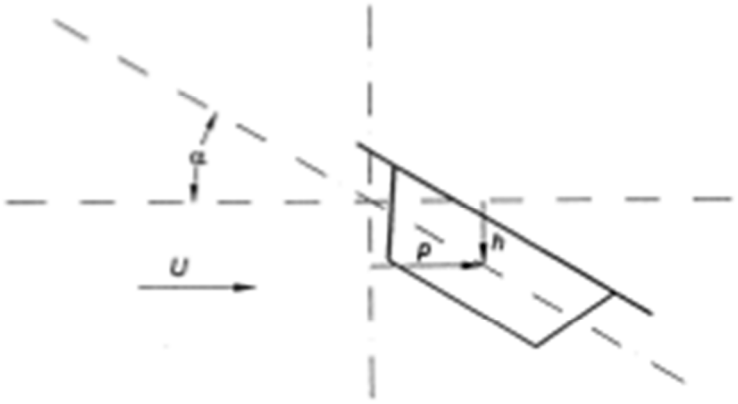

Fig. 7.5 Aerodynamic displacement components [7.1]

7.4.4.2 Spline discretization of aerodynamic forces

In conventional analytical methods and finite element method, the uniformly self-exited forces are linearly lumped along the structure whereby one-half of every element load acts

upon each element-end. Herein, the B3-spline interpolation is employed to distribute the aerodynamic forces along the plate. The spline discretization of aerodynamic forces leads to a more accurate distribution because of higher continuity degree (C2). In the finite strip formulation, it is more convenient to locate a nodal line passing through the aerodynamic line loads, acting on the centre of elasticity of the deck. Applying the principle of minimum potential energy in the environment of IFSM, the self-exited aerodynamic forces, originated from the wind velocity as an external wind-induced force, can be distributed on the knots along the nodal line of a spline strip. The work done by aerodynamic forces $\{f_{aer}\}$ is obtained by

$$\{f_{aer}\} = \int [N]^T q \, dA \tag{7-26}$$

where q represents the self-excited aerodynamic forces given by

$$q = L_f + D_f + M_f \tag{7-27}$$

Substituting Eq. (7-26) into (7-27) yields

$$\{f_{aer}\} = \int [\phi]^T [N_t]^T L_f \, dA + \int [\phi]^T [N_t]^T D_f \, dA + \int [\phi]^T [N_t]^T M_f \, dA \tag{7-28}$$

where $[\phi]^T$ is the longitudinal B3 spline function of Eqs. (7-6) or (7-8). $[N_t]$ is the transverse shape function of Eq. (7-13), where its integration $\int_0^b [N_t]^T \, dx$ over the width of the strip b corresponding to the aerodynamic forces L_f , D_f, and M_f is given by the following matrices respectively

$$\begin{bmatrix} 0 & 0 & 0 & 0 & 0 & 0 & 0 & 0 \\ 0 & 0 & 0 & 0 & 0 & 0 & 0 & 0 \\ 0 & 0 & 1 & 0 & 0 & 0 & 0 & 0 \end{bmatrix} \tag{7-29}$$

$$\begin{bmatrix} 1 & 0 & 0 & 0 & 0 & 0 & 0 & 0 \\ 0 & 1 & 0 & 0 & 0 & 0 & 0 & 0 \\ 0 & 0 & 0 & 0 & 0 & 0 & 0 & 0 \end{bmatrix} \tag{7-30}$$

$$\begin{bmatrix} 0 & 0 & 0 & 0 & 0 & 0 & 0 & 0 \\ 0 & 0 & 0 & 0 & 0 & 0 & 0 & 0 \\ 0 & 0 & 0 & 1 & 0 & 0 & 0 & 0 \end{bmatrix} \tag{7-31}$$

The integration of the spline representations of Eqs. (7-6) or (7-8) over the length of the strip L, for each degree of freedom (displacement parameter), results in m+3 values corresponding to the knots of a nodal line. This integral can be called $\{\phi_f\}$. Assuming the location of the aerodynamic loads on the first nodal line of the strip *i,* and after mathematical rearranging, the Eq. (7.28) is expanded to the following matrix formulation

$$\{f_{aer}\}=\frac{1}{2}\rho_{air}U^2K_w{}^2\begin{bmatrix} P_4^*[\phi_{fdiag}] & [0] & P_6^*[\phi_{fdiag}] & BP_3^*[\phi_{fdiag}] & & \\ [0] & [0] & [0] & [0] & zeros & \\ H_6^*[\phi_{fdiag}] & [0] & H_4^*[\phi_{fdiag}] & BH_3^*[\phi_{fdiag}] & & \\ BA_6^*[\phi_{fdiag}] & [0] & BA_4^*[\phi_{fdiag}] & B^2A_3^*[\phi_{fdiag}] & & \\ & & zeros & & zeros & \end{bmatrix}\begin{Bmatrix} u_i \\ v_i \\ w_i \\ \theta_i \\ u_j \\ v_j \\ w_j \\ \theta_j \end{Bmatrix}+$$

$$\frac{1}{2}\rho_{air}UBK_w\begin{bmatrix} P_1^*[\phi_{fdiag}] & [0] & P_5^*[\phi_{fdiag}] & BP_2^*[\phi_{fdiag}] & & \\ [0] & [0] & [0] & [0] & zeros & \\ H_5^*[\phi_{fdiag}] & [0] & H_1^*[\phi_{fdiag}] & BH_2^*[\phi_{fdiag}] & & \\ BA_5^*[\phi_{fdiag}] & [0] & BA_1^*[\phi_{fdiag}] & B^2A_2^*[\phi_{fdiag}] & & \\ & & zeros & & zeros & \end{bmatrix}\begin{Bmatrix} \acute{u}_i \\ \acute{v}_i \\ \acute{w}_i \\ \acute{\theta}_i \\ \acute{u}_j \\ \acute{v}_j \\ \acute{w}_j \\ \acute{\theta}_j \end{Bmatrix} \quad (7\text{-}32)$$

in which $[\phi_{fdiag}]$ is the diagonal form of $\{\phi_f\}$ with the order of (m+3) × (m+3) and is given by

$$[\phi_{fdiag}]=\begin{bmatrix} \phi_{f-1} & & zeros \\ & \ddots & \\ zeros & & \phi_{fm+1} \end{bmatrix} \quad (7\text{-}33)$$

7.4.4.3 Finite strip aerodynamic stiffness and damping matrices

The first and second matrices in Eq. (7-32) are, in fact, the aerodynamic stiffness and damping matrices of a spline strip respectively. As there are *m+3* knots on each nodal line, the number of each displacement parameter in Eq. (7-32) will be *m+3.* Applying the spline finite strip derivation, aerodynamic stiffness and damping matrix of a shell spline strip can be obtained by

$$[k_{aer}] = \frac{1}{2}\rho_{air}U^2K_w{}^2 \begin{bmatrix} P_4^*[\phi_{fdiag}] & [0] & P_6^*[\phi_{fdiag}] & BP_3^*[\phi_{fdiag}] & \\ [0] & [0] & [0] & [0] & zeros \\ H_6^*[\phi_{fdiag}] & [0] & H_4^*[\phi_{fdiag}] & BH_3^*[\phi_{fdiag}] & \\ BA_6^*[\phi_{fdiag}] & [0] & BA_4^*[\phi_{fdiag}] & B^2A_3^*[\phi_{fdiag}] & \\ & zeros & & & zeros \\ & & & & \end{bmatrix} \quad (7\text{-}34)$$

$$[c_{aer}] = \frac{1}{2}\rho_{air}UBK_w \begin{bmatrix} P_1^*[\phi_{fdiag}] & [0] & P_5^*[\phi_{fdiag}] & BP_2^*[\phi_{fdiag}] & \\ [0] & [0] & [0] & [0] & zeros \\ H_5^*[\phi_{fdiag}] & [0] & H_1^*[\phi_{fdiag}] & BH_2^*[\phi_{fdiag}] & \\ BA_5^*[\phi_{fdiag}] & [0] & BA_1^*[\phi_{fdiag}] & B^2A_2^*[\phi_{fdiag}] & \\ & zeros & & & zeros \\ & & & & \end{bmatrix} \quad (7\text{-}35)$$

Except for the spline strip with self-excited forces, the aerodynamic stiffness and damping matrices of the rest of the strips in the entire IFSM model is zero as there is no self-excited force acting on other elements of the model. The global aerodynamic stiffness $[K_{aer}]$ and damping $[C_{aer}]$ matrices are formed using the conventional assembling techniques. Finally, the aerodynamic equation of motion for the entire structural system in the environment of IFSM is formulated in the general form of Eq. (7-2).

7.4.5 Boundary conditions

The strip in the finite strip method must be defined with preset boundary conditions. There are several techniques that can be applied to model the boundary conditions of the strip [7.13]. Although the advantages of spline finite strip over the finite element method in terms of computational efficiency, handling of a complex amended scheme of local splines for considering the end and internal boundary conditions, keeps it solution untidy. In other words, current amendment schemes of boundary conditions are unable to be generalized. Dealing with boundary conditions using the standard techniques like penalty functions is complicated. Herein, a straightforward method for modelling boundary conditions based on replacing the spline displacement parameters with physical degrees of freedoms is proposed. This will result in developing a general unified formulation of otherwise very complex and tedious amended schemes of local splines, in the vicinity of the boundary supports and at

any internal support. This makes the method more versatile and adjustable with other numerical techniques.

For an equally spaced B3-spline function, one can rewrite the physical displacements $u_{phy}, v_{phy}, w_{phy}$ and the rotation θ_{phy} at the end knots of a nodal line *i* of a spline strip as

$$u_{phy0} = \frac{1}{6}(u_{-1} + 4u_0 + u_1)$$

$$v_{phy0} = \frac{1}{6}(v_{-1} + 4v_0 + v_1)$$

$$w_{phy0} = \frac{1}{6}(w_{-1} + 4w_0 + w_1)$$

$$\theta_{phy0} = \frac{1}{2h}(-\theta_{-1} + \theta_1) \tag{7-36}$$

$$u_{phym} = \frac{1}{6}(u_{m-1} + 4u_m + u_{m+1})$$

$$v_{phym} = \frac{1}{6}(v_{m-1} + 4v_m + v_{m+1})$$

$$w_{phym} = \frac{1}{6}(w_{m-1} + 4w_m + w_{m+1})$$

$$\theta_{phym} = \frac{1}{2h}(-\theta_{m-1} + \theta_{m+1})$$

where h is the spline section length. Dividing a spline strip into m equal sections will give 8(m+3) spline parameters which define the displacement function of the shell spline strip. Similarly, the displacements and rotations of the intermediate knots are also presented by spline parameters. The transformation matrix corresponding to each degree of freedom u_i v_i w_i θ_i u_j v_j w_j θ_j is expressed by

$$T = \begin{bmatrix} \frac{-1}{2h} & 0 & \frac{1}{2h} & & & & & & \\ \frac{1}{6} & \frac{4}{6} & \frac{1}{6} & & & & & & \\ & \frac{1}{6} & \frac{4}{6} & \frac{1}{6} & & & & & \\ & & & & & & & & \\ & & & & \ddots & & & & \\ & & & & & \frac{1}{6} & \frac{4}{6} & \frac{1}{6} & \\ & & & & & & \frac{1}{6} & \frac{4}{6} & \frac{1}{6} \\ & & & & & & \frac{-1}{2h} & 0 & \frac{1}{2h} \end{bmatrix} \tag{7-37}$$

where T is a $8 \times 8\ (m+3)$ matrix. The global transformation matrix of a flat shell spline strip is presented as

$$T_t = \begin{bmatrix} T & & & & & & & \\ & T & & & & & & \\ & & T & & & & & \\ & & & T & & & & \\ & & & & T & & & \\ & & & & & T & & \\ & & & & & & T & \\ & & & & & & & T \end{bmatrix} \tag{7-38}$$

Therefore, the transformed structural matrices can be obtained by

$$[K_{st}] = [T_t]^T [K_s][T_t] \tag{7-39}$$

$$[M_{st}] = [T_t]^T [M_s][T_t] \tag{7-40}$$

After transferring all degrees of freedom to the physical coordinate system, for each restrained degree of freedom a corresponding zero value is imposed on the physical displacement vector, which means the corresponding rows and columns in the structural and aerodynamic properties matrices are eliminated. The proposed amended scheme is more applicable to the equal section splines while for the unequal section splines the penalty function is used.

7.5 Flutter eigenvalue analysis

Eq. (7-4) is an eigenvalue problem which can be solved using techniques of either frequency domain or time domain analyses. In the present research, the flutter eigenvalue problem is solved in the environment of frequency domain method. The flutter response frequencies of the structure are primarily dependent on the natural frequencies of the system. Different schemes can be used for solving the flutter equation like PK, PK-F method, Jacobi diagonalization, QL, or QR transformation, subspace iteration, etc.

Herein, a simple method is proposed which is based on linearizing the quadratic flutter equation (7-4) as well as converting it into a steady-state problem. The philosophy of linearization of flutter eigenvalue problem is to allow one to use eigenvalue solution of an undamped system. Assuming $z = \{\dot{\delta}\}$, one can reformulate Eq. (7-4) as

$$\begin{bmatrix} [M] & [0] \\ [0] & [I] \end{bmatrix} \begin{Bmatrix} \{\ddot{\delta}\} \\ \{\dot{\delta}\} \end{Bmatrix} = \begin{bmatrix} -[C] & -[K] \\ [I] & [0] \end{bmatrix} \begin{Bmatrix} \{\dot{\delta}\} \\ \{\delta\} \end{Bmatrix} \tag{7-41}$$

or

$$\begin{bmatrix}[M] & [0]\\ [0] & [I]\end{bmatrix}\begin{Bmatrix}\dot{z}\\ \{\dot{\delta}\}\end{Bmatrix}=\begin{bmatrix}-[C] & -[K]\\ [I] & [0]\end{bmatrix}\begin{Bmatrix}z\\ \{\delta\}\end{Bmatrix} \tag{7-42}$$

In short form, Eq. (7-42) is presented by

$$[A]\{\dot{X}\}=[B]\{X\} \tag{7-43}$$

where

$$[A]=\begin{bmatrix}[M] & [0]\\ [0] & [I]\end{bmatrix} \tag{7-44}$$

$$[B]=\begin{bmatrix}-[C] & -[K]\\ [I] & [0]\end{bmatrix} \tag{7-45}$$

$$\{X\}=\begin{Bmatrix}z\\ \{\delta\}\end{Bmatrix}=\begin{Bmatrix}\{\dot{\delta}\}\\ \{\delta\}\end{Bmatrix}=\begin{Bmatrix}\lambda\{\psi\}\\ \{\psi\}\end{Bmatrix}e^{\lambda t} \tag{7-46}$$

$$\{\dot{X}\}=\begin{Bmatrix}\dot{z}\\ \{\dot{\delta}\}\end{Bmatrix}=\begin{Bmatrix}\{\ddot{\delta}\}\\ \{\dot{\delta}\}\end{Bmatrix}=\begin{Bmatrix}\lambda\{\psi\}\\ \{\psi\}\end{Bmatrix}\lambda e^{\lambda t} \tag{7-47}$$

7.5.1 Full-mode finite strip aeroelastic analysis

In the full-mode flutter analysis, the flutter eigenvalues of an original n degrees of freedom system, rather than an m order system, modified by m natural modes, is calculated. The full-mode aeroelastic analysis employs the vector iteration method to solve partial eigenvalues of Eq. (7-43). The iterative analysis must converge to the most dominant value of λ, which is equal to the highest frequency ω_f. For a complicated structural system like a long-span cable-stayed bridge with massive amount of degrees of freedom, the full mode eigenvalue flutter analysis requires a high amount of time which is computationally very inefficient. Research has shown that difference between the results of full-mode flutter analysis and multi-mode analysis is slight [7.1]. The flutter phenomenon usually occurs under the effect of the first few torsional and/or heave modes of the structure. For that reason, full-mode analysis might not be considered efficient for the eigenvalue flutter analysis.

7.5.2 Multi-mode finite strip aeroelastic analysis

A globally accepted algorithm for solving eigenvalue flutter problem, especially for linear

elastic structural systems, is the flutter modal analysis in which the aerodynamic response of the structure is discretized into *m* degrees of freedom, instead of high order *n* degrees of freedom. The multi-mode flutter analysis is an approximate approach in which the system flutter oscillation mode is assumed to be the combination of a few natural modes of the target structure. Herein, *m* is the number of natural modes involved in the flutter oscillation. When multi-mode flutter analysis needs to be performed, the flutter equation of motion (Eq. (7-4)) must be presented in the modal space, in which the structural and aerodynamic matrices are generalized as

$$[M^*] = [\psi]^T[M][\psi] \tag{7-48}$$

$$[C^*] = [\psi]^T[C][\psi] \tag{7-49}$$

or

$$[C^*] = [\psi]^T([C_s] - [C_{aer}])[\psi] = [\psi]^T[C_s][\psi] - [\psi]^T[C_{aer}][\psi] \tag{7-50}$$

and

$$[K^*] = [\psi]^T[K][\psi] \tag{7-51}$$

or

$$[K^*] = [\psi]^T([C_s] - [C_{aer}])[\psi] = [\psi]^T[C_s][\psi] - [\psi]^T[C_{aer}][\psi] \tag{7-52}$$

7.5.3 Solution procedure

In the case of full-mode flutter analysis, the generalization of the property matrices is not necessary because all natural frequencies of the system must be considered, and the natural mode shapes are not required to be decoupled. For both full-mode and multi-mode flutter analysis, the eigenvalue analysis of Eq. (7-4) yields a set of complex conjugate pairs of eigenvalues $\lambda_i = \mu_i \pm i\omega_i$ $(i = 1,2,\dots,m/2)$. The real part μ_i is in fact the logarithmic decrement of the structural system while the imaginary part ω_i is the flutter frequency response of the structure at a certain wind speed. The real part μ_i of at least one complex conjugate pair must be positive to identify the occurrence of the flutter instability. In other words, when the real part of the eigenvalue becomes zero for the first time at the lowest

wind speed, the flutter critical condition occurs. In performing the flutter eigenvalue analysis, the flutter critical speed U_f and critical flutter frequency ω_f can be solved simultaneously from the real and imaginary values of the resultant eigenvalue. The range of wind speeds U_{min} to U_{max} in increments of ΔU, as well as the iteration of the oscillation frequency from the initial value of the corresponding natural mode, are important factors in the investigation of flutter susceptibility. In the case of full-mode analysis, the number of eigenvalues λ is equal to *2n,* while for the multi-mode analysis this number is equal to *2m*. Eigenvalue equation of Eq. (7-4) (or Eq. (7-43)) is solved iteratively with incremental value of wind speed *U*. The aerodynamic derivatives are obtained from the flutter angular frequencyω_f. The critical wind speed and flutter frequency are traced when aeroelastic logarithmic decrement of the system becomes zero. The intersection of the flutter frequency curves of two or multiple modes determine the critical condition.

7.6 Numerical examples

In order to illustrate the effectiveness of the proposed finite strip solution in flutter analysis of long-span plates and bridge structures, two examples of frequency-domain flutter analysis are presented in this section. First, classical thin airfoil aerodynamics in the category of both multi-mode and full-mode analysis approaches is employed for numerical flutter investigation of a thin flat shell. In the second case study, the aerodynamic performance of Kap Shui Mun Bridge is evaluated.

7.6.1 Flutter of long-span flat shell

A long span plate with simply supported ends is selected as case study to investigate the accuracy of the proposed finite strip solution. For verification purposes, the material and geometric properties are the same as those addressed in reference [7.18] including plate length L=300 m, plate width B = 40 m, plate thickness t = 1 m, modulus of elasticity $E = 3.5 \times 10^3\ MPa$, plate mass density $\rho = 2.5 \times 10^3\ kg/m^3$, and Poisson's ratio $\upsilon = 1/6$, and the air density $\rho_{air} = 1.225\ kg/m^3$. The plate is divided into two strips of equal width in the transverse direction, and 10 equal-length sections in the longitudinal direction. The finite strip discretization of the plate is illustrated in Fig. 7.6. The angle of the wind speed is selected to be zero degrees.

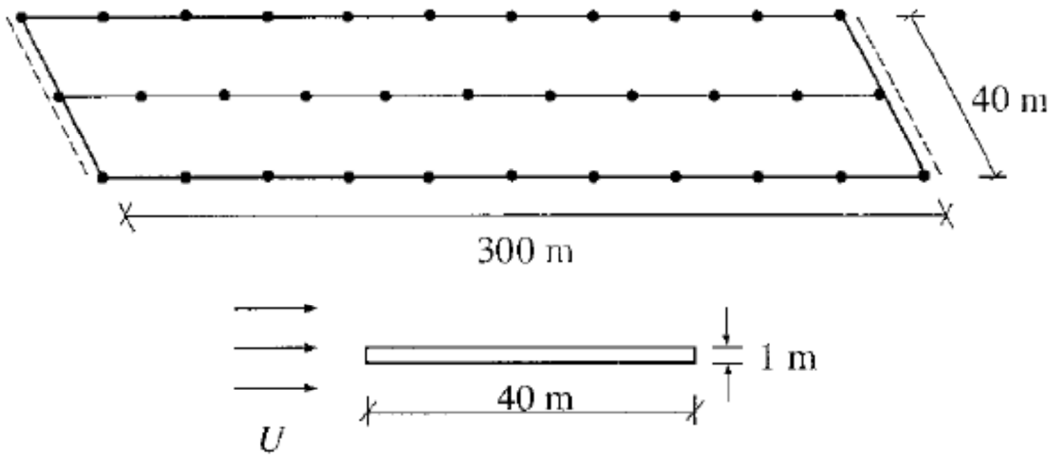

Fig. 7.6 Simply supported long-span flat shell [7.18]

First, a free vibration spline finite strip analysis is performed in order to obtain the natural frequencies and mode shapes of the plate. The developed finite strip program is also capable of 3D plotting of the deformed shape of the plate in different mode shapes. In Table 7.1 and Fig. 7.7 the first ten natural frequencies, as well as the mode shapes of the simply supported flat shell are presented. From the deformed shape of the plate, it can be concluded that the second and the fifth modes are corresponding to the first symmetric heave and torsional modes with the natural frequencies of 0.0189 Hz and 0.2050 Hz respectively. As can be seen in Table 7.1, the targeted natural frequencies are in excellent agreement with the frequencies of the same plate, as presented in Ref. [7.18] with the difference of less than 5%.

Table 7.1 Natural frequencies of the long-span thin flat shell

Mode number	Frequency f (Hz)		Angular frequency ω (rad/s)	Mode shape
	FSM	Ref. [7.18]		
1	0	-	0	-
2	0.0189	0.019	0.1185	symmetric heave 1
3	0.0755	-	0.4744	antisymmetric heave 1
4	0.1702	-	1.0694	symmetric heave 2
5	0.2050	0.194	1.2879	torsional 1
6	0.3035	-	1.9069	antisymmetric heave 2
7	0.4150	-	2.6076	torsional 2
8	0.4768	-	2.9961	symmetric heave 3
9	0.6351	-	3.9902	torsional 3
10	0.6939	-	4.3600	antisymmetric heave 3

mode 1

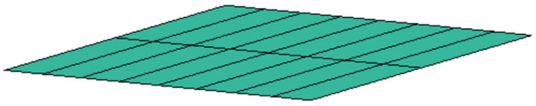

mode 2

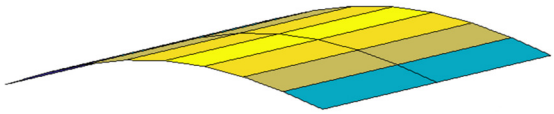

mode 3

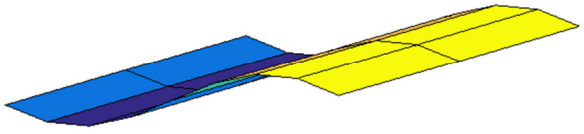

mode 4

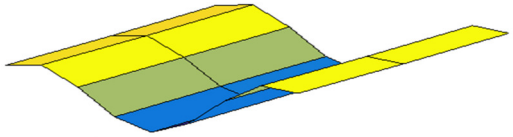

mode 5

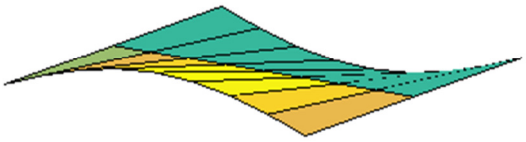

mode 6

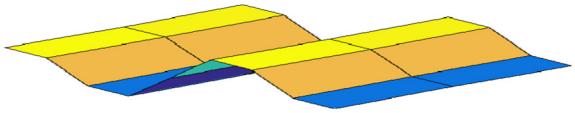

mode 7

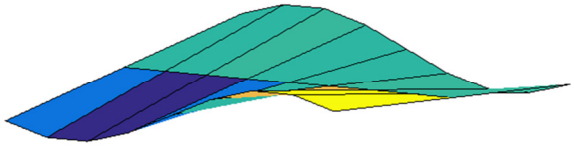

mode 8

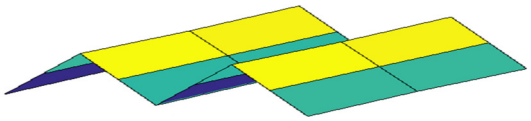

mode 9

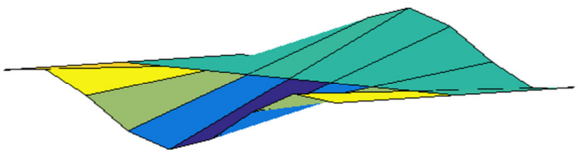

mode 10

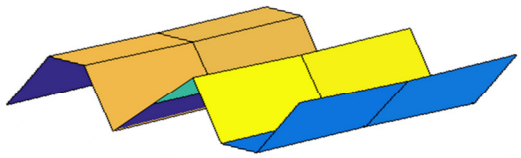

Fig. 7.7 Finite strip mode shapes of the simply supported thin flat shell

The Theodorsen's function [7.20] is used to calculate the aerodynamic flutter derivatives of a plate with uniform thin cross-section as

$$C(K_w) = F(K_w) + iG(K_w) \tag{7-53}$$

where

$$F(K_w) = 1 - \frac{0.165}{1+\left(\frac{0.0455}{k_w}\right)^2} - \frac{0.335}{1+\left(\frac{0.3}{k_w}\right)^2} \tag{7-54}$$

$$G(K) = -\frac{0.165\left(\frac{0.0455}{k_w}\right)}{1+\left(\frac{0.0455}{k_w}\right)^2} - \frac{0.335\left(\frac{0.3}{k_w}\right)}{1+\left(\frac{0.3}{k_w}\right)^2} \tag{7-55}$$

in which $k_w = 0.5\,K_w$. The values of Theodorsen's functions $F(K_w)$ and $G(K_w)$ against the k_w are illustrated in Fig. 7.8.

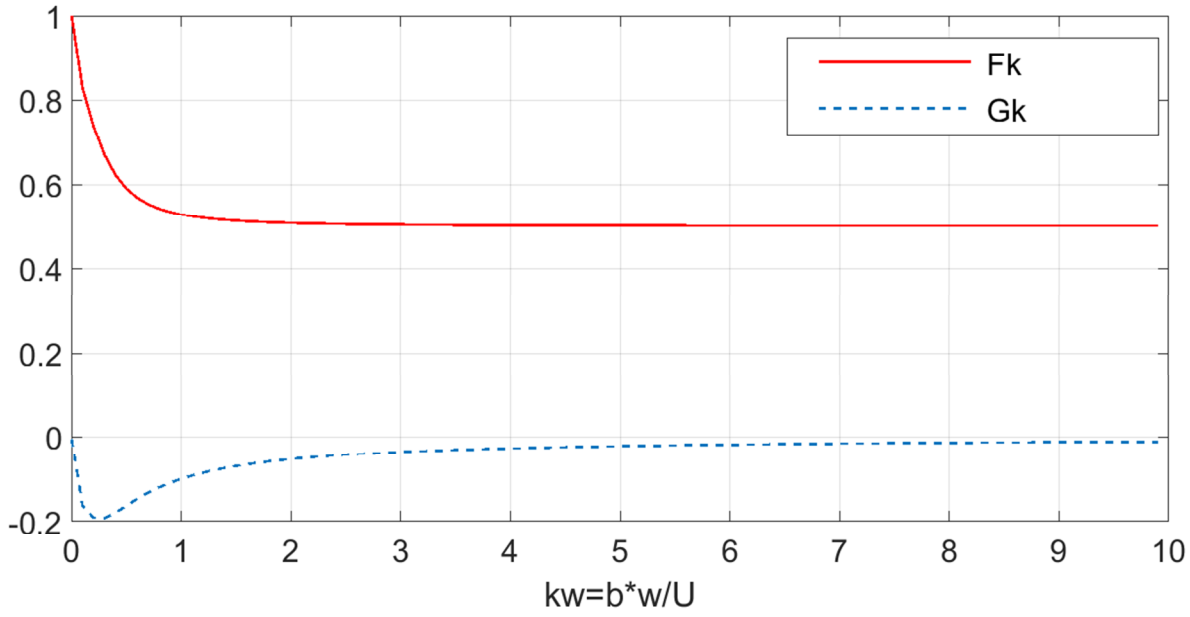

Fig. 7.8 Real and imaginary parts of the Theodorsen circularity function $C(K_w) = F(K_w) + iG(K_w)$

Using the Theodorsen's functions $F(K_w)$ and $G(K_w)$, the flutter derivatives H_i^* and A_i^* (i=1, 2, 3, 4) for a plate section can be analytically presented as follows

$$H_1^* = -2\pi\frac{F}{K_w}$$

$$H_2^* = -\frac{\pi}{K_w}\left(\frac{1}{2} + \frac{G}{K_w} + \frac{F}{2}\right)$$

$$H_3^* = -\frac{\pi}{K_w^2}\left(2F - \frac{K_w G}{2}\right)$$

$$H_4^* = \frac{\pi}{2}\left(1 + \frac{4G}{K_w}\right) \tag{7-56}$$

$$A_1^* = \frac{\pi F}{2K_w}$$

$$A_2^* = \frac{\pi}{K_w}\left(\frac{-1}{8} + \frac{G}{2K_w} + \frac{F}{8}\right)$$

$$A_3^* = \frac{\pi}{K_w^2}\left(\frac{K_w^2}{64} + \frac{F}{2} - \frac{K_w G}{8}\right)$$

$$A_4^* = -\frac{\pi G}{2K_w} \tag{7-57}$$

The variations of the theoretically calculated flutter derivatives H_i^* and A_i^* of the plate section against the reduced velocity are illustrated in Fig. 7.9.

In the environment of spline finite strip method and using an iterative frequency domain analysis, the response flutter frequencies of the plate for different wind speeds are obtained and expressed in Fig. 7.10. In addition, the variation of logarithmic decrement against the wind speed is shown in Fig. 7.11. Only the torsional mode has been considered in this study using both multi-mode and full mode flutter analysis. Also, the structural damping is neglected in this example.

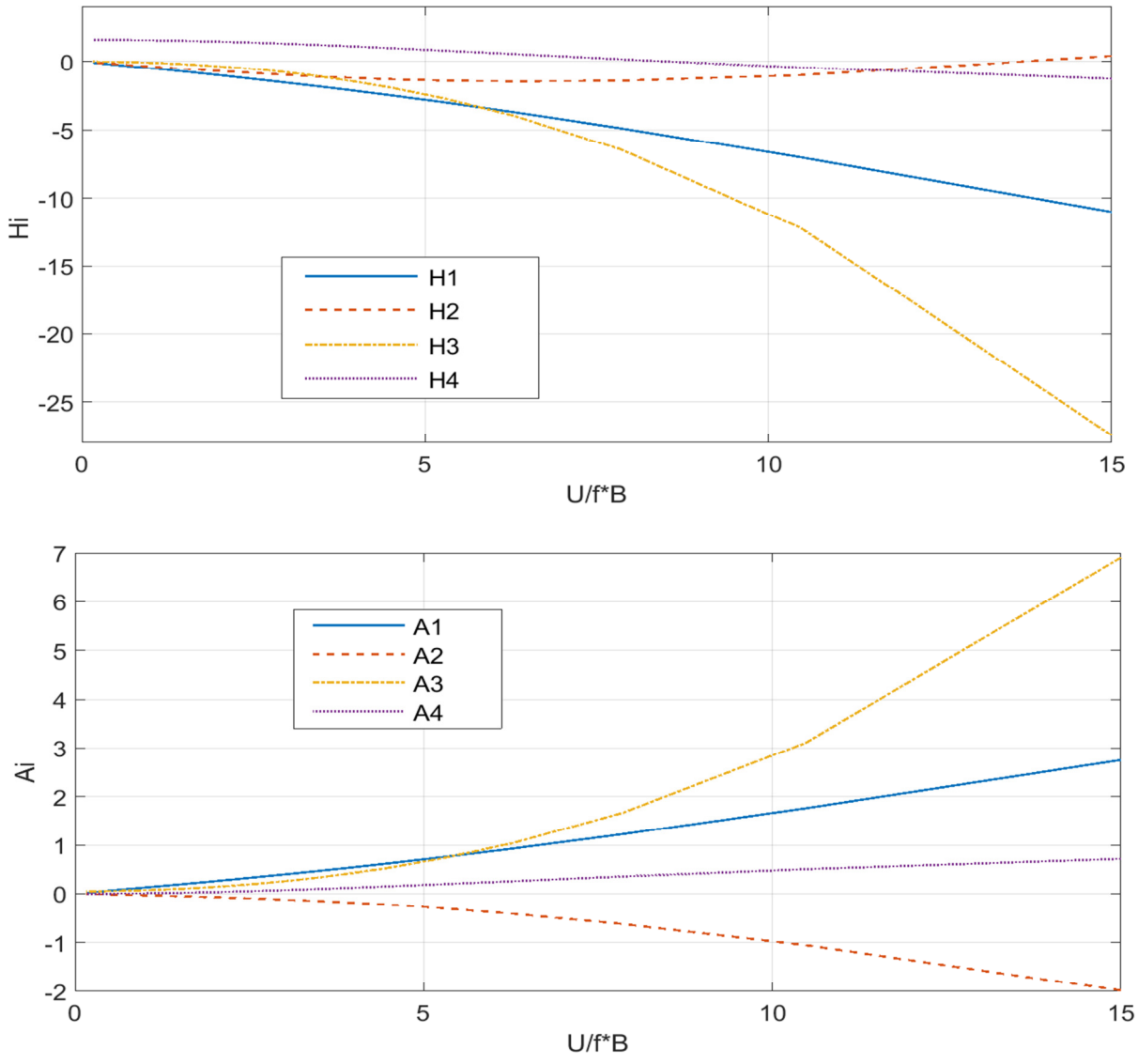

Fig. 7.9 Aerodynamic flutter derivatives of thin flat shell

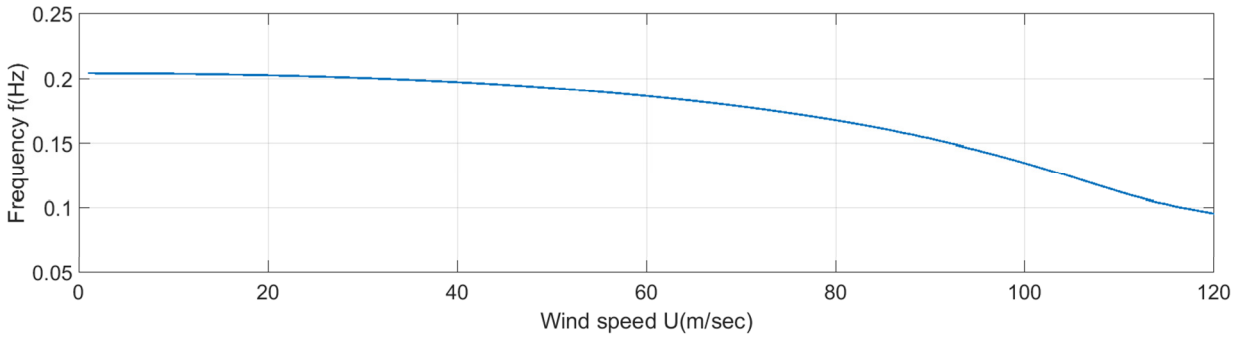

Fig. 7.10 Torsional flutter response frequencies of simply supported long-span plate

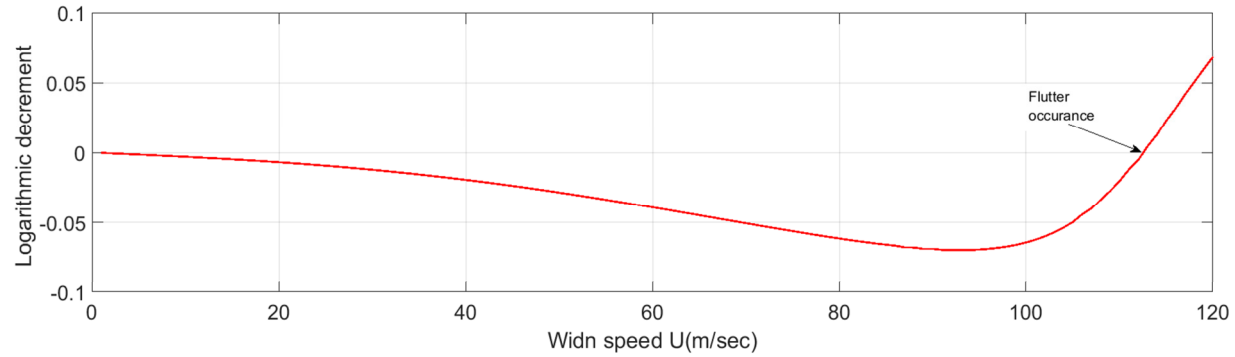

Fig. 7.11 Logarithmic decrement of simply supported long-span plate

According to Fig. 7.11, the logarithmic decrement becomes zero at the wind speed of 113 (m/sec) which shows the occurrence of flutter instability. The corresponding response frequency for the critical wind speed of 113 (m/sec) is 0.1055 (Hz) which represents the critical flutter frequency. In Table 7.2, the critical flutter wind speed and frequency of the present plate are comparted with the results reported by other researchers. The comparison between the results shows the maximum 2% and 11% difference between the critical flutter frequencies and critical flutter wind speeds respectively which confirms the accuracy of the present finite strip formulation and the corresponding flutter analysis scheme. Also, there is almost no difference between the numerical finite strip results of single-mode and full-mode analyses. It can be concluded that there is no need to include all the vibration modes in the flutter analysis. The reason for the higher critical wind speed in the case of PK-F finite strip flutter analysis [7.18] could be the spatial distribution of the self-excited loads in which the

magnitude of the aerodynamic forces allocated to each knot in a spline nodal line is slightly lower than that of the present finite strip formulation. Therefore, less wind energy is input into the structure. This initiates the occurrence of flutter at a higher speed. The other reason behind the difference between the critical wind speed of the present formulation and that obtained by Chang et al. [7.18], is originated in the spline distribution of the aerodynamic forces in the current flutter finite strip method versus the trapezoidal distribution of the same forces employed in the work of Cheng et al. [7.18]. In the spline distribution more forces are allocated to the middle knots than the knots close to the two ends of the plate, while in the trapezoidal distribution except the two ends of the nodal lines, the same amount of forces are allocated to the rest of the knots.

It is worth noting that a number of parametric studies were performed in the present research to investigate the convergence of the flutter frequency and flutter wind speed results against the spline finite strip mesh size. The results show that the number of sections in the longitudinal direction of the strip directly influences the convergence of the results while the number of strips has the lower impact on the accuracy and convergence rate of the solution. The reason is that the more the number of knots in the longitudinal direction of the spline strip, the more uniform distribution of the aerodynamic self-excited forces along the centre of elasticity of the deck. This results in faster and better convergence of the results.

Table 7.2 Flutter analysis results of simply supported long-span thin flat shell

Method	Single-mode	Full-mode	FEM	SFSM PK-F	Van der put formula
Reference	This paper	This paper	[7.21]	[7.18]	[7.18]
Critical flutter frequency f(Hz)	0.1055	0.1055	0.1034	0.1045	-
Frequency error %	-	0	+2	+0.9	-
Critical wind speed U_f(m/sec)	113.1	113.2	125.4	123.5	121.9
Wind speed error %	-	0	-11	-9	-7

7.6.2 Aerodynamic performance of Kap Shui Mun Bridge

For the second case study, the integrated finite strip method is employed to investigate the flutter performance of the Kap Shui Mun Bridge as illustrated in Fig. 7.12. The geometric and material properties of the deck are expressed in Fig. 7.13 and Table 7.3 respectively. The finite strip modelling of the west and east towers, as well as the 3D integrated finite strip modelling of the entire cable-stayed bridge system are displayed in Figs. 7.14 and 7.15 respectively. The detailed information regarding the integrated finite strip modelling of Kap Shui Mun Bridge system can be found in Ref. [7.15].

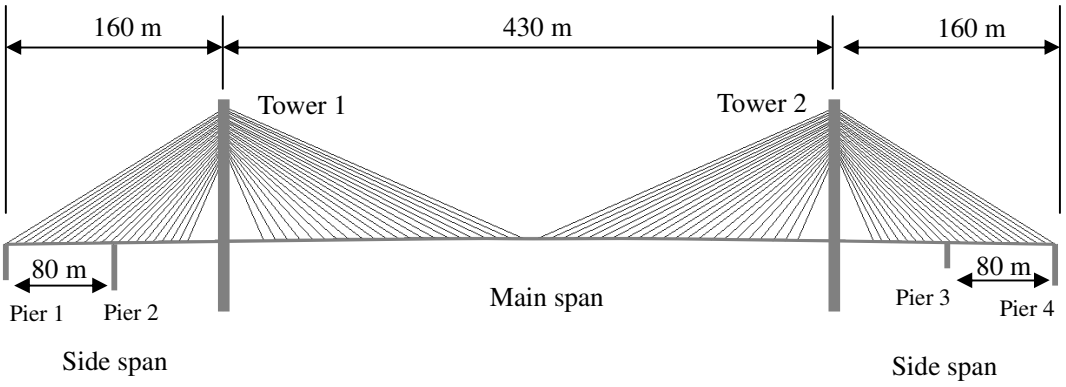

Fig. 7.12 Kap Shui Mun Bridge

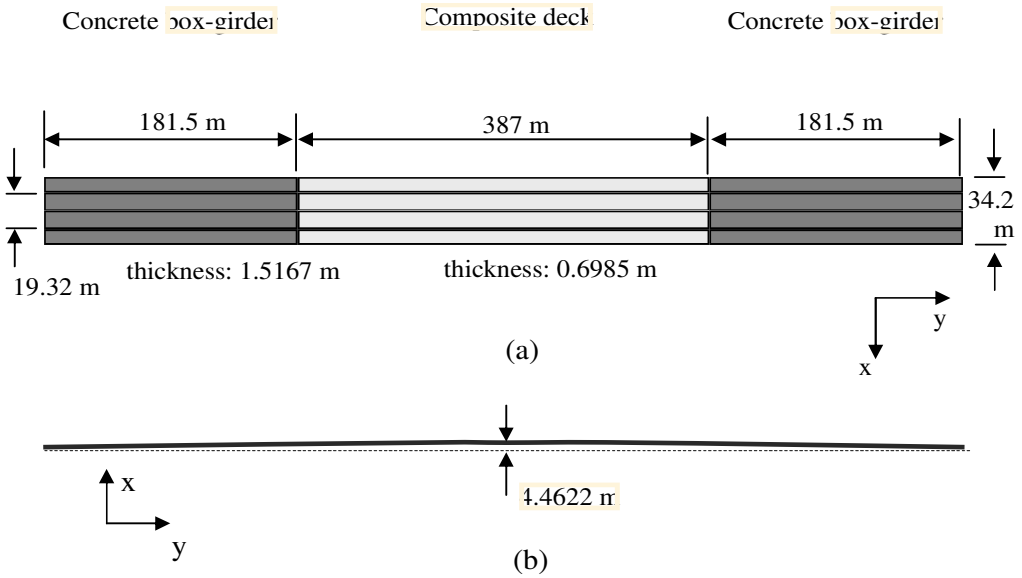

Fig. 7.13 Geometrical properties of the deck: (a) top view; (b) front view

Table 7.3 Material properties of deck

Properties	Main Span	Side Spans
Modulus of elasticity (kPa)	2.00×10^{8}	3.00×10^{7}
Mass density (kg/m^3)	3880	3630
Poisson's ratios	0.3	0.2
Moment of inertia (vertical) (m^4)	191	363
Moment of inertia (transverse) (m^4)	2530	5560

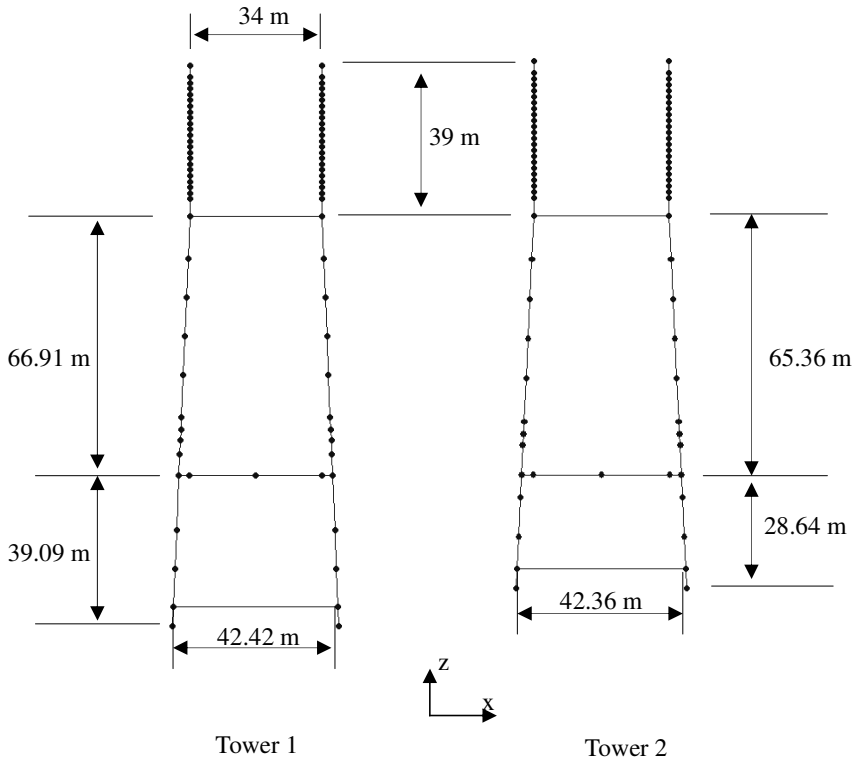

Fig. 7.14 Towers models of the Kap Shui Mun Bridge

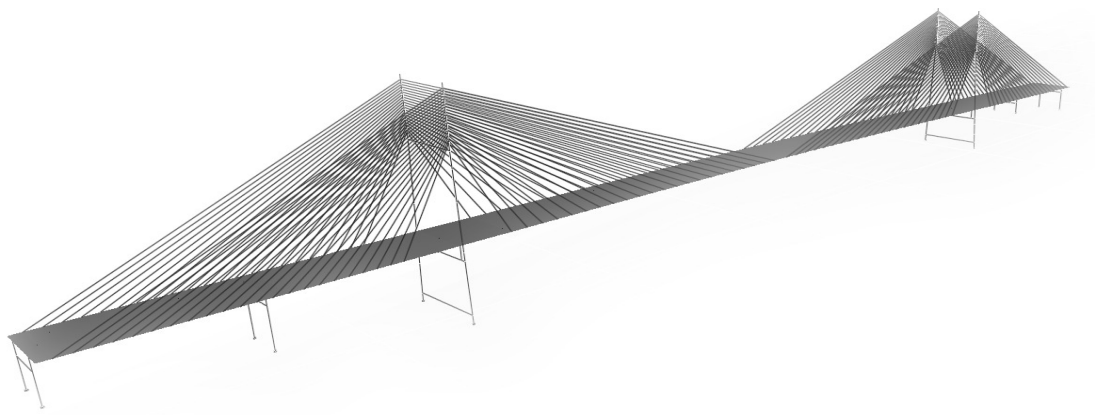

Fig. 7.15 Three-dimensional model of the Kap Shui Mun Bridge

7.6.2.1 Free vibration analysis

The flutter frequency analysis is performed by selecting the natural frequencies of one or a number of specific mode shapes as the start point of the response frequency. Therefore, free vibration analysis is a necessary step before flutter analysis. In this regard, a free vibration analysis is performed to obtain the natural frequencies of the Kap Shui Mun Bridge and their corresponding mode shapes. The first ten mode shapes of the bridge including the natural frequencies are obtained by IFSM and are presented in Table 7.4. The finite strip results are compared with those obtained from finite element (SAP 2000) analysis [7.15] as well as with the field measurements [7.22]. The very good agreement between the results validates the accuracy of the IFSM in frequency analysis. In Figs. 7.16 to 7.19 the first symmetric and antisymmetric heave and torsional mode shapes of the Kap Shui Mun Bridge are illustrated. The corresponding natural frequency for the first symmetric torsional and heave modes is 0.7526 (Hz) and 0.4250 (Hz) respectively, while this value is 1.3419 (Hz) and 0.8523 (Hz) respectively for the first antisymmetric torsional and heave modes.

Table 7.4 Modal characteristic of first ten modes of the Kap Shui Mun Bridge

Mode number	Natural frequency f (Hz)			Nature of mode shape
	IFSM (1)	FEM [7.15] (2)	Field tests [7.22] (3)	
1	0.2113	0.2061	---	tower
2	0.2409	0.2338	---	tower
3	0.4250	0.4226	0.39	symmetric heave mode of the deck
4	0.5217	0.5160	0.49	lateral bending of the deck
5	0.7526	0.7179	0.83	symmetric torsional mode of the deck
6	0.8523	0.8500	0.66	antisymmetric heave mode of the deck
7	0.9305	0.9257	0.90	lateral bending of the deck
8	1.0032	1.0023	1.07	heave mode of the deck
9	1.1381	1.1048	---	tower
10	1.1391	1.1058	---	tower

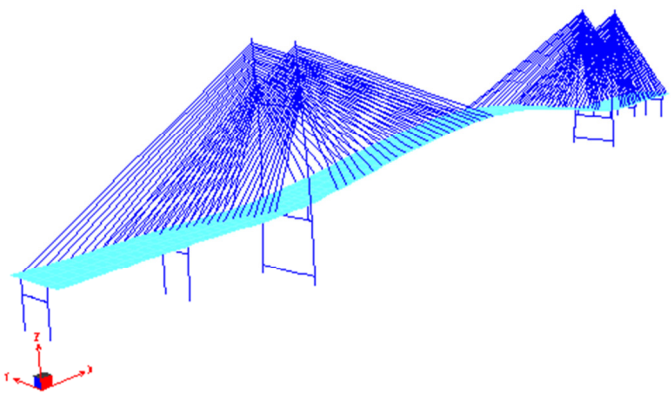

Fig. 7.16 First symmetric heave mode of the deck (0.4250 Hz)

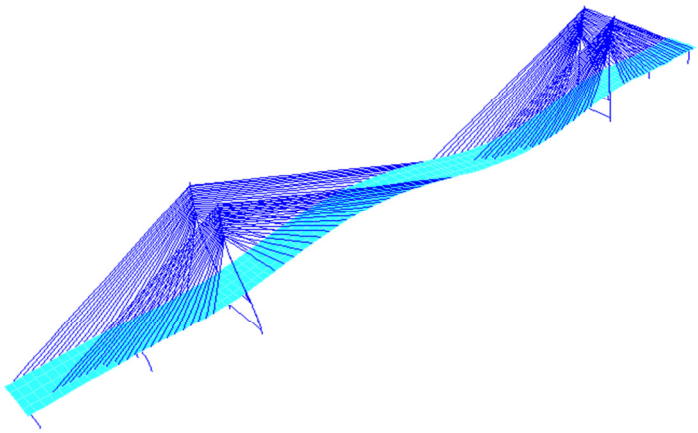

Fig. 7.17 First antisymmetric heave mode of the deck (0.8523 Hz)

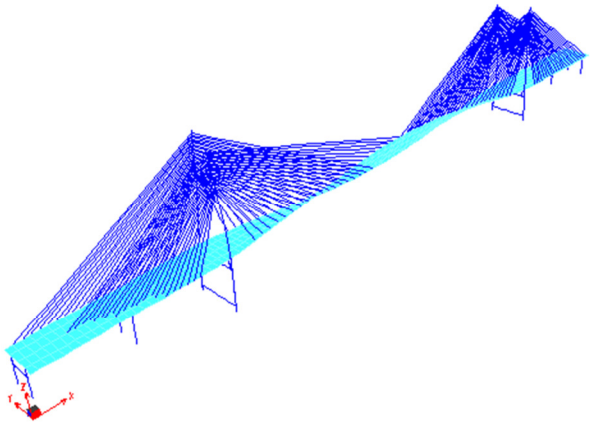

Fig. 7.18 First symmetric torsional mode of the deck (0.7526 Hz)

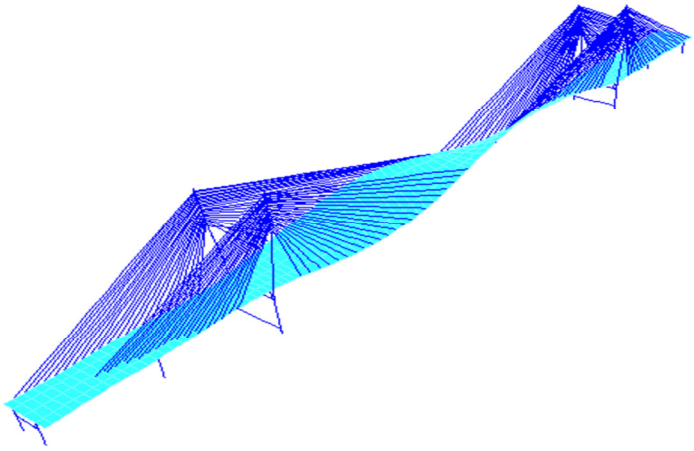

Fig. 7.19 First antisymmetric torsional mode of the deck (1.3419 Hz)

7.6.2.2 Kap Shui Mun Bridge flutter derivatives

In the design of Kap Shui Mun Bridge, because of the critical location of the bridge, the typhoon conditions have been considered in which the wind loading is much stronger (might need to consider up to 95 m/s of the wind speed) [7.23]. The Kap Shui Mun Bridge was tested for the aerodynamic derivatives to determine the critical wind velocities for bridge deck [7.24]. The aerodynamic flutter performance of Kap Shui Mun Bridge has been investigated through the experimental flutter derivatives of the Bridge reported by Jon Raggett in West Wind Laboratory at California in collaboration with Robert Scanlan at Johns Hopkins University [7.25]. The static aerodynamic coefficients and the aerodynamic flutter derivatives have been derived through the wind tunnel tests. The flutter derivatives $A*$ and $H*$ obtained experimentally are reproduced in Figs. (7.20) and (7.21). Herein, the deck width B is 35.7 m. All the flutter derivatives are related to the final main span bridge deck configuration with and without traffic in which the kerb is also considered. The vertical incidence angle of the wind, or sometimes called the angle of the wind attack, in the present study is -2.5 degrees.

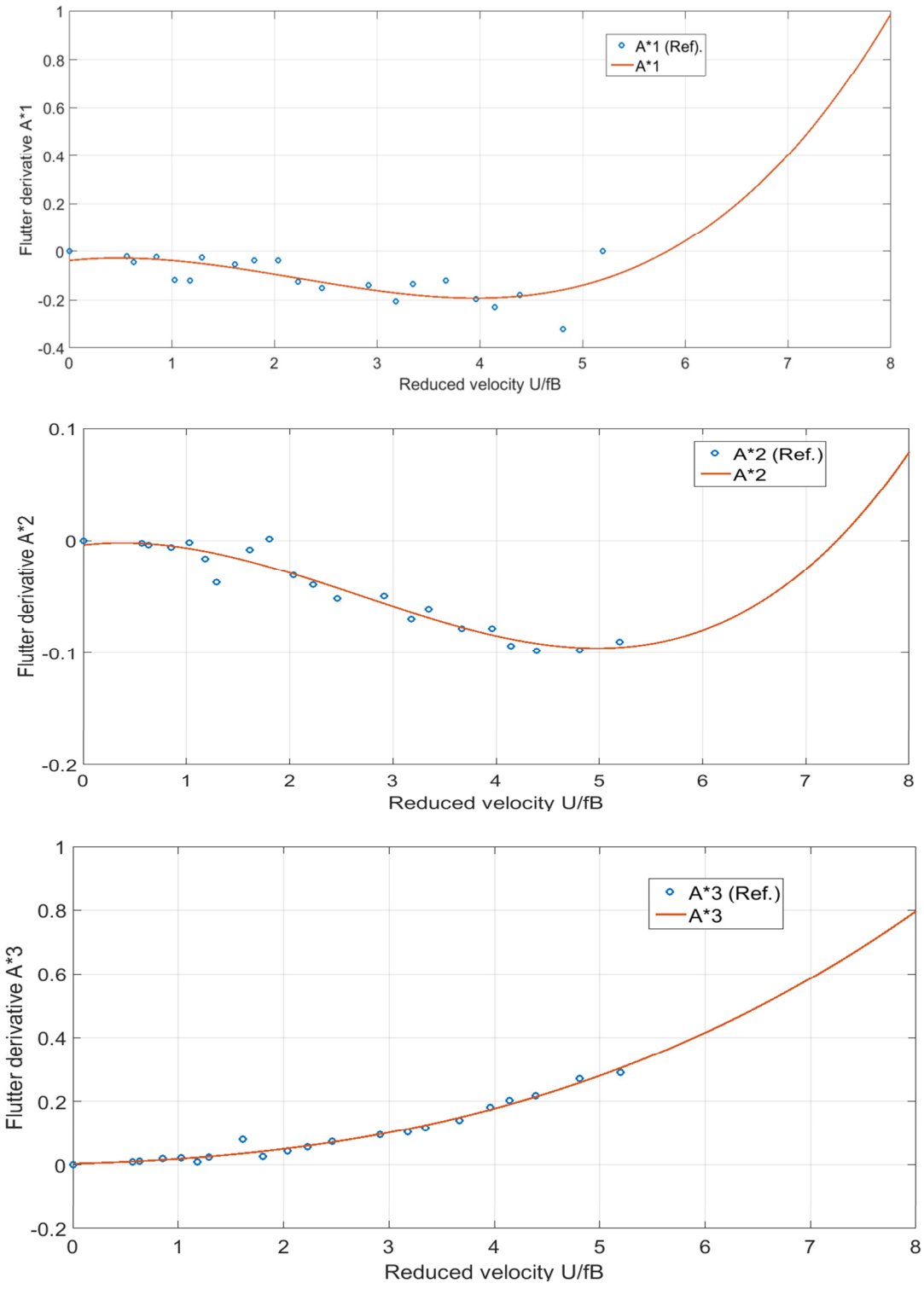

Fig. 7.20 Flutter derivatives A_1^* to A_3^* of Kap Shui Mun against reduced velocity

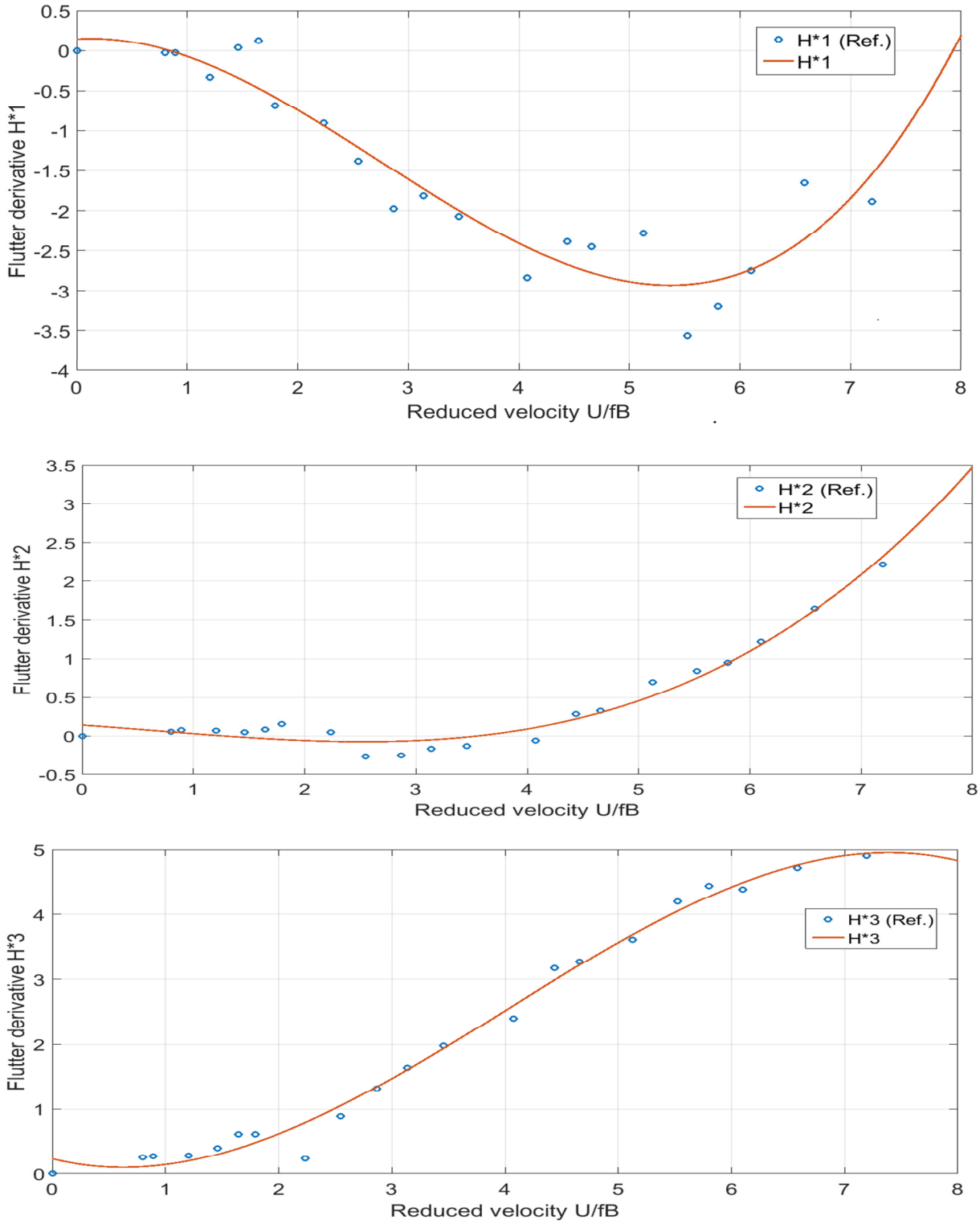

Fig. 7.21 Flutter derivatives H_1^* to H_3^* of Kap Shui Mun against reduced velocity

7.6.2.3 Flutter analysis of Kap Shui Mun Bridge

Having all structural properties and aerodynamic properties of the Kap Shui Mun Bridge by using the integrated finite strip method, the flutter analysis can be performed. The damping ratio of the bridge system is chosen to be 0.02. In the previous example, it was shown that the full-mode flutter analysis takes much more time storage and time comparing with the multi-mode flutter analysis, while the results are of both techniques are almost the same. The full-mode flutter analysis for such a massive structure like Kap Shui Mun Bridge with thousands of degrees of freedom will take a massive amount of storage and time. Therefore, multi-mode flutter analysis is applied in this example for aeroelastic analysis of the Kap Shui Mun Bridge. The first symmetric torsi

onal mode of the deck is taken as the critical mode shape for the flutter. The integrated finite strip flutter eigenvalue analysis results are plotted in Figs. (7.22) and (7.23), where the flutter frequencies, as well as the logarithmic decrements of the Kap Shui Mun Bridge for different wind speeds are calculated and displayed. The results show that both flutter frequency and logarithmic decrement decrease when the wind speed increases, which could be the sign of flutter instability occurrence. However, the logarithmic decrement never becomes zero, which means that the flutter instability does not happen within the standard values of wind speeds and even in the typhoon conditions for which the critical wind speed could be 95 m/sec. Therefore, it proves that the aerodynamic flutter design of the Kap Shui Mun Bridge meets the requirements of the aeroelastic stability.

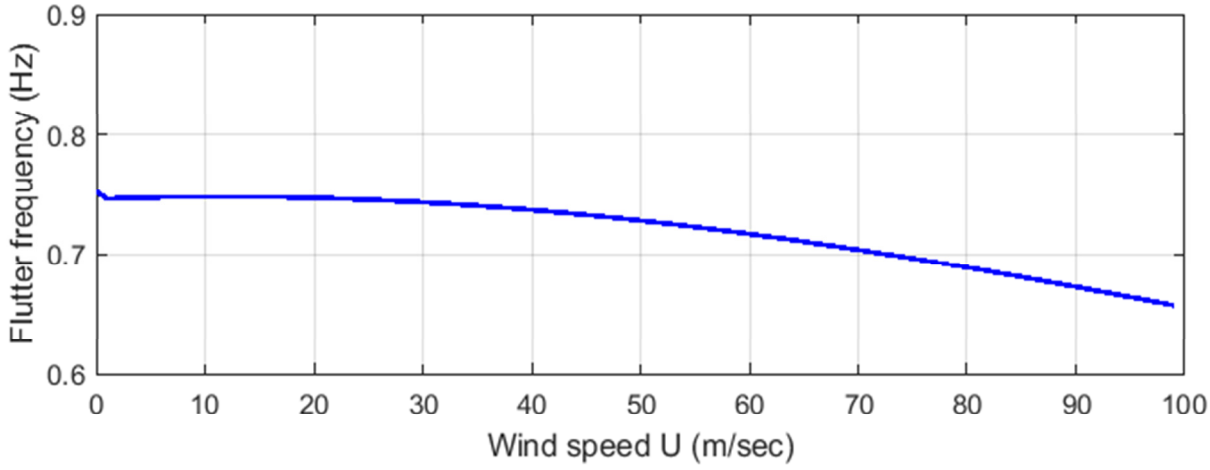

Fig. 7.22 Torsional flutter response frequencies of Kap Shui Mun Bridge

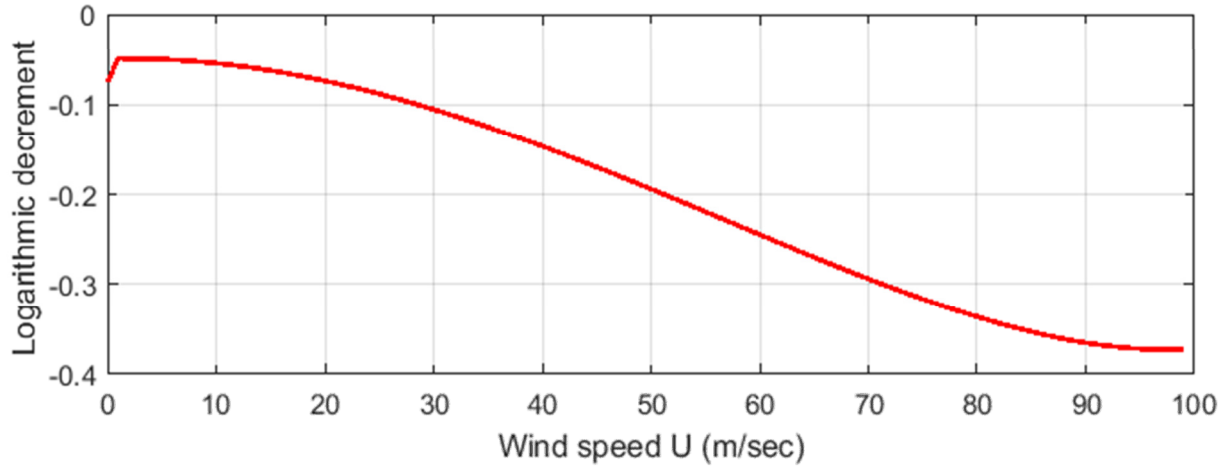

Fig. 7.23 Logarithmic decrement of torsional flutter of Kap Shui Mun Bridge

7.7 Conclusions

Integrated finite strip method was extended to the area of wind engineering where the aerodynamic flutter analysis can be performed in minimal computational time providing high accuracy and efficiency. Due to the semi-analytical nature and a narrow bandwidth of the dynamic properties of the system, the results converged rapidly with a few degrees of freedom. The aeroelastic damping and stiffness matrices were derived by using integrated finite strip method. The total potential energy of a shell strip was obtained from the algebraic summation of the in-plane and out-of-plane deformations. In the current finite strip solution, the boundary conditions were modelled by using a simple technique based on physical coordinate system. Also, the flutter problem was solved by a very straightforward eigenvalue frequency analysis. Both multi-mode and full-mode flutter analyses approaches have been outlined in the environment of IFSM for evaluating the critical flutter speed as well as the critical flutter frequency of the structural system. The numerical results show that performing the full-mode flutter analysis is extremely more time consuming than the multi-mode analysis, while the resultant critical flutter frequencies and the corresponding flutter wind speeds do not change significantly. Therefore, it is suggested to use the multi-mode technique for flutter analysis. Also, the results showed that the uniform distribution of self-excited flutter forces on the centre of elasticity of cross-section is reasonably good when

compared with the spatial distribution of aerodynamic forces on the entire surface of the deck. Last but not least, the method is capable to perform a three-dimensional flutter analysis. The successful extension of the finite strip method to the aerodynamic flutter analysis can open a new door for further development of this methodology on different areas of wind engineering, such as buffeting analysis of bridge, wind-vehicle-structure (WVS) interaction and aerodynamics of composite hybrid FRP bridge structures.

References

[7.1] Ge, Y.J., Tanaka, H., (2000), Aerodynamic flutter analysis of cable-supported bridges by multi-mode and full-mode approaches, J. Wind Eng. Ind. Aerodyn: 86, 123–153.

[7.2] Ding, Q.S., Chen, A.R., Xiang, H.F., (2002), Coupled flutter analysis of long-span bridges by multimode and full order approaches, J Wind Eng Ind Aerodyn: 90, 1981–1993.

[7.3] Ming-Hui Huang, Yuh-Yi Lin and Ming-Xi Weng, (2012), Flutter and Buffeting Analysis of Bridges Subjected to Skew Wind, Journal of Applied Science and Engineering, Vol. 15, No. 4, pp. 401E413 (2012) 401

[7.4] S. Chad Gibbs, Ivan Wang, Earl Dowell, (2012), Theory and experiment for flutter of a rectangular plate with a fixed leading edge in three-dimensional axial flow, Journal of Fluids and Structures 34 (2012) 68–83

[7.5] Teng Wu, Ahsan Kareem, Yaojun Ge, (2013), Linear and nonlinear aeroelastic analysis frameworks for cable-supported bridges, Nonlinear Dynamics, November 2013, Volume 74, Issue 3, pp 487–516

[7.6] E.S. Kreis and J.C. Andr´e, (2005), A numerical inquiry into the flutter phenomenon in long-span bridges, Latin American Journal of Solids and Structures 2 (2005) 321–337

[7.7] Masaru Matsumoto, Hisato Matsumiya, Shinya Fujiwara, Yasuaki Ito, (2008) New Consideration on Flutter Properties basing on SBS -Fundamental Flutter Mode, Similar Selberg's Formula, Torsional Divergence Instability, and New Coupled Flutter Phenomena affected by Structural Coupling, BBAA VI International Colloquium on: Bluff Bodies Aerodynamics & Applications Milano, Italy, July, 20-24 2008

[7.8] Duc-Huynh Phan, Ngoc-Trung Nguyen, (2013), Flutter and Buffeting Control of Long-span Suspension Bridge by Passive Flaps: Experiment and Numerical Simulation, Int'l J. of Aeronautical & Space Sci. 14(1), 46–57 (2013) DOI:10.5139/IJASS.2013.14.1.46

[7.9] Thomas Canor, Luca Caracoglia, Vincent Denoël, (2015), Application of random eigenvalue analysis to assess bridge flutter probability, Journal of Wind Engineering and Industrial Aerodynamics, Volume 140, May 2015, Pages 79–86

[7.10] Gui-hua Xie, Jie Yin, Rong-gui Liu, Bei Chen, Dong-sheng Cai, (2017), Experimental and numerical investigation on the static and dynamic behaviors of cable-stayed bridges with CFRP cables, Composites Part B: Engineering, Volume 111, 15 February 2017, Pages 235-242

[7.11] Yongxin Yang, Rui Zhou, Yaojun Ge, Xiaojie Zou, Lihai Zhang, (2017), Flutter characteristics of twin-box girder bridges with vertical central stabilizers, Engineering Structures, Volume 133, 15 February 2017, Pages 33-48

[7.12] N Lee, H Lee, C Baek, S Lee, (2016) Aeroelastic analysis of bridge deck flutter with modified implicit coupling method, Journal of Wind Engineering and Industrial Aerodynamics, Volume 155, August 2016, Pages 11–22

[7.13] Cheung, M. S., Li, W., and Chidiac, S. E. (1996) Finite strip analysis of bridges, 1st Ed., Spon, London.

[7.14] Cheung Y. K., Tham L. G. (1998) The finite strip method, USA: CRC Press; 1998

[7.15] Naderian, Hamidreza., Cheung, Moe M. S., Shen, Zhenyuan., Dragomirescu, Elena., (2015) Integrated Finite Strip Analysis of long-span cable-stayed bridges, Computers and Structures 158 (2015) 82–97

[7.16] Naderian, Hamidreza., Cheung, Moe M. S., Shen, Zhenyuan., Dragomirescu, Elena., (2015) Seismic analysis of long-span cable-stayed bridges by an integrated finite strip method, ASCE Journal of Bridge Engineering, ISSN 1084-0702

[7.17] Cheung, Y. K., Fan, S.C. and Wu, C.Q.(1982), "Spline finite strip in Structure Analysis", Proceedings, The international Conference on Finite Element Method, Shanghai, 704-709

[7.18] Lau, D. T., Cheung, M. S., and Cheng, S. H., (2000) "3D flutter analysis of bridges by spline finite strip method." J. Struct. Eng., 10.1061/(ASCE)0733-9445(2000)126:10(1246), 1246–1254.

[7.19] Scanlan, R. .H., Lin, W.H.(1978), "Effects of Turbulence on Bridge Flutter Derivatives' J. Engrg. Mech., ASCE, 104(4), 719-733.

[7.20] E. Simiu, R.H. Scanlan, (1996), Wind Effects on Structures, 3rd Edition, Wiley, New York, 1996.

[7.21] Cheng, S.H., (1994), “The 3D finite element flutter analysis of long-span bridge”, Master thesis, Tongji University, Shanghai, China

[7.22] Lau, C. K.; Mak, W. P.; Wong, K. Y.; Man, K. L.; Chan, W. Y.; Wong, K. F. (1999) Structural Performance Measurement and Design Parameter Validation for Kap Shui Mun Cable-Stayed Bridge, ADVANCES IN STEEL STRUCTURES, Vol.2, No.1

[7.23] Benedict Kai Kwan Yung. (2008), A CRITICAL ANALYSIS OF THE KAP SHUI MUN BRIDGE, Proceedings of Bridge Engineering Conference, 23 April 2008, England

[7.24] R.H. Scanlan, S.L. Stroh, J.D. Raggett, (1995), Methods of wind response investigation employed for the Kap Shui Mun Bridge, Journal of Wind Engineering and IndustrialAerodynamics54/55(1995)1-11

[7.25] Raggett Jon., Scanlan Robert, (1997), “Flutter derivatives of Kap Shui Mun Bridges using wind tunnel tests”, West Wind Laboratory, California & Department of Civil Engineering, Johns Hopkins University

Chapter 8
Conclusion and Future work

8.1 Conclusion

In this research, an integrated finite strip method (IFSM) was proposed for conventional and FRP long-span cable-stayed bridges. The method was applied to study the bending, free vibration, seismic, and aerodynamic analyses of long-span cable-stayed bridges.

In spite of the large number of publications on the use of finite strip method in long-span cable-stayed bridge analysis, the application of existing finite strip methods in static, dynamic, and aerodynamic analyses of long-span cable-stayed bridge has been restricted to the bridge super-structures or to the bridges with assumed sub-structure (towers, piers, cables) conditions only. The philosophy of the integrated finite strip method is to increase the capability of the finite strip method so that it can model the entire bridge system including deck, towers, piers, and cables. For this purpose, different strip elements were introduced including the flat shell spline strip and the laminate spline strip for modelling conventional and FRP laminated decks respectively, while the so-called column strip and cable strip were developed for modeling the towers, piers, and cables respectively. The unequally spaced B3-spline functions are the base for creating the integrated finite strip method. Using the latter concept, the transition section element is employed for modeling the joint knots of different structural components. Using the transition section elements, the joints are modelled and the structural interaction between different elements can be handled.

The free vibration analysis procedure in the integrated finite strip method environment was well performed. After solving an eigenvalue problem, the natural frequencies and mode shapes of the cable-stayed bridge structure were obtained. In the environment of the IFSM, the time history seismic analysis of long-span cable-stayed bridges was formulated. The Newmark scheme was employed for temporal discretization.

Through the development of the laminate strip, the IFSM was extended for modelling the entire bridge system and for performing dynamic analysis of long-span cable-stayed hybrid FRP bridges. The anisotropic characteristics, as well as the coupling effect between out-of-plane and in-plane degrees of freedom of the laminated FRP deck were taken into account. The results showed that the laminated strip is integrated well with both ordinary spline finite strip method for bending analysis of laminated FRP plates with different end conditions as well as integrated finite strip method for bending, free vibration, and seismic analysis of long-span cable-stayed hybrid FRP bridges, as well as continuous multi-span FRP bridges.

Following the primary phases of the present research, and as the main objective of this project, for the first time, a fully finite strip solution was extended to the area of wind engineering. Using the spline finite strip discretization, the aerodynamic stiffness and mass properties of a long-span cable-stayed bridge were derived. The aerodynamic properties along with the structural properties of the plates and long-span bridge are formulated in the flutter equation of motion. An innovative eigenvalue solution was proposed for solving the flutter problem which is based on linearization of aeroelastic equations of motions and converting the complex eigenvalue problem into a steady-state problem. Moreover, an innovative scheme was proposed for amending the B3 spline functions in order to handle different end boundary conditions in conventional SFMS and IFSM.

A series of computer programs were developed using C++ and MATLAB for analysis purposes. In addition, FEM simulations were made using SAP2000 and ABAQUS for verification and comparison purposes. A good agreement could be noticed between the numerical results of the integrated finite strip method and those obtained by finite element method as well as the field data. According to the time required for analysis, it was observed that the computational costs and efficiency in the finite strip method are much better than those of the finite element method. In particular, when it comes to the dynamic and aerodynamic analyses of long-span cable-stayed bridges in which the structure has a very large number of degrees of freedom, the finite strip method becomes more efficient and economic. Moreover, the simplicity of the input data in the finite strip environment is highly appreciated when comparing it with finite element method in which numerous parameters and criteria need to be controlled.

The set of computer codes developed through the proposed research is a unique tool for analyzing the dynamic and aerodynamic responses of the cable-stayed bridges constructed with both traditional and FRP composite materials. Moreover the computer codes will be much more efficient than the currently used structural commercial software, due to the use of the finite strip method. Details regarding the IFSM programs as well as the comprehensive information on finite strip discretization of the Kap Shui Mun Bridge model can be found in the user manual [8.1].

The outcomes of the research can be summarized as below:

- An integrated finite strip solution was proposed for long-span cable-stayed bridges.
- The entire bridge was modeled using the integrated finite strip method.
- The interactions between different components were considered in the analysis.
- The advantages of the method are simplicity of input data and high efficiency.
- The method is used for the static and free vibration analyses of Kap Shui Mun Bridge.
- Time history analysis of long-span cable-stayed bridges using Newmark scheme and in the environment of IFSM was introduced.
- Seismic responses of Kap Shui Mun Bridge under uniform and nonuniform excitations were evaluated.
- Numerical finite strip results were compared with finite element analysis and field measurements data.
- Laminate spline strip was developed for modelling laminated FRP plates with different boundary conditions.
- Anisotropy nature of the FRP deck as well as the coupling effects were considered in the finite strip analysis.
- The IFSM was extended to hybrid FRP continuous multi span bridges and hybrid FRP long-span cable-stayed bridges.
- Bending, free vibration, and seismic analysis of FRP cable-stayed bridges and continuous multi-span FRP bridge were solved using IFSM.
- An IFSM was proposed for aerodynamic analysis of long-span cable-stayed bridges.
- A simple scheme was developed for modeling different boundary conditions of the spline strips.
- An optimal eigenvalue flutter solution was proposed for solving the aeroelastic problem.

8.2 Future work

As a new stage in adapting the IFSM for bridges, such that this versatile method can integrate and simulate additional features, the following topics are suggested for extending the current research.

8.2.1 FRP hybrid bridges

In terms of cable-stayed FRP deck bridges, it is suggested that the FRP deck be modeled as a box FRP tube girder deck in finite strip environment and investigating how much it affects the stiffness of the hybrid system. It is predicted that the FRP box girder cross-section can significantly increase the stiffness of the laminated FRP deck. The developed integrated finite strip method is able to model all types of the cross-sections, including open thin-walled sections and box sections.

8.2.2 Future studies on aerodynamics using IFSM

Although the use of composite FRP materials in the bridge structural components make the bridges structures lighter and consequently prepare the conditions for extending the length of the bridge span, the aerodynamic stability becomes critical in the design step. Therefore, special attention should be paid to the aerodynamic flutter behavior of hybrid composite long-span cable-stayed bridges.

In addition, the current rapid development of transportation systems leads to longer bridge span and higher vehicle speed, which inevitably increase the potential risk of vehicles moving on a bridge subjected to strong cross winds. Recent bridge-vehicle-wind interaction studies highlighted the importance of predicting the bridge dynamic behavior by considering the bridge, the actual traffic load, and wind as a whole coupled system [8.2-8.5]. Thus, it is necessary to investigate the coupled vibrations of wind–vehicle–bridge (WVB) systems and to ensure the safety and normal working performance of both vehicles and bridge. Regarding the aerodynamic stability, buffeting responses of bridge deck under natural wind can be evaluated by the proposed finite strip solution.

8.2.3 Optimal temporal schemes for fluid-structure interaction

The flutter equation of motion is a complex eigenvalue problem. A numerical scheme called Runge-Kutta method has the great potential to be employed for solving the complex

eigenvalue flutter problem. Runge-Kutta method is suggested to be first applied to a simplified structural system and then to be generalized for solving the flutter of the bridges. As a further research, it is suggested to optimize the proposed Runge-Kutta scheme in order to increase the efficiency and proficiency of the analysis. Using integrated finite strip method and the proposed Runge-Kutta scheme, both spatial and temporal discretization of the system will be optimized. As a result, a very efficient and robust solution will be proposed for the flutter analysis. In the following, detailed explanations will be presented on proposing an optimal temporal scheme for fluid-structure interactions with emphasis on flutter of longs-span bridges.

When analyzing a long-span bridge for aerodynamic forces, a fluid-structure interaction (FSI) problem is created in which the bridge structure interacts with the surrounding wind flow. Flutter analysis of long-span cable-stayed bridges, as a FSI problem plays a prominent role in the safe and optimized design of these massive structures. A comprehensive study of such problems is still a challenge due to their strong nonlinearity and multidisciplinary nature.

For most FSI problems including flutter of long-span bridges, analytical solutions for modeling the equations are impossible to obtain, and laboratory tests results are limited. Therefore, to evaluate the fundamental physics involved in the complex interaction between wind as a fluid, and bridge as solid, numerical simulations may be employed. With recent advances of computer technology, simulations of scientific and engineering systems, including long-span cable-stayed bridges, have become increasingly sophisticated. To fill the technological gap, an efficient numerical algorithm can be used to investigate the interaction between wind flows and the response of the bridge structure. Such an investigation is typically multidisciplinary because the performance of the bridge is a result of the interaction between wind-induced flutter and structural dynamics.

Multi-stage Runge-Kutta schemes have been recognized as a suitable solving method for the temporal integration of Navier-Stokes equations in computational fluid dynamics owing to the low-storage requirements as well as large stability limits. Nevertheless, the main concerns in problems such as wave propagation and flutter could be dissipation and dispersion errors even if the stability limits are preserved to obtain the desirable results. As a result, low-dissipative low-dispersive numerical integration schemes have drawn attention in

the simulation of such physical phenomena. Optimal Runge–Kutta schemes for temporal discretization of the flutter problem can be introduced by optimizing an error function regarding the nature of the phenomenon, which maintains low dissipation and dispersion.

As the future steps of this research, temporal discretization of the flutter equation can be investigated to ensure low-dissipation and low-dispersion errors. Due to the benefits of Runge-Kutta schemes, it is believed that low-dispersion and low-dissipation Runge–Kutta schemes can be perfectly developed through the minimization of dissipation and dispersion errors. Deriving an optimal scheme for a specific type of problem is a growing approach in diverse fields of engineering including flutter analysis. In terms of Runge-Kutta schemes, both Explicit and Implicit RK methods can be applied for temporal discretization of the flutter problem. However, explicit schemes are well-known for the numerical stability concerns. To avoid instability, very small time steps may be required in some applications including the flutter analysis, which leads to high computational costs. For the same reason, main attention should be paid to implicit RK scheme and its optimized version for solving flutter problem. Different Runge-Kutta schemes must be introduced by optimizing the error and linear stability analysis for a flutter system of equations. The proposed scheme will be stable for a wide range of time steps. The procedure implemented in this study will be quite general and can be applied to flutter analysis of long-span cable-stayed bridges in the environment of integrated finite strip method. In order to develop an optimal temporal discretization scheme, a number of items need to be defined including objective function, order conditions, number of unknowns and equations as well as choosing free parameters which will be fully discussed in the final thesis.

The end result of the proposed research can lead to an efficient and accurate model that uses optimal schemes both for spatial and temporal integration of equations.

8.2.4 Integrated finite strip method for smart structural health monitoring of bridges

In North America, many of the bridge structures approach the end of their design life. Moreover, after natural disasters like earthquakes and typhoons, it is vital that emergency facilities such as bridges be investigated for safety criteria. Therefore, in order to increase the reliability of bridges, subjected to dynamic and aerodynamic hazards, innovative strategies need to be developed for structural health monitoring (SHM) of bridge structures.

With the rapid development of computer techniques like Internet of Things, etc., the application of smart wireless sensors in SHM of bridges is of great interest. An important feature in smart sensors is the capability of continuously monitoring the performance of the bridge structure in real time. This results in reducing the maintenance costs and increasing the safety to the public.

There are different SHM methods for detecting damages in bridge structures from which the vibration-based damage detection methods are more popular. After acceleration data is collected, modal parameters like natural frequency, damping ratio and mode shape can be obtained by using an adopted algorithm to assess the bridge health conditions through the change in modal properties.

Vibration-based damage detection algorithms that mesh well with the smart sensor system are highly desirable but currently very limited. Numerous vibration-based methods have been proposed like frequency changes methods, matrix update methods, flexibility-based damage methods, modal strain energy methods, etc. Although these methods can be effective, they are usually very complicated and not yet easily employed for continuous, real time online SHM of bridges with smart sensors.

It was shown in this thesis that the IFSM can be perfectly used for vibration analysis of bridges under seismic and aerodynamic effects. As the further step, the IFSM methodology can be extended to vibration based structural health monitoring of bridges. However, an algorithm needs to be developed in order to perform the continuous real time analysis of the bridge.

The performance of the proposed algorithms can be investigated based on the computational time, calculation efforts as well as the consistency and accuracy of the extracted results. The outcome of the research must provide a comprehensive framework for long-term structural health monitoring (SHM) of bridge structures using wireless smart sensors.

8.2.5 Further potential contributions of the proposed research

The remaining parts of the current research can potentially lead to further novel contributions as listed below:

- Time history flutter analysis of long-span cable-stayed bridges using Runge-Kutta method and in the environment of integrated finite strip method.

- Optimization of temporal schemes for flutter analysis using optimal Runge-Kutta method.
- Flutter analysis of long-span cable-stayed bridges using optimal Runge-Kutta method.
- Flutter analysis using Relaxation Method.
- Flutter analysis of long-span cable-stayed bridges using Relaxation Method.
- Flutter analysis using Implicit-Explicit (IMEX) Runge-Kutta Methods.
- Flutter analysis of long-span cable-stayed bridges using Implicit-Explicit (IMEX) Runge-Kutta Methods.
- Buffeting analysis of long-span cable-stayed bridges using Runge-Kutta methods and in the environment of integrated finite strip methods.
- Optimization of temporal schemes for buffeting analysis using optimal Runge-Kutta methods.
- Buffeting analysis of long-span cable-stayed bridges using optimal Runge-Kutta methods.

References

[8.1] Naderian, H., Cheung, Moe M. S., Finite Strip Analysis of Bridges: User Manual, Department of Civil and Environmental Engineering, Hong Kong University of Science and Technology, July 2013.

[8.2] Xu, Y.L., Guo, W.H., Dynamic analysis of coupled road vehicle and cable-stayed bridge systems under turbulent wind, J Struct Eng, ASCE, 2003; 25, 473–486.

[8.3] Cai, C.S., Chen, S.R., Framework of vehicle-bridge-wind dynamic analysis, J. Wind Eng. Ind. Aerodyn., 2004; (92)579–607.

[8.4] Chen, S.R., Cai, C.S., Unified approach to predict the dynamic performance of transportation system considering wind effects, Struct. Eng. Mech, 2006; (23), 279–292.

[8.5] Chen, S.R., Cai, C.S., Equivalent wheel load approach for slender cable-stayed bridge fatigue assessment under traffic and wind: Feasibility study, J. Bridge Eng., 2007; (12), 755–764.

Appendix A

The geometric properties as well as the initial prestress forces of the cables of the Kap Shui Mun Bridge used for the integrated finite strip model are given in Table A.1. The values of the temperature have been derived from the finite element model.

Table A.1 Geometric and prestress properties of the cables of Kap Shui Mun Bridge model

Cable number	Cable length (m)	Radius of cable section (m)	Initial prestress force at the first end (KN)	Initial prestress force at the second end (KN)	Temperature (C)
1	182.4869758	0.07	3321.982103	-3321.9821	92.2222
2	176.4736891	0.07	3321.982103	-3321.9821	92.2222
3	170.4814221	0.07	2961.76709	-2961.76709	82.2222
4	164.5124718	0.07	2241.337062	-2241.33706	62.2222
5	158.5694712	0.07	1881.122049	-1881.12205	52.2222
6	152.6554512	0.07	1160.692021	-1160.69202	32.2222
7	146.7739149	0.07	1160.692021	-1160.69202	32.2222
8	140.9289295	0.065	1932.581447	-1932.58145	62.2222
9	135.1252381	0.065	1621.987889	-1621.98789	52.2222
10	129.3683985	0.065	1311.394331	-1311.39433	42.2222
11	123.6649539	0.065	1000.800773	-1000.80077	32.2222
12	118.0226456	0.065	690.2072158	-690.207216	22.2222
13	112.4506766	0.06	1382.048852	-1382.04885	52.2222
14	106.9647674	0.06	1117.401087	-1117.40109	42.2222
15	101.5688014	0.06	1117.401087	-1117.40109	42.2222
16	96.28326497	0.06	852.7533218	-852.753322	32.2222
17	91.12737544	0.055	1606.06021	-1606.06021	72.2222
18	86.12442012	0.055	1161.304938	-1161.30494	52.2222
19	81.30263631	0.055	1383.682574	-1383.68257	62.2222
20	76.69620164	0.055	1606.06021	-1606.06021	72.2222
21	72.34626297	0.06	2705.287678	-2705.28768	102.2222
22	68.30184426	0.06	5748.736977	-5748.73698	217.2222
23	182.4869758	0.07	3321.982103	-3321.9821	92.2222
24	176.4736891	0.07	3321.982103	-3321.9821	92.2222
25	170.4814221	0.07	2961.76709	-2961.76709	82.2222
26	164.5124718	0.07	2241.337062	-2241.33706	62.2222
27	158.5694712	0.07	1881.122049	-1881.12205	52.2222
28	152.6554512	0.07	1160.692021	-1160.69202	32.2222
29	146.7739149	0.07	1160.692021	-1160.69202	32.2222
30	140.9289295	0.065	1932.581447	-1932.58145	62.2222
31	135.1252381	0.065	1621.987889	-1621.98789	52.2222

32	129.3683985	0.065	1311.394331	-1311.39433	42.2222
33	123.6649539	0.065	1000.800773	-1000.80077	32.2222
34	118.0226456	0.065	690.2072158	-690.207216	22.2222
35	112.4506766	0.06	1382.048852	-1382.04885	52.2222
36	106.9647674	0.06	1117.401087	-1117.40109	42.2222
37	101.5688014	0.06	1117.401087	-1117.40109	42.2222
38	96.28326497	0.06	852.7533218	-852.753322	32.2222
39	91.12737544	0.055	1606.06021	-1606.06021	72.2222
40	86.12442012	0.055	1161.304938	-1161.30494	52.2222
41	81.30263631	0.055	1383.682574	-1383.68257	62.2222
42	76.69620164	0.055	1606.06021	-1606.06021	72.2222
43	72.34626297	0.06	2705.287678	-2705.28768	102.2222
44	68.30184426	0.06	5748.736977	-5748.73698	217.2222
45	228.8944254	0.07	4402.627144	-4402.62714	122.2222
46	220.3366484	0.07	4042.412131	-4042.41213	112.2222
47	211.8040966	0.07	3682.197117	-3682.19712	102.2222
48	203.2997388	0.07	2601.552076	-2601.55208	72.2222
49	194.8270991	0.07	2241.337062	-2241.33706	62.2222
50	186.3903733	0.065	2243.175004	-2243.175	72.2222
51	177.9944369	0.065	1621.987889	-1621.98789	52.2222
52	169.645156	0.065	1311.394331	-1311.39433	42.2222
53	161.3496243	0.065	690.2072158	-690.207216	22.2222
54	153.1163152	0.065	0	0	0
55	144.9556657	0.06	588.1055566	-588.105557	22.2222
56	136.8803827	0.06	323.4577915	-323.457792	12.2222
57	128.9062664	0.06	0	0	0
58	121.0530525	0.06	0	0	0
59	113.3456629	0.055	0	0	0
60	105.8156702	0.055	0	0	0
61	98.50330935	0.055	0	0	0
62	91.46053806	0.05	0	0	0
63	84.75025427	0.05	224.6234663	-224.623466	12.2222
64	78.45579797	0.05	592.1898068	-592.189807	32.2222
65	72.68528003	0.06	1117.401087	-1117.40109	42.2222
66	67.57306188	0.065	4106.73635	-4106.73635	132.2222
67	228.8944254	0.07	4402.627144	-4402.62714	122.2222
68	220.3366484	0.07	4042.412131	-4042.41213	112.2222
69	211.8040966	0.07	3682.197117	-3682.19712	102.2222
70	203.2997388	0.07	2601.552076	-2601.55208	72.2222
71	194.8270991	0.07	2241.337062	-2241.33706	62.2222
72	186.3903733	0.065	2243.175004	-2243.175	72.2222

73	177.9944369	0.065	1621.987889	-1621.98789	52.2222
74	169.645156	0.065	1311.394331	-1311.39433	42.2222
75	161.3496243	0.065	690.2072158	-690.207216	22.2222
76	153.1163152	0.065	0	0	0
77	144.9556657	0.06	588.1055566	-588.105557	22.2222
78	136.8803827	0.06	323.4577915	-323.457792	12.2222
79	128.9062664	0.06	0	0	0
80	121.0530525	0.06	0	0	0
81	113.3456629	0.055	0	0	0
82	105.8156702	0.055	0	0	0
83	98.50330935	0.055	0	0	0
84	91.46053806	0.05	0	0	0
85	84.75025427	0.05	224.6234663	-224.623466	12.2222
86	78.45579797	0.05	592.1898068	-592.189807	32.2222
87	72.68528003	0.06	1117.401087	-1117.40109	42.2222
88	67.57306188	0.065	4106.73635	-4106.73635	132.2222
89	228.8944254	0.07	4402.627144	-4402.62714	122.2222
90	220.3366484	0.07	4402.627144	-4402.62714	122.2222
91	211.8040966	0.07	3682.197117	-3682.19712	102.2222
92	203.2997388	0.07	2601.552076	-2601.55208	72.2222
93	194.8270991	0.065	2864.36212	-2864.36212	92.2222
94	186.3903733	0.065	2243.175004	-2243.175	72.2222
95	177.9944369	0.065	1932.581447	-1932.58145	62.2222
96	169.645156	0.065	1311.394331	-1311.39433	42.2222
97	161.3496243	0.065	690.2072158	-690.207216	22.2222
98	153.1163152	0.065	379.6136581	-379.613658	12.2222
99	144.9556657	0.06	852.7533218	-852.753322	32.2222
100	136.8803827	0.06	588.1055566	-588.105557	22.2222
101	128.9062664	0.06	0	0	0
102	121.0530525	0.06	0	0	0
103	113.3456629	0.055	271.7943943	-271.794394	12.2222
104	105.8156702	0.055	0	0	0
105	98.50330935	0.055	0	0	0
106	91.46053806	0.05	224.6234663	-224.623466	12.2222
107	84.75025427	0.05	592.1898068	-592.189807	32.2222
108	78.45579797	0.05	775.972977	-775.972977	42.2222
109	72.68528003	0.06	1382.048852	-1382.04885	52.2222
110	67.57306188	0.06	5087.117564	-5087.11756	192.2222
111	228.8944254	0.07	4402.627144	-4402.62714	122.2222
112	220.3366484	0.07	4402.627144	-4402.62714	122.2222
113	211.8040966	0.07	3682.197117	-3682.19712	102.2222

114	203.2997388	0.07	2601.552076	-2601.55208	72.2222
115	194.8270991	0.065	2864.36212	-2864.36212	92.2222
116	186.3903733	0.065	2243.175004	-2243.175	72.2222
117	177.9944369	0.065	1932.581447	-1932.58145	62.2222
118	169.645156	0.065	1311.394331	-1311.39433	42.2222
119	161.3496243	0.065	690.2072158	-690.207216	22.2222
120	153.1163152	0.065	379.6136581	-379.613658	12.2222
121	144.9556657	0.06	852.7533218	-852.753322	32.2222
122	136.8803827	0.06	588.1055566	-588.105557	22.2222
123	128.9062664	0.06	0	0	0
124	121.0530525	0.06	0	0	0
125	113.3456629	0.055	271.7943943	-271.794394	12.2222
126	105.8156702	0.055	0	0	0
127	98.50330935	0.055	0	0	0
128	91.46053806	0.05	224.6234663	-224.623466	12.2222
129	84.75025427	0.05	592.1898068	-592.189807	32.2222
130	78.45579797	0.05	775.972977	-775.972977	42.2222
131	72.68528003	0.06	1382.048852	-1382.04885	52.2222
132	67.57306188	0.06	5087.117564	-5087.11756	192.2222
133	182.4869758	0.07	2961.76709	-2961.76709	82.2222
134	176.4736891	0.07	2961.76709	-2961.76709	82.2222
135	170.4814221	0.07	2601.552076	-2601.55208	72.2222
136	164.5124718	0.07	1881.122049	-1881.12205	52.2222
137	158.5694712	0.07	1520.907035	-1520.90703	42.2222
138	152.6554512	0.07	1160.692021	-1160.69202	32.2222
139	146.7739149	0.065	1932.581447	-1932.58145	62.2222
140	140.9289295	0.065	1621.987889	-1621.98789	52.2222
141	135.1252381	0.065	1621.987889	-1621.98789	52.2222
142	129.3683985	0.065	1311.394331	-1311.39433	42.2222
143	123.6649539	0.065	1000.800773	-1000.80077	32.2222
144	118.0226456	0.065	1000.800773	-1000.80077	32.2222
145	112.4506766	0.06	1646.696617	-1646.69662	62.2222
146	106.9647674	0.06	1382.048852	-1382.04885	52.2222
147	101.5688014	0.06	1117.401087	-1117.40109	42.2222
148	96.28326497	0.055	1828.437846	-1828.43785	82.2222
149	91.12737544	0.055	1383.682574	-1383.68257	62.2222
150	86.12442012	0.05	1878.671998	-1878.672	102.2222
151	81.30263631	0.05	1878.671998	-1878.672	102.2222
152	76.69620164	0.05	1878.671998	-1878.672	102.2222
153	72.34626297	0.06	2440.639913	-2440.63991	92.2222
154	68.30184426	0.06	5351.765329	-5351.76533	202.2222

155	182.4869758	0.07	2961.76709	-2961.76709	82.2222
156	176.4736891	0.07	2961.76709	-2961.76709	82.2222
157	170.4814221	0.07	2601.552076	-2601.55208	72.2222
158	164.5124718	0.07	1881.122049	-1881.12205	52.2222
159	158.5694712	0.07	1520.907035	-1520.90703	42.2222
160	152.6554512	0.07	1160.692021	-1160.69202	32.2222
161	146.7739149	0.065	1932.581447	-1932.58145	62.2222
162	140.9289295	0.065	1621.987889	-1621.98789	52.2222
163	135.1252381	0.065	1621.987889	-1621.98789	52.2222
164	129.3683985	0.065	1311.394331	-1311.39433	42.2222
165	123.6649539	0.065	1000.800773	-1000.80077	32.2222
166	118.0226456	0.065	1000.800773	-1000.80077	32.2222
167	112.4506766	0.06	1646.696617	-1646.69662	62.2222
168	106.9647674	0.06	1382.048852	-1382.04885	52.2222
169	101.5688014	0.06	1117.401087	-1117.40109	42.2222
170	96.28326497	0.055	1828.437846	-1828.43785	82.2222
171	91.12737544	0.055	1383.682574	-1383.68257	62.2222
172	86.12442012	0.05	1878.671998	-1878.672	102.2222
173	81.30263631	0.05	1878.671998	-1878.672	102.2222
174	76.69620164	0.05	1878.671998	-1878.672	102.2222
175	72.34626297	0.06	2440.639913	-2440.63991	92.2222
176	68.30184426	0.06	5351.765329	-5351.76533	202.2222